Karlsruhe Institute of Technology

Linking structure and functioning of hydrological systems

How to achieve necessary experimental and model complexity with adequate effort

Conrad Jackisch

LINKING STRUCTURE AND FUNCTIONING OF HYDROLOGICAL SYSTEMS

HOW TO ACHIEVE NECESSARY EXPERIMENTAL AND MODEL COMPLEXITY WITH ADEQUATE EFFORT

LINKING STRUCTURE AND FUNCTIONING OF HYDROLOGICAL SYSTEMS

How to achieve necessary experimental and model complexity with adequate effort

Zur Erlangung des akademischen Grades eines

DOKTORS DER NATURWISSENSCHAFTEN

von der Fakultät für
Bauingenieur-, Geo- und Umweltwissenschaften
des Karlsruher Instituts für Technologie (KIT)
genehmigte

DISSERTATION

von
Dipl. Geoökologe Conrad Jackisch
aus Großröhrsdorf

Tag der mündlichen Prüfung: 17. November 2015

Referent: Prof. Dr.-Ing. Erwin Zehe
Korreferent: Prof. Dr. Marco Dentz

Karlsruhe 2015

KIT – KARLSRUHE INSTITUTE OF TECHNOLOGY

Layout using the Tufte-LaTeX package http://code.google.com/p/tufte-latex/

The thesis is accompanied by a GIT repository.
To get access to most of the analyses and the model code, please visit https://github.com/cojacoo/.

Eidesstattliche Versicherung gemäß §6 Abs. 1 Ziff. 4 der Promotionsordnung des Karlsruher Instituts für Technologie für die Fakultät für Bauingenieur-, Geo- und Umweltwissenschaften:

1. Bei der eingereichten Dissertation zu dem Thema "Linking Structure and Functioning of Hydrological Systems" handelt es sich um meine eigenständig erbrachte Leistung.
2. Ich habe nur die angegebenen Quellen und Hilfsmittel benutzt und mich keiner unzulässigen Hilfe Dritter bedient. Insbesondere habe ich wörtlich oder sinngemäßaus anderen Werken übernommene Inhalte als solche kenntlich gemacht.
3. Die Arbeit oder Teile davon habe ich bislang nicht an einer Hochschule des In- oder Auslands als Bestandteil einer Prüfungs- oder Qualifikationsleistung vorgelegt.
4. Die Richtigkeit der vorstehenden Erklärungen bestätige ich.
5. Die Bedeutung der eidesstattlichen Versicherung und die strafrechtlichen Folgen einer unrichtigen oder unvollständigen eidesstattlichen Versicherung sind mir bekannt.

Ich versichere an Eides statt, dass ich nach bestem Wissen die reine Wahrheit erklärt und nichts verschwiegen habe.

Karlsruhe, 30.06.2015

Contents

List of Figures

List of Tables

List of abbreviations and symbols

Abbreviation	**Description**
CAOS	DFG Research Group "From Catchments as Organised Systems to Models based on Functional Units"
CRP-GL	Centre de Recherche Publique – Gabriel Lippmann (now LIST)
DFG	German Research Foundation
KIT	Karlsruhe Institute of Technology
LIST	Luxembourg Institute of Science and Technology
LMU	Ludwig-Maximilians-Universität München
TUBS	Technical University Braunschweig
UF	University Freiburg
EchoRD	Eco-hydrological particle model based on Representative structured Domains
EFU	Elementary functional unit
FU	Functional unit
GIS	Geographical information system
GPR	ground penetrating radar
LTE	Local thermodynamic equilibrium
MEP	Maximum entropy production
REW	Representative Elementary Watershed [Reggiani et al., 1998]
RS	Remote sensing
TDR	time domain reflectometry

Symbol	Description	Unit
$D(\theta)$	Diffusivity	$m^2\,s^{-1}$
E_{tkin}	Translatory kinetic energy	$kg\,m^2\,s^{-2}$
ET	Evapotranspiration normalised	m
η	Viscosity of water	$kg\,m^{-1}\,s^{-1}$
g	Gravitational acceleration	$m\,s^{-2}$
I	Impulse counteracting E_{tkin}	$kg\,m\,s^{-1}$
θ	Volumetric soil moisture	$m^3\,m^{-3}$
k_{sat}	Saturated hydraulic conductivity	$m\,s^{-1}$
$k(\theta)$	Unsaturated hydraulic conductivity	$m\,s^{-1}$
m	Mass	kg
P	Precipitation normalised	m
Pe	Péclet number	-
Ψ	Matric head	Pa
ψ	Matric head as column water	m
q	Flux	$m\,s^{-1}$
R	Macropore radius	m
$r_{particle}$	Particle radius	m
ρ	Density of water	$kg\,m^{-3}$
Q	Discharge normalised	m
s	Length	m
S	Storage normalised	m
t	Time	s
T	Temperature	°C
u	Advective velocity in matrix	$m\,s^{-1}$
v	Advective velocity in structures	$m\,s^{-1}$
V	Volume	m^3
x	Lateral distance	m
ξ	Random number 0..1	-
z	Depth	m

To all who strive for a sustainable world of freedom, equal rights and shared knowledge about the earth's processes.

I wish to thank the whole community who has made this thesis possible. As such I hope it will contribute back for all the efforts: Cleaning the institute building, taking care about my daughter, supporting me to devote my time to this work, and funding the endeavour is more than I could have asked for.

In particular I thank my advisor Erwin Zehe who was always an inspiring, creative fighter in the quest for new insights and to overcome nasty traps. I also want to acknowledge the support of Razije Fiden, Selina Baldauf, Jonas Lanz, Federico Fronza, Electra Ullrich and François Nyobeu during the fieldwork and laboratory analyses. Without the colleagues at KIT and the CAOS team, especially Niklas Allroggen, Lisa Angermann, Loes van Schaik, Simon Seibert, Ralf Loritz, Sibylle Hassler, Theresa Blume, Markus Weiler, Matthias Sprenger, and Britta Kattenstroth, I could not have achieved this.

Also the reliable financial support of the German Academic Foundation and the Deutsche Forschungsgemeinschaft is gratefully acknowledged.

Finally I wish to thank all my friends and comrades for backing me up to the real world.

Abstract

Hydrological processes in the earth's *Critical Zone* [Lin, 2010] like the infiltration and redistribution of rainfall, soil water storage and dynamics, and pedo-eco-hydrological interactions are some of the most common and crucial everyday phenomena. Rapid subsurface flow in structured soils arises from imperfect lateral mixing of fast advective flow in structures and diffusive flow in the soil matrix. It remains one of the most challenging topics in hydrology with respect to conceptualisation, observation and modelling [among many others Beven and Germann, 1982, 2013, McDonnell et al., 2007, Nimmo, 2011, Band et al., 2014]. Approaching a catchment as dynamic self-organised system, structures like macropores become an inherent property for fast dissipation of rainfall induced gradients [Zehe et al., 2013].

This thesis seeks to develop theories, experiments, concepts and modelling tools at the plot- and hillslope-scale suitable to integrate the "some degree of organisation" [Dooge, 1986], which results in threshold processes [Zehe et al., 2005], connectivity [Wainwright et al., 2011], patterns [Grayson et al., 2002] and landscape function [Schröder, 2006] at the lower meso-scale. It is motivated by outcomes of the initiative on predictions in ungauged basins [Sivapalan et al., 2003, Blöschl et al., 2013] and a critical reflection on the conceptual constraints in hydrology and hydrological modelling [Gupta et al., 2012].

The quest for minimum adequacy of model complexity, geophysical exploration and functional unit identification investigates examples from the Attert experimental basin in Luxembourg. With emphasis on a joined examination of theoretical concepts, experimental methodology and modelling approaches the thesis is addressing landscape and process analysis (chapter 2), targeted experiments at the plot- and hillslope-scale (chapter 3) and the development of a novel model framework (chapter 4).

Landscape analysis and functional unit identification
In the first part I contrast *in situ* measurements, pedo-physical anal-

yses of soil samples, an examination of the flow regimes and an investigation of GIS and remote sensing data. It is found that landscape features and process characteristics do not necessarily align. Landscape classes and pedo-physical property means are not sufficient to define functional units.

Experiments to measure advective flow in structured soils I present a series of plot-scale sprinkler experiments with Brilliant Blue dye tracer and Bromide salt tracer. They are accompanied by monitoring of soil moisture dynamics. In addition three experiments have been extended by 3D time-lapse ground penetrating radar (GPR) and stable isotopes. Moreover a hillslope-scale experiment addresses lateral subsurface structures by means of a dense TDR monitoring setup and GPR inferred trenches based on time-lapse radargrams.

For all sites, rapid subsurface flow in biogene, pedogene and geogene structures is found. While the binary Brilliant Blue stains allow for the identification of preferential flow paths, recovered Bromide concentration profiles enables a very detailed description of the advective flow field. Advance is achieved through the coherent combination of different tracers and methods. Primarily the discrepancies between the results spark a revision of the perception of the processes and the exploratory methods.

In the hillslope-scale experiment the findings from the plot-scale are extended. While vertically a fraction of the water largely bypassed the soil also lateral structures lead to fast transport. Further it is found very challenging to identify hydrologically relevant structures *a priori* in a single GPR survey. Also monitoring flow in structures even with a very dense network of soil moisture logs proves very difficult. However, the GPR inferred trenching based on repetitive measurements of the same profiles did clearly identify distinct flow paths.

Lagrangian model framework with a representative, structured domain
A major achievement of this thesis is a novel Lagrangian stochastic-physical model framework. It simulates soil water flow by means of a space domain random walk and advection of water particles in a representative, structured model domain. The central objective is the simulation of rapid flow fingerprints in different ecohydrological settings by making maximum use of field observables for parameterisation and to avoid non-observable parameters for macropore-matrix exchange. I present the hypothesis-driven iterative model development and its falsification based on suitable experiments and mon-

itoring data. Special emphasis is placed on how to estimate a) the distribution of advective velocity in soils, b) macropore-matrix exchange as key control for the self-limitation of advection, and c) key features of the macropore network in the model.

During the process-hypothesis testing the "echoRD" model proves as a powerful alternative to existing dual-domain models, allowing for topologically explicit structures based on experimental data. The model is successfully referenced against a large spectrum of experimental findings in the lab, on an agricultural site with biopores and on a forested site on periglacial slope deposits.

Pushing the basins – squeezing the models

Aside from the specific findings, a major point of this thesis is the joint consideration of theoretical concepts, experimental techniques and modelling approaches. It is highlighted in each aspect how much the perceptional model influences the respective method. The topic is concluded with a proposal to revise the procedure. Models of a more general type can be used to derive particular hypotheses. They are tested by experiments with strongly controlled boundary conditions and a coherent multi-method observation layout. Since real world experiments are limited, specific process models are employed to extend them in a virtual domain.

Zusammenfassung

Hydrologische Prozesse in der *Kritischen Zone* der Erde [Lin, 2010] wie Infiltration und die Verteilung von Regenwasser im Boden, das Speichern und Verlagern von Wasser als Bodenfeuchte sowie Wechselwirkungen in und zwischen der Pedo-, Öko- und Hydrosphäre sind alltägliche und grundlegende Phänomene. Präferenzielles Fließen in strukturierten Böden begründet sich darauf, dass der schnelle advektive Fluss in Strukturen und die diffuse Wasserbewegung in der Bodenmatrix nicht vollständig gemischt sind. Es bleibt eines der herausfordernsten Themen in der Hydrologie für diese Prozesse Konzepte, Beobachtungsmethoden und Modelle zu entwickeln [unter vielen anderen Beven and Germann, 1982, 2013, McDonnell et al., 2007, Nimmo, 2011, Band et al., 2014]. Mit dem Verständnis eines Flusseinzugsgebietes als dynamisches, sich organisierendes System sind Strukturen wie Makroporen eine inhärente Eigenschaft für den schnellen Abbau der durch Regen aufgebauten Gradienten [Zehe et al., 2013].

Diese Dissertation handelt von der Entwicklung von Theorien, Experimenten, Konzepten und Modellen auf der Skala zwischen Bodensäule und Hang, welche dazu geeignet sind, den Teil an Organisation auf der unteren Mesoskala [Dooge, 1986] zu integrieren. Letzterer ist das Resultat von Schwellwertprozessen [Zehe et al., 2005], Konnektivität [Wainwright et al., 2011], Mustern [Grayson et al., 2002] und Landschaftsfunktionen [Schröder, 2006]. Die Ergebnisse der Initiative für Vorhersagen in nicht-bepegelten Einzugsgebieten [Sivapalan et al., 2003, Blöschl et al., 2013] und eine kritische Reflexion der derzeitigen konzeptionellen Grenzen in der Hydrologie und hydrologischen Modellierung [Gupta et al., 2012] motivieren diese Arbeit.

Die Expedition für minimal adäquate Modellkomplexität, geophysikalische Exploration und Identifikation funktioneller Einheiten untersucht Beispiele aus dem Untersuchungsgebiet der Attert in Luxemburg. Mit einem Schwerpunkt auf der gemeinsamen Betrachtung von theoretischen Konzepten, experimenteller Methodologie und Modellentwicklung werden in dieser Dissertation eine Landschafts- und Prozessanalyse (Kapitel 2), zielgerichtete Experimente auf der

Skala von Bodensäulen und einem Hang (Kapitel 3) und die Entwicklung eines neuen Modellkonzeptes (Kapitel 4) behandelt.

Landschaftsanalyse und Identifikation funktioneller Einheiten

Im ersten Teil der Arbeit vergleiche ich *in situ* Messungen, pedophysikalische Analysen von Bodenproben, eine Untersuchung der Wasserhaushaltsdynamik und eine Studie von räumlichen- und Fernerkundungsdaten. Dabei stellt sich heraus, dass Landschafts- und Prozesseigenschaften nicht unbedingt kongruent sind. Funktionelle Einheiten sind nicht vollständig durch Landschaftsklassen und pedophysikalische Eigenschaften definiert – vor allem wenn deren Skalen nicht überein stimmen.

Experimente zur Erkundung von advektiven Flüssen in strukturierten Böden

Ich präsentiere eine Reihe von Beregnungsexperimenten mit Brilliantblau als Farb- und Bromid als Salztracer auf der Skala einzelner Bodensäulen. Drei der Experimente werden um multitemporale 3D Georadarmessungen und Analysen von natürlichen Isotopen (Deuterium) erweitert. Darüber hinaus werden laterale Fließstrukturen im Untergrund in einem Experiment auf der Hangskala mit einem dichten Netzwerk an TDR Bodenfeuchtemessungen und multitemporalen Georadarprofilmessungen untersucht.

In allen Fällen wird präferenzielles Fließen in biogenen, pedogenen und geogenen Strukturen beobachtet. Während die präferenziellen Fließpfade mittels Brilliantblau Färbungen identifiziert werden, kann mittels der Analyse von Bromidkonzentrationen in Bodenproben das Feld der effektiven Advektionsgeschwindigkeiten bestimmt werden. Fortschritt wird vor allem durch die kohärente Kombination verschiedener Tracer und Methoden erzielt. Die Diskrepanzen zwischen den einzelnen Ergebnissen stoßen die Revision der Annahmen über die Prozesse und der Untersuchungsmethoden an.

Mit dem Experiment auf der Hangskala werden die Erkenntnisse der lokalen Beregnungen erweitert. Während ein Teil des Beregnungswassers in den Strukturen große Bereiche des Bodens vertikal überbrückt, haben auch laterale Strukturen einen erheblichen Anteil an schnellem Transport. Dabei zeigt sich die Schwierigkeit die hydrologisch relevanten Strukturen *a priori* mit einer einzigen Georadaruntersuchung zu identifizieren. Zudem stellt sich die Beobachtung von Bodenwasserdynamik in strukturierten Böden sogar mittels eines dichten Netzwerks von TDR Rohrsonden als problematisch heraus. Die Fließstrukturen wurden durch multitemporale Messungen mit Georadar sehr gut identifiziert.

Lagrangesches Modellkonzept mit einer repräsentativen, strukturierten Domäne

Eine der zentralen Errungenschaften dieser Dissertation ist ein neues Lagrangesches, stochastisch-physikalisches Modellkonzept. Es simuliert Bodenwasserflüsse durch eine Zufallsbewegung und Advektion von Wasserpartikeln in einer repräsentativen strukturierten Domäne. Ziel ist die Simulation von Fingerabdrücken präferenziellen Fließens in verschiedenen öko-hydrologischen Situationen. Dabei sollen nicht beobachtbare Parameter vermieden werden und möglichst viele Informationen aus Beobachtungen und Experimenten vom Modell genutzt werden können. Ich stelle die hypothesengestütze Modellentwicklung und deren Falsifizierung gegen passende Feldexperimente und Beobachtungen in einem iterativen Lernprozess vor. Zentral dabei sind die Verteilung advektiver Flüsse im Boden und der Austausch zwischen Makroporen und Bodenmatrix als zentrale Kontrolle der Eigenlimitierung advektiver Flüsse.

Während des Testens der Prozesshypothesen erweist sich das "echoRD" Modell als mächtige Alternative zu bisherigen Mehrdomänenmodellen. Im Gegensatz zu ihnen bildet es topologisch explizite Strukturen ab, die in Experimenten identifiziert werden. Das Modell wird erfolgreich in einem großem Spektrum an experimentellen Erkenntnissen aus dem Labor, auf Agrarflächen mit Bioporen und an einem bewaldeten Standort auf periglazialen Schuttdecken getestet.

Einzugsgebiete als Labor – Modelle als Lupe

Neben den spezifischen Ergebnissen ist die gemeinsame Betrachtung von theoretischen Konzepten, experimentellen Techniken und Modellansätzen zentral. In jedem der Aspekte stelle ich heraus, wie sehr die Annahmen und Vorstellungen von den Prozessen die jeweilige Methode und somit das Ergebnis bestimmen. Das Thema wird mit einem Vorschlag einer alternativen Herangehensweise abgeschlossen: Modelle allgemeineren Typs (Wasserhaushaltsdynamik) können dazu genutzt werden, spezielle Hypothesen an die Landschaft zu formulieren. Diese müssen dann in Experimenten mit klar kontrollierten Randbedingungen und einem kohärenten Untersuchungsaufbau verschiedener Methoden getestet werden. Da die Möglichkeiten für Experimente sehr begrenzt sind, werden spezifische Modelle entwickelt und verwendet, welche die Analysen im virtuellen Raum erweitern.

1
Introduction

Hydrological processes in the earth's *Critical Zone* [Lin, 2010] like the infiltration and redistribution of rainfall, soil water storage dynamics and pedo-eco-hydrological interactions are some of the most common and crucial everyday phenomena. Nonetheless it remains challenging to understand, observe and model them. The task to develop techniques to measure integrated fluxes and storages at useful scales is – as Beven [2006a] puts it – the most important problem in hydrology of the 21st century, followed by the search for appropriate closure schemes. Reviews of applied exploration and modelling in hydrology point out that interlinked scales, heterogeneity and patterns, non-stationary processes and non-universality of hydrological models are key restrictions for advancing the understanding of the water cycle.

To investigate system dynamics, there is a growing interest to use models as virtual exploratorium. For this application it is crucial to revise the model development process and their capability and limitations [Gupta and Nearing, 2014]. In many cases it is very difficult to consequently treat models as testable hypotheses [Clark et al., 2011] and to differentiate between the different sources of uncertainty and errors. As much as singular measurements are challenged to be representative and to go beyond case studies, also models are confronted with deeply rooted conceptual assumptions.

This thesis is motivated by the concept of approaching catchments as dynamic self-organised systems [Zehe et al., 2013] – hence not a random, well distributed coincidence. As such I will seek to develop theories, experiments, concepts and modelling tools at the plot- and hillslope-scale suitable to account for spatial organisation which according to Dooge [1986] cause complex catchment functioning at the lower meso-scale. This includes to investigate threshold processes [Zehe et al., 2005], to unravel connectivity and patterns which reflect spatial oranisation [Wainwright et al., 2011, Grayson et al., 2002, respectively] and those which are caused by it, and to include ecological controls on landscape function [Schröder, 2006].

A special focus lies on rapid subsurface storm flow in structured soils as one manifestation of this self-organisation of dissipative structures. It confronts us with a multitude of different eco-hydrological influences, which need consideration [Band et al., 2014]: Earthworm burrow configurations [Blouin et al., 2013], their spatio-temporal dynamics [Palm et al., 2012, van Schaik et al., 2013] and burrow coatings [Rogasik et al., 2014] are studied and dramatically effect infiltration and water redistribution. Also other structure creating animals like rodents and moles have impact [Botschek et al., 2002]. Plant roots effect water uptake and redistribution dynamically [Nadezhdina et al., 2010]. Connected flow paths [Wienhöfer and Zehe, 2014] and periglacial cover beds [Heller, 2012] may change the hydrological regime completely. All of these are rather complex and specific in detail. Most of the study will reduce the question to macropore-matrix interaction as a common challenge to current model concepts since the advective processes take place in explicit structures (with respective connectivity and spatial covariance) interacting with the soil matrix. However, the target is an adequate generalisation of these processes in concepts, exploration and modelling.

Another focus lies in the joint consideration of theoretical concepts, experimental techniques and modelling approaches. Seeking for minimal adequacy of landscape exploration and model complexity inevitably poses the question for what, where and how processes are, can and should be observed and modelled.

This chapter will introduce the current state regarding the relevant research aspects concluding with my specific research questions and an outline of the thesis.

1.1 *Energy Perspective – to treat a catchment as dynamic, self-organised geo-eco-hydrological system*

From a general standpoint a catchment can be seen as a dissipative system driven by gradients imposed upon it by atmospheric and radiation forcing. Figure 1.1 presents the fundamental idea after Zehe et al. [2013]. The different forcings (radiation, precipitation) cause a deviation from the local thermodynamic equilibrium (LTE) state into different directions:

1. Radiation causes evaporation and drying. This creates a higher matric potential which I express as capillary binding energy [after Kleidon and Schymanski, 2008]. This gradient is depleted by wetting to return to LTE.

2. Rainfall imports mass to the system. This potential energy excess

needs drainage to relax back to LTE.

From the second law of thermodynamics[1] the hypothesis is formulated that hydro-geo-ecosystems evolve to a state of maximum free energy dissipation. As such they expose structures which facilitate large mass fluxes in rainfall driven conditions and a storage to feed large energy dissipation in radiation driven conditions. At the same time hydrologic cycling within the earth system is bound by some limit as maximum conversion rate of thermodynamic gradients into mechanical work such as the Carnot limit for heat induced mechanical work [Kleidon and Renner, 2013].

Bejan and Lorente [2011] point out that structures are an emergent property of natural systems exhibiting a large similarity. More specifically Kleidon [2004] and Dewar [2005] formulate arguments of the maximum entropy production (MEP) hypothesis: Aiming fundamentally at processes in the climate system it suggests that given many degrees of freedom physical, dissipative processes evolve to states at which the production of entropy is maximised. Kleidon [2009] and Kleidon and Schymanski [2008] show in more detail how the MEP principle can also be applied to processes in the water cycle. It was extended by Zehe et al. [2013] who linked the same principle as free energy dissipation to process hydrology.

[1] The second law of thermodynamics is also known as "the arrow of time" or "law of increased entropy". It states that $\Delta S = \partial Q/T \geq 0$ or $\Delta S_{univ} = \Delta S_{system} + \Delta S_{environment} \geq 0$ and adds to the first law (conservation of matter and energy).

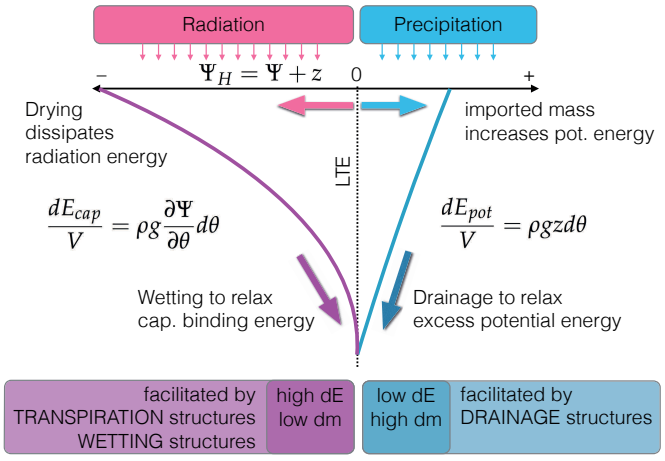

Figure 1.1: Catchment as dissipative system depleting gradients imposed by climatic forcing as positive (rainfall) or negative (capillary forces) hydraulic head after Zehe et al. [2013].

Based on this the hypothesis is specified further: Structures and the system's dissipation limits are inherently linked. They arrange in a way to minimise the time to recover LTE. In the example of preferential flow[2] in structured soils it facilitates vertical mass transfer against differences in geo-potential or large gradients in matrix potential, which emerge during dry spells in cohesive soils and lead to a faster depletion of the gradients. This implies a faster reduction (dissipation and export) of free energy of soil water during rainfall

[2] The terms rapid flow, subsurface storm flow and preferential flow are used rather synonymously. Rapid flow shall emphasis the existence of a fast flow domain which is significantly exceeding the expected average diffusive flow velocity. Subsurface storm flow does indicate towards mass induced processes. Preferential flow is giving more emphasis on the existence of structures.

driven conditions due to enhanced mixing into the main direction of the preferential flow path [Zehe et al., 2013], although it hinders lateral mixing. Also exchange between the diffusive and advective flow domains is associated with dissipation of kinetic energy and thus momentum [Kutilek and Germann, 2009].

1.1.1 *Mass induced gradients*

The depletion of rainfall induced gradients and associated dissipation is characterised by generally large fluxes of mass with relatively low energy. For example, the potential energy of rainfall water at some elevated point is converted into kinetic energy for its discharge at a lower point. As such, the limitation may be searched in the elevation gradient and the resistivity against the flow. Zehe [1999] points out that a single earthworm burrow (d=8 mm) can transport equivalent to 1 m^2 of loess soil. A more common example is that of stream networks which efficiently drain a basin.

In hydrology the theme has been taken up by several groups: Rodriguez-Iturbe and Rinaldo [1997] analysed the self-similarity of rivers (and coastlines) at different scales resulting in the proposal of scaling laws and a vision for inter-dependent self-organisation of climate-soil-vegetation dynamics [Rodriguez-Iturbe, 2000]. At the catchment scale Rinaldo et al. [2014] propose "optimal channel networks" as an inherent feature which could be used for hydrologic system characterisation and comparison. Using drainage density as an index for basin characteristics is not a new approach [Kirkby and Chorley, 1967]. A similar idea has also been applied to hillslope and channel lengths [Lazzaro, 2008].

However, the explicit consideration of structures in hydrological concepts has been limited to the more apparent structure of surface flow networks for a long time. McDonnell [2013] provocatively stated that *all runoff processes are the same*. Hergarten et al. [2014] argue that surface and subsurface structures may share similar mean residence times but their distributions differ strongly. In terms of the MEP hypothesis functional optima are non-unique. Thus different structural setups may maximise entropy production.

Zehe and Flühler [2001] and Weiler and Flühler [2004] took the first steps to study the role of macroporous structures and how to infer flow types from tracer recovery and dye pattern distributions. A considerable body of preferential flow literature has emerged [Beven and Germann, 1982, 2013] and Schulz et al. [2006] highlight the importance of spatial structures in more general terms. Nevertheless, it remains challenging to unravel the *science in which all processes are preferential* [Uhlenbrook, 2006] in the face of energy dissipation and

ecohydrological redistribution feedbacks [Nadezhdina et al., 2010].

1.1.2 *Radiation energy induced gradients*

The depletion of gradients induced by radiative forcing is rather different in nature. Here we are faced with high fluxes of energy and low mass exchange (e.g. evaporation of soil water as latent heat flux cooling the radiated surface). As such also the structures for the processes differ and limitations may be found in the resistivity against energy fluxes.

Naturally, the respective processes are mainly connected to transpiration and soil-water-retention. While the latter appears relatively well studied going back to the work of Buckingham [1907] the former poses more open questions since the interaction of plants within the hydrological system has long been reduced to a loosely defined sink term accounting for 10-80% of the water balance. It is commonly calculated as a function of atmospheric vapour pressure deficit after Penman-Monteith [Allen et al., 1998], Shuttleworth and Wallace [1985], Szilagyi and Jozsa [2008] or the simpler Hargreaves [Droogers and Allen, 2002]. Schymanski [2006], Schymanski et al. [2008] introduced a shift in the perspective by addressing transpiration of plants as a byproduct of the more fundamental carbon cycle. Although the concept of *plants as carbon factories* has yet to be made utilisable in hydrological process models, it proved applicable at larger scope [also Lei et al., 2008]. Many other studies succeed in explaining vegetation patterns by directly or indirectly linking them to some sort of optimality in the competition for resources [e.g. Caylor et al., 2005, Ursino and Contarini, 2006, Schymanski et al., 2009, Stavi et al., 2015]. At large and global scales the concepts of optimality and MEP have proven highly insightful [e.g. Kleidon, 2012, Kleidon et al., 2014].

1.1.3 *Evolution of dissipative structures*

Besides the co-evolution of landscape ecology and catchment hydrology [Schröder, 2006], joint evolution of dissipative structures is a central concern as they are the result of past work of eventually the same or at least similar processes we currently observe [Zehe et al., 2014, Beven, 2015]. On the one hand, one may use such patterns [e.g. Sivapalan, 2005, Ali et al., 2012] and the behaviour of the resulting processes [Wagener et al., 2007, Harman et al., 2011] for system characterisation. On the other hand, unraveling the inherent optimality principles can highly reduce the ambiguity of heterogeneity, scaling estimates and observation requirements [e.g. in the REW framework Reggiani et al., 1998, Tian et al., 2006] [and in more general terms Ehret et al., 2014]. An enhanced understanding of the dissipative ca-

pacity of an environmental system also opens perspectives for the assessment of system resilience and adaption to changes of external drivers.

While the general concept appears rather trivial it has proven challenging to find experimental, observational and modelling tools to test and develop specific hypotheses for such organisation processes. I thus state the hypothesis more precisely that advective and diffusive flow paths are intrinsic structures of an eco-hydro-pedosphere. As such the topology and connectivity of these structures evolved under the given climatic forcing, the geogene and pedogene degrees of freedom, and ecological and societal modifications to a state of persistence of the dissipative structures.

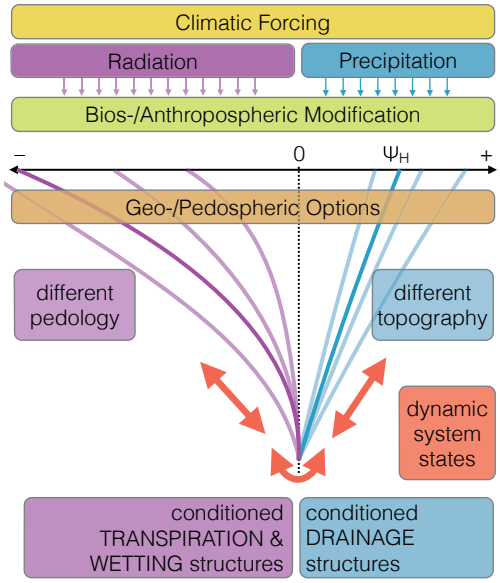

Figure 1.2: Evolution of dissipative structures by cycles of radiation and precipitation induced deviation from equilibrium given the respective amplitude, frequency and degrees of freedom after Zehe et al. [2013]

Figure 1.2 illustrates this concretisation, where a system may evolve during cycles of radiation and precipitation induced deviation from equilibrium given the respective amplitude, frequency and degrees of freedom. As such new questions about resulting system properties and dynamics emerge: When do systems operate at their thermodynamic limits? What constrains these limits and how can they be identified?

To answer these, models with sufficient physical rigour, thermodynamic consistency, and degrees of freedom are required. Conceptually they have to be capable to allow hypothesis testing. And they must be driven by observable parameters with physical meaning and the ability to adapt or change over time.

1.2 *Process perspective – a journey through scales*

Macropore settings may be very different in their topology, their temporal dynamics and their interface characteristics to the soil matrix. Figure 1.3 gives just a glimpse into some types we commonly observe. They extend over pore-, plot- and hillslope-scale.

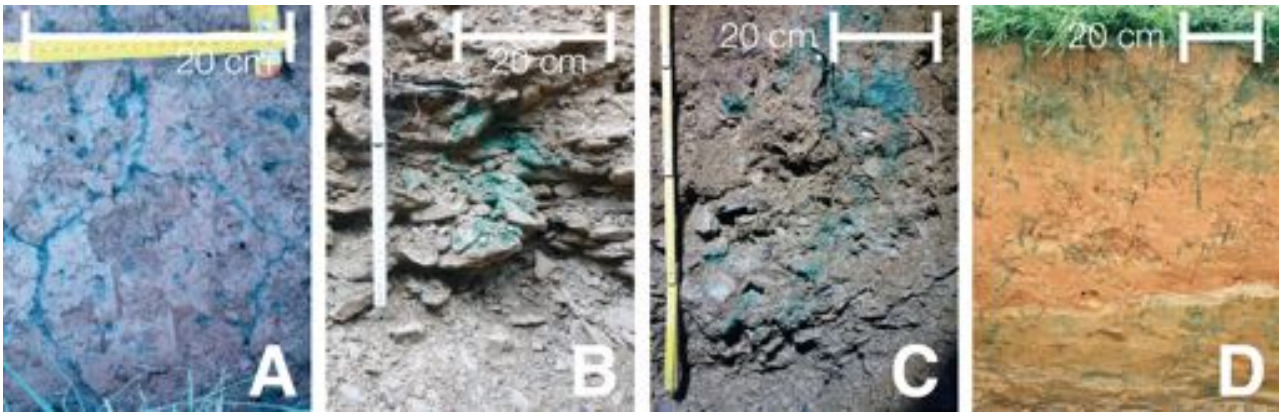

Figure 1.3: Macropores with different origin: A) Cracks - pedogenic aggregates and water stress; B) Soil skeleton - geogenic structures and landscape evolution; C) Roots - biogenic structures, state, activity and life cycle; D) earth worms - biogenic structures, activity cycle, abundances.

Preferential or rapid subsurface storm flow is omnipresent in hydrology [Uhlenbrook, 2006] and is today accepted as being the rule rather than the exception [Flury et al., 1994]. Originally, the term *preferential flow* was coined after it was realised that water flow in non-capillary soil structures was much faster than would be expected from the classical theory of flow and transport in porous media. A considerable number of studies and model approaches have been proposed to solve the issue [especially pinpointed in these reviews: Beven and Germann, 1982, Šimůnek et al., 2003, Gerke, 2006, Jarvis, 2007, Weiler and McDonnell, 2007, Köhne et al., 2009b, Beven and Germann, 2013, Germann, 2014]. However, rapid flow in structured soils is still a challenge to current means of observation, modelling and process understanding.

1.2.1 *A rough sketch through scales*

Instead of repeating the reviews mentioned above, I briefly sketch the processes at different scales inspired by Vogel and Roth [2003]:

At the hillslope scale connectivity of structures are of main concern [e.g. McGuire and McDonnell, 2010, Jencso and McGlynn, 2011, Wienhöfer and Zehe, 2014] although not necessarily attributed to preferential flow alone. Owing to the strong difference in diffusive and advective transport velocity, the establishment of connectivity is

considered to control the threshold process of fast catchment reaction [e.g. Bachmair and Weiler, 2013, van Meerveld et al., 2015].

AT THE PLOT SCALE the separation of different (interacting) flow phases adds to connectivity [e.g. Sanders et al., 2012, Gerke, 2012]. Starting with the initiation of macropore infiltration [Weiler and Naef, 2003] and eventually draining to a larger structure [e.g. like a tile drain Klaus and Zehe, 2010] this may be regarded as the effective scale of rapid subsurface flow in conductive structures as in figure 1.3. However the controls of the processes may not uniquely be derived at this scale. While Flury et al. [1994] did not find clear relation to antecedent soil moisture, Roth and Hammel [1996] pointed out friction control in the flow paths as a dominating process.

HENCE THE PORE SCALE processes at the interface between structures and matrix and in the matrix itself exhibit some control for the apparent process. Besides water retention due to capillary forces, this is shown by Leue et al. [2013] through organic coatings at biopore and crack interfaces or by Snehota et al. [2015] who found redistribution of entrapped air towards the coarse fraction to block flow there. Although there is good reason to take the study even to smaller pores as foam flow [Or and Assouline, 2013], networks of pores [Vogel and Roth, 1998] or the establishment of mobile/immobile phases due to pore size distribution [Bijeljic et al., 2013] this is left for future projects.

OF COURSE SCALES MATTER [Bloschl and Sivapalan, 1995]. What likely confuses the discussion is that hydrological processes in structured systems are studied at all scales often without an adequate unifying concept. Depending on the scope, a considerable proportion of structure may be attributed to heterogeneity in the sub-ordinate scale [e.g. Tetzlaff et al., 2010, Dentz, 2012] or comprised in scaling procedures [e.g. Or, 2008, Jury et al., 2011]. Despite the large body of literature about such issues, the general process description in most hydrological models is of a diffusive, well-mixed percolation in the vadose zone and hydraulic conduction in the saturated zone. This imposes a remarkable fragmentation of theories, observation techniques and perceptional models as it obstructs non-diffusive, structured, and scale- and process-specific representations.

1.2.2 *Advection, diffusion and pressure wave translation*

In the debate about celerity as the apparent velocity [McDonnell and Beven, 2014] it is emphasised that observation of water levels or soil

moisture results in a non-decomposable signal of water and pressure wave propagation. This is also found through much progress in the assessment and modelling of transit time distributions [Soulsby et al., 2010, Harman, 2015, respectively]. With regard to flow in structures the same problem occurs.

Roth [2008] concludes that, in contrast to large fluid systems, fluid properties in porous media are deeply entangled with the geometry of the pore spaces and are often non-stationary. This imposes inherent limits to upscaling and the application of the Richards equation for many environmental systems. At the pore-scale many studies search for approaches to flow conditions, where the assumptions of the Richards equation are not met [e.g. Jury et al., 2003, Lepore et al., 2009, Neuweiler et al., 2012]. However, under conditions of capillary bound soil water and a continuous, harmonic matric potential field, the Richards equation is an efficient way to simulate diffusive water transport.

Hence a physically consistent process description needs to approach all three forms of apparent water flux. This implies that soil water dynamics are insufficiently described with the mass balance alone.

1.3 *Exploration perspective – Assessing landscape organisation and structured hydrological dynamics*

What is a representative sample? What monitoring location adequately corresponds to landscape elements and processes? How can we comprehensively and objectively approach a catchment respecting all the knowledge we have, its generic self-organisation and functional dependencies? What data add information? While a qualitative evaluation from the expert's perspective can (although likely perceptually biased) comprehend most of these aspects – a distinct objective delineation into functional units[3], a determination of their topology and connectivity, and a quantitative description appears far more challenging.

[3] A functional unit (FU) is hypothesised as concept which revises the static hydrological response units towards a process oriented description [Zehe et al., 2014]. It proposes a hierarchy of spatially organised entities which are dynamically allocated based on similar dissipation characteristics and eco-hydrological functioning. See below in section 1.3.2 for details.

1.3.1 *Static maps of a dynamic system*

Grayson et al. [1997] point out preferred states of patterns in soil moisture in temperate Australia. They conclude that a single wetness index may not be able to represent the observed patterns. Grayson and Blöschl [2001] comprehensively link patterns and processes through scales which is seen as key for advances in hydrological sciences by Schulz et al. [2006]. Zehe et al. [2010b] highlight that spatial organisation of patterns may self-organise in a manner to maximise

the dissipation associated with the depletion of driving gradients.

Dynamic system soil properties change in time due to abrupt changes (land use, strong erosion, cracking), gradual adaptation (erosion, swelling and shrinking, carbon accumulation), slow pedogenesis (lessivation, leaching) or different conditions (hysteresis cycle, structure maintenance). The knowledge about pedogenesis is the basis of all soil maps founded on relatively few profile and auger samples. Terribile et al. [2011] impressively show that soil maps and hydrological application are not necessarily well-aligned. Bloschl and Sivapalan [1995] show that single measurements can be largely misleading when the process-scale is ignored.

However, a detailed map of proxies for hydrologically relevant processes is only one possible strategy to identify and extrapolate observed properties at the point scale to the catchment. Baveye and Laba [2015] critique the self-determination of soil heterogeneity in many studies and conclude that clear attention to the underlying causes of that "heterogeneity" has to be given. In the example of preferential flow, which is one of the most significant causes of spatial heterogeneity, Beven and Germann [2013] conclude that little progress has been made in the last 25 years.

1.3.2 *The functional unit concept*

An alternative approach has been introduced with the functional unit hypothesis [Zehe et al., 2014, Ehret et al., 2014]. On the one hand it is a thermodynamic reinterpretation of the hydrological response unit concept. On the other hand it is a process-aware, theoretically consistent catchment delineation strategy.

Figure 1.4 outlines the idea with a description in the caption. One fundament of the functional unit hypothesis is the concept that it is possible to identify a hierarchy of spatial entities with similar process characteristics with respect to either energy or mass exchanges. Due to self-organisation and process interrelation, only very few of all possible combinations of elementary functional unit (EFU) descriptors are comprising most of the system. Thus it is proposed that in-depth examination of few representatives allows one to assign this typical behaviour to the class. Reversely it may be feasible to infer the catchment dynamics from simulations of such representatives without lumping across the organisational hierarchy.

From this it is apparent that both mapping and functional unit identification require distinctly different exploration. This thesis tests the feasibility the functional unit approach, which allows for processes exploration at adequate scales. It is not contradicting any mapping effort but strongly alters the workflow: Potential representatives

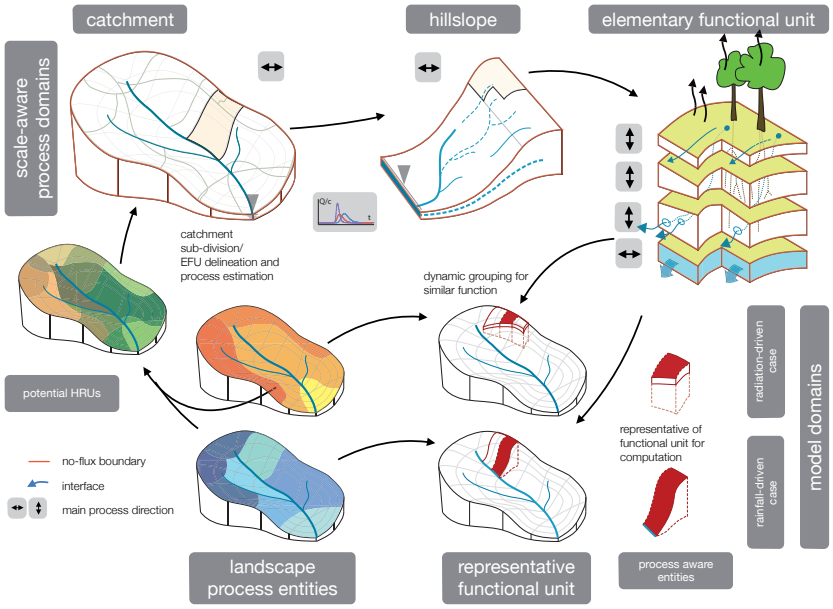

Figure 1.4: Functional unit concept after Zehe et al. [2014]. Landscape elements dynamically group for similar processes. Shown in the lower left are two possible examples like evapotranspiration which may be an imprint of exposition and land use (top) and runoff generation which connects hillslopes to the river network (bottom). As data is available at specific locations for specific attributes instead of extrapolating the data to the landscape a representative at the respective scale and for the specific process is taken to simulate the dynamics. To do so elementary functional units (with prevailingly vertical processes) recompose depending on state and forcing.

are derived from a preparatory analysis of existing data. Experiments and monitored dynamics inform models which are used as hypotheses to infer the behaviour of similar functional units. Ultimately this can lead to the identification of appropriate proxies for the processes and a map of functional units including their general behaviour.

A minimal-adequate exploration appears demanding: Advective and diffusive flows are dissipating gradients in a basin. Furthermore, a confusion of heterogeneity with sub- or super-scale structures needs to be avoided. It is also argued for less ambiguity in hydrological case studies in a review of exploration methods for subsurface connectivity [Blume and van Meerveld, 2015]. New avenues in landscape analysis could avoid this overwhelming demand by following the concept that catchment structures and properties are the most probable result of past work during the continuous depletion of gradients. Experiments can be constrained as specific hypotheses based on a broad primary exploration and data analysis. With elevated physical coherence such experiments (both real and virtual) will lead to a more reliable process analysis. They will also be more appropriate to prepare predictions of responses under change.

1.4 *Modelling perspective – extending experiments and allowing hypothesis testing*

Much of the hydrological modelling efforts may be attributed to rainfall-runoff prediction. In the last decades hundreds of powerful

tools have been developed with different scope and scale in dynamic water balance simulation. To frame the field TOPMODEL [Beven and Kirkby, 1979], HBV [Bergström, 1976], Superflex [Fenicia et al., 2011], mHM [Samaniego et al., 2010], THREW [Tian et al., 2006], SWAP [van Dam et al., 2008], WASA [Güntner et al., 2004], Catflow [Zehe et al., 2001], CATHY [Niu et al., 2014], MIPs [Davies et al., 2011] and many more are superb tools which also exhibit vast details beyond the discharge reference. However, their strength lies in aspects different from supporting and extending exploratory experiments.

1.4.1 *Process models for rapid subsurface flow*

Preferential flow arises from imperfect lateral mixing between the fast advective fraction of water and solutes traveling in soil structures and the slow diffusive fraction traveling in the soil matrix [Blöschl and Zehe, 2005, Neuweiler and Vogel, 2007]. The proposed approaches to deal with this imperfect mixing range from

a) the early concept of stochastic convection i.e. no mixing at all [Jury and Roth, 1990], over

b) the scale way idea to represent structural fingerprints in flow and transport across scales [Vogel and Roth, 2003],

c) dual porosity and permeability approaches relying on overlapping and exchanging continua [Gerke, 2006], to

d) spatially explicit representation of macropores as vertically and laterally connected flow paths [Vogel et al., 2006, Sander and Gerke, 2009, Klaus and Zehe, 2011].

In particular the last approach emphasizes the crucial importance of reliable field data/estimates characterising surface density and depth distribution of the macropores and their optional connection to lateral preferential flow paths for successful predictions.

1.4.2 *Models to extend experiments*

Virtual laboratories or modelling studies are a common and insightful tool in hydrological system analysis. In most studies, the models are taken as true reality without much examination of their structural adequacy [Gupta et al., 2012] for the exploration target. This makes it particularly difficult to unravel the different sources of information coded in these models [Gupta and Nearing, 2014]. From this perspective the debate about equifinality [Beven, 2006b] or the non-uniqueness of non-independent model parameters points out that it

is rather challenging to sort out the useful from the "wrong" models [Box, 1976].

For rapid subsurface flow in structured soils, the models also rely on crucial assumptions about spatial redistribution in the fast phase and interaction between both phases – if at all represented. Despite the fact that there has been considerable progress in the understanding of preferential flow, the topic remains one of the most challenging in particular with respect to scale and sub-scale representation of preferential flow and transport in hydrological models [Beven and Germann, 2013] as well as feedbacks between soil ecology and soil hydrology [van Schaik et al., 2013].

We rely on models which are capable to extend the few possible real world experiments. But the application of current models is harshly limited, given that diffusive and advective flow need to be considered and that structures are an emergent system property of the same dissipation processes.

1.5 *Research questions and thesis outline*

My master thesis aimed at the application of state of the art tools to an ungauged basin in NW India to analyse impacts of different land use strategies on the water balance of a meso-scale catchment [Jackisch et al., 2014]. Although complying with what is recommended as best practice in the PUB synthesis report [Chapter 13 in Blöschl et al., 2013], I soon faced limitations in modelling feedbacks in the eco-hydrological system. At the same time, common grounds of hydrological methodology, observation and conceptualisation were challenged severely by the question what may be a sustainable land use strategy for this area.

The overall aim of this thesis is to examine a more rigorous means of hydrological exploration and modelling to advance the knowledge about minimal adequate system representation. To do so I present findings from data analyses, experiments and the development of a novel Lagrangian model framework.

From the introduced perspectives I derive the following overarching research questions:

Rapid subsurface storm flow: What factors control advection in macropores? How can they be identified and measured? What temporal and spatial scales matter? What are suitable adaptive modelling strategies for advection and diffusion in structured soils?

Functional units and landscape delineation: Do functional units exist as hypothesised? What are appropriate means to test the hypothesis? How can functional units be identified and monitored?

Free energy conversion and dissipation in hydrology: How do preferred equilibrium states depend on system structure and states? What is the role of connected structures in re-establishing these preferred states? How can thermodynamics be used as closure to hydrological process calculations?

The link of functional similarity to similarity of catchment descriptors is not a straight forward procedure. In fact, they can even appear contradictory when their scales and scopes are not coherently aligned, as will be shown later. To identify and improve appropriate and scale-aware catchment descriptors one needs to develop current modelling tools, monitoring strategies and experiments beyond the current state of the art. This motivates this thesis to explore a more rigorous means of hydrological system analysis with emphasis on a unified perspective on the three aspects.

Chapter 2 (p.15) presents a first attempt to link functional similarity to similarity of catchment descriptors by an exploration of the Attert basin under study. The hydrological and soil property analysis is extended by a GIS study of the basin.

Experiments to address advective and diffusive water dynamics at the plot- and hillsope-scale are studied in chapter 3 (p.41).

In chapter 4 (p.67) I will come back to the gradient dissipation concepts in the development of a new, Lagrangian, stochastic-physical model framework for advective and diffusive soil water dynamics based on water itself as particles and a representative domain. Macropore-matrix interaction is represented by means of energy dissipation optimisation. In the final section 4.8 (p.94) the model is used to investigate controls of preferential flow in two different landscape settings.

A joint discussion of the subjects is given in chapter 5 (p.99), followed by an overall synopsis (p.119).

The appendix (p.123) holds additional results and insights contributing to the presented findings. This work is accompanied by several repositories with the respective analyses and software used and developed during the study[4]. It can be accessed through `https://github.com/cojacoo/phd_thesis`.

[4] All software is given under GNU General Public License (GPLv3) and Creative Commons Attribution-NonCommercial-ShareAlike License (CC BY-NC-SA 4.0) "as is" with explicitly no warranty or liability of any kind.

2

Preparatory Exploration

As foundation for the forthcoming analysis of this thesis I introduce the Attert experimental basin in this chapter. It is followed by water balance analysis of available data (section 2.2), preparatory exploration of eco-hydrological setting by means of *in situ* and laboratory measurements (section 2.3), and a first attempt to identify functional units based on GIS and remote sensing data (section 2.4). The chapter provides some fundamental understanding of the basin's dynamics and setting as prerequisite to formulate specific hypotheses lateron.

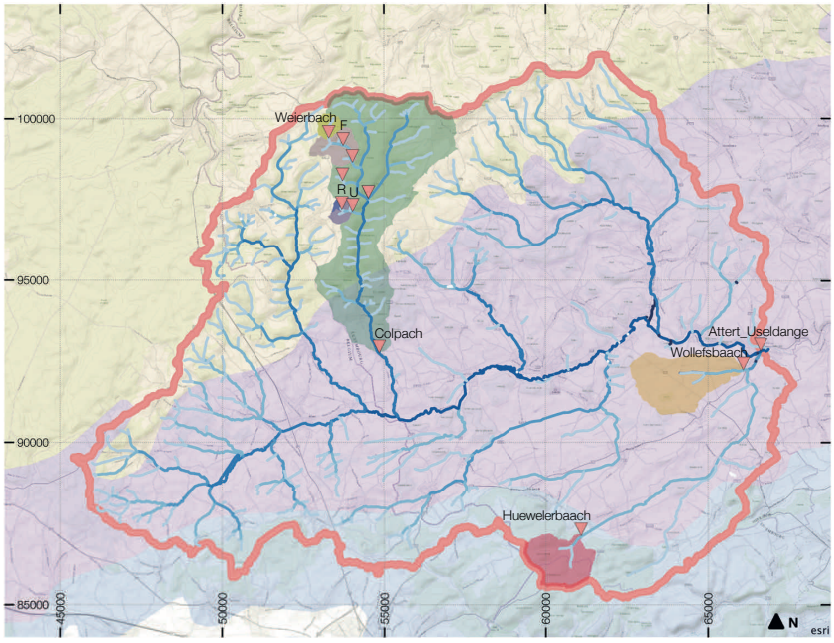

Figure 2.1: The Attert Basin. The three main geological settings are marked in yellow (Schists of Ardennes Massif), purple (Marls in the central basin) and blue (Sandstone of the Paris Basin). The nested experimental sub-basins are given as shaded colours with the gauge position (triangles). CRS Luxembourg 1930, EPSG:2169, map units in metre. Backgrounds: Esri ArcGis World Topo and EuroGeoSurveys 1:1.5M Bedrock Age. See map 7.1 (p.125) for more details.

2.1 Site description – the Attert experimental basin

The Attert experimental basin is located in the central western part of the Grand Duchy of Luxembourg stretching into Wallonia in Belgium. It is situated at the transition of the Ardennes Massif in the north, locally called *Oesling*, and the sedimentary Paris Basin, called *Gutland*, in the south. As such a remarkable hydrological spectrum is comprised in the 246.7 km^2 basin upstream the gauge Useldange (figure 2.1).

Since 2003 the former Centre de Recherche Publique – Gabriel Lippmann (CRP-GL), now Luxembourg Institute of Science and Technology (LIST), has studied and monitored the catchment intensively. Since 2012 the DFG Research Group "From Catchments as Organised Systems to Models based on Functional Units" (CAOS) extends the monitoring with additional 48 eco-hydro-meteorological measurement sites, massive field campaigns and many specific experiments.

HYDRO-CLIMATOLOGICALLY the study area is located in a pluvial oceanic regime with mean annual rainfall of 850 mm (1971–2000). Mean monthly temperatures lie between a maximum of about 18 °C in July and a minimum of 0 °C in January [Pfister and Hoffmann, 2002]. Low flows are observed from July to September due to high summer evapotranspiration, while high flows occur mainly from December to February. A more detailed analysis of the hydrological regime is given in the following section 2.2.

GEOLOGICALLY the basin can be subdivided into the three major groups sandstone, marls and schists as given in figure 2.1. The geological setting also determines pedogenesis and in this case ecological setting. It is this variability in direct proximity which makes the Attert an exceptional exploratory. The three general classes are described next:

2.1.1 Schist on the Ardennes Massif

The northern part of the basin is situated in Schist of the Ardennes Massif which originates in the Variscan orogeny as NE-SW-trending fold system transforming the Devonian epicontinental sea deposits into schists and slates. Characteristically, the rivers drain in narrow valleys with relatively steep forested (spruce, fir and beech) slopes and shallow young soils. Headwaters show more gentle topography and mostly blueberry-beech forests. This stands in contrast to agriculturally used plateaus of the massif.

Juilleret et al. [2011] elaborate that pedogenesis is dominated by slope deposit cover beds formed under Pleistocene periglacial climatic conditions. They are composed of eolian loess deposits and weathered schist debris that were relocated by solifluction causing a often horizontally orientation. At the hillslopes, the deposit layer is overlain by shallow top soil of less than 1 m depth. The Devonian schist bedrock below is strongly inclined with almost vertical foliation and considered relatively impermeable [van den Bos et al., 2006].

2.1.2 *Marls in the central basin*

The central part of the basin consists of Late Triassic Keuper marls. This is interspersed with older shell limestone and variegated sandstone formations. Soils are generally very silty, loamy and clayey with low matrix permeability. The undulating topography with very low relief energy tends towards plateau formation. Most of the marls have a long history of agricultural use as crop- and grasslands. Tile drains and subsurface channels are common. Discharge generally reacts quickly to events with surface runoff and rapid subsurface stormflow through cracks and earthworm burrows.

2.1.3 *Sandstone of the Paris Basin*

The southern ridge of the basin is formed by arenaceous sediments of the late Eifel Depression in early Jurassic as Luxembourg Sandstone. Soils on permeable sandstone are homogeneously weathered sandy Cambisols. Beech forests prevail in the area. The well-drained conditions with deep percolation imprint in a sparse river network with mostly base flow controlled dynamics. The aquifer feeds many springs, eventually emerging at the contact zone between marl and sandstone layers.

2.2 *Water balance and hydrological regime*

The Attert basin in this study has a network of nested catchments. Figure 2.1 outlines them. I present some of the observed characteristics of the sub-basins with regard to rainfall-runoff dynamics and storage behaviour[1] as foundation for the upcoming chapters.

2.2.1 *Runoff dynamics and water balance*

The annual runoff coefficient (RC) at the basin outlet (blue line) ranges at 0.42 ± 0.073. The Huewelerbach basin (yellow line) has a much lower RC of 0.28 ± 0.04. Wollefsbach basin (purple line) and Weierbach basin (green line) show higher inter-annual variability with RC of 0.29 ± 0.08 and 0.44 ± 0.07 respectively.

In figures 2.2 & 2.3 the inter-annual and seasonal dynamics of catchment response to precipitation are presented as double-mass curves of cumulated precipitation against cumulated discharge.

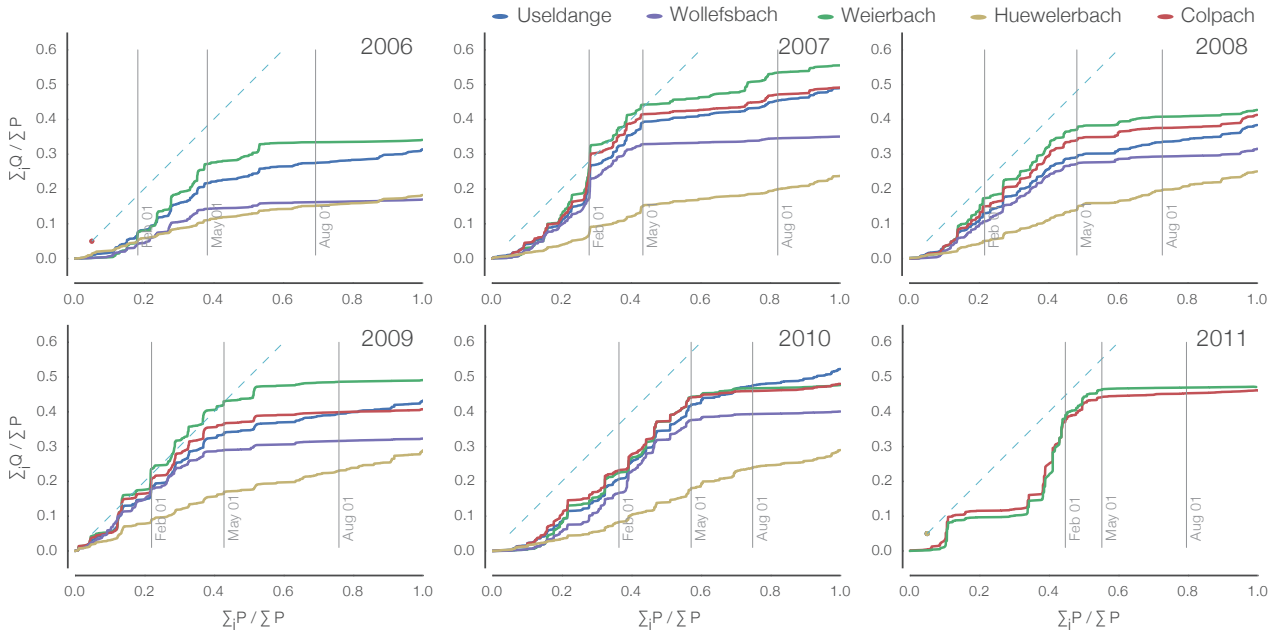

Figure 2.2: Rainfall-runoff dynamics of some of the Attert sub-basins. Double-mass curves for each hydrological year (01-Nov until 31-Oct) as cumulated precipitation against cumulated discharge, both normalised by total precipitation. The data basis is hourly aggregated precipitation at the station Useldange and unit discharge. Since the Ardennes receive more precipitation due to orographic uplift precipitation is scaled with reference to the short data series at the station Roodt by a factor of 1.38.

Both are normalised by total precipitation. Especially for the Colpach and Weierbach basins the first 40% fall very close to the one-to-one line (RC≈1.0). Here, step-like graphs with slopes>1 suggest strong event-specific mobilisation of water and preferential flow. It is followed by a period of almost no event-reaction (RC≈0.04) and very low base-flow. Notice that the Weierbach basin is nested in the Col-

[1] The data for this analysis have been provided by the Luxembourg Institute of Science and Technology, Department Environmental Research and Innovation and the CAOS Research Group. All the efforts which went in the generation of this data set is gratefully acknowledged. Special thanks go to Jeff Iffly and Laurent Pfister (Luxembourg Institute of Science and Technology, ERIN), Sibylle Hassler and Theresa Blume (Helmholtz Centre Potsdam - GFZ German Research Centre for Geosciences), and Britta Kattenstroth and Markus Weiler (University of Freiburg, Hydrology).

pach basin covering only 2%. Yet, both exhibit very similar process characteristics.

A similar picture is exhibited in the Wollefsbach basin with a strong but more mediated runoff reaction at the beginning (RC≈0.8) which speaks for moderated preferential flow. Afterwards only few events can cause some minor reactions. In contrast, the Huewelerbach basin presents a rather constantly low RC. It is mostly base-flow controlled with very few events causing a direct stream reaction.

The Useldange gauge is dominated by the strong reaction to rainfall in the young soils of the Ardennes and macroporous soils in the marls. With the beginning of summer when the contribution of the former areas becomes very low it is fed by the more continuous base-flow from the southern sandstone areas.

Basin	Area $[10^{-5}\,m^2]$
Useldange	24672
Colpach	1903
Weierbach	45
Huewelerbach	270
Wollefsbach	450

Table 2.1: Subbasin sizes in the Attert catchment.

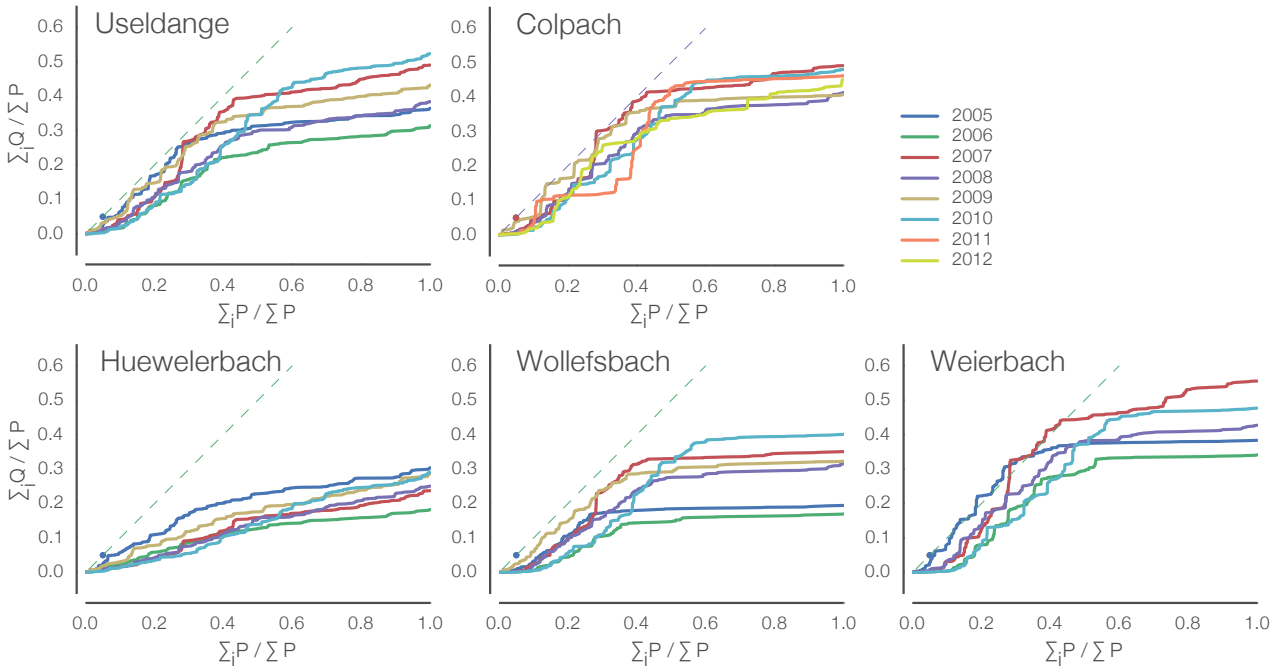

Figure 2.3: Rainfall-runoff dynamics of some of the Attert sub-basins. Double-mass curves as in figure 2.2 but arranged for inter-annual comparison. Since the x-axis is given in relative received precipitation of each year, the timing varies for each line.

It is noteworthy that the ranks of these curves differ between the sub-basins and that similar precipitation can result in very different behaviour. Table 2.2 gives the annual precipitation (Useldange) and discharge sums for the regarded gauges. Year 2006 has the lowest RC, 2010 scores relatively high in all subbasins. However the recorded precipitation is very similar slightly below the longterm average. The dry year 2005 scores average in Useldange and the schist basins but is low in Wollefsbach and highest in Huewelerbach. The wet year 2008 resides around the mean ranks for all basins.

Table 2.2: Annual sum of precipitation (P) and discharge (Q) [mm] for hydrological years in Attert basin.

Year	2005	2006	2007	2008	2009	2010	2011
P Useldange	667	780	834	1032	686	718	531
Q Useldange	243	247	410	397	297	379	-
Q Huewelerbach	203	143	199	259	199	210	-
Q Wollefsbach	130	133	293	326	222	292	-
Q Colpach	233	-	568	590	387	479	339
Q Weierbach	354	373	642	611	465	476	347

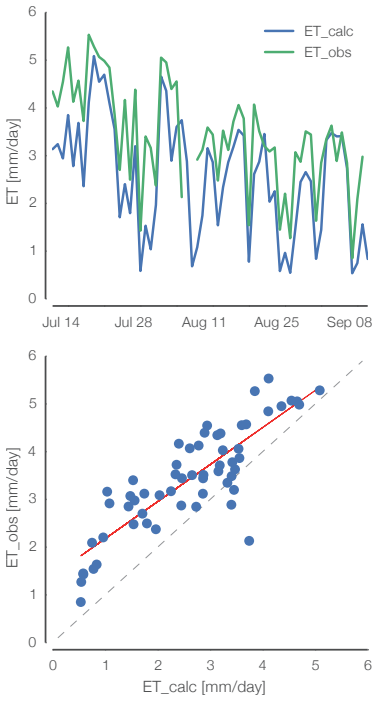

Figure 2.4: Daily evapotranspiration - measured with a Scintillometer in Ell and calculated after Szilagyi and Jozsa [2008] with meteorological data at Useldange. r 0.85, SE 0.064, KGE 0.7, ρ 0.8.

[2] These data have been provided by Elisabeth Thiem, BOKU Vienna, which is gratefully acknowledged.

[3] The meteorological observations of the measurement campaign lack global radiation, which is a crucial input to the model. Hence complete and consistent data of the closest station are chosen as reference.

Evapotranspiration (ET) is not monitored at the stations in the Attert basin. In order to address storage dynamics of the different sub-basins I refer to an estimate from meteorological data in the water balance calculations.

In a comparison of different methods to calculate ET McMahon et al. [2013] found the modified Advection-Aridity model after Szilagyi and Jozsa [2008] as possible compromise for daily actual ET in water balance applications in temperate climate. It is an extension of the original Advection–Aridity model [Brutsaert and Stricker, 1979] which was modified by Morton [1983] utilising the Bowen ratio and air temperature to iteratively optimise surface temperature. The model is using daily observation of air temperature (min/max), relative air humidity (min/max), average wind speed, and radiation gain. Vegetation is included as Penman-Monteith land use factor α for albedo and an estimate for the evaporation surface level z_0. It is set to $\alpha = 0.23$ [green grass albedo Allen et al., 1998] and z_0 =0.02 m.

Data from a measurement campaign of actual ET (ET_{act}) using a dual disk large aperture scintillometer (Scintec AG, Rottenburg) is used to validate the model in the basin. The campaign was realised for two months in summer 2013 at a field near Ell (marls, central catchment)[2]. In figure 2.4 it compares with modelled daily ET_{act} based on data at the meteorological station Useldange[3].

Although the general behaviour is reproduced, the negative bias of the simulation could tend to a slight underestimation by the model. A discussion of the assumptions and restrictions of this model is postponed to the end of this section. With the moderate fit (coefficient of correlation of 0.85, Kling-Gupta Efficiency of 0.7 and Spearman rank correlation coefficient of 0.8) the model is accepted for the purpose to serve as reference.

Water balance of the three tributaries and the total basin is compared in figure 2.5. Following the simple water balance equation $\Delta S = P - Q - ET$ and the assumption that the storage is fully renewed each hydrological year, the difference between ET_{act} and $P - Q$ can be used to identify periods of storage accumulation, deple-

tion and deficit. Note that ET_{act} is used as theoretical reference here, since it is a model result and not a measured entity. The good correlation at Useldange and stronger deviations in the tributary basins could also be explained by local differences in rainfall because precipitation input and especially ET reference are based on data at the Useldange meteorological station.

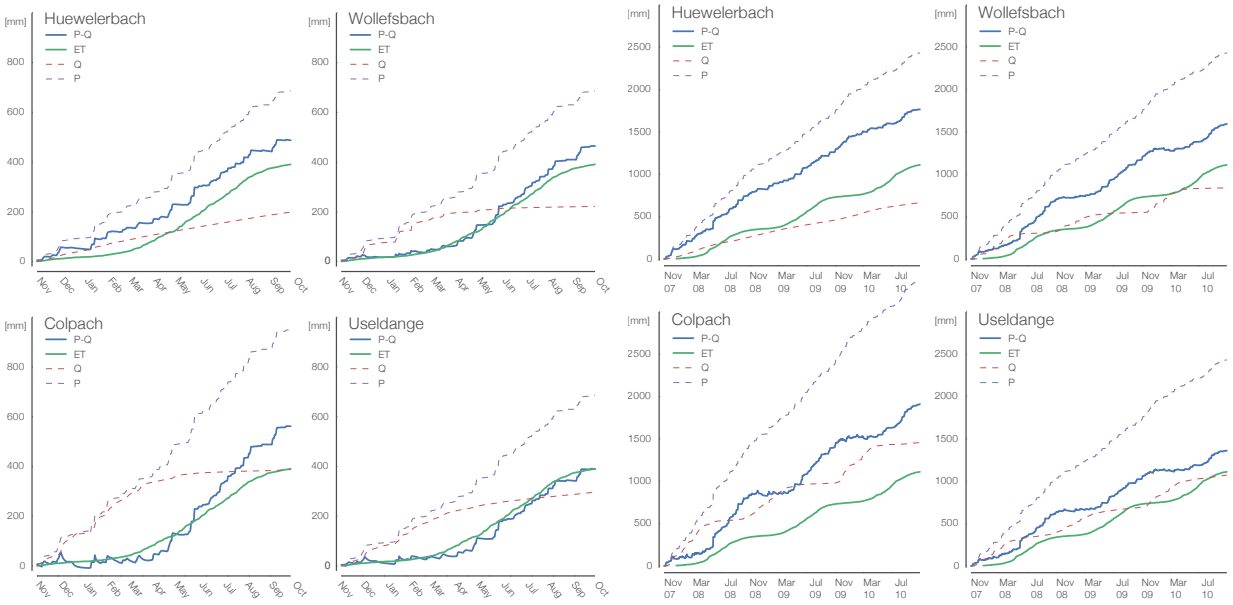

Figure 2.5: Water balance calculation for the Attert basin (Useldange) and three tributaries for Nov 2008 to Oct 2009 (left) and a longer period from Nov 2007 to Oct 2011 (right). ET is estimated after Szilagyi and Jozsa [2008] based on daily aggregated meteorological data at station Useldange.

Overall, the water balance closes well with the two independent variables. The sandstone sub-basin Huewelerbach shows almost no seasonality, while the schist sub-basin Colpach has the two distinct seasons. This seasonality mostly depends on the vegetation period. A closer look at the dynamics in the Colpach basin (figure 2.6) hints to the aforementioned break in the behaviour in April with the onset of vegetation.

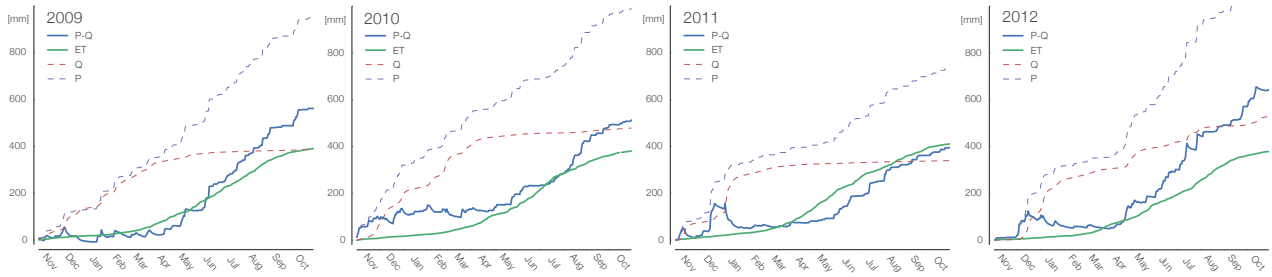

Figure 2.6: Water balance calculation for the Colpach basin. ET is estimated after Szilagyi and Jozsa [2008] based on daily aggregated meteorological data at station Useldange with scaled precipitation.

Variations in precipitation appear less influential and more related to occasional positive shifts in the water balance. When looking at a

longer period the three tributaries reveal this general positive trend in the storage (area between ET (green) and P-Q (blue)). While the Huewelerbach sub-basin accumulates this storage continuously, specific wet periods build up the storage surplus in the other sub-basins.

It could also be due to an underestimation of ET in the vegetation period by the model, which is likely for the Colpach sub-basin. The inter-annual comparison for four years (figure 2.6) supports both arguments: Steep inclines in the accumulated precipitation (blue dashes) mark the areas of departure of the modelled and balanced ET estimates. And as the model results are very static over the years it is neither capturing the dry year 2011 nor the wet 2012 well (531 mm and 846 mm in Useldange). Notice that further examination is needed to test whether or not spatial non-uniformity of precipitation can explain the deviances.

2.2.2 *Event runoff dynamics in the schist basins*

In order to scale down towards processes at the hillslope- and plot-scale during single events I present two exemplary events in the schist. Figure 2.7 shows the reaction to two summer storm events in 2013 and 2014. Both exhibit a strong separation into double peaks of an immediate quick reaction and a large and strongly retarded event reaction the following days. Although not all events follow this pattern, it is regarded as stereotype for the basin particularly visible at the Holtz tributary gauges R and U with 9 and 46 ha respectively.

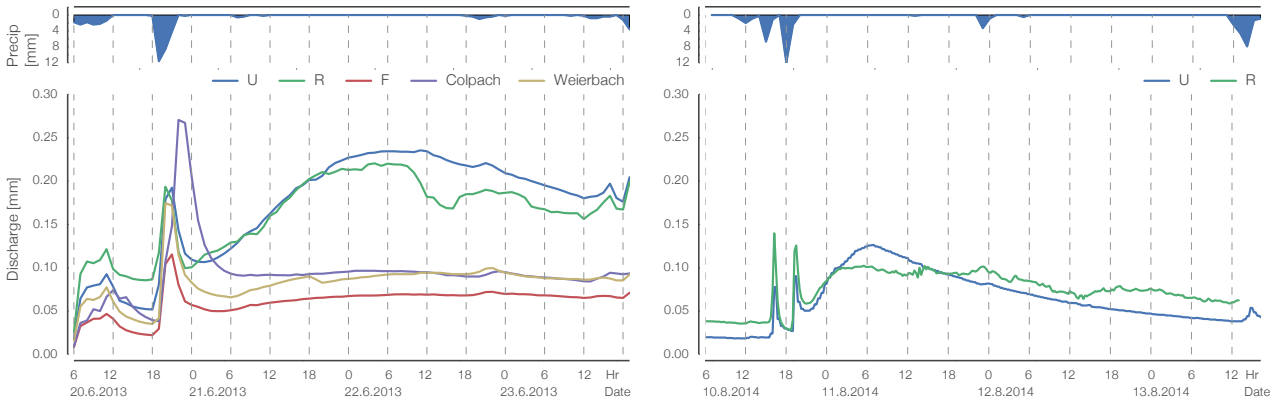

Figure 2.7: Discharge reaction in the schist basins to two storm events on June 20, 2013 (left) and August 10, 2014 (right). The first event had 24.8 mm after a more gentle 12 mm priming. The second example is a succession of three events with 3.9 mm,7.9 mm and 14.4 mm.

It is noteworthy that also the soil moisture sensors react as quickly - especially in lower depth. Figure 2.8 combines the observations and their explanatory content for event water. In the event water balance the first peak reveals no significance. After 48 h about 30%

of the precipitation has left the basin. The soil moisture sensors in the top 0.6 m (assumed 0.2 m increment) resemble 30% of the event water at the end of the storm. However soil moisture declines again immediately after the event and returns to pre-event state after ±24 h on the hillslope. Only the topmost sensor and the plateau sensors register slightly increased pore-bound water storage. The temporary changes of soil moisture can thus be attributed to preferential flow.

70% of the total event water balance is not observed by topsoil moisture change and discharge. It is likely advectively transported and stored in structures and local fill and spill sinks or contribute to a deeper groundwater body. Since the annual and long-term water balance is only slightly positive, much speaks for a combination of both.

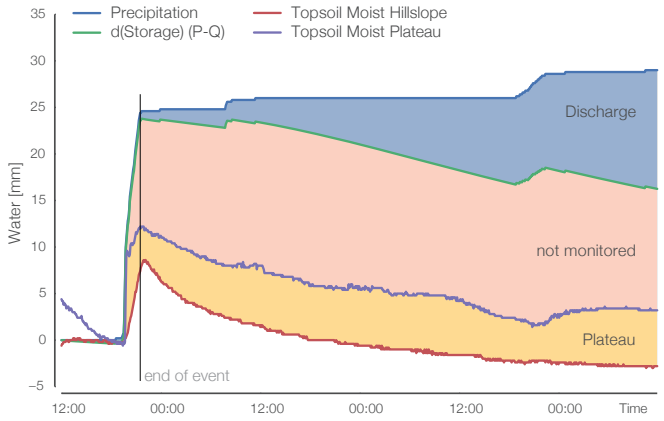

Figure 2.8: Event water balance of a storm event on June 20, 2013 in the Holtz tributary (gauge U). The first peak (as shown in figure 2.7) does not account for a significant share of the water balance. The soil moisture sensors (in −0.1 m, −0.3 m and −0.5 m) react immediately on the forested slope (Cluster V). On the plateau grass land (Cluster I) the also quick reaction accounts for more recovered mass. Especially on the hillslope soil moisture also quickly declines again and returns to pre-event state after 1 day. As such, a major share of the event water is not monitored in the topsoil.

2.2.3 *Discussion and conclusion of the water balance*

Although the general water balance is relatively well explained by the data and conceptual storage dynamics, single events exhibit more questions about the actual processes and domains [compare to Fenicia et al., 2007, Wrede et al., 2014]. Especially because preferential flow dominates the hydrological behaviour in the marl and schist sub-basins, many of such conceptual ideas cannot be scaled down in space and time to single events and hillslopes. I have shown that soil moisture and gauge monitoring leaves room for improvement in addressing preferential flow paths, connectivity dynamics, ephemeral subsurface storages and ground water bodies, deep percolation and interaction at the bedrock interface.

This rough assessment has many open threads. Besides the issue of complementary and consistent data sets (see discussion in section 5.1, p.99) some assumptions were introduced to fill unobserved gaps:

ET makes up for 30 % to 60 % of the water balance dominating it

during vegetation period. Except for measurements of sap-flow (not used in this study) it is not monitored in the experimental basin. The reference model after Szilagyi and Jozsa [2008] and episodical measurement campaigns are giving some reference. However, both time series represent relatively well-defined conditions above agricultural and grass land. Forests on young soils will likely impose more uncertainty. Local micro-climatical effects like the redistribution of moist air in the step terrain are neglected, too.

Rainfall distribution in a mesoscale catchment may explain much of the local variances. A single station record is imposing significant uncertainty to the real value in the basin ($2.14 \times 10^{-2}\,m^2$ tipping bucket against $2.47 \times 10^{8}\,m^2$ catchment size). The divergence score [Weijs and van de Giesen, 2011] and general rain field patterns have not been assessed for this study. Hence the conclusions from figures 2.2 to 2.8 need some precaution regarding the absolute balance values.

Double-mass curves and RC are thus not to be seen as fixed values. The southern sandstone sub-basins could receive generally less precipitation due to their leeward location. With this the respective RC would increase quickly. Given the climatical oceanic regime with relatively evenly distributed rainfall conditions (except for some summer storms), the comparison of the seasonal differences is still valid as the shape of the curves does not depend on the amplitude.

To CONCLUDE this section, the hydrological regimes of the Attert sub-basins are, except for the sandstone areas, strongly shaped by rapid subsurface flow and threshold behaviour. During vegetation period ET is a strong control. This imposes challenges to adequate monitoring strategies – especially at lower spatial and temporal scales, where the processes take place.

In line with findings of Fenicia et al. [2014] marls and schists are very similar with respect to their rainfall-runoff dynamics. This functional similarity will be confronted with findings from functional soil analyses and a GIS analysis in the two following sections.

2.3 *Functional soil exploration – lab analyses, in-situ experiments and data recalculation*

As foundation for modelling and process understanding *in-situ* and laboratory measurements of site properties are fundamental. But since I question what has to be measured and observed to characterise a mesoscale catchment this task is vaguely defined. This section presents the collection of the exploration efforts in the CAOS project[4]. The value of each sample and an interpretation of the sampling strategy will be discussed in section 5.1 (p.99).

[4] While I focused on the experimental sites, Benjamin Müller (LMU) and Loes van Schaik (TUBS) contributed many of the spatially more distributed samples. Moreover Christophe Hissler and Jérôme Juilleret (LIST), and countless student assistants massively contributed to this data. Especially the great support by our laboratory assistant Raziye Fiden (KIT) is acknowledged.

2.3.1 *Soil core samples*

Pedo-physical properties of the soil matrix such as bulk density, texture, pH-value, saturated hydraulic conductivity and soil water retention characteristics can be best defined by analyses based on undisturbed core samples. Fig. 2.9 presents the locations, numbers and analyses of our data set.

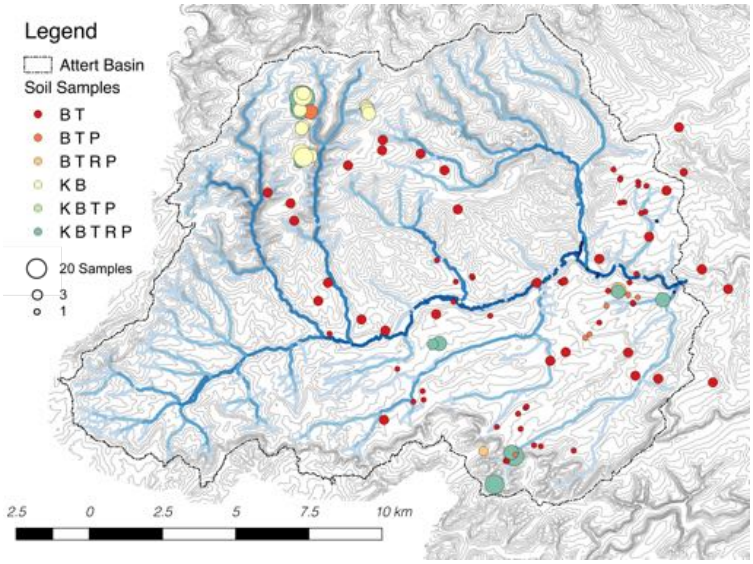

Figure 2.9: Location of soil core samples in the Attert basin. Colours indicate the respective analysis set, size give the number of samples at each location. B: Bulk Density (382 samples), T: Texture (wet sieving and sedimentation) (265 samples), P: pH (128 samples), R: Retention Curve (HYPROP apparatus) (120 samples), K: Ksat (Ksat apparatus) (223 samples).

Soil texture analysis was performed using wet sieving of ground soil without rocky fraction >2 mm into the classes of coarse sand >630 µm, medium sand >200 µm and fine sand >63 µm. In addition the sedimentation method after Köhn (ISO 11277) was employed to analyse the smaller fractions of coarse silt >20 µm, medium silt >6.3 µm, fine silt >2 µm and clay <2 µm. In compliance with the ISO organic compounds were destroyed through application of Hydrogene-peroxid. Salt-removal was performed through repetitive washing and centrifugation of the samples with de-ionised water.

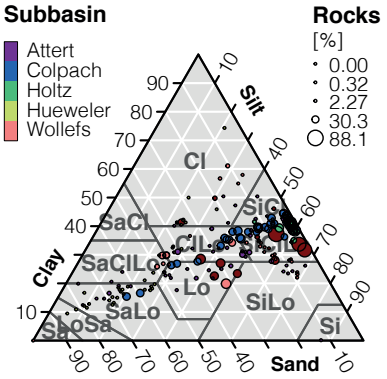

Figure 2.10: Texture and content of gravel (size and taint of dot) of soil core samples in the Attert basin.

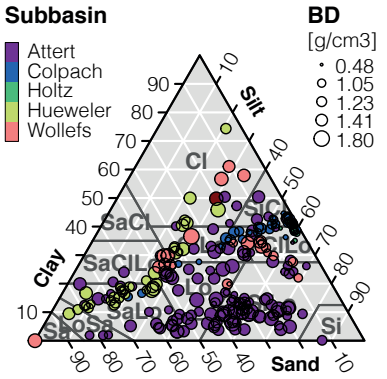

Figure 2.11: Texture and bulk density (size and taint of dot) of soil core samples in the Attert basin.

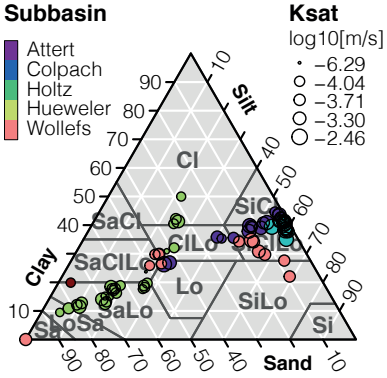

Figure 2.12: Texture and saturated hydraulic conductivity (size and taint of dot) of soil core samples in the Attert basin.

In addition, I performed a number of tests with new methods for texture analysis like laser diffraction and image processing. This technical analysis is given in Appendix 7.3.1.

SATURATED HYDRAULIC CONDUCTIVITY was measured with undisturbed 250 ml ring samples with the Ksat apparatus (UMS GmbH, Munich). The method is following the Darcy approach applying a flux trough a saturated porous medium. The apparatus records the falling head of the water supply though a highly sensitive pressure transducer which is used to calculate the flux.

SOIL WATER RETENTION CURVE of the drying branch is measured with the same samples in the HYPROP apparatus (UMS GmbH, Munich) and subsequently in the WP4C potentiameter (Decagon Devices Inc., Hopkins Court). The HYPROP records total mass and matric head in two depths in the sample over some days when it is exposed to free evaporation. Referenced to the dry weight the relation of soil water content and matric head can be derived up to a head of about −800 hPa bound by the air entry point of the tensiometers.

A small fraction of about 10 g is then transferred to the WP4C where soil water potential is measured based on a chilled mirror approach. Subsequent weighing, further drying and measuring contributes further references to the water retention curve.

RESULTS in figures 2.10 to 2.12 highlight that the distinct geologic settings are well captured in the soil texture composition with sandy samples in Huewelerbach, silty clayey samples with great amount of gravels in the Colpach and silty samples in the Wollefsbach. Generally, the Attert basin comprises a remarkably large set of soil classes. Moreover, measured saturated conductivity and the fraction of coarse or rocky material shows considerable heterogeneity - also within one geological region. However, some of the spread can also be attributed to inconsistencies between the laboratories as discussed in appendix 7.3.1.

Regarding soil water retention the results are also dominated by the general geological situation. Figure 2.13 explicitly highlights the great heterogeneity within the Attert experimental basin. As expected and locally observed, the Huewelerbach sub-basin samples show sandy and marly characteristics. In the Wollefsbach sub-basin a large spread of retention properties is resembled. The mean curve shows silty characteristics. Samples from the Colpach sub-basin correspond to larger pore spaces near saturation. For greater tensions they resemble the silty curves.

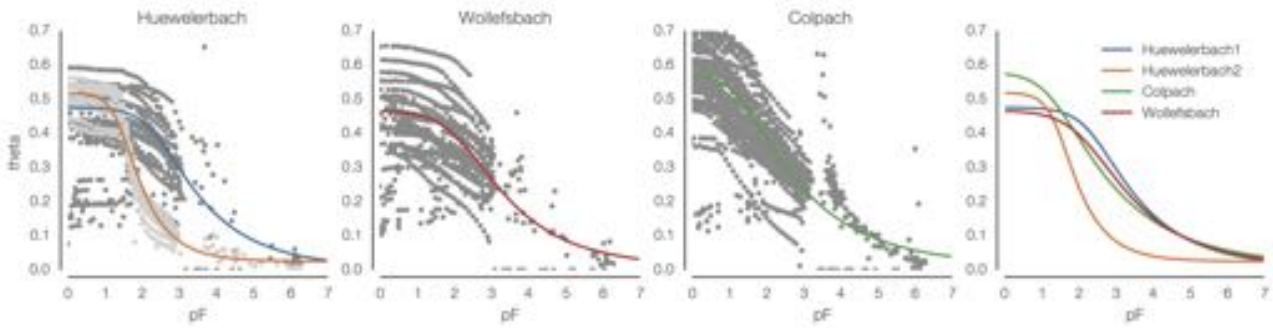

Figure 2.13: Soil water retention curves of soil core samples in the Attert basin. All measured data (HYPROP and WP4C) on the drying branch. Master retention curve fitted to the mean of all individually fitted van Genuchten curves. The parameters are given in table 2.3.

With regard to functional similarity the very close match of the mean retention curves is particularly interesting. The marls in the Huewelerbach and Wollefsbach tributaries are very closely related. For the finer pore spectrum (or larger tensions) this is also true for the schists and the marls. The two classes also exhibit similar hydrological properties (section 2.2) and also their soil water storage dynamics. Because the soilwater dynamics above field capacity is additionally controlled by macropores (although different in structure and origin), the similarity of both regions is also supported by the soil analysis.

2.3.2 *Hydraulic properties at schist focus site*

At the transect of cluster S_D to cluster S_I in the northern Colpach sub-basin (figure 2.14) we analysed 74 soil cores, measured infiltration capacity at 40 spots (Hood Infiltrometer, UGT GmbH, Müncheberg) and saturated hydraulic conductivity at 32 borehole logs (Constant Head Permeameter, Ksat Inc., Raleigh).

The Hood Infiltrometer was applied after removing the loose litter layer if existing. We aimed at an application at three to four tensions. In cases of very high infiltration capacity (mostly due to direct connection to structures with large capacity) only measurement at zero tension was possible.

		Huewelerbach (marly)	Huewelerbach (sandy)	Colpach	Wollefsbach
θ_{sat}	[$m^3\,m^{-3}$]	0.476	0.518	0.579	0.467
θ_{res}	[$m^3\,m^{-3}$]	0.007	0.025	0.013	0.010
α	[m^{-1}]	0.44	3.77	4.94	0.66
n	-	1.12	1.73	1.05	0.87
k_{sat}	[$m\,s^{-1}$]	4.3e-5	1.5e-4	7.1e-4	2.9e-4
ρ_{bulk}	[$kg\,m^{-3}$]	1.46	1.30	1.03	1.38

Table 2.3: Van Genuchten parameters of mean soil types of the different tributaries of the Attert basin. Values derived from least square fit to mean of all curve realisations in the respective sub-basin.

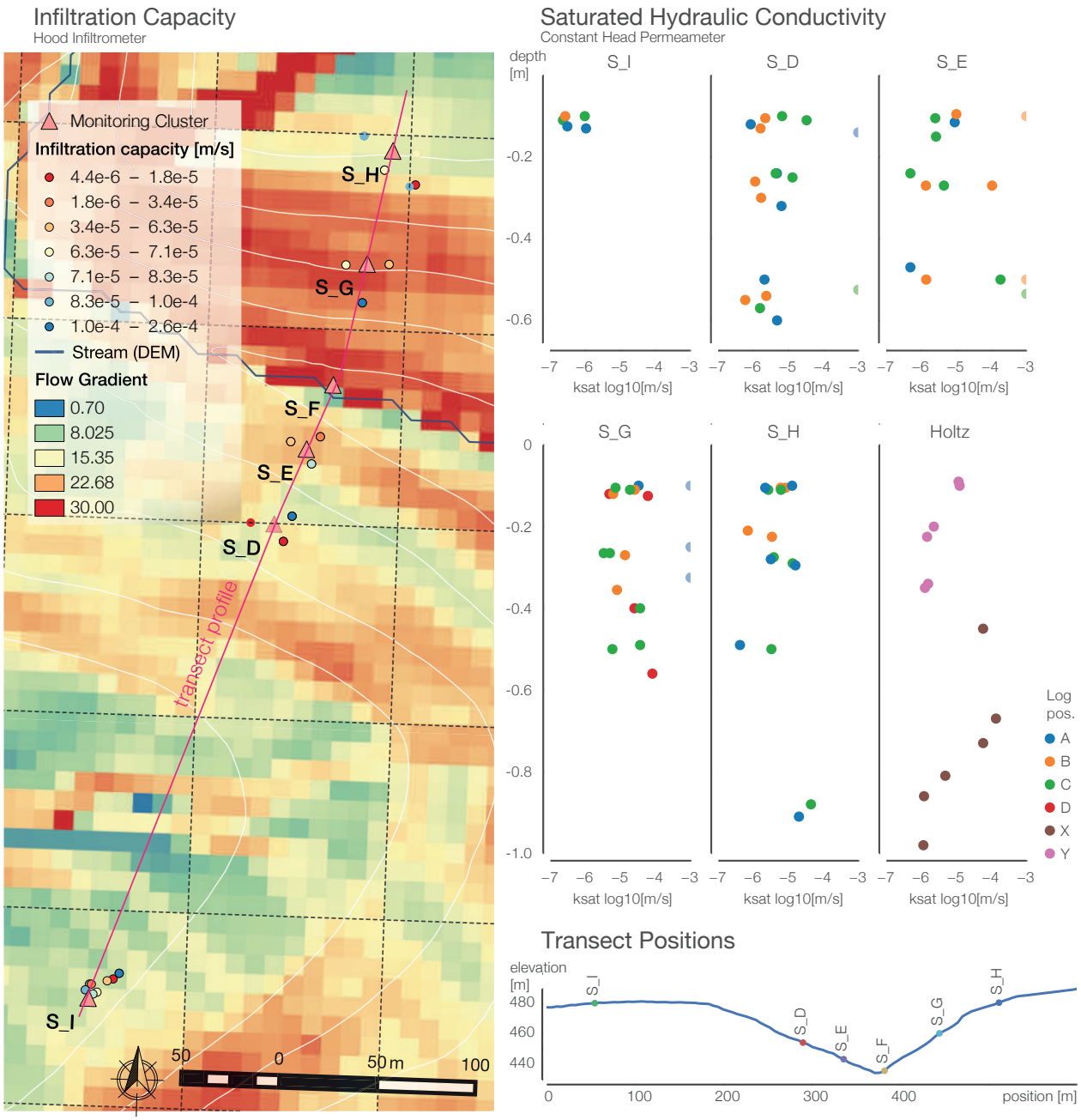

Figure 2.14: Left: Infiltration capacity (values in colour) measured with hood infiltrometer in the Colpach sub-basin. Basemap with flow gradient (section 2.4.3), topography contour lines and positions of eco-hydro-meteorological monitoring clusters. Coefficient of correlation to this and other landscape attributes is given in table 2.4. Right bottom: Elevation profile of cluster transect as characteristic landscape feature in the sub-basin. Right: Saturated hydraulic conductivity measured with a constant head permeameter in the Colpach sub-basin. Individual log position at cluster colour coded (2 measurement holes with dist=1 m). Values exceeding the device capacity set to 10^{-3} m s^{-1}.

The Constant Head Permeameter (CHP) was used in a successively drilled borehole. The high gravel and rock content in the soil prevented equally spaced measurement depths. However, we aimed to establish at least three measurements per borehole log ($dz \approx 0.2\,\mathrm{m}$). At most locations manual drilling could not surpass the first deposit band at about $-0.7\,\mathrm{m}$.

Figure 2.14 presents the large spread of results without much spatial autocorrelation. Correlation to landscape attributes is given in table 2.4 and supports this. At many borehole logs I found layers with almost no hydraulic conductivity followed by highly conductive structures exceeding the devices capacity. It is noteworthy that the theoretical assumption of a plume-like spread of the infiltrating water is most likely violated by all experiments in this area. Thus the *in situ* measurements are valid to describe the behaviour of free water in the found structured soils but may not adequately represent k_{sat} for saturated flux through the matrix or as reference for an estimated propagation of a theoretical wetting front.

Attribute	$R_{pearson}$
L7 NDVI	0.253
L7 NDWI	-0.244
STI	-0.082
TWI	-0.007
dist. stream	-0.065
flow gradient	0.098
relative TWI	-0.071

Table 2.4: Coefficient of correlation (Pearson) of measured infiltration capacity (log transformed) to landscape attributes in section 2.4 at the same locations. L7: Landsat 7 indexes, STI: soil topographic index, TWI: topographic wetness index, relative TWI is calculated based on elevation above stream.

A comparison of *in situ* and laboratory derived saturated hydraulic conductivity values reveals that the latter likely overestimates the situation (figure 2.15) due to few dominating macropores in the 250 ml samples. At the same time the former could also underestimate the situation due to local siltation and methodological constraints induced by the apparatus or erroneous assumptions about the referred infiltration surface and strong local soil anisotropy.

2.3.3 *Intermediate discussion and conclusion of the soil exploration*

After having analysed so many samples and after lots of *in situ* measurements I am still reluctant to infer much new information. It is clearly shown, that even hundreds of single measurements can only be attributed to heterogeneity at this scope. One also might come up with some cluster or principal component analysis of the data – and recover the major geological formations. Especially for the purpose of using the soil data as input for hydrological models this data may render uninformative.

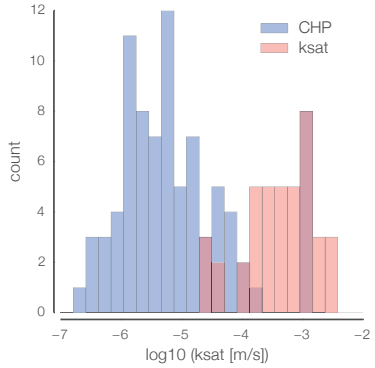

Figure 2.15: Histograms of saturated hydraulic conductivity of schist soils. Comparison of *in situ* measurement with constant head permeameter (blue, CHP) and lab measurement in 250 ml core samples with ksat apparatus (red, ksat). Notice that the CHP has a upper measurement limit at about $10^{-4}\,\mathrm{m\,s^{-1}}$.

In structured soils *heterogeneity* is a core property. It manifests itself in large spreads in soil characteristics. However it is by no means a simple random occasion with some central *true* mean value. For saturated hydraulic conductivity samples at structures will have much higher values than less connected locations. In the silty soil matrix values around $10^{-6}\,\mathrm{m\,s^{-1}}$ are already high. Still, the hillslopes will react much faster as soon the structures become connective as has been shown in many studies. This likely ranges at the conductivity of these structures around $10^{-3}\,\mathrm{m\,s^{-1}}$ which was highlighted earlier

considering the quick event runoff in section 2.2. Despite all scatter at the local scale, the mean retention curves for the three sub-basins in sandstones, marls and schists fall very much in line with the hydrological similarity assessment earlier.

Hence instead of discussing pros, cons and uncertainties of the respective methods this section closes by pointing out the relevance and necessity of specific scale-aware experiments and spatially distributed geophysical imaging techniques to functional soil exploration. Single measurements need to be put into spatial and process context to be informative. This will be addressed in the following chapter.

2.4 GIS analysis – preliminary functional unit identification

In the Attert sub-basins also previous studies have shown a distinct conditioning of the hydrological regime by the geological setting [van den Bos et al., 2006, Hellebrand et al., 2011, Wrede et al., 2014]. I will take a look into the setting beyond these general classes as geographic information system (GIS) case-study towards functional unit identification.

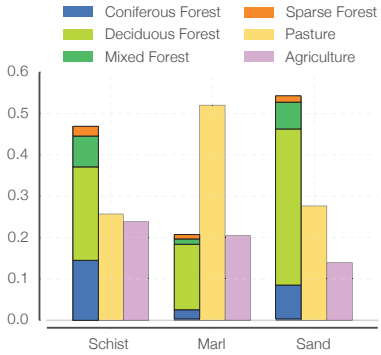

Figure 2.16: Normalised land cover shares in the three main geological settings based on land cover data for Luxembourg and Belgium and respective geological maps.

2.4.1 GIS data preparation

The analysis in this section is based on the following GIS data:

- DEM (digital elevation model), Modèle Numérique de Terrain de Luxembourg, 5m LIDAR. Relief de la Wallonie - Modèle Numérique de Surface, 10m LIDAR.
- Geological Map of Luxembourg, Scale 1:25 000, 1949. Service géologique du Luxembourg. Grand-Duché de Luxembourg.
- Land Cover, Occupation Biophysique du Sol, Scale 1:15 000, 1999. Based on color IR areal images. Grand-Duché de Luxembourg. And Carte d'Occupation du Sol de Wallonie, Scale 1:10 000, 2011, Service Public de Wallonie, Direction Générale opérationnelle Agriculture, Ressources Naturelles et Environnement
- Soils, Sols des plateaux et des pentes, Scale 1:100 000, 1969. Ministère de l'agriculture, de la viticulture et du Développement rural-Administration des services techniques de l'agriculture-Service de pédologie, Grand-Duché de Luxembourg. And Carte Numérique des Sols de Wallonie, 2007. Service Public de Wallonie, Direction Générale opérationnelle Agriculture, Ressources Naturelles et Environnement
- MODIS near-IR reflection (2005-2011, 14 day timestep, 250 m resolution, MOD13Q1) (accessed through USGS Earth Explorer).
- Landsat 7 – 32 day composite of the Normalised Difference Vegetation Index (NDVI, using red (0.66 µm) and near-IR (0.83 µm) reflection bands, 30m resolution) (accessed through google earth engine).
- Landsat 7 – 8 day composite of the Normalised Difference Water Index (NDWI, using near-IR (0.83 µm) and mid-IR (1.65 µm) reflection bands, 30m resolution) (accessed through google earth engine).

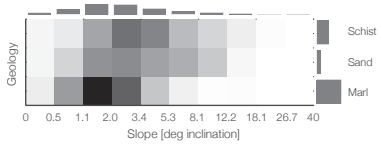

Figure 2.17: Distribution of slopes in different geological settings based on DEM analysis. Gird of shares normalised in each geology class.

The data basis and quality of both DEMs differed and both DEMs were clipped to the national borders. In oder to create a common basis, the resolution of the Luxembourgian DEM was downsampled to 10m. For the few overlapping pixels a moving window smoothing filter was applied. For further analysis the resulting DEM was further processed with a D8 filling algorithm (r.fill.dir) removing all apparent local sinks.

From the resulting DEM slope was calculated based on a least squares fitted plane approach [Horn, 1981] (r.slope.aspect). Flow direction has been derived based on single flow direction D8 [O'Callaghan and Mark, 1984] and triangular multiple flow direction algorithm MD∞ [Seibert and McGlynn, 2007].

In this section I use gridded plots of spatial class coincidence. Two given maps of classified values are evaluated for grid cells which belong to the respective two classes. The number of such cells is presented in the plots as black referring to the maximum and white referring to the minimum. In addition, the overall histograms of both input maps are given as marginals.

2.4.2 *Landscape setting – common sets of slope and land use*

Not surprisingly the different geological areas in the Attert basin manifest distinct forms of land use. The arable silty plains of the marls are predominantly used as pasture and agricultural lands (80%). The much more sloped sandstone and schist areas are about 50% forested. Figure 2.16 summarises the main land cover classes.

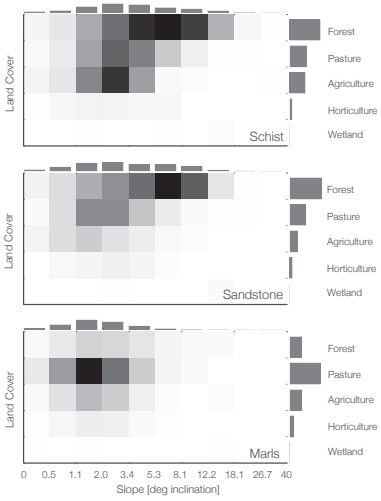

Figure 2.18: Distribution of land cover classes in different geological settings at different slopes based on DEM analysis.

The topographic setting in the geology classes is described in figure 2.17. The marls have the greatest share of the basin (60%) and comprise the most gentle topography with slopes generally below 5° inclination. In the schist area (30%) we find the steepest slopes and very few flat patches. The distribution peaks around 3° but spreads above 25°. The sandstone area presents also some topographic diversity which is relatively evenly distributed between 1° and 12°.

To bring together land cover, slopes and geology class figure 2.18 points out their respective distributions. In the schist area a gradient of land cover and slope is apparent. On the plateaus agriculture is prevailing. With more sloped surface the plateau edges are used for pasture. The steep slopes are forested. A similar but less pronounced pattern is found for the sandstone with slightly more evenly distributed slopes and less agriculturally used area. Since the marls are generally rather flat here a less skewed distribution is found - or in other words slope is no strong predictor for land cover.

In the schist 23.3% of the area are sloped (>3.4°) forests, 22.9%

agricultural and 21.0% pasture plateau ($\leq$3.4°). That means, that these three classes comprise 2/3 of the area already. In the sandstone 32.9% is covered with forests on medium slopes (2.0°< slope <12.2°) and 18.3% with forests on flat areas (<2.0°). 12.7% are pasture on gentle slopes (1.1°< slope <5.3°). Again three classes make up for 2/3 of the area. In the marls 50.1% are covered with non-sloped (<3.4°) pasture. 20.2% fall into non-sloped agriculture.

2.4.3 *Topographic and thermodynamic gradients*

So far, this was broad first order statistics of areal shares. For the two major drivers of the hydrological cycle (rainfall and solar radiation) I calculate areal references and compare their setting.

Solar radiation can be quickly calculated in GRASS GIS with the r.sun package [Hofierka and Šúri, 2002]. It is an implementation of the clear-sky solar radiation model after Scharmer and Greif [2000] based on European data and climate conditions. I used an accumulation of monthly sample days to estimate a potential annual solar radiation gain based on elevation, aspect and slope. The resulting map is given as map 7.9.

Topographic gradients are less simple to derive as they rely on much more assumptions about the influence of the topography and the subsurface on runoff generation and storage dynamics. While in general the potential energy of a water particle may be determined by the topographic elevation above stream or another reasonable reference like groundwater table where applicable, it is less straight forward to estimate accumulation and decay of kinetic Energy on the water particle's course to the river. Beven and Kirkby [1979] introduced the topographic wetness index (TWI) as fundament of Topmodel for that purpose

$$TWI = \ln(\frac{\alpha}{\tan(\beta)}) \tag{2.1}$$

where α is the area drained per unit contour length at a point (flow accumulation) and β is the slope. Under temperate humid conditions in strongly storage controlled basins TWI is very successfully applied [Buytaert et al., 2008]. Buchanan et al. [2014] recently compared different applications of this index based on different data. Especially a decision tree for best practice application and the originally foreseen integration of hydraulic soil conductivity (k_s) and soil depth (z_s) as soil-topographic wetness index

$$STI = \ln(\frac{\alpha}{k_s z_s \tan(\beta)}) \tag{2.2}$$

[Walter et al., 2002] is highlighted.

Maps 7.6-7.8 present TWI, STI and a flow gradient estimate. The TWI map has been calculated with the respective SAGA toolbox [Conrad, 2006]. For the derivation of the STI map saturated hydraulic conductivity has been estimated based on the soil maps of Belgium and Luxembourg. In table 2.5 the respective reclassification scheme to Carsel and Parrish [1988] standard values is given. Moreover, soil depth to the first restrictive layer was estimated based on the findings in the field. Accordingly a depth of 0.8 m, 1.2 m and 6.0 m has been assigned for schist, marls and sandstone respectively.

Soil Map Belgium Drainage Class	Soil Map Luxembourg Soil Class	Carsel and Parrish Texture Class	Ks value [m/s]
a - excessive	-	Sand	8.25×10^{-5}
b - slightly excessive	sandy, loamy sand	Loamy Sand	4.053×10^{-5}
c - moderate	sandy loam, loamy	Sandy Loam	1.228×10^{-5}
d - moderately low	loam	Loam	2.889×10^{-6}
-	loamy stony	Silt Loam	1.25×10^{-6}
-	clayey, structured	Sandy Clay	3.333×10^{-7}
e, f, h, i - low	silty stony	Silty Clay Loam	1.944×10^{-7}
g - very low	heavy clay	Silty Clay	5.555×10^{-8}

Table 2.5: Reference table assigning estimates for saturated hydraulic conductivity after Carsel and Parrish [1988] to mapped soil classes for soil-topographic wetness index estimation. Notice that these references deviate strongly from the observed values in the previous section.

Furthermore, a flow gradient estimate is calculated inspired by Florinsky [2012]. The calculations use the watershed analysis tools in GRASS GIS [Metz et al., 2011] and Whitebox Geospatial Analysis Tools (John Lindsay, University of Guelph). In order to derive a stream network consistent with the topographic map, the DEM and the observations two networks have been extracted from the D8 and Rho8 flow accumulation map based on different accumulation thresholds: 8.9 for schist, 10.6 for sandstone and marls. These thresholds have been identified based on expert knowledge about stream existence. Consequently, both maps have been patched for the respective geology classes and manually cleaned to eliminate fragments and to maximise compliance with the topographic map.

The resulting stream network is then used with the GRASS GIS addon r.stream.distance [Jasiewicz and Metz, 2011] to calculate distance to (d_{rel}) and elevation above (z_{rel}) stream in the basin (downstream method). With the least squares fitted plane approach [r.slope.aspect after Horn, 1981] the respective local derivates of both maps are calculated. After Florinsky [2012] the slope gradient of this stream-relative topography is calculated as

$$G = arctan(\partial z_{rel} / \partial d_{rel}) \tag{2.3}$$

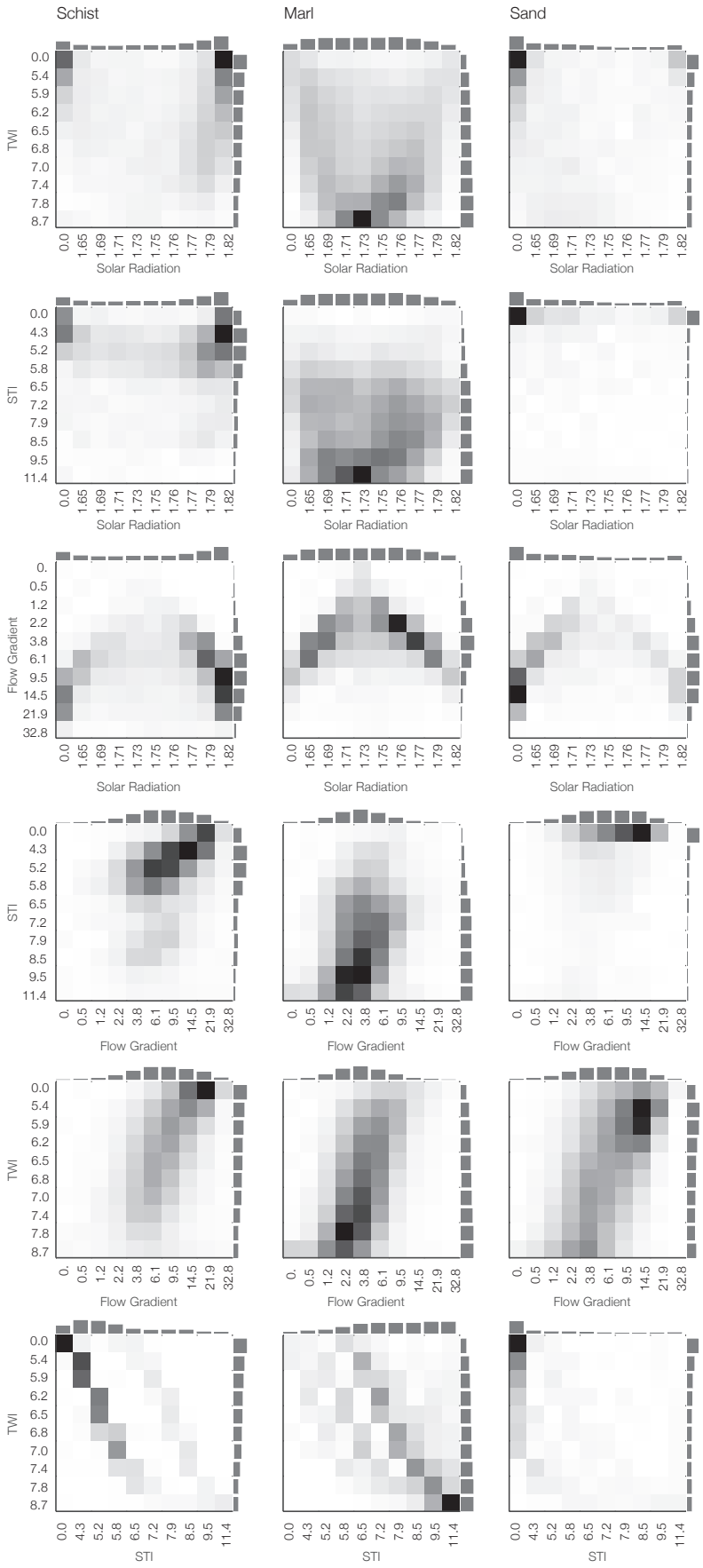

Figure 2.19: Spatial coincidence of landscape gradient classes in the different geology classes. Marginals give the overall distribution of the respective attribute in the geology class. Grid with black for maximum number of cells to belong to both respective classes. White refers to the minimum.

which is given as flow gradient estimate.

A LANDSCAPE COMPARISON of these four derived index maps is given in figure 2.19 as geology class specific relative distributions. The resulting maps are classified based on the respective quantiles (0.1 steps, 10 bins) of the total distribution in the basin for solar radiation, TWI and STI; The log-normally distributed flow gradient map was resampled based on log-normal bins. The axis labels mark the lower bound value of the respective class. At the top and right edges again the overall histograms of the classes are given. The grey shade of the grid points out higher occurrence with darker stain.

The first apparent result is that all four indexes are non-redundant, although they are statistically by no means independent as they result from the same DEM. The approach is intended as strongly data driven identification support for potential EFUs.

2.4.4 *Remote sensing for landscape dynamics*

Remote sensing (RS) is used as last reference in this analysis. Using Google Earth Engine I extracted cloud-free scenes of the Landsat7 (L7) 32 day composite of the Normalised Difference Vegetation Index (NDVI, using red (0.66 µm) and near-IR (0.83 µm) reflection bands) and 8 day composite of the Normalised Difference Water Index (NDWI, using near-IR (0.83 µm) and mid-IR (1.65 µm) reflection bands). For this analysis six scenes for early spring and autumn in 2011, 2013 and 2014 were selected. The resolution is 30 m. In addition MODIS near-IR reflection (2005-2011, 14 day timestep, 250 m resolution, MOD13Q1) was evaluated.

The L7 scenes have been processed for mean and standard deviation of each grid cell over time. For the girds in the MODIS stack the mean of the annual median and standard median deviation over time is calculated, resulting in respective maps for MODIS IR, L7 NDVI and L7 NDWI 7.10-7.15. For this analysis, again the spatial coincidences of different classes were analysed. Figure 2.21 and following use the same approach as above.

2.4.5 *Interpretation of the results*

In the following a brief interpretation of the landscape gradient indexes and remote sensing data is given for the different geology classes. Figures 2.19-2.23 and maps 7.6-7.15 have been introduced as reference.

The schist area is characterised by relatively low TWI and STI, high flow gradients and a positive bias in solar radiation gains. The sandstone area appears similar in many regards but clearly peaks

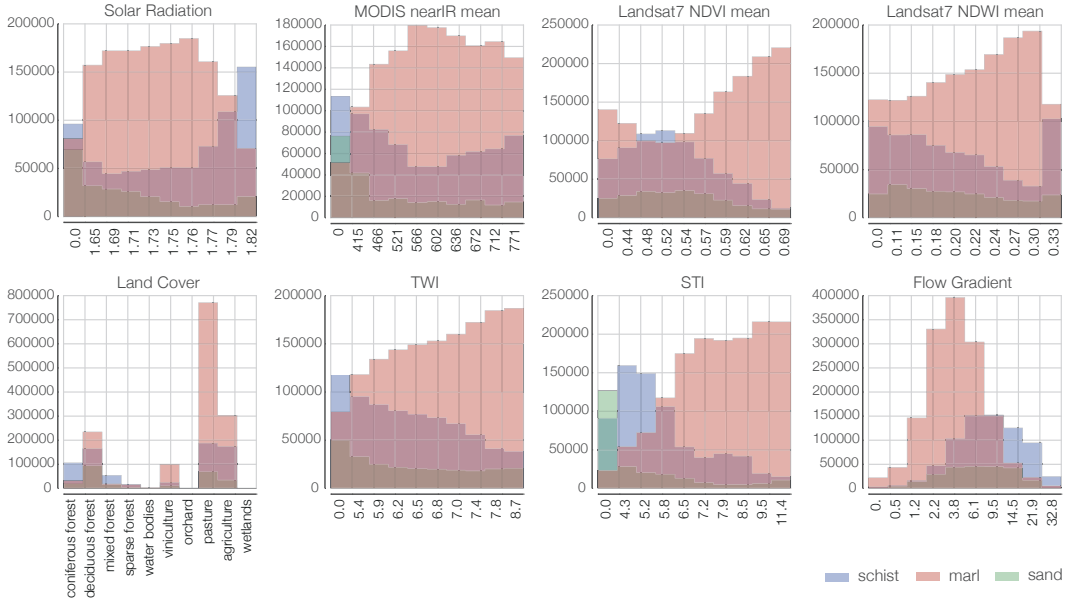

Figure 2.20: Histograms of the areal shares landscape gradient and remote sensing classes in the three geology classes. Since the distributions given in figures 2.21–2.23 and 2.19 are normalised within the geology class, this is a reference to avoid over-interpretation of the plots. That the spatial coincidence cannot be inferred from these histograms is especially apparent for TWI and NDWI as given in figure 2.24. Count on y-axis is number of grids of 100 m^2.

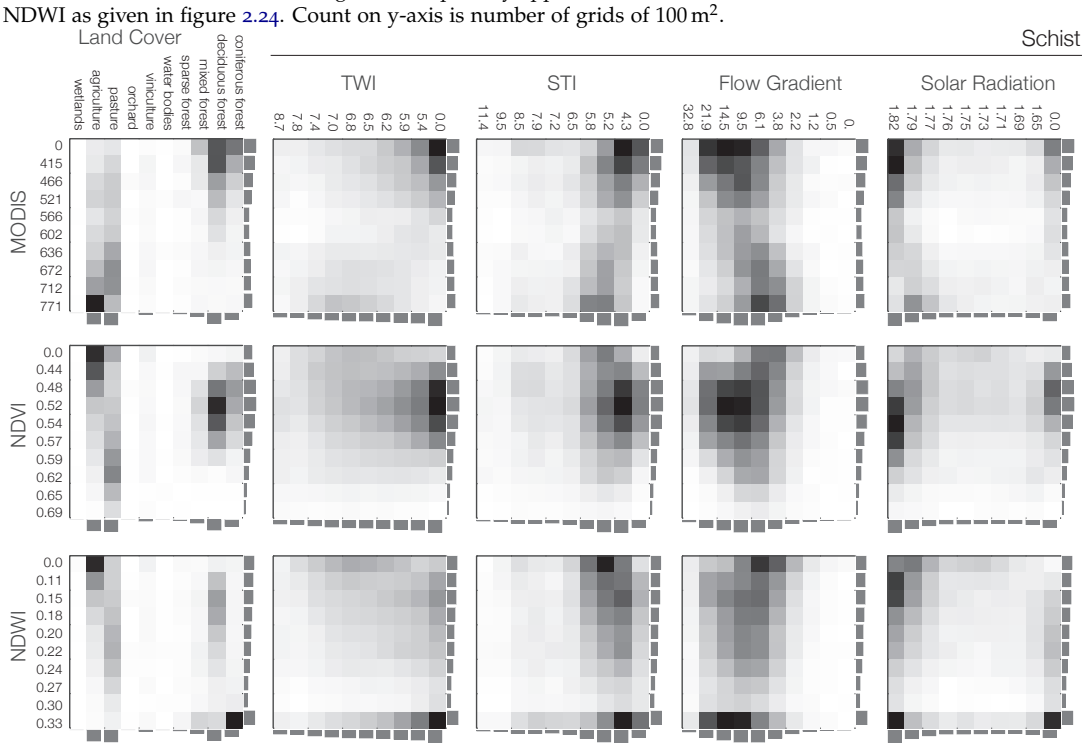

Figure 2.21: Matrix of spatial coincidence of remote sensing classes with landscape gradients and indexes in the schist areas of the Attert basin.

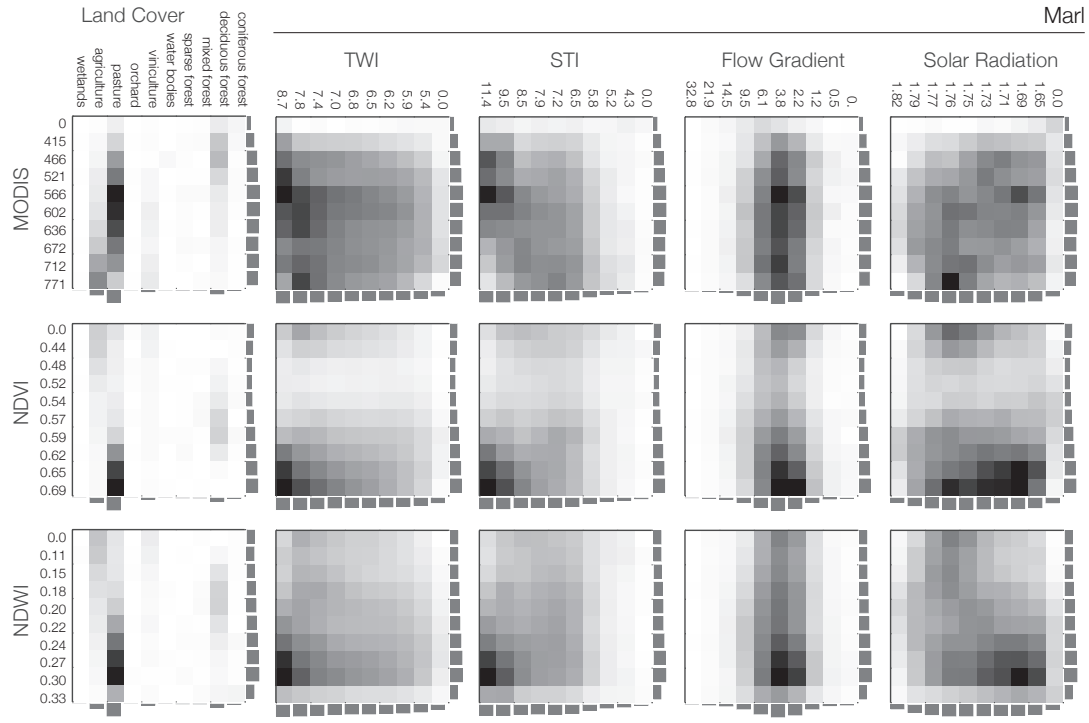

Figure 2.22: Matrix of spatial coincidence of remote sensing classes with landscape gradients and indexes in the marl areas of the Attert basin.

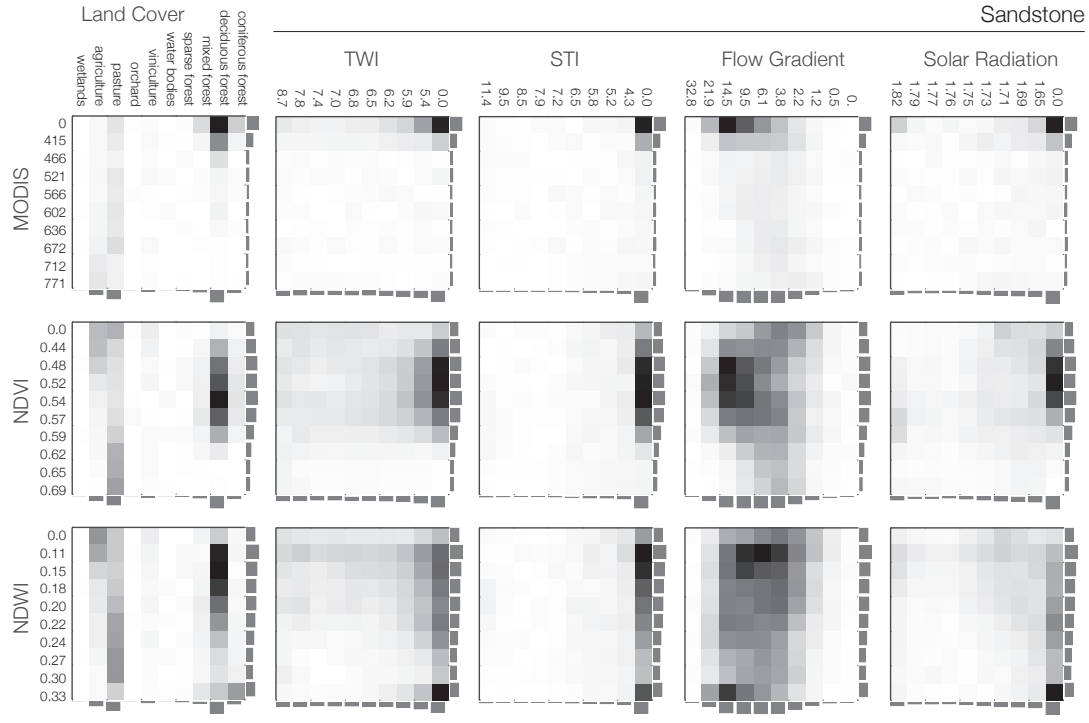

Figure 2.23: Matrix of spatial coincidence of remote sensing classes with landscape gradients and indexes in the sandstone areas of the Attert basin.

at very low STI. Here, solar radiation has a negative bias and solar radiation is more evenly distributed. The relation of TWI to STI is least which is caused by a dominance of the deep draining soils with high saturated hydraulic conductivity over the topographic gradients. As such, this area is the driest with moderate flow gradients. In contrast, the marls have the lowest flow gradients and the highest TWI and STI. Hence it can be classified as relatively wet area with low discrimination power of topography. These contrasting pairs are also reflected in the remote sensing data with one interesting peak of high NDWI in the schist.

The similarity of the patterns in schist and sandstone is also apparent in the more detailed comparisons. One should note that the differences are mainly attributed to solar radiation gain, distribution of flow gradients and STI in figure 2.19. Although the derived NDVI and NDWI are more evenly distributed in the sandstone the more pointed distribution of the landscape gradients suggest easily identifiable EFU candidates.

The marl patterns are pointing to more wet conditions and less distinctly identifiable prevailing classes.

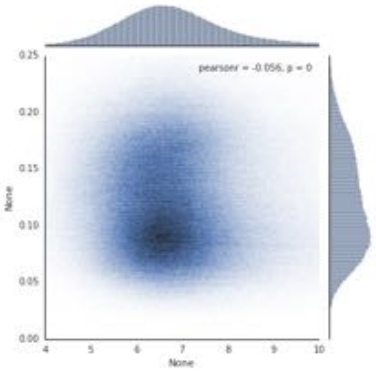

Figure 2.24: Joint plot of TWI and NDWI mean for the Attert basin. TWI and NDWI are showing very similar histograms. However, a direct comparison of spatial coincidence at the grid level does not reveal much correlation.

2.4.6 *Intermediate discussion and conclusion*

The resulting maps and comparison matrices do not automatically lead to the identification of EFU candidates or hypotheses. However, they suggest that the simple delineation of the catchment into the three geology classes may not be the only avenue to head for. Contrasting the results from hydrological process analyses, the sandstone and schist areas exhibit very similar patterns regarding landscape gradients and remote sensing derivatives. Similarity according to these measures is inconsistent with the derived functional similarity. This also means that GIS analyses alone may leave ambiguous or erroneous conclusions to processes which are not predominantly related to longterm surface properties.

Since the results strongly rely on geology class as primary identifier, next steps should include a multivariate geo-statistical analysis of the data to identify possible clustering and descriptors without bondage to them. Also a closer look into temporal dynamics of RS data with much higher resolution (in space and time) is suggested, which falls in line with the conclusion made earlier, that the scales of the processes and the observation need to match.

3
Field experiments

Numerous measurements and experiments have been conducted to find adequate descriptors for the settings of mediated rapid subsurface storm flow and soil water retention. This chapter presents plot- and hillslope-scale experiments as foundation for the concept, model development and discussion of the findings. Most experiments already anticipate conceptual ideas I present in the later chapters as they are part of an iterative learning process of hypotheses and respective tests. The discussion in chapter 5.4 (p.114) will link the different aspects back into the big picture.

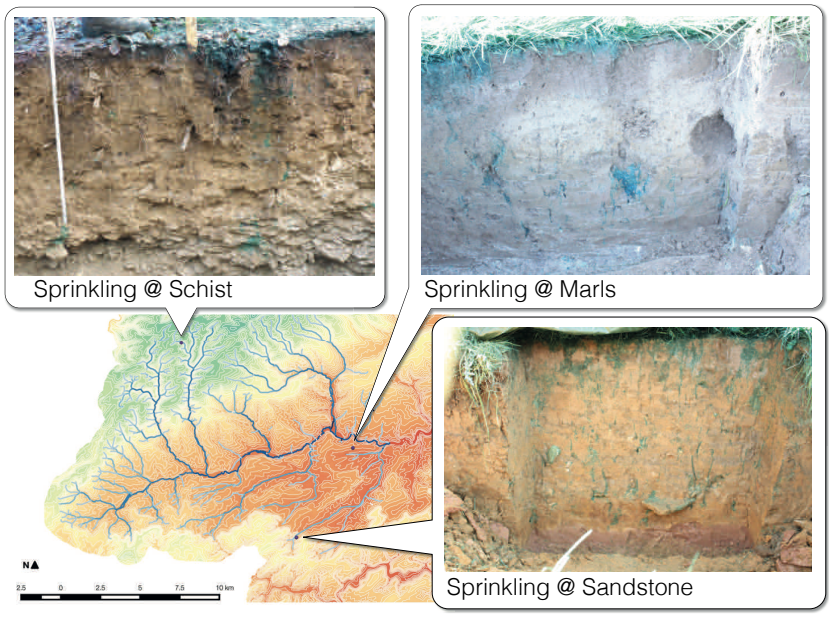

Figure 3.1: Location of plot-scale sprinkler experiments in the Attert basin. Basemap with topography and stream network, zoomed exemplary Brilliant Blue stain profiles.

3.1 *Plot-scale sprinkler experiments for rapid subsurface stormflow measurement*

Within the three distinct geological settings we conducted a series of plot-scale sprinkler experiments as outlined in figure 3.1.

I hypothesise that flow within a macropore system can be representatively characterised by sprinkling experiments at 1 m^2 plots, which:

- push the macropore network near to its hydraulic capacity by using a large sprinkling amount at an intensity which avoids ponding or macropore clogging,
- assume low but sufficient diffusive interaction between macropore and soil matrix,
- employ a rapid soil sampler assuring a fast collection of soil samples at high resolution down to a depth of up to 2 m.

Moreover, I assume that the impact of drop splash [Iserloh et al., 2013] and macropore drainage area connectivity [Weiler and Naef, 2003] are negligible since the used sprinkler produces a very fine drop spectrum and vegetation remains undisturbed.

3.1.1 *Setup of plot-scale sprinkler experiments and analysis*

The experiments were conducted with spray irrigation of 50 mm in 1 h on 1 m^2. The sprinkling water was enriched with 5.0264 g l^{-1} Potassium bromide (KBr) salt tracer and 4.0 g l^{-1} Brilliant Blue dye tracer. I used a sprinkler setup with one centred 120° full-cone nozzle (Spraying Systems Co., Wheaton) at 1 m height in a fully wind-protected tent.

Soil moisture was monitored employing a TDR soil moisture tube probe (Pico IPH Imko Modultechnik GmbH, Ettlingen) throughout the experiment. This probe has an elliptically shaped measurement footprint of about 3 l. Hence in each depth increment of 10 cm three repeated measurements with 120° twist were performed. The deviation of these three measurements can be used as indicator for local heterogeneity.

The plot was excavated the next day after ≈24 h down to the deepest spot of Brilliant Blue recovery. Vertical and horizontal images of the dye pattern profiles were taken. Moreover, vertical profiles of 21.2 ml soil cores in a 5×5 cm grid for Br^- analysis were taken using a rapid sampler.

The rapid sampler is a repeatedly deployable core sampler with the aim of quickly withdrawing undisturbed samples with equivalent

volume, making a reference to soil mass and volume possible. The cores are directly transferred from the sampler into brown glass bottles.

In the laboratory these soil samples were dried at 105 °C for 72 h and after weighing are subsequently suspended in de-ionised water. For full suspension the samples were placed in an overhead shaker for another 72 h at 9 rotations per minute. The samples were then left for 4 days for sedimentation to exfiltrate the excess through a) filtration paper (5 µm to 13 µm) and b) 0.45 µm PP micro-filter. The extracts were analysed in an Ion Chromatograph (Metrohm 790 Personal IC) with an anion separation column (Metrosep A Supp 4 - 250/4.0) for Br^- concentration[1].

[1] I sincerely thank Elly Karle and the colleagues at KIT Engler-Bunte-Institute for the processing of many hundreds of such samples.

From these results I gain classical qualitative binary dye tracer images of the outcrop faces and horizons, and a quantitative Br^- concentration profile. In addition the dynamics of a 1D soil moisture log are recorded.

3.1.2 *Derivation of travel velocities from tracer profiles*

To determine the travel velocity distribution from the tracer profiles I employ a cumulative curve method [Leibundgut et al., 2011]. The distribution of the advective velocity v_{advect} is set to the depth z distribution of the Br^- concentration c_{Br^-} at the time of fixation t_{fix}. For the profile I gain:

$$v = z/t_{fix}, \tag{3.1}$$

$$\Phi(v^z_{advect}) = c^z_{Br^-} / \sum c_{Br^-}, \tag{3.2}$$

where Φ is the cumulative distribution function (CDF). Obviously, the estimated travel velocity pdf depends strongly on the selection of t_{fix} somewhere between irrigation and excavation. This can scale v several orders of magnitude. It further depends on the sampling resolution as well as on the cross sectional fraction of the macropore system. This is discussed in section 5.1.3.

3.1.3 *Results of sprinkler experiments*

In total we conducted nine such experiments throughout the Attert basin[2]. The results are given in figure 3.1.

[2] In the marls and sandstone area I collaborated closely with Loes van Schaik (TUBS), in the schist area with Niklas Allroggen (UP) and Matthias Sprenger (UF). Their support is gratefully acknowledged.

It is remarkable to note that in all experiments sprinkling water drained to a lower subsurface structure or great depth mainly through soil structures. Although different in the respective specifics, macroporous structures were found in all kind of soils: cracks in silty clay, earthworm borrows through clay and loamy sand, and voids in young periglacial deposits. As such also large proportions of the

soil remained without any interaction with the sprinkling water. In the Wollefsbach basin the dry and cracked layer at about −0.3 m did simply act as transfer zone without moisture reaction to the 50 mm irrigation event. In the Hoevelerbach basin irrigation water did bypass a 0.5 m thick clay band through single earthworm burrows and even reached through highly diffusive loamy sand to a depth of −1.9 m. In the Colpach basin the tracer was also recovered far offset from the irrigation spot.

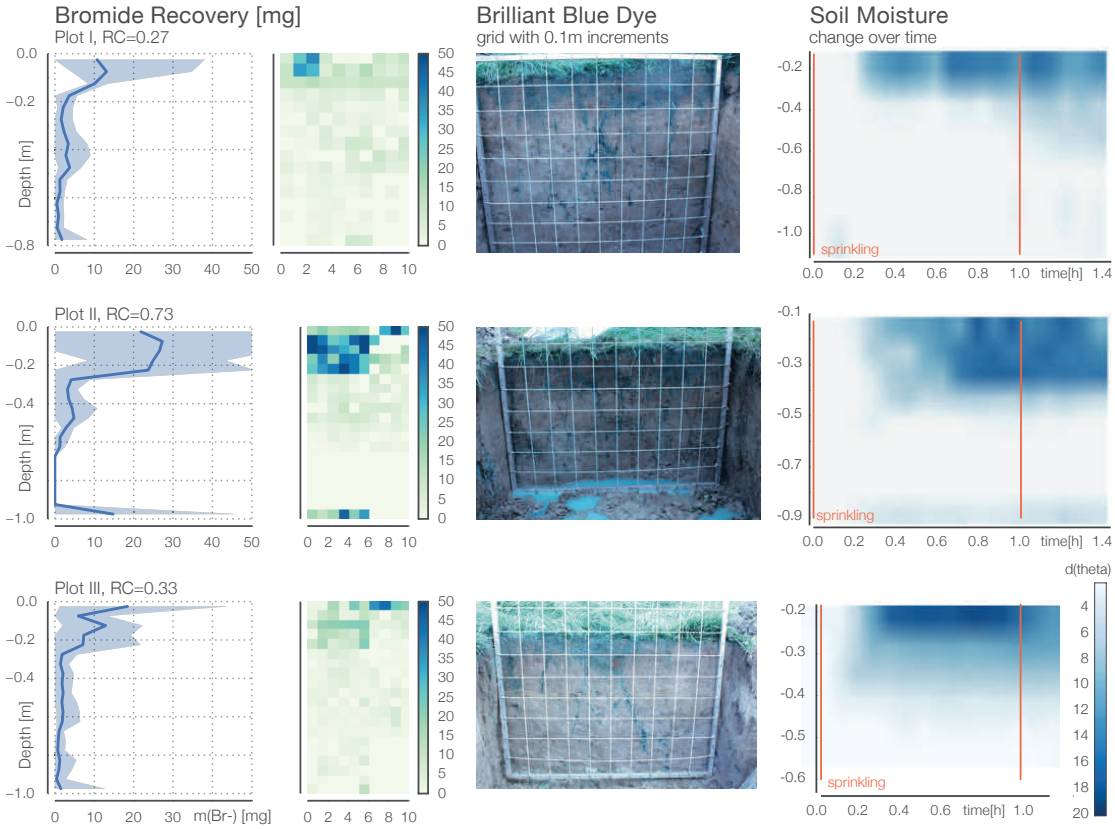

Figure 3.2: Plot-scale sprinkler experiments Wollefsbach basin. Marls with tile drains. Results from experiments with 50 mm spray irrigation for 1 h. Left: Recovered Bromide mass profiles. Center: Photo of excavated profile with Brilliant Blue stains. Right: Observed soil moisture change referred to the first measurement shortly before onset of irrigation.

These findings are inline with many experiments all over the world. However they challenge the common reduction of soil water dynamics to (effective) diffusive flow. This challenge is long standing [e.g. Beven and Germann, 1982, 2013, Germann, 2014] and will also be central in this thesis.

Figures 3.2–3.4 present the recovered Br^- mass profiles, excavated soil profiles with Brilliant Blue stains and the observed soil moisture dynamics referenced to the first measurement shortly before irrigation onset. The given recovery coefficient (RC) is calculated by

$$RC = \Sigma_{profile} m_{Br^-} \frac{z_{max} * A_{irr}}{\Sigma V_{sample}} / c_{Br^-_{irr}} V_{irr} \tag{3.3}$$

with m_{Br} as the recovered Bromide mass in the samples [mg], V_{sample} the sample volume of 21.1 ml, z_{max} the maximum depth of the sampling [m], A_{irr} the irrigated area of 1 m^2, $c_{Br_{irr}}$ the concentration of Bromide in the sprinkling water with 3.37 g l and V_{irr} the irrigated water volume. For plot X, XI and XII the percussion drill core sample is also taken in account.

Generally, the RC for all plots is relatively low which is expected under the given conditions due to a sampling of about 0.5% of the heterogeneous and structured total affected soil volume. With respect to additional samples from the drilled cores (figure 3.4) all RCs decline, which points towards low representativeness of the sampling.

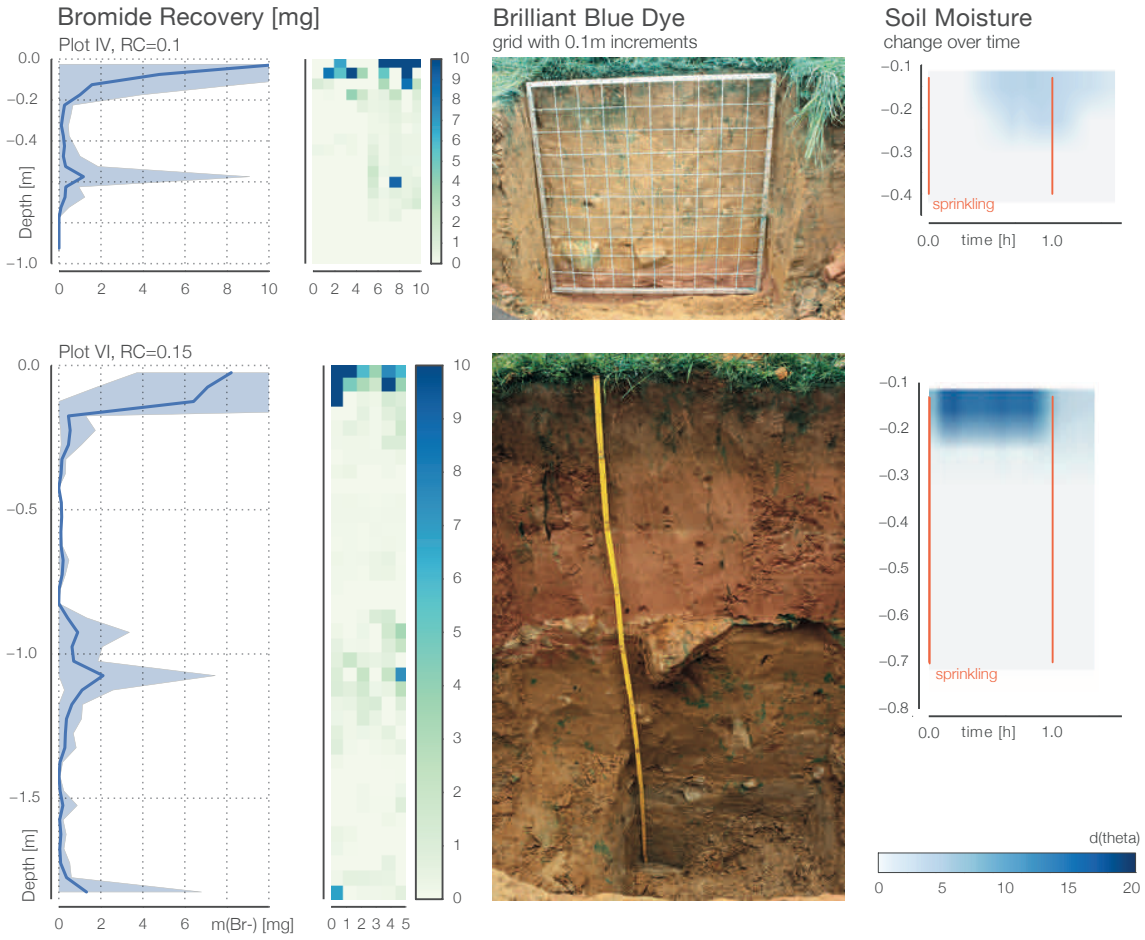

Figure 3.3: Plot-scale sprinkler experiments Huewelerbach basin. Marls and clay over loamy sand. Results from experiments with 50 mm spray irrigation for 1 h. Left: Recovered Bromide mass profiles. Center: Photo of excavated profile with Brilliant Blue stains. Right: Observed soil moisture change referred to the first measurement shortly before onset of irrigation.

However, losses to greater depth are observed but not assessed by this method. In the cases of the Wollefsbach basin, a sandstone layer prohibited further excavation. In the Colpach basin the deposit layer could not really be sampled due to the rocky material. The example of the Huewelerbach plot VI (figure 3.3) shows that even excavation to the end of the earth worm burrows at −1.9 m did not result in a

RC near 1.

Both tracer results reveal distinct site characteristics.

Wollefsbach: many cracks and earthworm burrows. large vertical redistribution along the cracks.

Huewelerbach: very few earthworm burrows make the water and tracer bypass the clay layer with almost zero recovery there. peak below clay in loamy sand but further vertical redistribution in macropores. lateral spread due to diffusive transport is low in clay and loam but high in loamy sand.

Colpach: very patchy pattern. concentration in first deposit layer could not be measured since sampling was almost impossible - problem of retention in non matrix soil material.

Soil moisture dynamics are a bit more difficult to interpret. In the following section 3.3 (p. 57) the topic is taken up at the hillslope scale. The observed reaction in the marls is strongest. It also resembles the observed very dry layer below $-0.3\,\mathrm{m}$. There the water is largely bypassing the soil in cracks to greater depth. In plot II an impermeable layer at the bottom appears to constrain further percolation.

In the sandstone experiments[3] the observed reaction differs a lot. Especially for plot VI the record may be erroneous with water flowing along the tube of the probe, which has been installed only shortly before the measurements. Nevertheless it is apparent that the sandstone plots are wetting up far less compared to the marl sites.

[3] Notice that the soil characteristics are also marly here. The sites are located in the northern Huewelerbach sub-basin (sandstone) where the marls cover a sandy basis. This is also found in the retention curve analysis (section 2.3).

The schist plots also have a very low reaction. In the following section figure 3.9 gives a more detailed view on the same data. However it can be pointed out that the moisture reaction appears very late and for plot X and XII a strong reaction in about $-0.8\,\mathrm{m}$ is noticeable.

3.1.4 *Intermediate conclusion from the plot experiments*

The plot sprinkler experiments allow a much greater insight into the advective and diffusive water redistribution compared to soil moisture dynamic monitoring alone. With the conservative tracer Bromide the binary information of Brilliant Blue stains is quantitatively extended. From the tracer concentration profiles the apparent advective velocity flow field can be inferred.

Notwithstanding, the method has by no means solved the open questions in rapid subsurface flow observation. It remains unclear whether the samples are representative for the whole flow field or not and how much of the not recovered tracer was lost to greater depth or lateral spread. A throughout discussion is given in section 5.1.3 (p. 102).

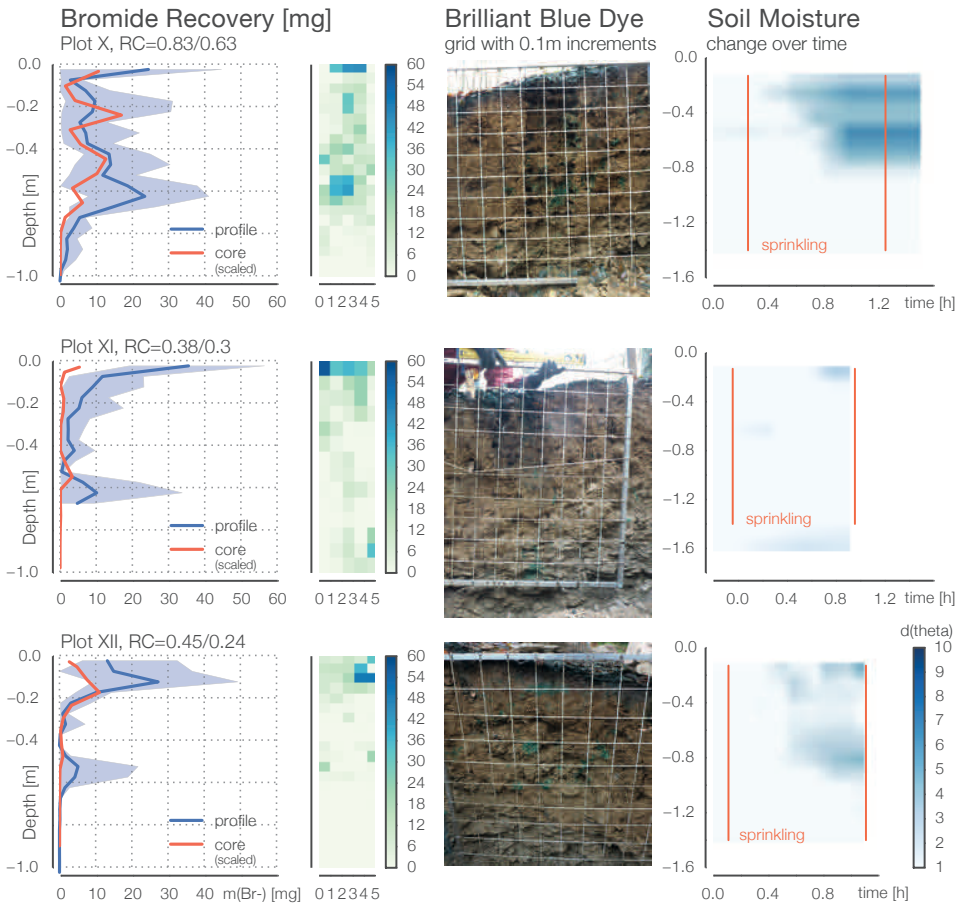

Figure 3.4: Plot-scale sprinkler experiments Colpach basin. Young soils on periglacial cover beds. Results from experiments with 50 mm, 30 mm and 50 mm spray irrigation for 1 h. Left: Recovered Bromide mass profiles. Core sample mass is rescaled to the profile samples. Recovery coefficient (RC) calculated for profile (first value) and the profile including core samples (second value). Center: Photo of excavated profile with Brilliant Blue stains. Right: Observed soil moisture change referred to the first measurement shortly before onset of irrigation.

3.2 *Complementary multi-tracer sprinkler experiments and 3D time-lapse GPR measurements* [4]

[4] These experiments were jointly conducted with Matthias Sprenger (UF) who analysed the stable isotope concentrations, and Niklas Allroggen (UP) who headed and performed the GPR analysis.

The three sprinkler experiments in the Colpach sub-basin have been conducted on three successive days in October/November 2013. To conserve identical starting conditions, the plots have been covered from the first experiment onward. Evaporation was negligible with relatively low temperatures and high air humidity. These sprinkler experiments were accompanied by a 3D time-lapse Ground Penetrating Radar (GPR) survey. Moreover, we sampled a 80 mm percussion drill core sample for joint stable isotope and Br^- analysis with a vertical resolution of 5 cm. GPR data were collected using a PulseEKKO Pro GPR system (Sensors and Software Inc., Mississauga) equipped with 500 MHz shielded antennas. Sampling interval was set to 0.1 ns recording a total trace length of 100 ns at an internal stacking rate of 8. Since sub-centimetre-precise positioning and accurate repeatability are key requirement, we used an automatic-tracking total station and a specially constructed portable measuring platform guiding the antennas on equally spaced lines (2 cm). Figure 3.5 shows the experimental setup *in situ*.

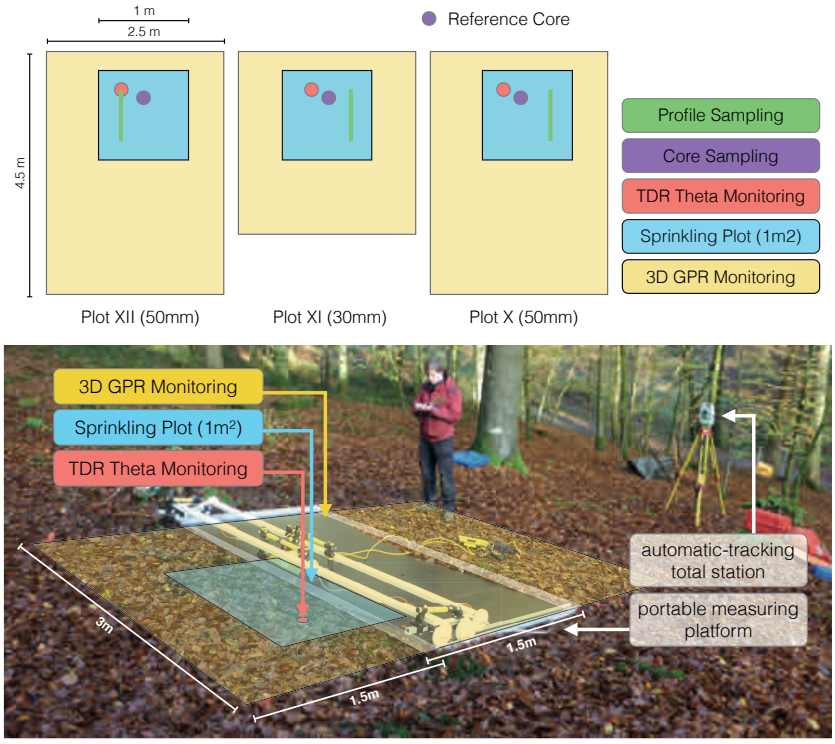

Figure 3.5: Experimental setup of complementary multi-tracer sprinkler experiments and 3D time-lapse GPR measurements in Colpach subbasin.

Three GPR data cubes have been acquired for each plot: The first

directly before sprinkling, the second directly after sprinkling and a third 20 h after sprinkling. One complete scan took about 45 min. The first data cube is used as reference to calculate the deviance of the amplitudes for the two other scans. As we did not observe any wetting front and as the soil consists of many voids, this very simple approach is found appropriate for a qualitative identification of changes in soil moisture. However precise positioning (especially in depth below 0.1 m accuracy) or quantitative interpretation is not possible with this technique. This setup explores the subsurface between -0.5 m to -2.5 m depth.

Stable isotopes $\delta 18\,O$ and $\delta 2\,H$ have been analysed using a Cavity Ring Down Spectrometer (Picarro Inc., Santa Clara) in the gas phase of dry air having let for equalisation with pore water for two days. It is given as deviation to the Vienna Standard Mean Ocean Water.

3.2.1 *Results*

Figures 3.6–3.9 present an overview of the multi-tracer und multi-method findings. In all cases water and tracer was transported to the deposit layer. Especially there a lateral relocation further downslope was observed. Even at lower sprinkler intensity of 30 mm on Plot XI tracer was recovered relatively far offset the sprinkler area. Although the three plots are very close to each other and distributed parallel to the contour line they reveal considerable differences. Plot X shows a much more evenly distributed tracer recovery and fast reaction of the soil moisture down to ≈ -0.6 m. There also the observed difference between the moisture plume directly and 24 h after irrigation show little difference. However, plot XI&XII point out substantial further lateral relocation of the irrigation water close to the deposit band.

The GPR data cubes also reveal, that the irrigation water quickly reached a depth of -1.4 m. Soil moisture reaction in -1 m is already recorded soon after irrigation start. That speaks for advective velocities of $10^{-4}\,m\,s^{-1}$ to $10^{-3}\,m\,s^{-1}$.

The Br^- and Brilliant Blue excavations propose very patchy macropore-matrix interaction and water flow which is limited to the macropore network. This is also captured by the Br^- core logs. The stable isotope analyses of the same samples generally suggest a more diffusive flow. It is noteworthy that the irrigation water was not especially enriched. Hence the difference to the isotope signature in the soil is relatively low and interpretations have to be drawn with attention to this low signal.

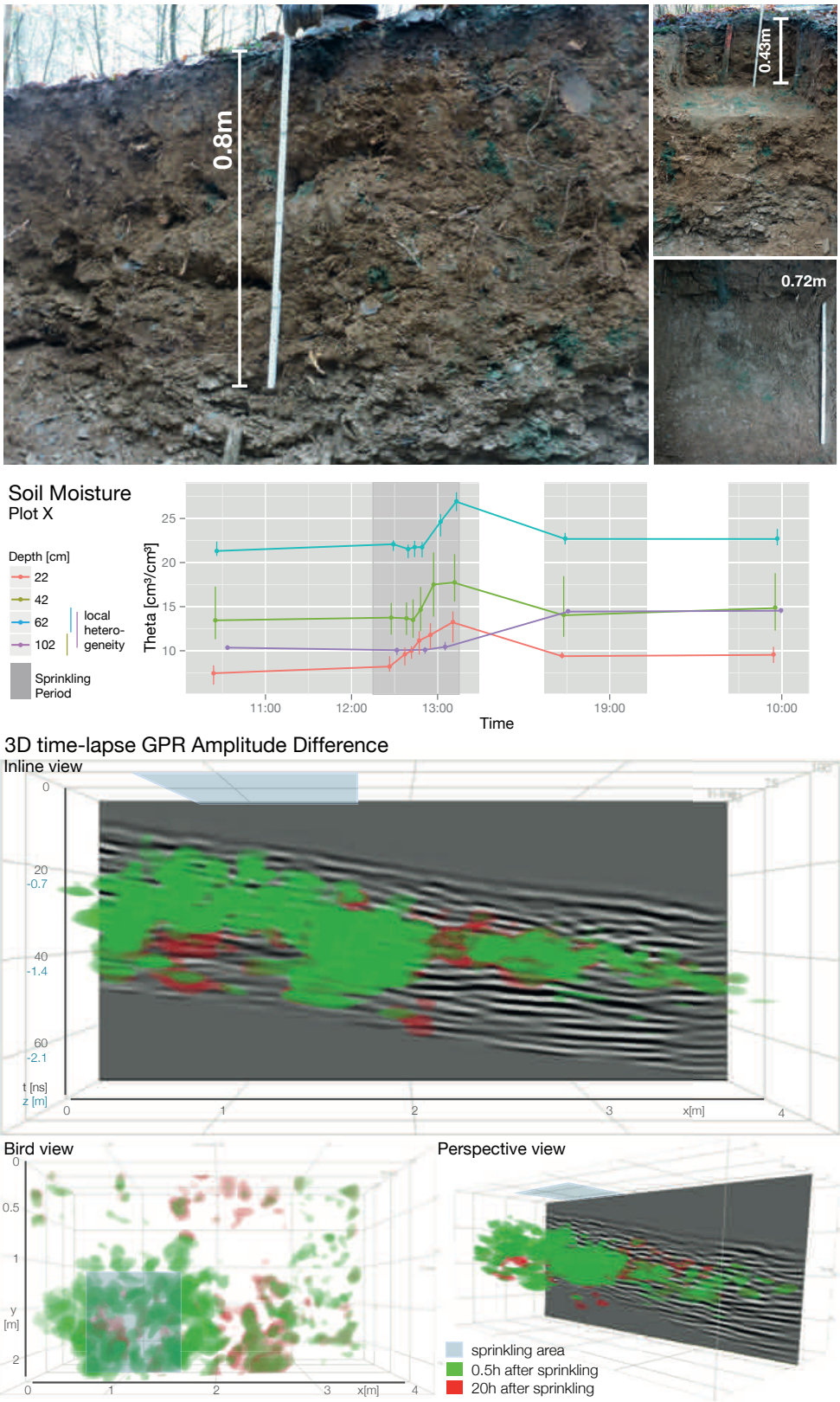

Figure 3.6: Sprinkling experiment plot X (50 mm, 1 h). Top: Excavated Brilliant Blue stains. Mid: Observed soil moisture dynamics (mean and spread in different depths). Bottom: 3D time-lapse GPR amplitude difference to pre-event state 0.5 h and 20 h after irrigation.

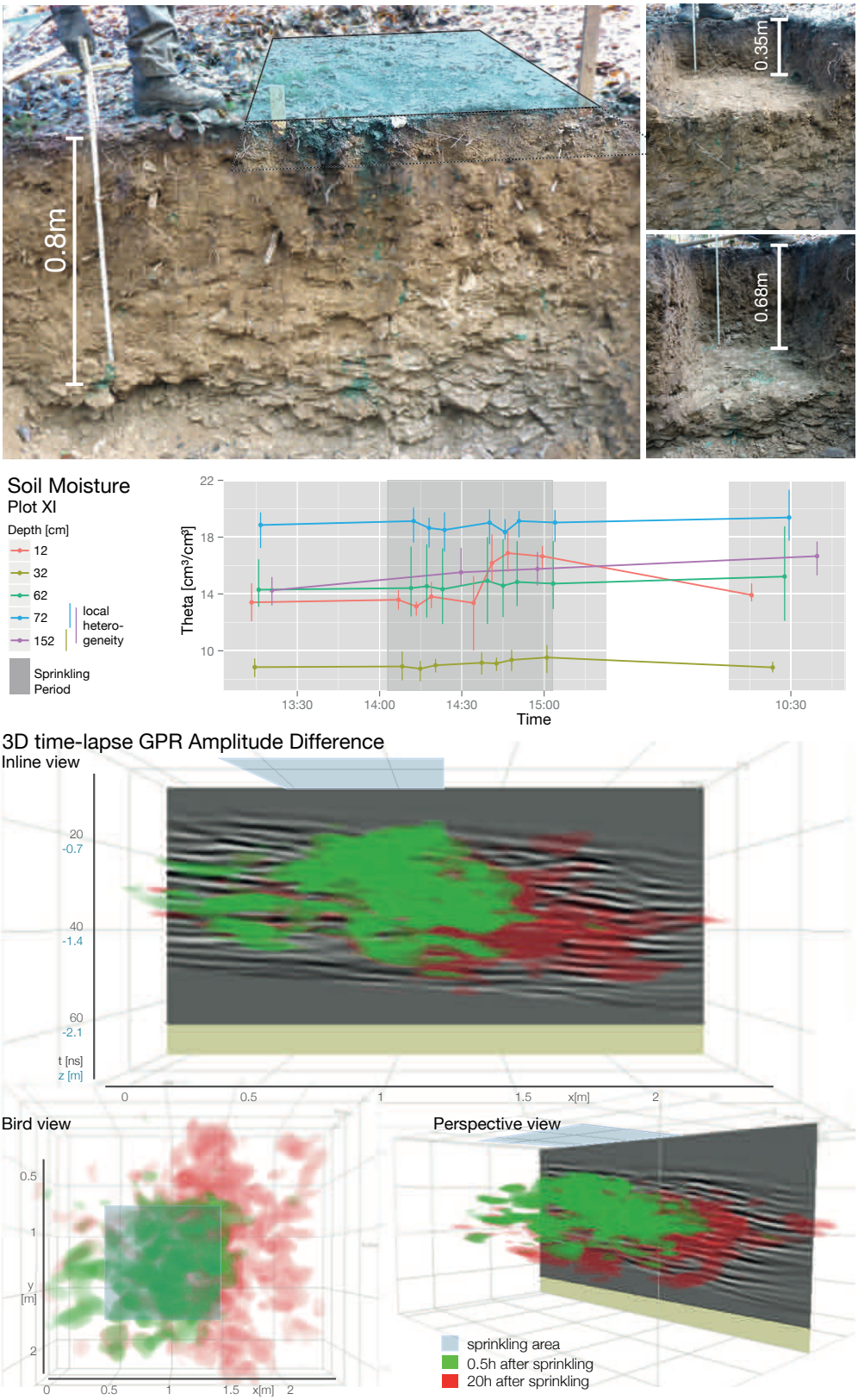

Figure 3.7: Sprinkling experiment plot XI (30 mm, 1 h). Top: Excavated Brilliant Blue stains. Mid: Observed soil moisture dynamics (mean and spread in different depths). Bottom: 3D time-lapse GPR amplitude difference to pre-event state 0.5 h and 20 h after irrigation.

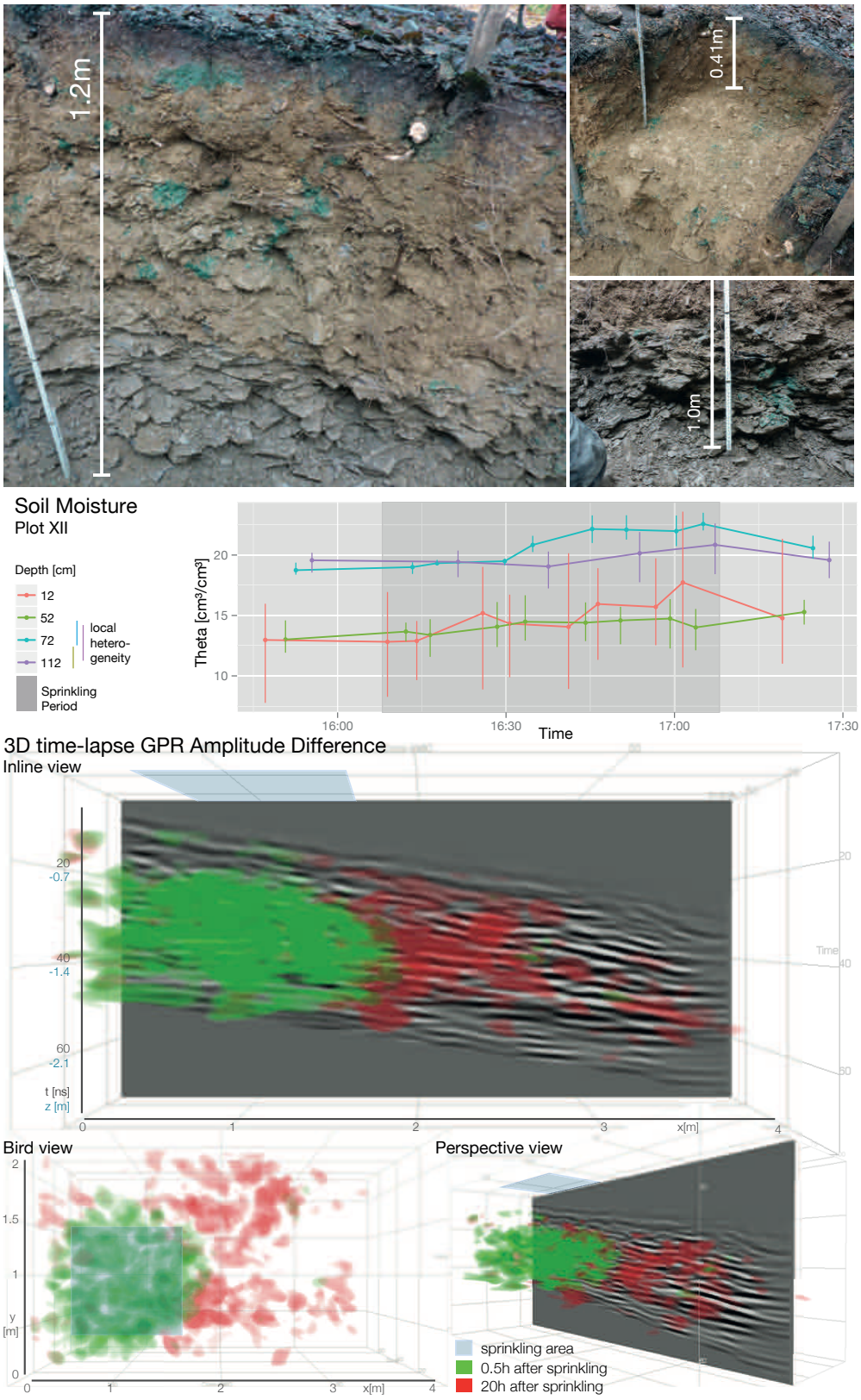

Figure 3.8: Sprinkling experiment plot XII (50 mm, 1 h). Top: Excavated Brilliant Blue stains. Mid: Observed soil moisture dynamics (mean and spread in different depths). Bottom: 3D time-lapse GPR amplitude difference to pre-event state 0.5 h and 20 h after irrigation.

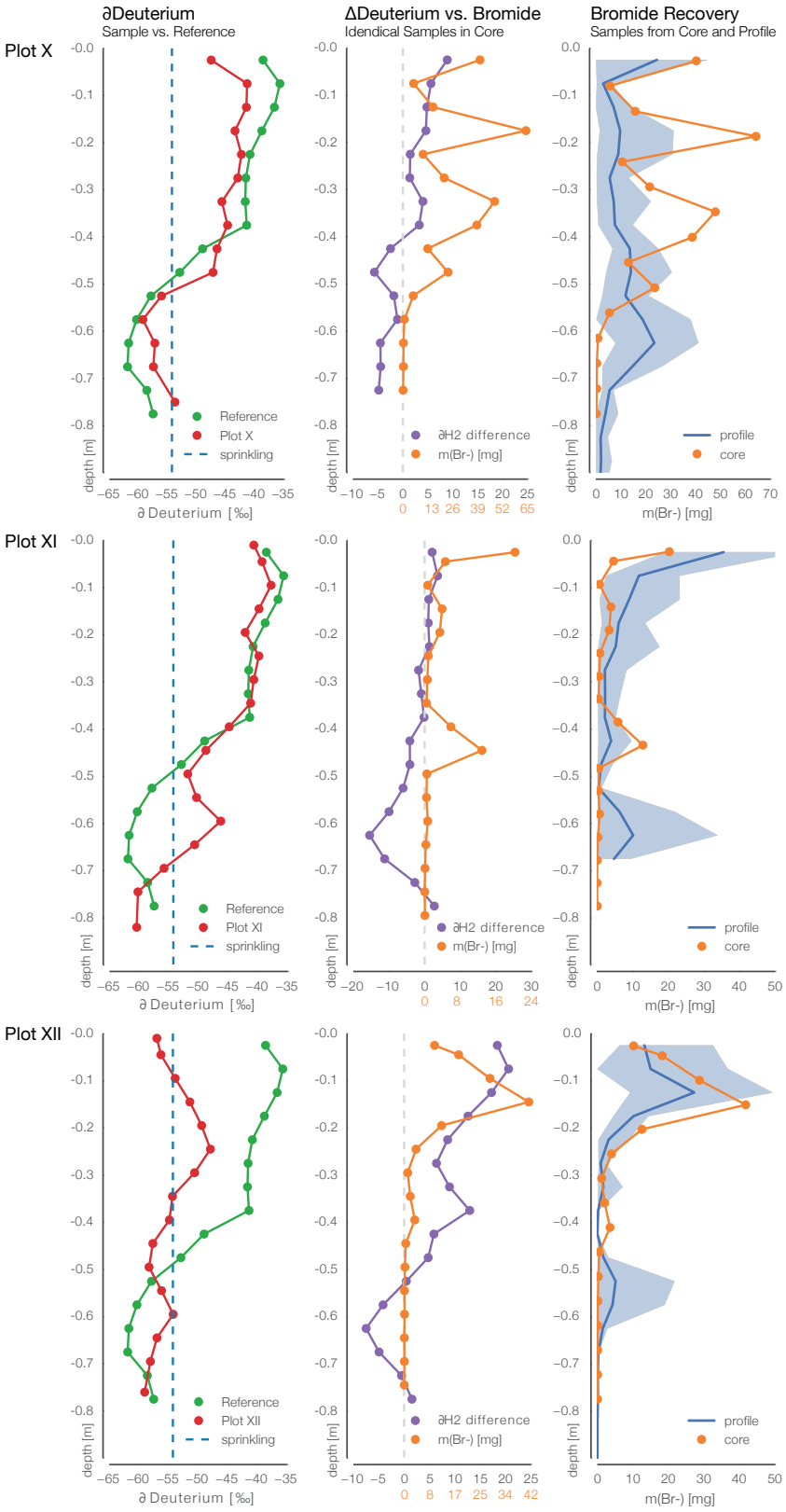

Figure 3.9: Multi-tracer sprinkling experiment plot X, XI, XII. Recovered changes in Deuterium concentration in percussion drill core sample logs and profiles and retrieved Bromide in the same samples and at the examined profiles.

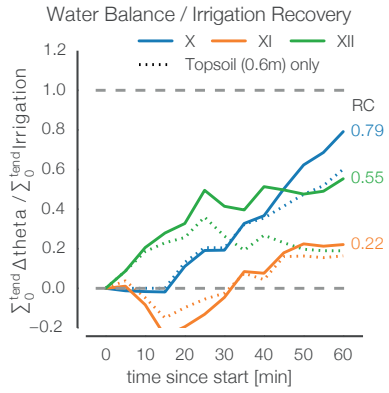

Figure 3.10: Water balance of recovered irrigation in soil moisture change for plots X, XI and XII. Recovery coefficient (RC) at the end of the experiment is given. $\Delta\theta$ referenced to start of irrigation. Log integrated over 1.4 m depth. Top soil share (dotted lines) in top 0.6 m.

3.2.2 *Complementary process interpretation*

The different complementary approaches give room for different interpretation of the observed process. I present one possible interpretation of the results referring to figures 3.6–3.9. The discussion is given in section 5.1.4 (p.104).

Soil moisture measurements show different reaction in respective depths. None of the plots fully resembles the irrigated water volume as shown in figure 3.10. Soil moisture change below −0.6 m has a noteworthy contribution to the recovery coefficient. All plot excavation clearly points to non-uniform soil moisture distribution. The large differences in one layer at the same time but with shifted sensor orientation (3x120°) and a strong reaction in greater depth in plot X and XII point to the existence of multi-phase flow. Decline in soil moisture after the event hints to further drainage of free water to greater depth. Low overall recovery coefficients and the stagnating recovery in the top soil of plot XII suggest that a share of the water is quickly drained either laterally or to deeper drainage.

Brilliant Blue recovery in the young soils fails to reveal the flow paths directly. However the generally L-shaped distribution proposes a quick vertical displacement with successive lateral flow in the deposit layer. This is also true for lower intensity of 30 mm h^{-1} with even more patchy recovery. Redistribution appears to be mainly controlled by the void network. Roots were only occasionally found stained - apparently when decayed. Combining horizontal and vertical excavation faces hints to about 80% of the total soil volume not taking part in the irrigation experiment – at least for the advective part.

With an average pre-event soil moisture of 20%, 1 m^2 irrigation surface and stained travel distances of about 2 m (vertical and lateral component), the irrigation water could only account for 2.5 or 1.5% change in soil moisture respectively to 50 or 30 mm if distributed evenly. However, we recorded 5-10% change in the soil moisture signal even for the lower intensity corroborating the estimate of about a great proportion of the soil not taking part in the event dynamics.

Bromide recovery generally resembles the observed patchy stains although the sampling volume often mixes several flow paths. With relatively high recovery rates the quantitative representativeness of the sampling needs to be reconsidered. Since the drilled cores generally match the sampled profiles pretty well the representation of the tracer signal appears to be sufficient within the error margins

of the method itself. The very large deviation of the concentrations in one depth level prohibits the existence of a wetting front. With this, Bromide recovery also points to largely advective transport bypassing a large proportion of the soil. Soil moisture monitoring suggests that between 30 and 80% of the water may be lost to further drainage.

STABLE ISOTOPE ANALYSIS compares post-event percussion drilled core samples against one pre-event reference. Notice that the isotopic signature (δ Deuterium) of the sprinkling water does not deviate much from the soil water. As such the interpretation needs some precaution. The logs generally suggest considerably distributed interaction in the top $-0.6\,\mathrm{m}$ for plot X&XII. Plot XI shows only a small reaction in $-0.6\,\mathrm{m}$ to $-0.7\,\mathrm{m}$. Contrastingly to plot X&XI the third plot suggests very intense mixing, shifting the log close to the signature of the irrigation water. As such the measurements primarily corroborate the findings of non-uniform wetting of the soil. But they also hint to much more interaction of soil water and irrigation water.

Since the core log samples have been analysed for stable isotopes and Bromide, a comparison of the two signals is more insightful. In general it is apparent that the two signals show considerable deviation. While in plot XII the overall shape may be somehow matched, one may interpret an faster propagation of Br^- as observed in other studies [e.g. Rühle et al., 2013, 2015]. However, plot XI suggests the opposite: Br^- peaks at 0 and $-0.45\,\mathrm{m}$ while the stable isotopes can be interpreted as low but evenly distributed interaction in the top $0.2\,\mathrm{m}$ and a peak in $-0.65\,\mathrm{m}$, hence faster transport of the isotope signal. Moreover at plot X the Br^- signal shows strong peaks which are not followed by the stable isotopes. The latter hint to more diffusive interaction than would be supported by the Br^- recovery. A different behaviour of the signals among the three plots may propose different interaction of the mobile and immobile phases as already pointed out by Roth et al. [1991].

3D TIME-LAPSE GPR also highlights quick transport of irrigation water to greater depth and further prevailingly lateral relocation along the deposit layer. In plot X I recovered changes in soil moisture about 4.5 m from the irrigation surface directly after the experiment. This suggests velocities up to $1 \times 10^{-3}\,\mathrm{m\,s^{-1}}$. Here the water appears to have only slightly been relocated after the experiment. In plot XI&XII there is a clear lateral propagation of the patchy moisture plume between the second and third scan. It is noteworthy that all scans result in a very similar final plume shape with a strong lateral component in the deposit layer. Although the structure is only loosely confined deep percolation appears not to a prevailing process. Intensity mostly

controls the lateral spread of the plume while its vertical spread is always around 1.4 m.

3.2.3 *Intermediate conclusion from the multi-method experiments*

This complementary interpretation of the results of three very close and very similar experiments resulted not at all in a repetitive picture. Neither do the methods reveal a congruent image nor do the plots behave the same. All measurements show clearly: Rapid subsurface flow dominates the experiments. However, interpretation of the different data is not as concordant. Especially the degree of macropore-matrix exchange or interaction of mobile and immobile phase leave room for different interpretation. Our study shows once more that inference from single sites, single methods or across scales may be misleading - especially for processes far from well mixed states.

3.3 *Hillslope-scale irrigation experiment with GPR inferred trenching*[5]

[5] This experiment has been jointly designed and conducted with Lisa Angermann (GFZ), Niklas Allroggen (UP, GPR measurements) and Matthias Sprenger (UF, stable isotopes in core logs and piezometres). I thank Theresa Blume (GFZ) and Markus Weiler (UF) for the great support and challenging discussions about it.

The plot scale experiments, discussions in the CAOS team and general ambiguity of the interpretation of single measurements led to the development of this hillslope-scale irrigation experiment. Rapid subsurface flow experiments suffer from a general un-observability of the processes. Blume and van Meerveld [2015] present a comprehensive review about experimental state of the art in hydrology for rapid flow and connectivity studies. They distinguish between hillslope- and stream-centred approaches. Moreover they point out specific capabilities and shortcomings of the different techniques. As hillslope-centred-approach trenching is found highly appropriate but very costly and with the problem of the artificial boundary condition resulting in overestimation of flow during wet and underestimation during dry conditions. Blume and van Meerveld [2015] also highlight the benefit of piezometers for monitoring ground- and ephemeral water tables.

The methodological setup of the experiment was developed based on three major aspects: i) local soil moisture dynamics, ii) spatial pattern of soil moisture changes, and iii) comparability of observed processes and structural properties of the experimental area. As advancement of a) trenching with artificial boundary conditions and b) plot sprinkler experiments with limited interpretability of processes during the irrigation and the interaction at the hillslope we came up with a technique of *GPR-inferred trenching*.

The sprinkling setup is characterised by a sharp transition between the sprinkled uphill area and the downhill monitoring area. This design was chosen to enable a separate investigation of vertical flow processes which are dominant on the sprinkled area, and lateral flow processes dominating the downhill monitoring area. The whole setup is shown in figure 3.11 and described in more detail in the following section.

3.3.1 *Experimental setup*

The experimental site is located at the lower part of a north facing hillslope in the northern Colpach subbasin. Topographic gradient is about 14°. Vegetation is dominated by beech forest (*fagus sylvatica*) of different age. However, the experimental site is placed in an area with no major trees. Except for few young trees at the downhill monitoring area, all shrubs were removed from the experimental site to accomplish GPR measurements and allow for undisturbed and homogeneous sprinkling.

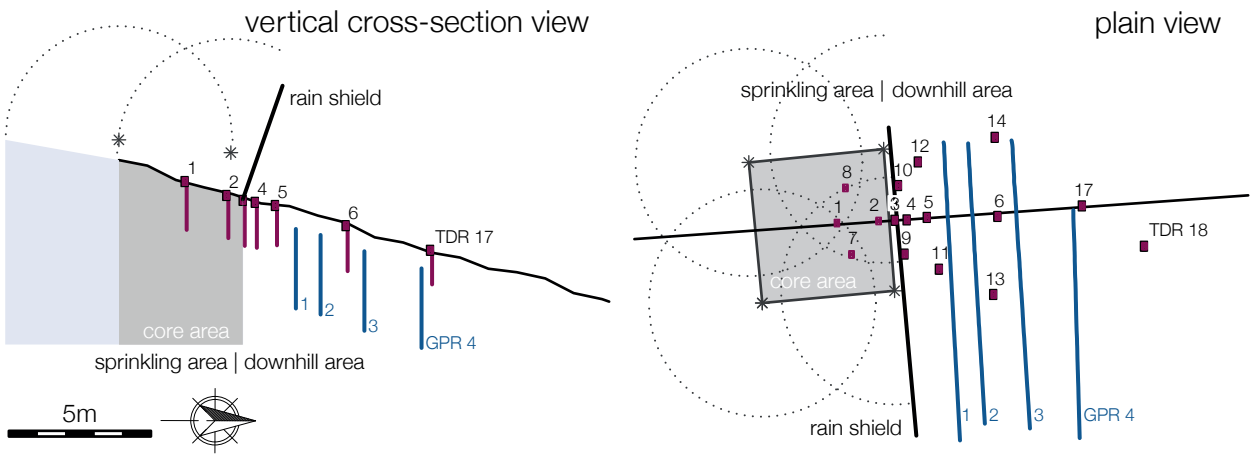

Figure 3.11: Setup of the GPR-inferred trenching hillslope irrigation experiment as vertical cross section with observed topography (left) and plain view (right). Sprinkler as asterisk with dashed circle as respective reach of 5 m. The core area with homogeneous irrigation and the rain shade as sharp divide marked with black lines. TDR tube probes as red dots with number. GPR profiles as blue lines with respective number.

Four circular irrigation sprinklers (Wobbler, Senninger Irrigation Inc., Clermont) were arranged in a 5 m by 5 m square in the upper part of the experimental site. This 25 m^2 area spanned by the sprinklers is referred to as the core area with relatively homogeneously distributed sprinkling intensity. A rain shield at the lower boundary of the core area was spanned to create a sharp transition to the non-irrigated area below. The water from the rain shield was collected with a gutter and routed away from the investigated area. Due to the sprinkler setup there was a buffer of 4 m on the other sides of the core area with less intense sprinkling, mitigating boundary effects and resulting in an overall sprinkled area of approximately 120 m^2.

Irrigation was realised with a 1 m^3 reservoir which was continuously refilled with stream water. The main water supply of the sprinkling system was monitored by a flow meter to measure the absolute water input, one tipping bucket to monitor the temporal variability of applied sprinkling and 42 mini rain collectors evenly distributed across the core area to check spatial heterogeneity of the sprinkling intensity.

Moreover, a surface runoff collector was installed across 2 m of the lower boundary of the core area. It was built from a plastic sheet installed approximately 1 cm below the interface between litter layer and Ah horizon of the soil profile. At the downhill end of the sheet, the water was captured by a buried and covered gutter. An in-ground tube was attached to the deepest point of the gutter to conduct the water to a tipping bucket downhill of the investigated area. The tube has been filled with water prior to the experiment to ensure an immediate reaction to the occurrence of surface runoff.

SOIL MOISTURE MONITORING was realised by a network of 16 access tubes for the TDR probes (Trime Pico IPH and T3, IMKO GmbH, Ettlingen), covering a depth down to −1.8 m. Two versions of the TDR sensors were used: two with 12 cm measurement integration over depth (T3) and one with 18 cm measurement integration (Pico IPH). Given a mean penetration depth of the microwave impulse of 5.5 cm and a tube diameter of 4.2 cm this yields an integration volume of approximately 21 and 31 respectively.

Four soil moisture logs were located in the lower half of the core area, the rest was arranged in three diverging transects across the downhill monitoring area (figure 3.11). The three TDR probes were in use to take manual measurements of the installed access tubes, following a flexible measuring routine to cover active soil profiles with higher frequency. Measurements were conducted with 0.1 m depth increments with the sensor head always pointing uphill to avoid influences of local heterogeneity on the elliptical integration volume.

Prior to the experiment, initial soil moisture was measured for every borehole log. Some logs were measured with all three TDR probes to assure their comparability. The time interval between two measurements during sprinkling was about 0.3 h to 1 h. Measurements were continued for 5 h after sprinkling and repeated during the following 2 days until soil moisture was down to approximately initial conditions again.

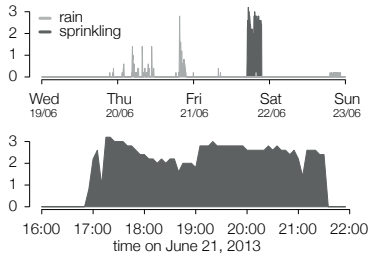

Figure 3.12: Natural rain and irrigation of hillslope sprinkling experiment.

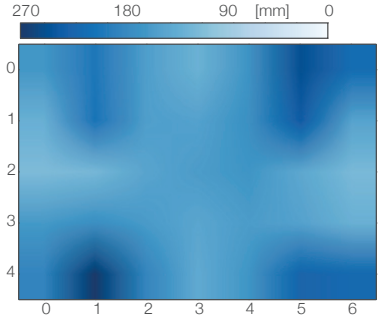

Figure 3.13: Distribution of received total irrigation at mini rain collectors on core area during hillslope sprinkling experiment.

GPR PROFILES have been measured with a similar setup as in section 3.2 (p. 48). Here we used wooden guides across the hillslope for exact repeatability of the 2D profile scanning. Each profile was assessed 8 times before, during and after irrigation. In addition a 3D exploration for potentially hydrologically active structures has been conducted on the hillslope before setting up the experiment.

3.3.2 *Realisation*

The experiment was preceded by a natural rainfall event of 44 mm on moderately dry pre-conditions on June 20th, 2013. Experimental sprinkling on the core area was 170 mm in 4.5 h with only weak fluctuations due to gradual clogging of the intake socket filter (figure 3.12).

The spatial distribution of the sprinkling intensity on the core area was influenced by the sprinkler setup and the slope of the experimental site, resulting in a mean intensity of $38 \pm 9\,\mathrm{mm\,h^{-1}}$ (figure 3.13).

Although surface runoff was recorded with a 20 min time lag from

irrigation start it was negligibly small with less than 0.04 mm (0.02%).

3.3.3 *Soil moisture dynamics*

The four logs on the core area show a rather similar behaviour. Figure 3.14 presents the changes in soil moisture over depth and time for TDR 2. We observed a quick reaction at the bottom which evolves to a strong soil moisture increase in −1.2 m to −1.5 m depth. A similar reaction is observed in the topsoil. However, between −0.5 m to −1 m only after 3 h of sprinkling a weak reaction was recorded which declined immediately after the end of irrigation. Thus water may have largely bypassed here and may have not been bound in the matrix.

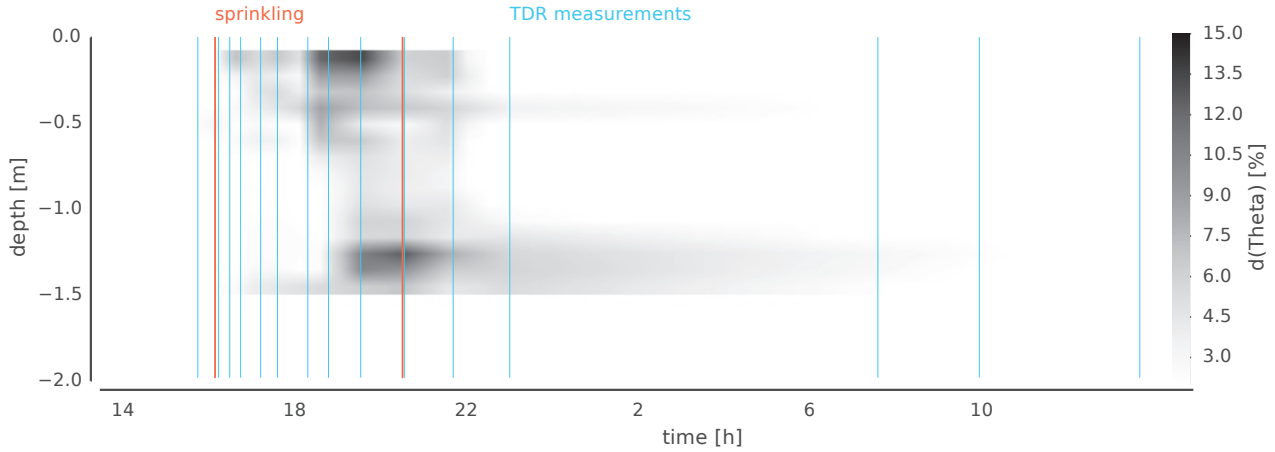

Figure 3.14: Soil moisture dynamics during Holtz irrigation experiment in TDR log 2 on the core area. Change in soil moisture referenced to the pre-experiment state. Linear interpolation between records.

This picture is extended by observed dynamics in most logs and in accordance with the findings from the plot scale earlier. Figure 3.15 presents them.

The other logs at the core area TDR 8 and some layers in TDR 7 and 2 do not at all show any reaction in this increment. At the core area (TDR 7, 2 and 8) the log reacts almost immediately to sprinkling. Although the signal in the top layer is strongest, the quick and remarkable reaction in the bottom layer is noteworthy. The mid layer shows the weakest reaction. Here some areas do not at all react All signals decline quickly after the end of sprinkling, which points to a significant proportion of mobile water. The intermediate decline in top soil moisture after about 100 min may be associated with a slight decrease in sprinkling intensity during this time. It may also be related to the initialisation of structure connectivity since at TDR 7 and 8 no further increase in soil moisture was recorded after that time.

Directly below the rain shield (TDR 9, 3 and 10) reaction in the bottom layer (−1.5 m) is strongest. Despite the onset of reaction varies between 80 min to 200 min the general reaction and quick decline after the sprinkling period is seen in all logs. The mid layer shows the weakest signal. Since no surface runoff was observed, top soil response may be attributed to lateral flow in that layer. The three logs are still very close (0.2 m to 0.5 m) to the core area.

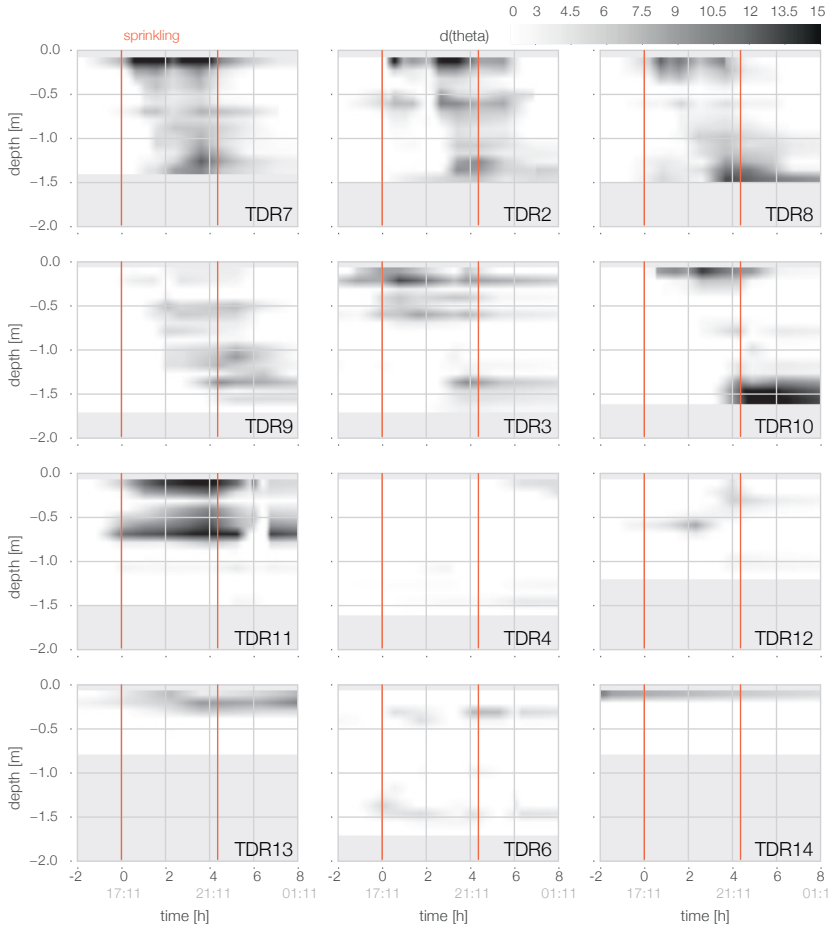

Figure 3.15: Soil moisture dynamics during Holtz irrigation experiment in TDR logs. Columns are downhill direction, rows at the same contour line. For consistency with the time-lapse GPR difference attribute all changes are referenced to the last measurement.

With a distance of 1.7 m to 2.1 m TDR 11, 4 and 12 exhibit a greater ambiguity for the interpretation of the less crisp observations. In general also here a fast reaction of the top layer after about 100 min suggests laterally connective structures for advective flow. TDR log 11 shows a significant signal in the bottom layer (−0.7 m) after about 5 h.

TDR logs 13, 6 and 14 have a distance of 5 m from the rain shield. It remains speculative if the reaction in TDR 13 is due to the sprinkling.

3.3.4 2D time-lapse GPR profiles – GPR inferred trenches

At distances of 2 m, 3 m, 5 m and 7 m four GPR profiles have been measured 9 times before, during and after sprinkling. To identify differences of time-lapse GPR radargrams in structured soils is not a standard procedure. Allroggen et al. [2015] discuss this issue and propose two more robust methods to distinguish amplitude (contrast similarity) and time-shift (structural similarity) variations related to differences between individual time-lapse GPR data sets.

Figure 3.16 shows calculated difference attributes[6] referring to the last scan 24 h after irrigation start. Time labels are referring to the start time of the experiment. The last shown profile 18 h after sprinkling start already exhibits very low difference to the reference. With this we are confident that the difference attributes are detecting mobile water.

I discriminate water from the preceding natural rain event (green), and water from the experimental sprinkling (blue). For each pixel the propagation over time is calculated. As long the values stay constant or decline I consider this to belong to the natural rain event. Once the values start rising by more than 0.05 after sprinkling start they are attributed to our sprinkling experiment.

In addition to the recorded two-way travel time (TWT) the y-axes are labeled with estimated depth derived from measured effective radar velocity of $0.07\,\mathrm{m\,ns^{-1}}$ and the sampling rate of 0.2 ns. This estimate assumes static conditions of the air-water-soil system which especially means no existing of any wetting front.

[6] The derivation of the difference attribute matrices has been done by Niklas Allroggen (UP). This contribution in gratefully acknowledged.

At PROFILE 1 the radargrams at sprinkling start and the reference show only very low difference. This may also clarify the noise-level for our experiment. Before that water of the storm event is still mobile. After about 3 h a strong signal occurs at the western edge of the profile (near TDR log 12) in −1.3 m depth. Some more structures in about −3 m depth start to react. After 5.25 h directly after the sprinkling period the maximum is reached with distinctly reacting structures which generally slowly decline during the next 1.5 h. Nevertheless some structures only appear at time 6:43h.

PROFILE 2 shows storm water until 1.5 h after sprinkling start. In the next scene at time 3:20h the difference attribute generally is at the noise level with some newly activated structures. From here on more reaction especially in a depth around −2.5 m establish and increase.

PROFILE 3 has an even longer trace of the natural storm water. This makes it more difficult to really identify structures which reacted due

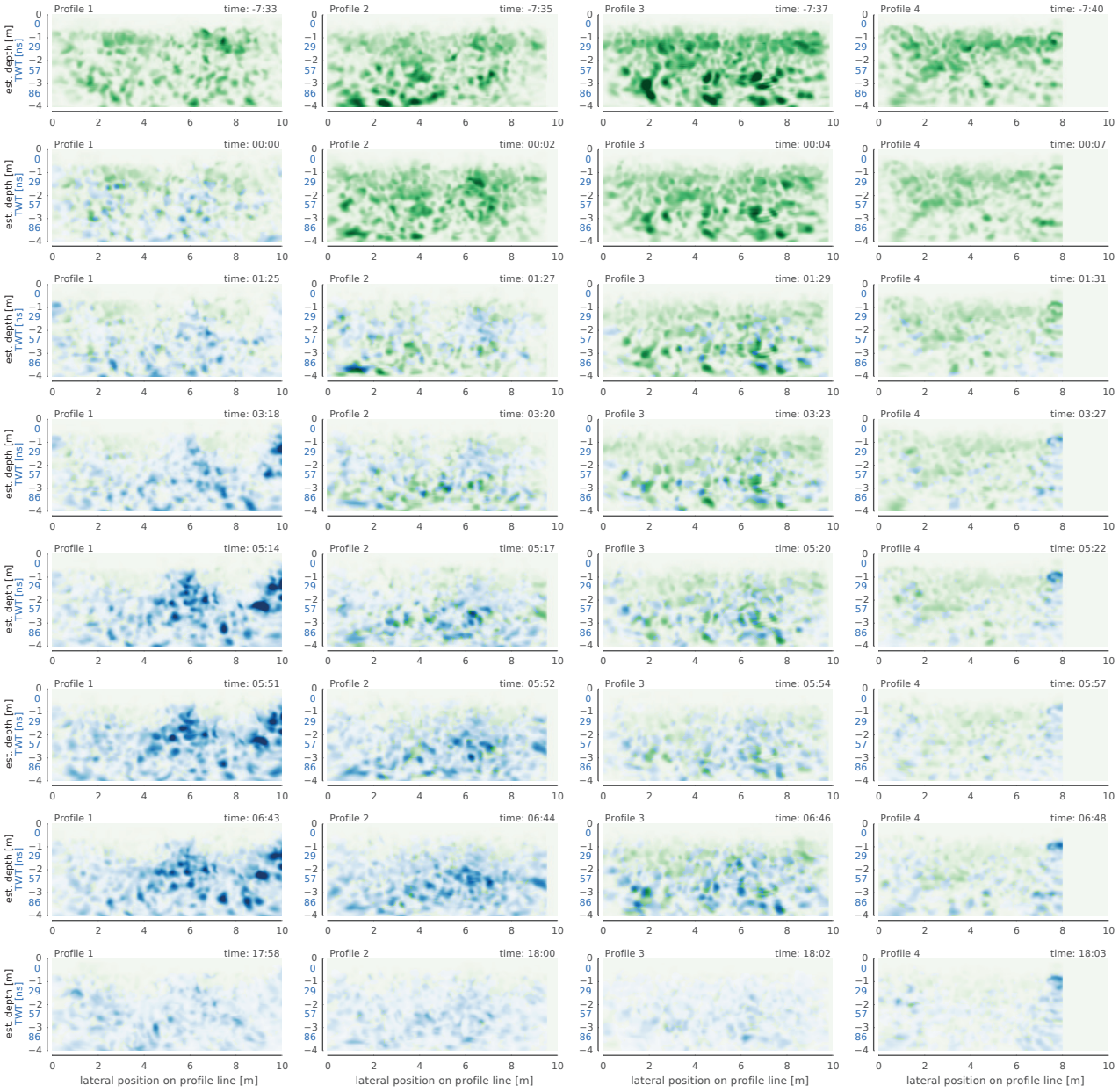

Figure 3.16: Time-lapse GPR profiles at Holtz sprinkling experiment. Difference attribute referenced to last radargram 24 h after the experiment (mobile water in flow structures). Water from the preceding natural rain event (green) is identified by declining difference intensity. Water from the experimental sprinkling (blue) is identified by a rise of the difference attribute > 0.05 after sprinkling start. Within one column the rows give a sequence over time. Columns proceed downhill.

to the sprinkling. However, with a minimum difference at time 5:53h and a strong increase to the next scene 50 min later falls in line with the general observation.

At PROFILE 4 the reaction to the natural and experimental forcing is generally low, when relying on the GPR difference attributes. This may be best interpreted as low deviance from the reference state. Either the mobile water shows relatively few dynamics (in total mass over time) or water is less confined to specific structures. Overall, the experiment does not appear to have effected this profile much. The apparent re-activation of a structure at the very western edge of the profile is equally vague and could be caused by fringe effects.

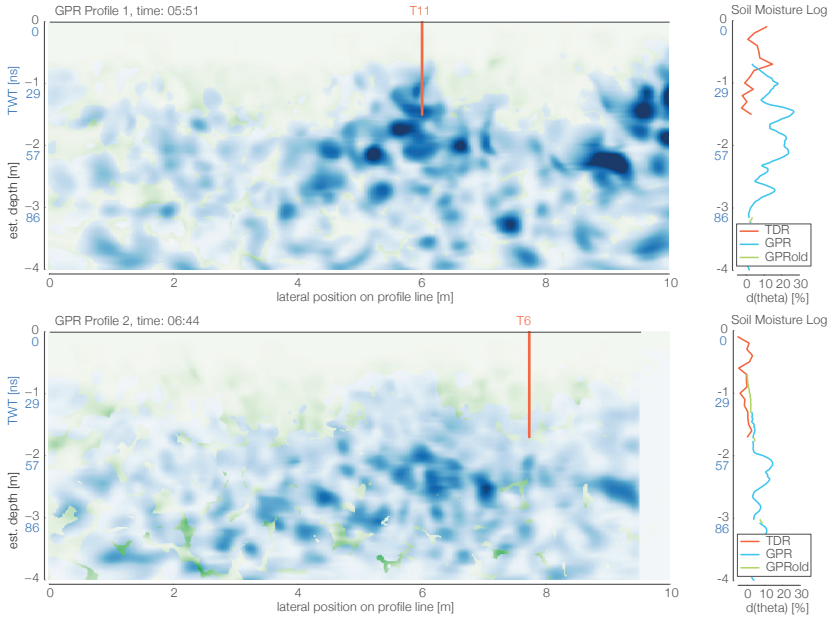

Figure 3.17: Time-lapse GPR profiles at Holtz sprinkling experiment with soil moisture log position (left). Measured soil moisture and referring GPR difference attribute log (right). GPRold refers to pre-experiment water (green) and GPR to new changes in soil moisture (blue). The GPR signal is arbitrarily scaled. Top: Profile 1 at 5:51 h with TDR log 11. Bottom: Profile 2 at 6:44 h with TDR log 6.

3.3.5 *Combining TDR and GPR*

With the given situation of observed soil moisture logs (quantitative) and GPR inferred trenches (qualitative) a combination of both suggests itself. Figure 3.17 shows, that both signals represent the situation in accordance. Although direct conversion of the difference attribute to soil moisture and vice versa is not feasible, at locations with low reaction (TDR6) both signals show no reaction while the preferential paths (TDR11) are causing distinct spikes in the logs.

To go into more detail of the derived data figure 3.18 presents the temporal dynamics of TDR log 11 and the nearest vertical log in the GPR profile. Although the temporal dynamics of the observed

maxima of the logs over time correspond well, the overall position of these reacting structures remains uncertain.

Because any device and tube directly at the GPR profile would massively disturb the GPR signal, we have to work with some spatial and temporal distance between logs and profiles (figure 3.11). With the given dependency of the radar velocity on soil moisture more interpretation needs precaution as the spatial overlap of both methods is limited and the connectivity of the observed structures unknown. I will discuss the issue in section 5.1.2 (p. 101).

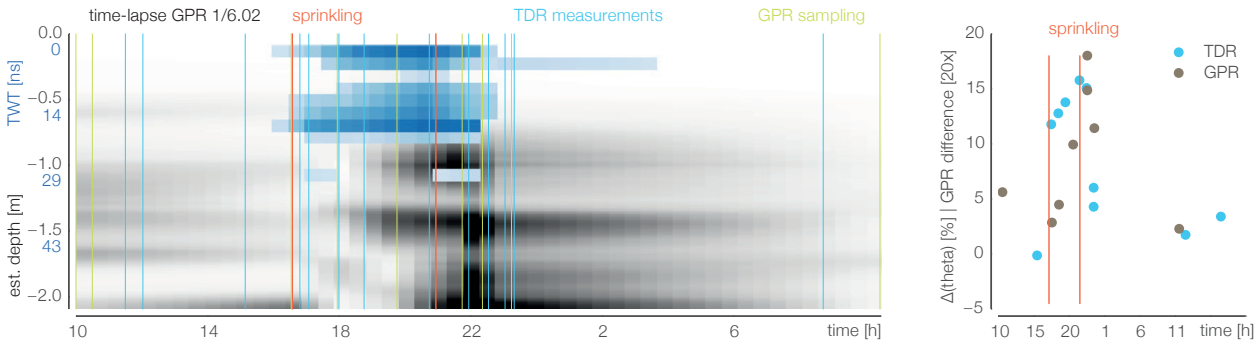

Figure 3.18: Time-lapse of GPR and TDR log at Holtz sprinkling experiment. Left: Temporal dynamics of soil moisture (TDR log 11, blue) and GPR difference attribute (grey). Right: Observed maximum at GPR and TDR logs over time.

3.3.6 *Identification of flow structures*

With the given experiment the identification of specific active flow paths was possible through 2D time-lapse GPR and difference attribute identification of different radargrams. During initial exploration and the installation of the experiment the existence of preferential flow structures was known already. Drilled soil cores suggested a first layer in about $-0.8\,\mathrm{m}$ and a second in approx. $-1.7\,\mathrm{m}$ depth. The general location of such structures at the hillslope scale was identified based on a 3D GPR survey and is given in 3.19.

However the rough estimates contrast the observed structures, which have been relatively well confined at a scale of few centimetres. In figure 3.16 especially profile 3 at time -7:33h and profile 1&2 at time 5:50h exhibit such structures for the natural and the experimental event respectively. A comparison reveals that hydrologically relevant structures in the given young soils and periglacial deposits cannot be identified without an assessment of their reaction to forcing.

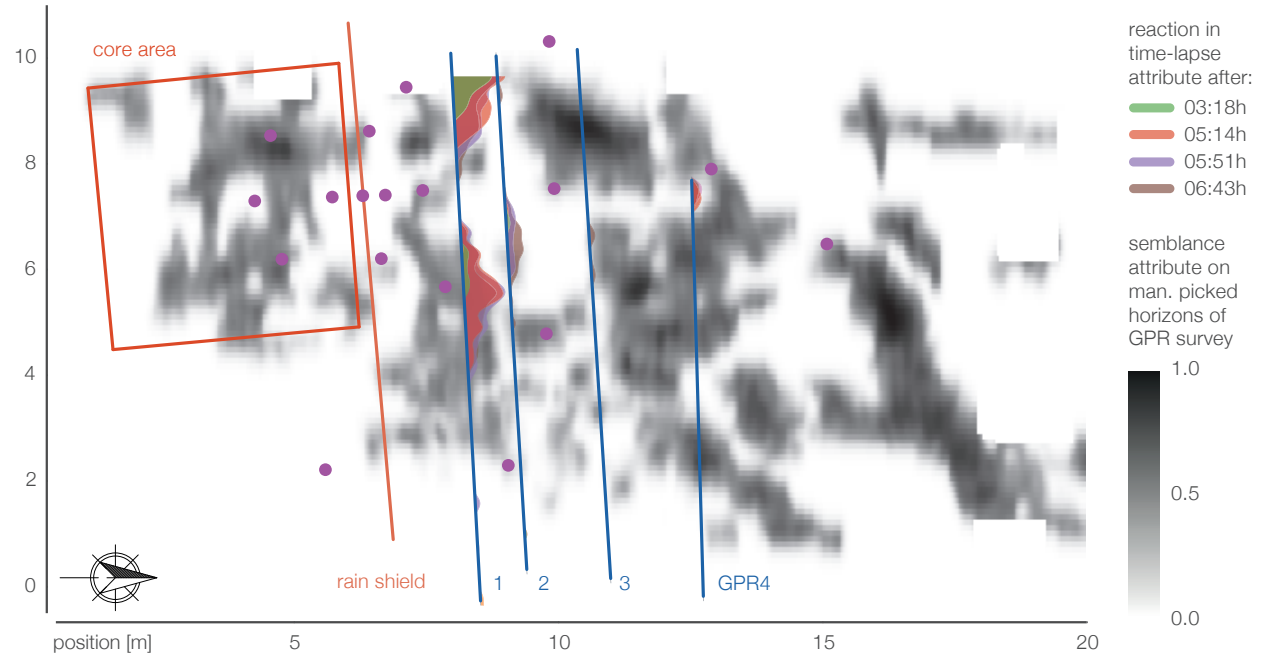

Figure 3.19: Structure identification based on 3D GPR survey and reaction on profile lines in hillslope sprinkler experiment. Greyscale patches: Picked horizons in 3D data cube supported by similarity attribute of semblance in dip steering cube. Quadratic values of attribute as greyscale. Notice that the depth information is neglected. Along GPR profile lines: Identified amplitude of time-lapse difference attribute of sprinkler water (see figure 3.16) accumulated over depth (−0.7 m to −2.5 m) at the given reference times after the start of the experiment. Spatial axes in m.

3.3.7 *Intermediate conclusions from the hillslope experiment*

The combination of plot and hillslope observation enabled us to identify vertical and lateral advection. With the experiment relatively well-controlled conditions for the observation of lateral flow paths were created.

Time-lapse GPR was proven as alternative, non-invasive trenching method. Although important as local reference and quantitative observation, the dense network of TDR logs alone could not fully capture and describe the lateral processes.

The experiment adds to the examples of diffusive and advective flow. About 50% of the irrigated water has not been captured by the matrix at the core area. However it is still not fully clear whether or not the lateral processes cause the quick reaction of the catchment, because much of the advective water was captured in the structures or probably lost to greater depth.

4
Simulating rapid flow in subsurface structures - linking observables and model structure in a Lagrangian model framework

4.1 Introduction

As discussed in the introduction (p.12) current models are limited by the attribution of advective and diffusive flow to an effective hydraulic conductivity, a lack of spatial explicitness in dual domain approaches or strongly conceptual assumptions about the interaction between a fast and slow domain.

This chapter presents the development of an alternative model framework which treats soil water flow by means of a space domain random walk of water particles. I hypothesise (H1) that this is already feasible for the case of pure matrix flow, because the Richards equation in the soil moisture based form is equivalent to a non-linear convection-dispersion equation [Jury and Roth, 1990] with a trivial advection term (drift term) describing gravity driven water flow. This implies that a simulation with a Richards solver and stochastic simulation with the corresponding non-linear random walk step equation should yield the same results (within the margin of numerical errors). As lumped 1D representation (H2) diffusive-advective flow in an apparent macropore system is simulated by adding a non-trivial stochastic advection term to the random walk step equation. To our knowledge similar Lagrangian approaches were only followed by Ewen [1996] and Davies et al. [2011].

The main objectives of the proposed approach are to a) simulate the fingerprint of preferential flow in the travel distance probability density function (pdf in the following) of water (and optionally so-

lutes) scale independently as long as the ensemble with respect to the forcing, soil and macropore structure remains the same and b) base the parameterisation strictly on field observables.

The non-linear diffusion parameter and trivial advection term are estimated based on soil water characteristics. The pdf of advective flow velocities in the macropore system are retrieved from tracer travel depths or travel time distributions obtained by plot-scale sprinkler experiments as specified in section 4.4.2 (H3a) or even more simply based on values reported in the literature (H3b). The related macropore density and depth distributions may be estimated either from direct mapping, analyses of dye staining or time lapse GPR using image analysis, or even through using predictions from species distribution models as in the case of biotic macropores [Palm et al., 2012].

Current model approaches for macropore flow preserve either the topology of the macropore network by explicit representation of macropore structures, with the drawback of not accounting for local disequilibrium. Or they account for local disequilibrium by treating matrix and macropore flow in separate continua, with the challenge to describe their exchange based on non-observable parameters and the drawback of smearing out the localised macropore topology into a continuum [Gerke, 2006, Zehe et al., 2014]. In the forthcoming rejection of H2 I develop a representative, structured domain (H4) as least adequate delineation of observed topology and macropore-matrix exchange.

Referring to the framework for improving model structural adequacy Gupta et al. [2012], Gupta and Nearing [2014] this study is structured along an iterative learning process to develop a model concept that shall ideally merge the strength of double domain and explicit approaches and thereby avoid the use of non-observable parameters for macropore-matrix exchange.

An overview about the iterative model development is given in table 4.1. In each step I state the model theory and structure as a hypothesis and test the model against an experiment. The next iteration presents a successive refinement of the model and its test against a suitable benchmark experiment.

H1 Within the first iteration I present the basic model concept and compare our first 1D model version with observations and Richards solvers for diffusive flow.

H2&H3 The second iteration introduces an additional stochastic drift term for lumped representation of advection and diffusion. Advection is informed by observed advective velocity distributions inferred from plot scale sprinkler experiments. Diffusion relies on pedo-

Iter	Model	Aspect	Experiment	Hypothesis	
I	1D diffusive RW	comparison against observation and Richards solvers	nocturnal redistribution after storm event (Weiherbach)	space domain random walk of water particles feasible to simulate soil water flow	H1
II	1D RW with additional stochastic drift term	determination of v from tracer profiles comparison w/ experiment	plot-scale sprinkler experiment with Br- and Brilliant Blue (Weiherbach)	lumped 1D diffusion-advection sufficient to reproduce flow fingerprint advective velocity PDF from tracer recovery profiles	H2 H3
IIIa	echoRD model w/ single macropore	macropore-matrix exchange lateral diffusion	sandbox experiment with "artificial macropore"	structured domain with macropore-matrix exchange capable	H4 X
IIIb	echoRD model w/ well-defined macropores	testing of process hypotheses simulation of experiment	sprinkler experiment (Weiherbach, loess soils, earthworm macropores)	representative, structured domain feasible, test of process-hypotheses	H4 XIF
IIIc	echoRD model w/ losely-defined macropores	testing of process hypotheses simulation of experiment	sprinkler experiment (Attert, young soil, periglacial cover beds)	application to different macroporous structures with model preprocessor	H4 XIF

Table 4.1: Overview about model iterations, referenced experiments and hypotheses H1-H4. Letters X,I,F stand for the process hypotheses for macropore-matrix exchange, infiltration and film flow respectively. The colors in the right column indicate success of the test.

physical parameters.

H4 The third iteration provides a detailed description of the final echoRD model (eco-hydrological particle model based on representative structured domains) which relies on two representatively distributed exchanging but spatially explicit domains. I present a successive test of the model concept and hypotheses: a) macropore-matrix interaction and lateral diffusive flow, b) simulation of a sprinkler experiment under well-defined conditions, and c) simulation of a sprinkler experiment under less well-defined conditions.

The chapter first introduces additional experiments. It then follows the iteration cycles with methods and results. A discussion is given in section 5.2 combining findings from experiments, methods and results.

4.2 *Experimental references – Linking observed tracer travel depth and macropore density distributions to advective velocities and exchange processes*

As introduced, macropore settings can be very different with respect to their topology, their temporal dynamics and their interface characteristics. The multitude of different ecohydrological influences, structure formation and system organisation has been explored in the previous chapters.

In addition to the Attert data set I reference the model development to data from the Weiherbach experimental basin [Zehe and Flühler, 2001, Klaus and Zehe, 2010] – a hilly loess area in south-west

Germany with agricultural use (not to confuse with the Weierbach headwater catchment in the Attert basin). The relatively homogeneous soils exhibit mostly macropores created by earthworms. The data set comprises long-term hydro-meteorological monitoring, pedo-physical analysis, findings from sprinkler experiments and macropore network characteristics.

Moreover I introduce an artificial macropore experiment of Germer and Braun [2015], Stadler et al. [2014] addressing macropore-matrix interaction and lateral diffusion as reference for macropore-matrix exchange and lateral diffusion. The experiments and model iterations will provide means to derive a comprehensive domain and process abstraction with respect to processes, exploration and modelling. At the end of the forthcoming iterations our model concept shall ideally avoid the use of non-observable parameters for macropore-matrix exchange.

Table 4.2: Pedo-physical van Genuchten parameters for the modelled soils in this chapter.

Sample	k_{sat} [m s^{-1}]	θ_{sat} [m^3 m^{-3}]	θ_{res} [m^3 m^{-3}]	α [m^{-1}]	n [-]	depth [m]
Attert_1	1.0E-04	0.7160	0.01	4.12	1.26	-0.1
Attert_2	3.0E-04	0.6617	0.00	7.50	1.22	-0.2
Attert_3	9.0E-04	0.6370	0.00	8.58	1.22	-0.3
Attert_4	1.6E-03	0.6315	0.00	6.70	1.24	-0.4
Attert_5	6.0E-04	0.5273	0.00	4.84	1.20	-1.2
Weiherbach_1	5.00E-05	0.4	0.04	1.9	1.25	-0.3
Weiherbach_2	3.70E-05	0.43	0.11	3.8	1.2	-1.2
Column_Sand	5.83E-05	0.336	0.071	0.015	15.0	-1.1

4.2.1 *The alternative in case of biopores – map the worm burrow system and measure water fluxes in worm burrows*

Zehe and Bloschl [2004] proposed an alternative approach to estimate the travel velocities in macropores based on a mapping of the surface density and depth of macropores of different radii and measurements of water flow through soil samples containing macropores in the lab. This approach is, however, only feasible if the macropore system consists solely of anecic earthworm burrows in soils with a high aggregate stability such as Loess soils.

The Weiherbach data set[1] contains such macropore observations and similar plot-scale sprinkler experiments. In contrast to the experiments presented above, this one was not designed to explore the hydraulic capacity of the macropore system but the rapid mobilisation of herbicides. This sprinkler experiment was conducted at a 1 m^2 plot with a cumulative irrigation of (25 mm in 2 h) 21 mm in

[1] This data has been part of the Weiherbach project [Zehe, 1999, Plate and Zehe, 2008]. I thankfully acknowledge the provision of this data as thorough reference for the model development.

1.3 h with a KBr tracer concentration of $0.165\,g\,l^{-1}$ and $4\,g\,l^{-1}$ Brilliant Blue. Excavation was also carried out after one day, however, the sampling took place in a 0.1 m grid at two profiles. The macropore system and its hydraulic capacity was observed as spatial density of macropores of different radii and their respective depth distribution [Zehe and Bloschl, 2004].

4.2.2 *Artificial macropore experiment addressing macropore-matrix interaction and lateral diffusion*

To reduce the ambiguity in exchange processes in the experiments I reference macropore-matrix exchange and lateral diffusion to a laboratory experiment of Germer and Braun [2015], Stadler et al. [2014][2].

A single 0.01 m wide "artificial macropore" (filled with coarse sand for stability) in a 1.2 m tall and 1 m wide half cylinder of homogeneous fine sand is irrigated over 24 h at a constant flow rate of $3.81\,h^{-1}$. A camera and 24 tensiometers (T5 UMS GmbH Munich) monitor the experiment. Figure 4.1 illustrates this experimental setup of of Germer and Braun [2015].

[2] This experiment is one of a series of tests performed by Kai Germer and colleagues at the Institute for Modelling Hydraulic and Environmental Systems, Stuttgart University. The provision of the data is gratefully acknowledged.

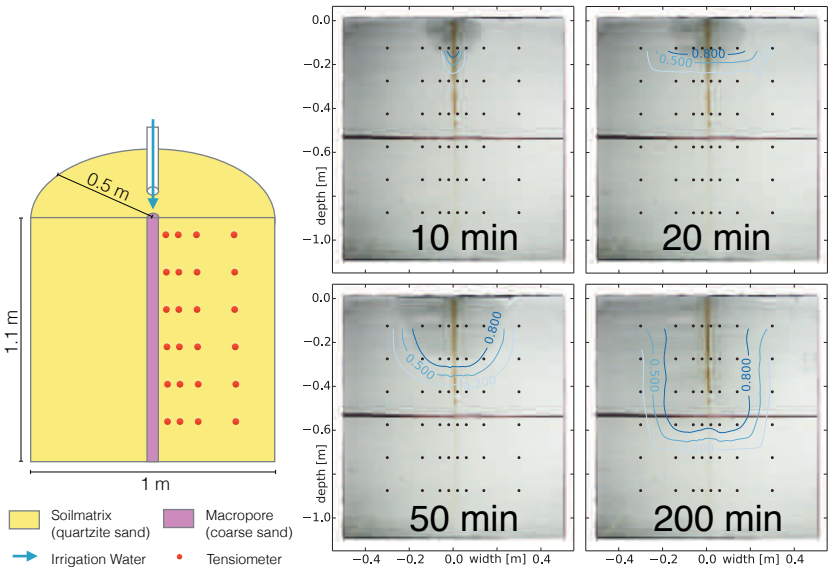

Figure 4.1: Artificial macropore experiment of Germer and Braun [2015]. A single 0.01 m wide macropore (filled with coarse sand for stability) is placed within a quartzite sand packed half-cylindrical container. During the experiment only the macropore is irrigated with $3.81\,h^{-1}$. Soil water propagation is monitored with 24 tensiometers and visually at the fibre-glass face. Right: Observed dynamics of the wetting front with contour lines of interpolated soil moisture measured with tensiometers.

As shown in figure 4.1, lateral diffusive transport – although in an artificial substrate – dominates water redistribution. Exfiltration from the irrigated "artificial macropore" must be at higher rates than percolation at the given intensity of $3.81\,h^{-1}$. Note, the flow in the artificial macropore is in fact also matrix flow and thus diffusion with highly increased saturated hydraulic conductivity compared to

the surrounding matrix. Although the experimental setup has some limitations (e.g. operates as an open water balance for the first hours of the experiment in which we are most interested), it does provide nevertheless a valuable benchmark for the revised model with respect to lateral exchange among a localised fast and a surrounding slower domain. It model will be qualitatively referred to it in section 4.7.1.

4.3 *First order iteration – Lagrangian model for diffusive water flow in the soil matrix*

4.3.1 *A 1D non-linear space domain model*

Particle tracking is usually employed for simulating advective dispersive transport of solutes, but not for the water phase itself [e.g. Delay and Bodin, 2001, Metzler and Klafter, 2004, Berkowitz et al., 2006, Koutsoyiannis, 2010]. Thus, most random walk applications rely on a continuous time domain representation as it performs well at minimum computational cost [Delay et al., 2008, Dentz et al., 2012]. This approach is, however, not feasible when the diffusivity itself depends on the particle density as is the case for water particles. I thus employ a non-linear random walk of water particles in the space domain. Our first iteration is a 1D vertical space domain which does not distinguish between the fast macropore and the slow matrix domain. Similar Lagrangian approaches were also followed by Ewen [1996] and Davies et al. [2011] at larger scale.

The starting point for my theory is the Richards equation in the soil moisture based form:

$$\frac{\partial\theta}{\partial t} = \underbrace{-\frac{\partial}{\partial z}k(\theta)}_{u(\theta)} + \underbrace{\frac{\partial}{\partial z}\left[k(\theta)\frac{\partial\psi}{\partial\theta}\frac{\partial\theta}{\partial z}\right]}_{D(\theta)} \tag{4.1}$$

The first term corresponds to a trivial drift term $u(\theta)$ characterising downward water fluxes driven by gravity, the second term represents diffusive water movements driven by the soil moisture gradient and controlled by the diffusivity, $D(\theta)$, of soil water:

$$D(\theta) = k(\theta)\frac{\partial\psi}{\partial\theta} \qquad \text{and} \qquad u(\theta) = k(\theta) \tag{4.2}$$

Soil water content and related particle density

The soil water content as a function of depth is represented by the density of water particles, which are constant in mass (and volume at this stage). Interaction between the particles such as exchange of contaminants, heat and momentum or bulking of particles to larger entities is not considered yet. Particles are chosen to be small enough

to suit the selected model domain and grid size, which is necessary for calculating particle densities and thus D, through a model parameter.

Particle density is calculated by accounting for the depth distribution of the particles. It is then referred to the respective soil properties (θ_s, van Genuchten parameters) for state determination. In the first example I assume that the resolution is sufficiently fine at a maximum number of 500 particles per grid increment of 5 mm resulting in a particle mass $m_{particle} = 6\,\mu g$.

Non-linear random walk equation for water particles

Water particles may move in a random manner controlled by the diffusivity $D(\theta)$ and advectively based on a re-sampling from either an advective velocity distribution derived from tracer data (compare next subsection) or based on u. Since $D(\theta)$ depends on soil moisture and thus the particle density as well as on the soil water retention curve, diffusivity is neither constant over the time step nor constant along the soil profile. This requires short time stepping or a predictor corrector scheme to allow for updating. A spatially non-uniform diffusivity requires a correction of the drift term, since the Fokker-Planck-Equation and the convection-dispersion equation are not equivalent Uffink [1990], Uffink et al. [2012], Kitanidis [1994], yielding the Itô random walk step scheme:

$$z_{t+\Delta t} = z_t + \left[u(\theta_{z,t}) + \frac{\partial D(\theta_{z,t})}{\partial z_t}\right]\Delta t + \xi\sqrt{2D(\theta_{z,t})\Delta t} \tag{4.3}$$

Both the diffusivity D and the drift term u are parameterized after Van Genuchten [1980] with eq. 4.2. Alternatively, Kutìlek and Nielsen [1995] derives D from the retention curve model as eq. 4.4:

$$D(\theta_E) = \frac{k_s(1-m)\theta_E^{1/2-1/m}}{\alpha m(\theta_s - \theta_r)}\left[(1-\theta_E^{\frac{1}{m}})^{-m} + (1-\theta_E^{\frac{1}{m}})^{m} - 2\right] \tag{4.4}$$

$$\text{with:} \qquad \theta_E = \frac{\theta - \theta_r}{\theta_s - \theta_r} \tag{4.5}$$

As such I can solve D as a function of the particle density and use this in the random walk equation.

4.3.2 *Comparing the Lagrangian model to the Richards equation in the case of pure matrix flow – Nocturnal diffusion in Loess soil after storm event*

In this first benchmark I evaluate the first version of the Lagrangian model against soil moisture dynamics observed during pure matrix flow conditions. I propose that nocturnal diffusion in the top

soil shortly after a rainfall event is likely to be neither influenced by preferential flow nor by soil evaporation. Thus soil moisture data observed at 3 cm, 10 cm, 20 cm, 30 cm and 40 cm depth in a Loess soil profile located in the Weiherbach catchment for a period after a 78.6 mm storm event is selected. In addition the redistribution was irritated by a small second rain event of 2.5 mm 2.8 h after the storm.

I simulated soil moisture dynamics for this period starting with observed initial conditions 21:35 h on June 27, 1994 until 06:00 h the next day. The Lagrange model and two solvers of the Richards equation (SimpegFlow, https://github.com/simpeg, [Cockett et al., 2015] and a simple predictor-corrector solver) both after Celia et al. [1990] in the potential form were parameterised according to pedophysical characteristics measured within this soil profile (compare table 4.2). All models were operated at a constant spatial grid size of 0.05 m either to solve the Richards equation or to calculate soil moisture dynamics based on particle density dynamics. Particle size was chosen to be equivalent to 6 µg amounting to 12000 over the profile. All rainfall infiltrated as advective phase. The top boundary condition of the Richards solvers was updated to the state of the Lagrange model in the case of infiltrating particles at each output time step of 1 min.

The comparison of simulated and observed soil moisture dynamics is given in figure 4.2 A-C. It reveals that the particle solver performs not only not worse but even slightly better than the Richards solver. Infiltration of the additional event is primarily overestimated in the top soil. However the Lagrange model quickly resembles the observed drying curve as the fast new particles drain deeper.

Transport of water particles was in both cases strongly dominated by diffusive mixing as corroborated by Péclet numbers around 0.05. As soon the advective phase appears, these numbers rise well above 10 - but only for less than 1% of the particles. In addition to the soil moisture profiles, the Lagrange model allows insights in the particle composition (figure 4.2 A-C, right panels).

Overall, I may thus state that the proposed approach to simulate soil water dynamics by means of a non-linear space domain random walk (H1) is a feasible and mass-conservative alternative to the Richards equation in the case of pure matrix flow i.e. low Péclet numbers. To reproduce these results, use `1D_test` in the repository.

4.4 *Second order iteration – stepping to structured soils and macropore flow*

The main objective of this second iteration step is to confront the Lagrangian model developed and successfully tested in the previous

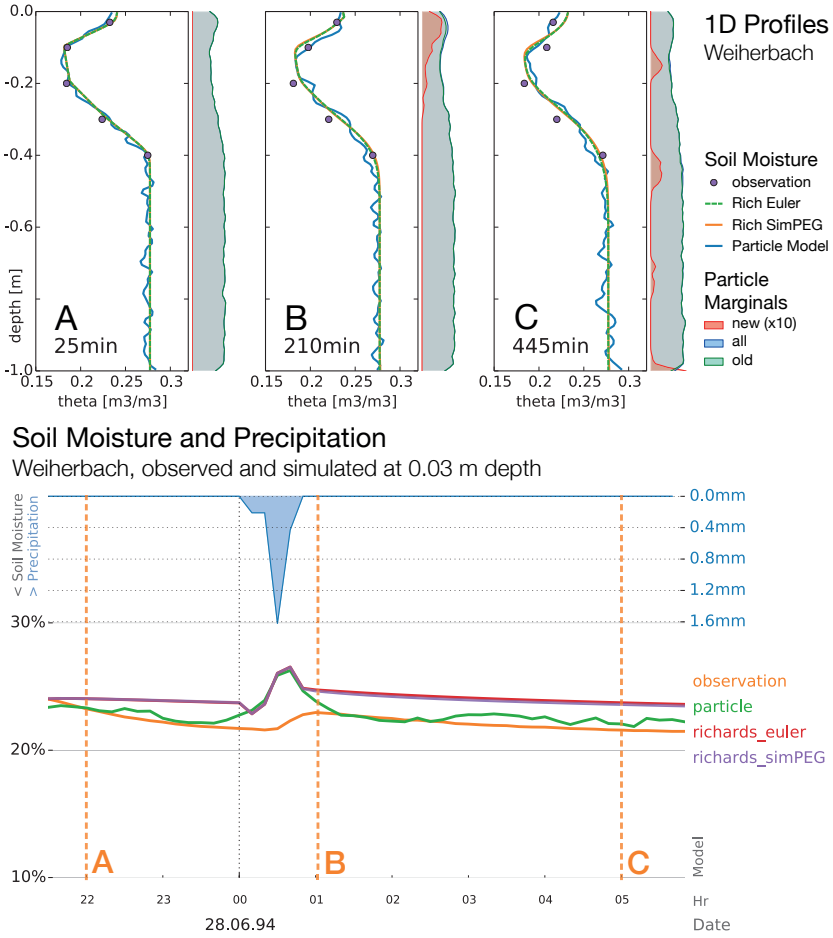

Figure 4.2: Simulations of nocturnal diffusion after a 78.6 mm summer storm event in a Loess soil profile (Weiherbach basin). **Top:** Soil moisture profiles simulated with the Lagrangian model (blue), the Richards solvers (green and yellow) as well as observed soil moisture (purple dots) at three instances. Particle density and composition over depth are shown in each right-hand panel. The graph of new particles is amplified by a factor of 10. **Bottom:** Time series of observations and simulations in the top soil at 3 cm depth. Marked times for top profiles.

step with macroporous soils. This requires suitable experiments characterising rapid flow in structured soils as discussed in subsection 4.2 as well as inclusion of an additional stochastic drift term into the random walk.

4.4.1 *Rapid macropore flow in the 1D Lagrangian model*

As a first attempt I implicitly represent the macropore system in a lumped 1D model concept as advective particles, which draw their velocity from the observed pdf (section 3.1.3, p.43). Depending on observed recovery, a certain fraction of infiltrated precipitation can be assigned as advectively active.

Advective movement of water particles in the macropore volume is represented by adding a second stochastic drift term to the random

walk step equation (Eq. 4.3) as given in Eq. 4.6:

$$z_{t+\Delta t} = z_t + \left[u(\theta_{z,t}) + \frac{\partial D(\theta_{z,t})}{\partial z_t}\right]\Delta t + \xi\sqrt{2D(\theta_{z,t})\Delta t} + v\Delta t \qquad (4.6)$$

This advective velocity v is one realisation of the pdf derived from a tracer recovery profile. The several columns are treated as separate stochastic stream tubes avoiding lateral averaging. For the 1D version I assume that infiltrating rainfall event water, which is represented by new particles in the model, enters the macropore volumetric fraction exclusively until its capacity is reached. New particles are randomly assigned to a stream tube, start and keep on traveling at an advection velocity, which is randomly drawn from the travel velocity pdf defined in Eq. 3.2 (p.43) and kept constant. This builds on our assumptions that a) infiltration into macropores dominates during rainfall driven conditions, b) macropore flow consists predominantly of event water and c) that there is negligible lateral mixing in the rapid flow volume during the transport event. Pre-event water particles move diffusively and with the trivial drift term as specified in Eq. 4.3.

4.4.2 *Lumped Lagrangian model to reproduce a sprinkler experiment*

As a second benchmark the 1D model is used to reproduce a plot-scale sprinkler experiment on the Weiherbach data set with the same setup as the first benchmark (section 4.3.2). Figure 4.3 presents the simulated depth distribution of irrigated particles (blue lines) compared to two observed tracer profiles (orange lines). To reproduce these results, use `1D_sprinkler` in the repository. The model resembles the observed tracer profile after 2 h which is as expected, since the model draws its advective velocity for irrigated particles from the given depth distribution of tracer concentrations at a estimated fixation time of 2.3 h. However, percolation continues during further simulation. The same phenomenon can be observed in figure 4.2B and C. Although the 1D Lagrange model is capable of also simulating rapid flow, some exchange parameter for decreasing advection velocities due to the increasing influence of lateral mixing is required. Davies et al. [2011] solve this issue by means of a particle interaction or mixing parameter.

A single mixing parameter cannot account for the multiple concurring influences. Conceptually it is also apparent that an 1D approach can neither resolve the topology of the macropore system, nor account for local disequilibrium conditions, nor cope with dynamic interaction of the different pathways. At the end of the forthcoming iterations, therefore, my model concept shall ideally meet the initially listed requirements and thereby avoid the use of non-observable parameters for macropore-matrix exchange.

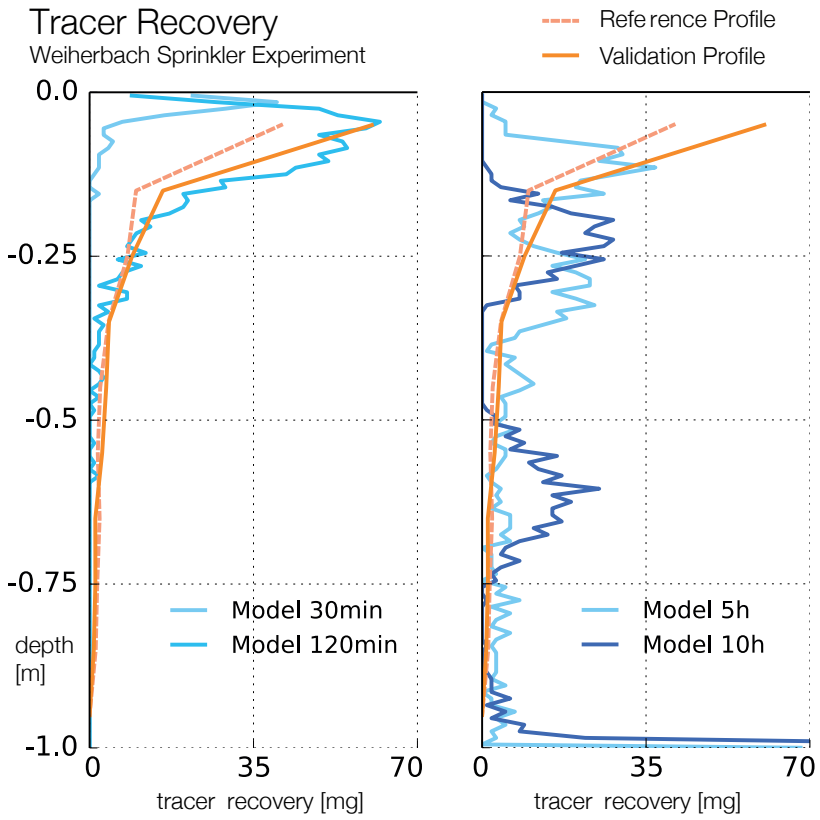

Figure 4.3: Simulated and observed tracer profiles of the Weiherbach sprinkling experiment for the time steps 30 and 120 min (left) and 5 and 10 h (right). Tracer recovery profile (yellow line) and simulations with the 1D random walk model including advective drift term (blue lines). Advective velocities estimated from tracer depth distribution of a second reference profile profile (dashed yellow line) with fixation time t_{fix} set to 2.3 h. Observed tracer recovery profile is captured after 2 h simulation. However, further simulation overshoots the observations.

The rejection of H2 calls for a revision of our lumped model concept towards several interacting domains.

4.5 *Third order iteration – extending the model concept to 2D, multiple domains and pathway interaction*

Although rapid flow in soil structures happens under far from well-mixed conditions, water does not simply bypass the soil matrix without any interaction. In contrast, I suggest that interaction with the surrounding matrix may be the central control for the dissipation of the advective momentum. This third iteration presents a largely extended model concept with regard to pathway interaction by introducing multiple topologically explicit 1D rapid flow domains and a representative 2D diffusive flow domain. This final version is named the echoRD model (eco-hydrological particle model based on representative structured domains).

4.5.1 *Revised model concept and underlying assumptions*

We propose a generalisation of the different rapid flow processes (section 4.2) based on the following hierarchy of assumptions:

1. The macropore density and topology exerts a first order control on the deviation of the flow process from laterally well-mixed flow conditions.
2. As advective flow is driven by gravity and thus has a unit gradient, it is mainly controlled by dissipative losses. The drainage capacity of the macropore system is hence crucially determined by the cross-sections and lengths of connected flow paths.
   - 2.1. In the case of wet conditions dissipation of kinetic energy is mainly determined by tortuosity and configuration of the macropore network, which dominates over minor exchange with the surrounding matrix. Thus mechanic friction controls advective flow velocities.
   - 2.2. In the case of dry conditions, the kinetic energy of advective flow is additionally dissipated through mass exchange with the surrounding matrix, which limits and stops advective flow at a certain stage.
3. A representative 2D matrix domain with topologically explicit (but flexible) connected 1D rapid flow elements is a reasonable abstraction balancing generality and specificity.

To illustrate the first assumption one may imagine two hypothetical cases: 1) A given soil volume exhibits one single macropore and low diffusivity. The contrast in velocities and the long mixing-distance from the macropore will likely lead to distinctly different flow regimes, where interaction might be negligible. 2) A soil volume possesses a high density of macropores and high diffusivity. Infiltrating water will quickly be mixed laterally and reach the full domain extent. This likely leads to an accelerated apparent diffusive flow describable as a single regime with an effective parameter. In most cases one may find an intermediate setting.

The exchange 2.2 is associated with a depletion in the matrix potential gradient between the interface and the surrounding matrix, which in turn implies a reduction in free energy of the surrounding soil and production of entropy [Zehe et al., 2013].

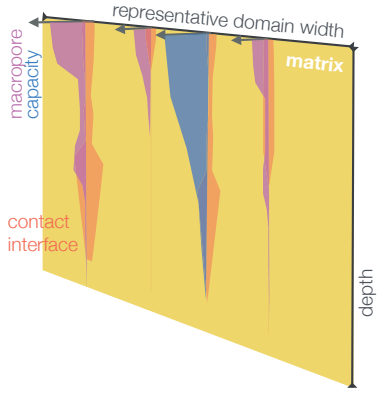

Figure 4.4: Representative macropore-matrix domain. A 2D matrix with cyclic lateral boundary hosts several 1D macropores with their respective capacities, interfaces and lateral distributions.

The representative macropore-matrix domain

I define a representative macropore-matrix domain with explicit topology as illustrated in figure 4.4. Soil matrix is projected as periodic 2D domain with a cyclic lateral boundary. Macropores are

represented as vertical 1D elements linked to the matrix. As there is usually no information about spatial clustering of macropores, they are placed at random distances according to observed densities. Given the cyclic lateral boundary of the matrix domain, it is not the macropore positions but their relative distances that matter. The minimum density of the macropores at a given depth determines the lateral extent of the domain. One may also chose to take a multiple of the least representative as setup for instance to describe interactions with less densely occurring structures such as occurs with subsurface pipe flow.

The 2D soil matrix possesses a grid for particle density calculation. The 1D macropore domains have an internal grid with a lag of one particle diameter for water film calculations. In addition, the 1D macropore domains have an interface area with the soil matrix domain. In this area particles are considered for exchange between the domains.

Reconfiguration of the 1D macropore elements during simulations is possible whenever the macropores are empty to allow for dynamic changes in macropore density, maintenance, depth or other properties.

Despite some sites having cohesive, homogeneous soil texture, direct mapping of preferential flow channels (earthworm burrows) [Zehe and Bloschl, 2004, van Schaik et al., 2013] is rarely possible. Hence, I propose that an estimate of flow path diameter distributions from observations is also sufficient and that dye tracer stains are reasonable estimators (see section 3.1) of the spatial distribution of preferential flow paths and its interaction with the matrix. In Appendix 4.6.2 I present the processing of such images for site parameterisation.

Diffusion in the matrix based on a 2D random walk

Diffusive soil water flow as non-linear, space domain random walk is taken to the 2D domain by combining Eq. 4.3 and a simple diffusive random walk for vertical and lateral movement respectively:

$$\begin{aligned} z_{t+\Delta t} &= z_t + \left[u(\theta_{z,x,t}) + \frac{\partial D(\theta_{z,x,t})}{\partial z_t}\right]\Delta t + \xi_z\sqrt{2D(\theta_{z,x,t})\Delta t} \\ x_{t+\Delta t} &= x_t + \xi_x\sqrt{2D(\theta_{z,x,t})\Delta t} \end{aligned} \tag{4.7}$$

Projected drainage capacity and maximum velocity

The preferential flow network exhibits large drainage capacity. Zehe [1999] estimates that a single burrow of a *Lumbricus terrestris* ($r = 4.5\,\text{mm}$) may drain the equivalent of $1\,\text{m}^2$ saturated soil matrix. Literature values for direct measurement of advective velocity in

earthworm macropores range closely around $0.075\,\mathrm{m\,s^{-1}}$, as given in table 4.3. In cracks and periglacial structures the advective velocity might be even higher.

Table 4.3: Measured mean maximum advective velocity in burrows of the earthworm *Lubricus terrestris* at a mean radius of 4.5 mm and theoretic value after Hagen-Poiseuille.

advective velocity $[ms^{-1}]$	**mean of n trials** [-]	**Source**
0.072	27	Shipitalo and Butt [1999]
0.056	29	Shipitalo and Butt [1999]
0.077	16	Weiler [2001]
0.058	12	Zehe [1999]
0.102	53	Bouma et al. [1982], Wang et al. [1994] in Weiler [2001]
24.78		after Hagen-Poiseuille

As an alternative to advective velocity estimation based on tracer recovery profiles (H3a, section 3.1.2), I suggest that a reference to the mean maximum advective velocity is sufficient (H3b). Advection is thus structurally limited by the drainage depth of a macropore and its size. Dynamic limitation through interaction with the matrix is self-controlled and depends on the pedo-physical properties.

Macropore-Matrix-Interaction

Macropore-matrix interaction depends on the matric head, the wetting of the macropore wall [Klaus et al., 2013] and is optionally affected by organic coatings which may act hydrophobic [Jarvis, 2007, Rogasik et al., 2014]. Moreover, it is dependent upon the flow velocities. Current double domain approaches treat this key process as either based on a leakage/exchange coefficient and the potential difference between the domains [Gerke, 2006] or by using the geometric mean of the saturated hydraulic and actual hydraulic conductivity and the potential gradient between both domains. The latter depends on an exchange length [Beven and Germann, 1981]. The drawback of these approaches is that neither the exchange length nor the leakage parameter are observable, and depend on model grid size and on event characteristics [Köhne et al., 2009a].

Direct experimental evidence about water dynamics at the macropore-matrix interface hardly exists. Some orientation is given by findings of Hincapié and Germann [2010], Moebius and Or [2012]. Other techniques like time-lapse X-ray or μCT tomography just emerge to be applied [Koestel and Larsbo, 2014]. Thus I propose two alternative process hypotheses for describing this key process which do not introduce additional parameters:

H4_Xa RW diffusion: A simple stochastic approach based on a random walk step where diffusivity is a state variable of the surrounding matrix.

H4_Xb E dissipation: A thermodynamic approach based on the Bernoulli equation that relates kinetic energy dissipation of a water particle that enters into the soil matrix to associated change in chemical/capillary binding energy of soil water.

A detailed description is given in section 4.5.1.

MACROPORE ADVECTION

The conceptualisation of macropore-matrix exchange over the pore wall requires the consideration of boundary effects and wetting processes. Generally, I assume particles to move along the macropore wall as film flow. If particles overlap their vertical positions, they form a second film layer, not being in contact with the matrix.

For the propagation of water as film flow in the macropores, I propose the following hypotheses:

H4_Fa dynamic film: Particles at a higher level in a film do not experience drag or friction and travel without retardation until they reach the lowest wetted position within a continuous film. Drag and friction are only experienced as negative acceleration on its further course.

H4_Fb stream tubes: Alternatively, particles experience the mean drag from the matrix and friction in the pore system along the projected course independent of their position within the film.

4.5.2 *Technical implementation of processes and of the representative structured domain*

While the fundamental concept of the echoRD model was introduced in the previous sections, here the technical realisation is presented as briefly as possible.

From a process perspective I resolve:

1. infiltration at the top boundary into matrix and macropores,
2. diffusive matrix flux as spatially explicit 2D random walk,
3. advective flux in the macropore,
4. macropore matrix interaction (infiltration and exfiltration).

Moreover, I handle:

5. dynamic time stepping

6. drainage at the lower boundary

INFILTRATION INTO MACROPORES AND THE MATRIX DOMAIN

With the extension of the model to 2D, infiltration became an important aspect of the model. As pointed out by Weiler [2005] initialisation of the macropores is critical and non-trivial. I use two hypotheses in the current model. In both precipitation is converted into particles which are randomly distributed over the top boundary.

H4_Ia Macropore drainage area: This is a generalisation of the concept of macropore drainage areas Weiler [2005], Weiler and Naef [2003]. All particles which happen to fall on soil first form a film layer. Excess precipitation or particles directly falling on macropores are redistributed to the macropores according to proximity and capacity. If one macropore's capacity is reached, it is excluded from the redistribution process. Particles in the film layer are included in the diffusive calculation step. Particles in the macropore domain are treated as advection and possible infiltration from the macropores into the matrix. Thus, infiltration is only limited by the transport capacity of matrix and macropores.

H4_Ib Maximum power in infiltration: The alternative hypothesis is based on the power and thus flow against the driving potential gradient is maximised [Zehe et al., 2010b, Kleidon and Renner, 2013]. As such I calculate infiltration capacity in each macropore from the observed velocity distribution (section 3.1) and the matrix. Incoming particles are hierarchically redistributed to the domains where the flux will be maximised.

MACROPORE FLOW AND MACROPORE-MATRIX INTERACTION

Macropore flow is represented as 1D dynamics of the particles. I assume a vertical movement at a macropore wall with variable film thickness depending on the number of particles in each depth. Figure 4.5 illustrates the general concept of projected advective translatory kinetic energy (E_{tkin}) which is depleted by friction and exchange with the matrix. In either hypothesis, the projected maximum advective velocity is decelerated resulting in a reduced velocity and thus reduced advective step length.

STOCHASTIC EXCHANGE BASED ON A RANDOM WALK DIFFUSION (H4_XA): In this approach the advective step of each particle is projected based on its advective velocity as $s_{proj} = v_{adv}dt$. A diffusive displacement step is estimated based on the actual diffusivity in the surrounding matrix. This step length is scaled by the share of free interface length (s_{free}) at the pore wall along the projected advective

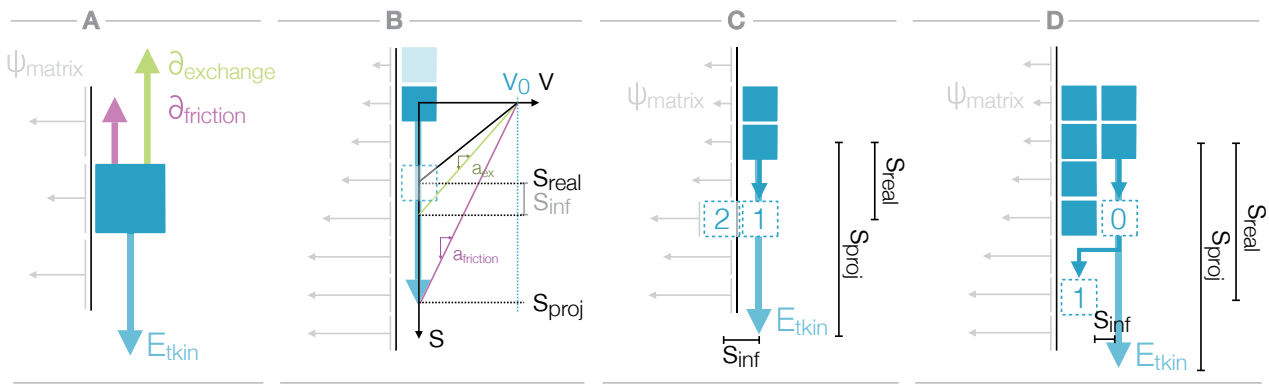

Figure 4.5: Macropore flow concept. A: Concept of a water particle at the pore wall possessing a translatory kinetic energy E_{tkin} which is depleted by friction in the macropore network and exchange with the matrix due to the matric potential ψ_{matrix}. B: Projected advection of a particle where the potential advective velocity v_0 is decelerated by the $a_{friction}$ and $a_{exchange}$ it experiences along the projected path s_{proj} resulting in a reduced step length s_{real}. C: Reduced advection with macropore-matrix exchange (1), and possible infiltration s_{inf} (2). D: Fast advection of a particle as film flow to the end of the film (0) and further decelerated advection (1).

step:

$$s_{diff} = \xi \cdot \sqrt{2dt \cdot D(\theta_{z,t})} \cdot \frac{s_{free}}{s_{proj}} \tag{4.8}$$

The result is used to reduce the advective step by the share of projected infiltration step of the particle into the matrix:

$$s_{red} = s_{proj} \cdot \begin{cases} \frac{d_{part} - s_{diff}}{d_{part}}, & \text{if } d_{part} \geq s_{diff} \\ 0, & \text{otherwise} \end{cases} \tag{4.9}$$

If the infiltration step is larger than the particle diameter d_{part}, the particle will be transferred to the matrix domain.

Solution based on energy dissipation calculation (H4_Xb): To solve macropore-matrix interaction on a physical basis without introducing more parameters I formulate a hypothesis fundamentally based on the Bernoulli equation:

$$\underbrace{0.5\varrho \overbrace{v_{adv}^2}^{const.}}_{E_{tkin}} + \underbrace{\varrho g z}_{E_{pot}} + \overbrace{p}^{=0} + \partial_{friction} = const. \tag{4.10}$$

In table 4.3 several studies with measured advective velocity in macropores are cited. These measurements compare with a theoretical laminar flow velocity through a pipe of the same cross-section, after Hagen-Poiseuille u_{mx}, with a factor of about 300. With this and assuming a unit pressure gradient, one may estimate the drag loss by friction $I_{friction}$ counteracting the hypothetical translatory kinetic energy as:

$$u_{mx} = 2 \cdot \frac{\rho g R^2}{8 \cdot \eta} \tag{4.11}$$

$$E_{tkin} = 0.5 m_{particle} u_{mx}^2 \tag{4.12}$$

$$I_{friction} = E_{tkin} / u_{real} \tag{4.13}$$

Following Kleidon and Schymanski [2008] and Zehe et al. [2013] soil water experiences a certain capacitative (or capillary binding) energy density $dE_{cap} = \Psi dV_\theta$, as matric potential is a negative energy density. Wetting and drying due to macropore-matrix exchange affects its capillary binding energy approximately as [Zehe et al., 2013]:

$$\partial_{exchange} = dE_{cap} = \varrho g \frac{\partial \Psi_z}{\partial \theta_z} \cdot \theta d\theta \tag{4.14}$$

For the infiltration of one particle a drag can be estimated by using the particle volume and a projected infiltration flux:

$$I_{exchange} = \varrho g \frac{\partial \Psi_z}{\partial \theta_z} \frac{V_{part}}{q_{exchange}} \tag{4.15}$$

The projected infiltration rate $q_{exchange}$ is calculated as Darcy flux $q_{exchange} = k_u \cdot -\psi / 2r_{particle}$. All state-dependent variables are formulated as geometric mean of the references at z_i and z_{proj}.

Hence the reduced advective velocity of a particle is estimated using friction and exchange drag acting against the maximum kinetic energy of the particle in steady state:

$$u_x = -\frac{E_{tkin}}{I_{exchange} + I_{friction}} \tag{4.16}$$

If the projected infiltration exceeds the particle radius $q_{exchange} \cdot dt > r_{particle}$ the particle will be transferred to the adjoining matrix. Figure 4.6 presents the general function of both assumptions in terms of advection speed reduction. However, the final particle behaviour of macropore flow can only be judged from the stochastic result with many particles and may be a combination of both approaches for capillary and saturation controlled conditions.

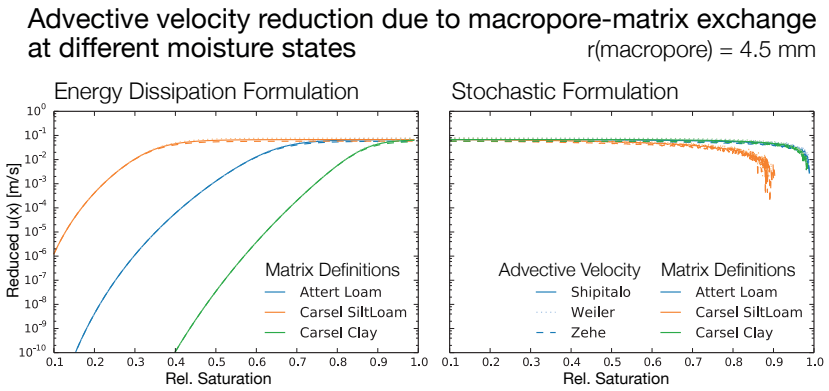

Figure 4.6: Reduced advective velocity as theoretically projected with the energy dissipation method and the stochastic formulation given different free advective flow velocity assumptions (Shipitalo: 0.0676, Weiler: 0.0774, Zehe: 0.058 m/s) and different pedophysical settings. Note, that the final particle behaviour of macropore flow can only be judged from the stochastic result with many particles.

TIME STEPPING, PROCESS SEQUENCING AND NUMERICS

In order to test the proposed concepts, I chose numerical schemes as robust and simple as possible. I rely on sequential calculations of the process domains. Thus the infiltration domain is handled first, second comes the diffusive flux in the matrix domain and third the macropore domain follows. Checks for infiltration into the macropores, saturation and percolation are performed afterwards. The time step is controlled through a Courant and Neumann criterion.

For diffusive water movement, the state update from particle density is based on a stratified subsampling. Within a time step state, updates are calculated after the simultaneous processing of a certain proportion of all particles. In the macropore domains, stratified subsamples are used according to the filling of the pore. Both account for the self-dependent state properties and are numerical strategies to avoid recalculation after each single particle has been processed. It can be controlled by respective simulation parameters.

4.6 Data requirements and preprocessing

Before I demonstrate tests of the echoRD model, this section presents the setup requirements and procedure for it.

4.6.1 Observable parameter driving the model

In order to facilitate the model as tool to analyse the influence of structural settings on the advective and diffusive flow it needs to be based on observable parameters. In most models the preprocessing and setup naturally determines the model results much more than the actual parameters of any element.

The echoRD model requires the following data:

- Soil layer arrangement
- Soil water retention parameters of the soil matrix for each layer (van Genuchten parameters)
- Distribution of macropores as horizontal Brilliant Blue stain images, time-lapse GPR data or direct observations of spatial density, depth distribution and diameters of macropores
- Estimate of the friction controlled maximum advective velocity in the preferential flow network (alternatively a distribution of observed advective velocities can be used)

The initial condition of the soil can be given as soil moisture or tension log. As forcing a rainfall time series or block rain has to be pro-

vided. In addition some numerical parameters control the general setup of the model:

- Size of calculation grid cells and number of particles per cell at saturation
- Rate of stratified subsampling of particles in diffusive dynamics calculations which controls how many update cycles are performed within one time step
- Size of a gaussian smoothing window for soil moisture calculations

4.6.2 *Automatic image analyser as preprocessor for the echoRD model*

The distribution of connected flow paths over depth and their topology is a crucial input to the echoRD model. In the example of Loess soils of the Weiherbach, biopores can be easily identified, counted and measured. However, in most situations the structures are much harder to identify. The schist experiments revealed stained patches which did not even show a clear connection.

I developed an image analyser for Brilliant Blue stain images and GPR difference attribute data. It is used as preprocessor for the echoRD model which automatises the domain setup procedure by identifying the distribution of macropores in given depths. Based on the derived information and the assumption, that a connectivity structure can be implicitly assumed, the representative domain is spanned and macropores are distributed on it.

Method

Most of the analysis is realised with the Python image processing tools of scikit-image [van der Walt et al., 2014]. Moreover the packages Shapely and Descartes [Gillies, 2013], SciPy and NumPy [Oliphant, 2007], and Pandas [McKinney, 2012] are used.

The tool loads a stack of rectified horizontal stain images or GPR difference attribute layers with given layer depth, resolution and signal threshold. Employing the Sobel operator and a watershed approach patches of flow paths are identified and statistical attributes for distance, size, perimeter are calculated.

The least populated layer is used as reference to calculate the representative domain width. The representative domain is defined to hold at least one macropore in each layer. Hence the scaling factor is given by the least number of macropores ($n_{macropore}$) in a layer (l_n):

$$F_{scale} = min[n_{macropore}]_{l_0}^{l_n} \tag{4.17}$$

The domain width is defined by the maximum of the minimal distances over all layers scaled by the number of macropores:

$$x_{max} = max[F_{scale} median(min(distance))]_{l_0}^{l_n} \quad (4.18)$$

The positions of the macropores on the 2D matrix are derived from the distance distributions with a random first location and further positions respectively. Contact interfaces of macropore and matrix are calculated from the observed stain perimeters for each macropore and layer. Patch sizes are used as proxy for macropore crossection and thus capacity.

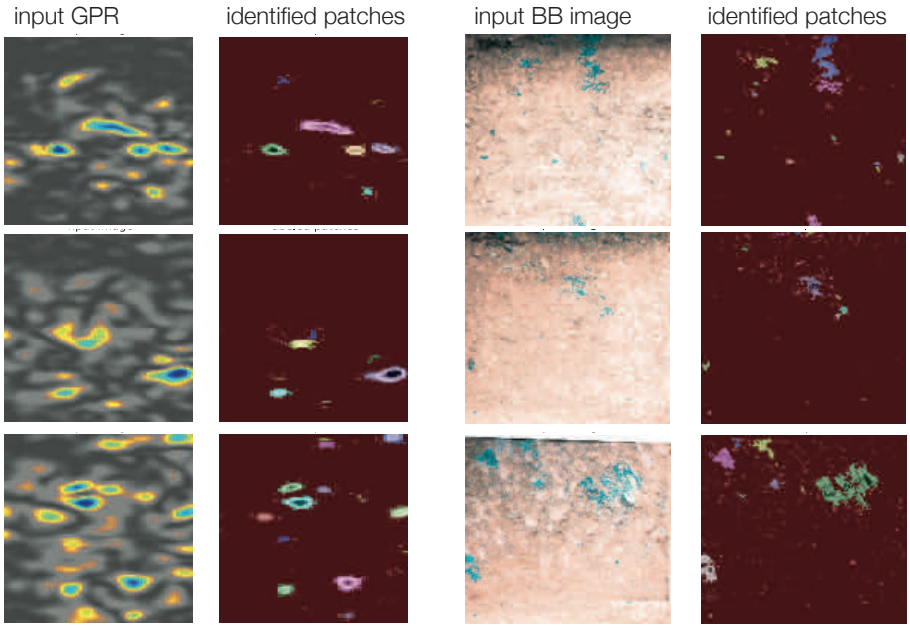

@46cm	GPR	BB
mac. count	7	13
share	0.038	0.029
avg. area[1]	26.81	13.56
avg. diameter[2]	5.29	3.44

@61cm	GPR	BB
mac. count	5.5	9
share	0.022	0.011
avg. area[1]	22.02	7.46
avg. diameter[2]	4.78	2.66

@71cm	GPR	BB
mac. count	15	8
share	0.056	0.057
avg. area[1]	18.49	42.32
avg. diameter[2]	4.40	5.93

Figure 4.7: Image analysis to automatically interpret horizontal dye stain photographs for macropore network characteristics. Exemplary data from Colpach sprinkler experiment plot XI. Left stack: Horizons of GPR amplitude difference attribute and identified structures. Right stack: Horizontal excavations of Brilliant Blue stains of the same experiment. Tables present the derived descriptors for each layer based on both inputs: Number of macropores, areal share covered by the signal, average area of a single patch [cm^2], average diameter of the patches [cm].

Results

Figures 4.7&4.8 present results based on the plot XI experiment in the Colpach basin (section 3.2, p.48). Clearly the images are not identical. Due to a lack of common reference it was not possible to aligne them or to analyse differences directly. Instead the tables and the resulting representative domain setups are given for comparison. Generally Brilliant Blue allows a higher spatial resolution and thus identifies also smaller patches. This is why the domain is set up lager because in some layers only very few flow paths are sufficiently large to be detected by the measurement.

Discussion and conclusions

Primarily the tool is intended to enable the setup of the echoRD model based on data alone. Instead of images, also a macropore

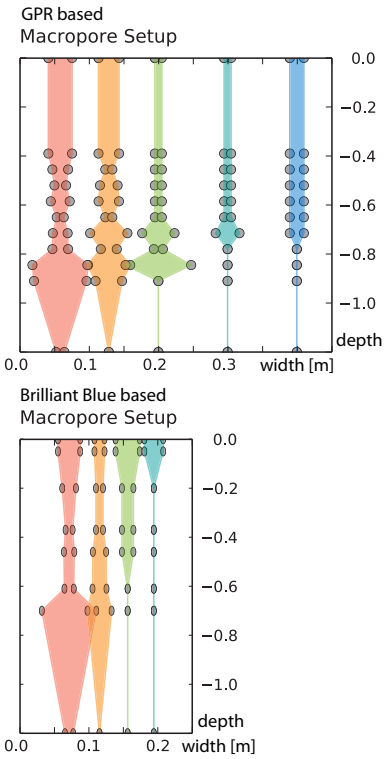

Figure 4.8: Resulting macropores with matrix interface areas. Depth and width given in [m].

distribution can be provided directly. The topology of the macropore network is reduced to the distance between macroporous structures. Connectivity, kurtosis and other properties are reduced to the simple 1D representation with a variable interface area to the matrix and capacity.

For the two examples (section 4.5, p.77) the concept works well. It is in line with the general proposition of the FU concept, that at the plot scale mainly vertical processes need to be resolved. Lateral processes are either negligible or contribute to a superordinate structure, which has to be taken care of elsewhere.

4.7 *Model testing and different process hypotheses*

In the following I test the echoRD model concept and in particular the different hypotheses on how to a) estimate advective velocities, b) describe infiltration, macropore flow and dissipative macropore-matrix exchange. I start with a simulation of the "artificial macropore" experiment to check plausibility of lateral diffusive exchange between two different porous media, and then present simulations of sprinkler experiments in the Weiherbach and the Attert catchments (section 3.1).

4.7.1 *Simulation of the "artificial macropore" experiment*

I set up two versions of the echoRD model as 1 m wide and 1 m high homogeneous soil matrix with a) one explicit macropore and b) a 1.5 cm wide column of coarse sand in the center. The underlying grid resolution for particle density calculation is set to 5 mm and one water particle is defined at 9.5 µg. Hydraulic properties of the soil matrix are taken from analysis of the silica sand (table 4.2). To reproduce the preprocessing and results, refer to `2D_column_trial` in the repository.

Figure 4.9 presents the observed and simulated soil water distribution. Both model setups a&b show the same results, which is discussed in section 5.1.6. Generally, the observed behaviour of the lateral diffusion and wetting front propagation is reproduced well, although the shape of the simulated wetting front is a little more conical. During the experiment, break through at the bottom was observed after about 8 h. The model proposed an earlier breakthrough after about 5 h.

Unfortunately a quantitative comparison of observed and simulated wetting is not feasible. This is because the silica sand posses an almost step-like retention curve, thus a translation of observed matrix potentials into soil moisture is highly uncertain with respect

to the wetting front. This is also corroborated by the fact that the water balance in the early hours of the experiment is far from being closed. However, I conclude that the model is capable of simulating 2D soil moisture dynamics and lateral exchange between a fast and a slow domain. In appendix 7.4.1 an additional comparison of different geometry assumptions for the 2D convolution is given.

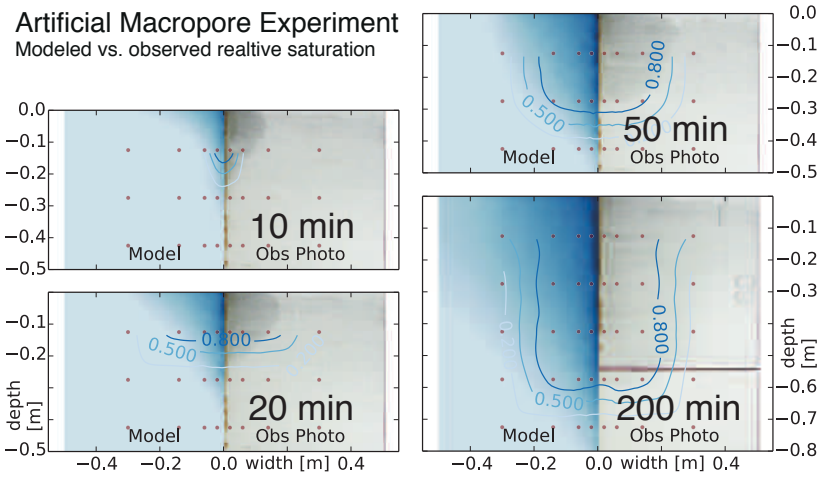

Figure 4.9: Simulation of single artificial macropore irrigation experiment with echoRD model. Simulated relative saturation (left), photo of experiment state (right), overlaid by tensiometer positions (red dots) and interpolated relative saturation (blue contour lines) measured as matric head.

4.7.2 *Reproduction of sprinkler experiments*

Weiherbach data set

The second benchmark is the reproduction of the observed tracer profile in the Weiherbach experiment with self-limited advection. Since the Weiherbach data set provides unique data for depth distribution of macropores of different diameters, this allows a model setup with very little preprocessing assumptions especially concerning macropore density and depth distribution. The model setup and parameters are identical to the earlier 1D version in section 4.4.2. But I now employ the full model on a representative domain of 0.34 m width. Refer to `echoRD_Weiherbach` in the repository to reproduce the results.

As introduced, I explored several process hypotheses. A comparison is given in figure 4.13 based on simulated tracer transport and moisture patterns.

In the following I present results based on macropore drainage area infiltration (H4_Ia), advective velocity after Shipitalo and Butt [1999] (H3b), energy dissipation based macropore-matrix exchange (H4_Xb) and dynamic film flow with no exchange in the higher film layers (H4_Fa). Tracer transport of the irrigation water is bound to

the particles and thus fully advective with the water. Dispersion of the tracer due to concentration gradients and dispersion are neglected.

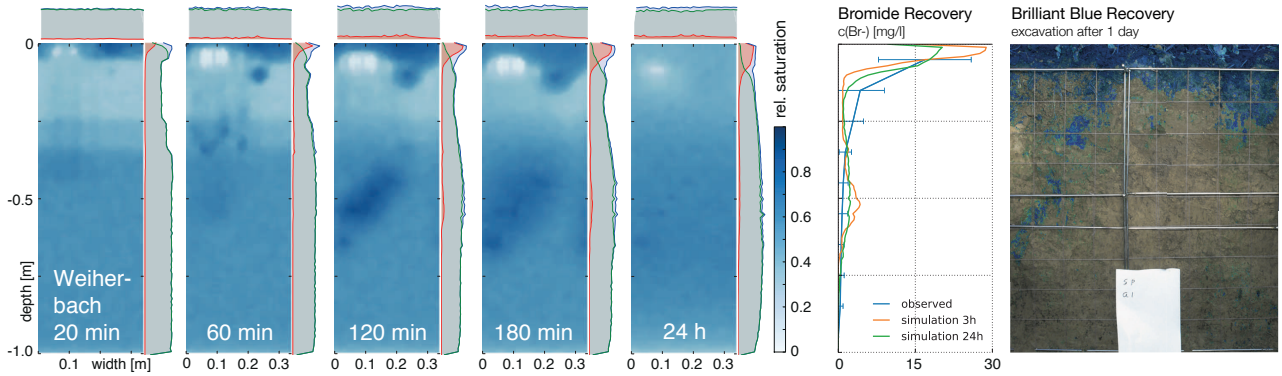

Figure 4.10: Simulation of a plot-scale sprinkler experiment of the Weiherbach data set with the full echoRD model (infiltration based on macropore drainage area (H4_Ia), advective velocity after Shipitalo and Butt [1999] (H3b), macropore-matrix interaction with energy dissipation approach (H4_Xb), dynamic film flow (H4_Fa)). Modelled soil moisture dynamics in representative domains at different times after irrigation start with marginal distributions of new (red), old (green) and total (blue) particles. Irrigation stops after 70 min. Right: Comparison of observed and modelled bromide tracer concentration profile (after 3h and 24h) and excavated Brilliant Blue profile for qualitative reference.

The simulation results are presented in figure 4.10. It first needs to be pointed out that the soil moisture dynamics match the dye stain characteristics very well without any calibration. Moreover, the salt tracer profiles are reasonably well recovered, although our model appears to underestimate vertical dispersion.

The key feature of self-limiting advection is achieved. After ≈2.5 h simulation diffusive flux dominantes and Péclet numbers fall below 1. Although the model is capable of diffusive flux one may use such reference to then utilise a more efficient Richards solver. This good match also highlights that transport in the near field dominates the process and that dispersion is of minor importance, as was also suggested by Roth and Hammel [1996].

Attert: Young soils on periglacial cover beds with geogenic voids

In the northern Attert basin, the last test of our proposed model is located in a setting far different from earthworm burrows in soils with high aggregate stability. On periglacial deposits on a weathered schist young soils with deposit bands present a completely different macropore system. Notice that this is also one of the very few studies on preferential flow modelling on forested sites [Laine Kaulio et al., 2014]. Figure 3.9 (top row) may serve as illustrative reference. *In situ* measurements of saturated hydraulic conductivity with a Constant Head Permeameter (CHP Ksat Inc., Raleigh, NC) revealed the full spectrum of $10^{-8}\,\mathrm{m\,s^{-1}}$ to $10^{-3}\,\mathrm{m\,s^{-1}}$ in a single borehole log. More details have been given in chapter 2 (p.15).

The model was setup based on observed horizontal dye stain im-

ages using the echoRD pre-processor described in appendix 4.6.2, measured pedo-physical parameters given in table 4.2 and the literature value for advective velocity after Shipitalo and Butt [1999] (table 4.3, H3b). Although I again examined the different process hypotheses, these results refer to MDA infiltration (H4_Ia), energy dissipation exchange (H4_Xb) and dynamic film flow (H4_Fa) as found most appropriate earlier.

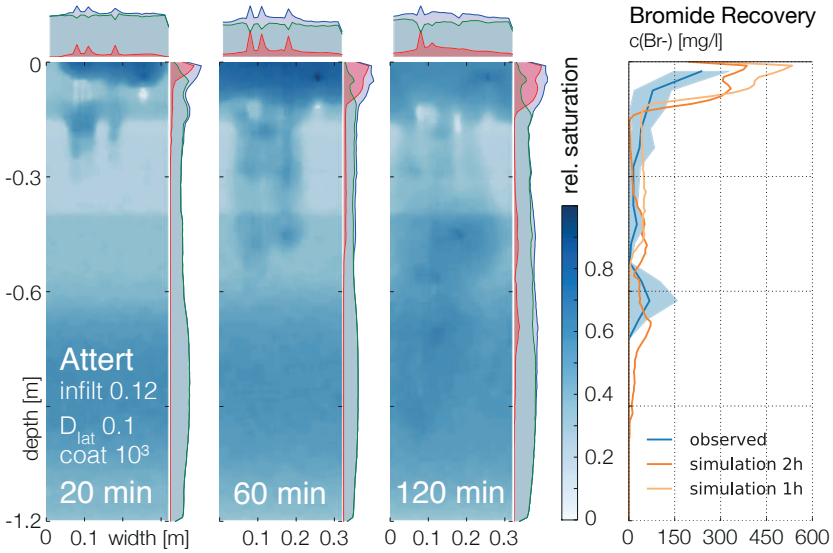

Figure 4.11: echoRD recalculation of a plot-scale sprinkler experiment Colpach in the northern Attert basin. Modelled soil moisture dynamics in representative domain at different times after irrigation start with marginal distributions of new (red), old (green) and all (blue) particles. Bromide tracer recovery (right). Irrigation stops after 60 min. Compare with observations in figure 3.4 (bottom).

The initial model results (not shown) have underestimated the observed fast vertical transport, suggesting most water captured in the top soil. This contradicts our experimental observations, where most water is quickly mobilised to greater depth, resulting in a very patchy recovery pattern.

Since the irrigation was mediated through the litter layer, I used the dye image at the Ah-horizon interface as reference to scale the irrigation directly fallen on the matrix. The analysis with a patch size threshold of 1 cm^2 resulted in 12% dye coverage. Moreover, I hypothesised faster advective velocity, since geogene structures are considerably larger compared to biopores. In addition after finding lateral diffusion being overestimated I also scaled lateral dispersion by a factor of 0.1.

The resulting simulation is given in figure 4.11. Please refer to `echoRD_Attert` in the repository. It shows, that only after harshly limiting the exchange by reducing lateral diffusion in the matrix, the model matched the observations. Although this simulation employs parameters which were not *a priori* directly derived from observations, the test provides a first indication of the concept's and model's

capabilities beyond well-definable macropore-matrix systems. It also pinpoints that the processes in biopores and geogene macropores may require specific representations.

4.7.3 *Hypotheses for macropore-matrix exchange, advective velocity reference, film flow, infiltration and macropore coating*

With the particle approach properties of the domains and much of the fluid are to a large degree unraveled. This allows us to treat them separately (e.g. temperature dependent viscosity or dynamic macropore density) and permits the formulation of process hypotheses.

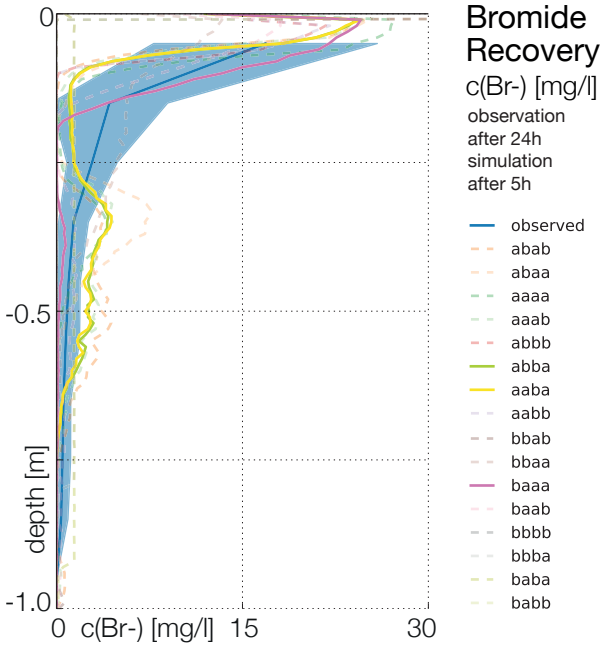

Figure 4.12: Bromide recovery profiles after 5 h. Laterally averaged simulation results with identical setup of the Weiherbach testcase for the different process-hypotheses: (1) infiltration H4_I, (2) advective velocity H3, (3) macropore-matrix exchange H4_X and (4) macropore film flow H4_F. The code presents the alternative hypotheses a&b at position 1 to 4 respectively.

For infiltration and macropore flow initialisation I implemented a macropore drainage area approach after Weiler [2005] (H4_Ia) and an approach based on maximum dissipation of free energy [Zehe et al., 2010b] (H4_Ib).

Advective velocity was referenced to observed tracer pdfs (H3a) or constant values from the literature (H3b). For macropore-matrix exchange a stochastic (H4_Xa) and an energy-based (H4_Xb) approach was formulated. For macropore flow dynamics I considered a dynamic film flow with a simple velocity estimate (H4_Fa) and stream tubes (H4_Fb). In addition optional model parameters controlling coating and lateral diffusion were introduced.

All these were comparatively run with the same setting for the Weiherbach and Attert testcase. Figure 4.12&4.13 show a comparison of the differently modelled tracer recovery and moisture patterns

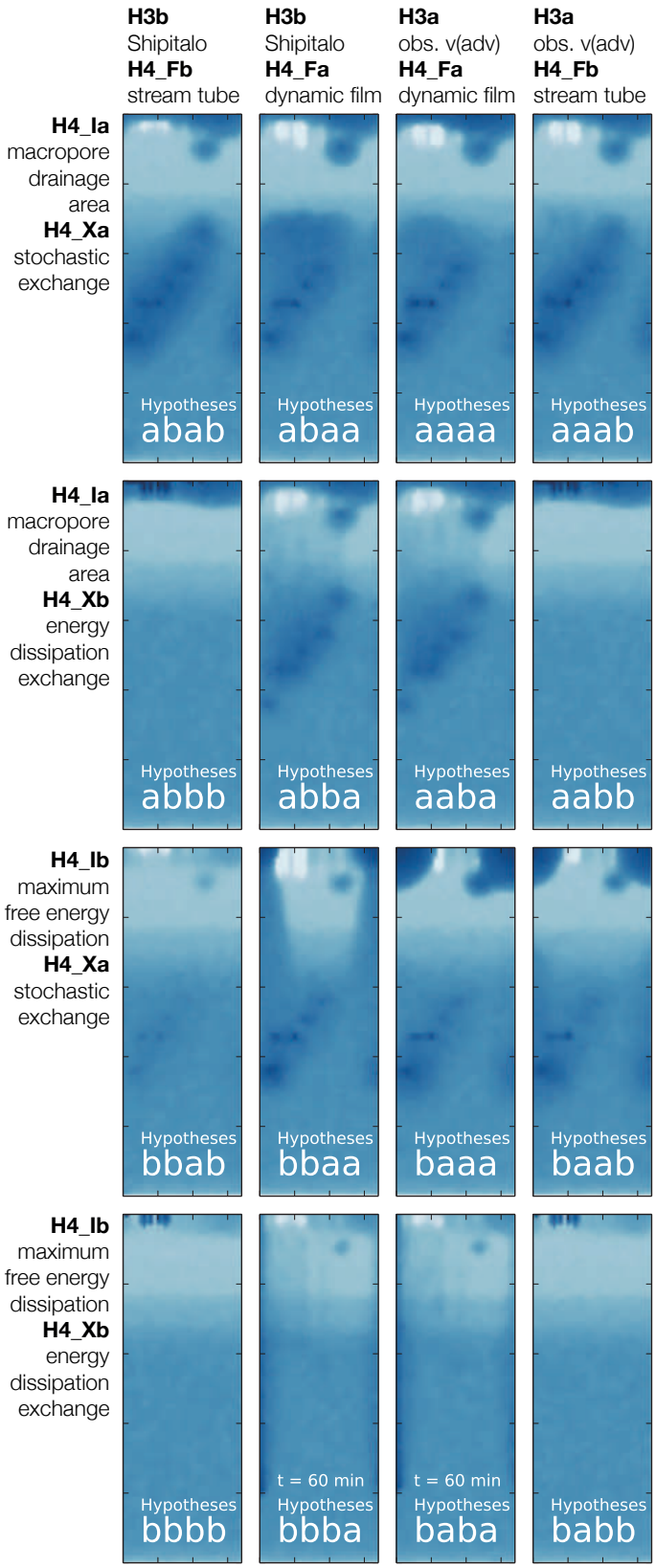

Figure 4.13: Distribution of relative saturation in the representative domains after 2 h simulation. Results with identical setup of the Weiherbach testcase for the different process-hypotheses: (1) infiltration H4_I, (2) advective velocity H3, (3) macropore-matrix exchange H4_X and (4) macropore film flow H4_F. The code presents the alternative hypotheses a&b at position 1 to 4 respectively.

to observations. It can be highlighted that the setup with hypotheses H4_Ia, H3b, H4_Xb and H4_Fa without any coating or diffusion parameter reproduce the observed infiltration patterns at the Weiherbach best. With regard to Br^- a reference to the laterally accumulated vertical tracer recovery after 24 h simulation reveals a similar result. Although the Attert test case had to introduce further hypotheses about lateral diffusion and infiltration, I come to the same conclusion with regard to the process hypotheses.

A test where I extended the Weiherbach model run by imposing noise to the soil matrix definition (standard deviation of the observed hydraulic conductivity) highlights that the general behaviour remains unchanged, while only local gradients are amplified.

4.8 *Application of the echoRD model as virtual laboratory*

Since the model is intended as virtual laboratory to explore the self-organisation of pedo-eco-hydro-systems through preferential flow structures, the final test is an investigation of simulations with different forcing.

I use the behavioural setups of the echoRD model from the previous section 4.7 for the Weiherbach and Colpach sample plots and run them with different intensity and duration of a block rain event. Intensity classes are $5\,mm\,h^{-1}$, $10\,mm\,h^{-1}$, $15\,mm\,h^{-1}$, $20\,mm\,h^{-1}$, $30\,mm\,h^{-1}$, $40\,mm\,h^{-1}$, $60\,mm\,h^{-1}$ and $100\,mm\,h^{-1}$. Durations of 10 min, 20 min, 60 min, 120 min and 240 min are simulated for 12 h.

During the simulations the Péclet number (Pe) is calculated for each particle every 1 min. In a review Huysmans and Dassargues [2005] conclude that for environments with low permeability it is advisable to scale diffusion to the respective accessible porosity. I hence use the following approach:

$$Pe = \frac{d_{particle}\frac{z_{t-1}-z_t}{dt}}{D_{t,x,z}\theta^*_{t,x,z}} \tag{4.19}$$

For each cell the mean Pe of all respective particles is stored during the simulations.

In addition I trace the depth distribution of all new particles throughout the simulation as count per depth increment of 0.01 m. The resulting time series of advection and Péclet numbers is given similar to the plots of soil moisture dynamics in section 3.3.3 (p.60). The number of new particles is plotted as grey shades (white = low, black = high), the Péclet number in colours (while all $Pe < 0.5$ are removed). Both attributes are given on a logarithmic colour scale with time on the x-axis and depth on the y-axis.

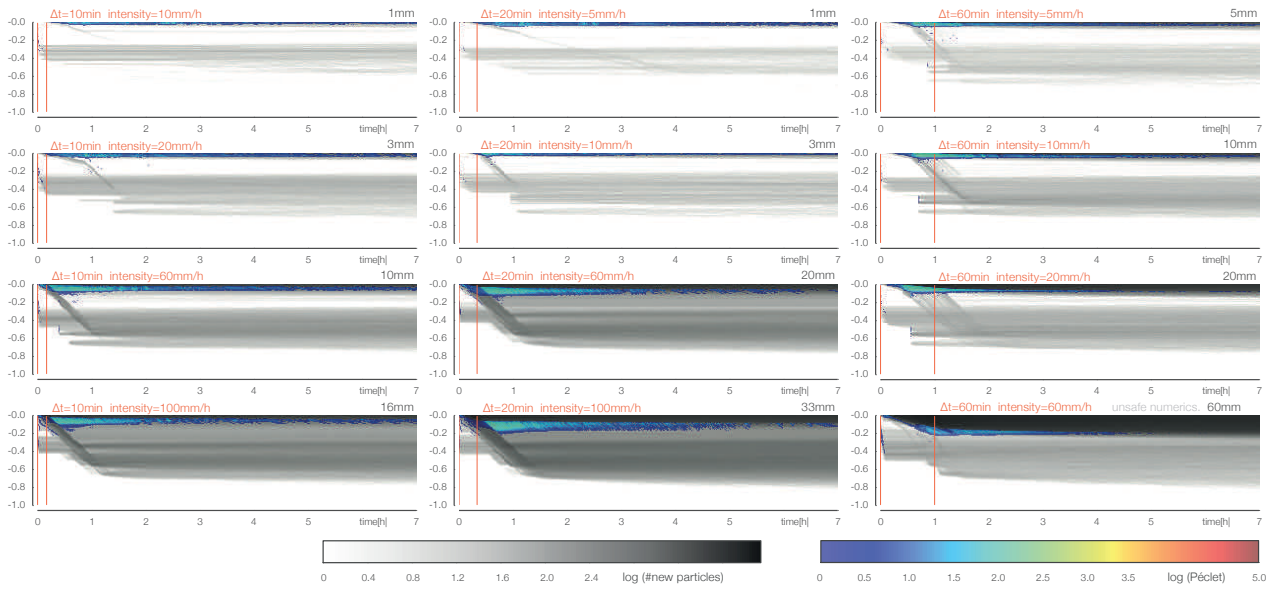

Figure 4.14: Modelled density of new particles (greys) and Péclet numbers (colour) of events of different duration and intensity in the Weiherbach setup of the echoRD model. X-axis is depth [m], Y-axis is time [h]. Notice some quickly transported advective particle bulks (immediate appearance or vertical grey lines) and their diffusive spread over time.

4.8.1 *Results, interpretation and discussion*

Figures 4.14 and 4.15 present some of the results for the Weiherbach and Colpach sample plots respectively. The block irrigation duration is marked with orange lines.

The Weiherbach case

In all cases new particles immediately reach greater depth. However, it appears that this distribution is not solely a function of irrigation amount. With longer duration a formation of a deep reaching wetting front is suggested by the model. At the wetting front high Péclet numbers occur especially for high intensities. For the flow in macropores this seems to be only the case at the beginning of the event. Soon after this, the drained particles are captured in the matrix and move diffusively. This can be seen by the diverging grey bands. Notice that I calculate the mean *Pe* for each grid cell here. As rapid flow in structures is observed in all simulations by the fast vertical redistribution of new particles, this simply means that the fraction of advective particles in a cell is to low to elevate the mean above 0.5.

Concerning the model test the results highlight the importance of the numeric stability criterions. This can especially be seen in the last shown example of 60 mm in 60 min. Although this has the largest rainfall amount, the Péclet numbers seem to be underestimated. More tests are needed to investigate this.

The Colpach case

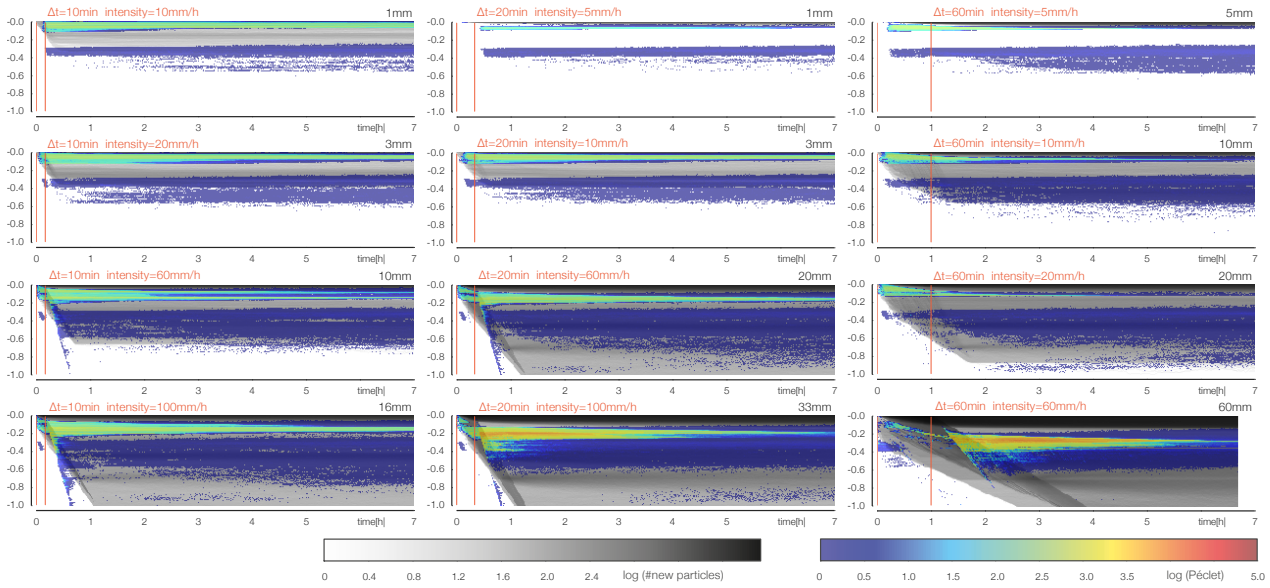

Figure 4.15: Modelled density of new particles (grey shades) and Péclet numbers (colour) of events of different duration and intensity in the Colpach setup of the echoRD model. X-axis is depth [m], Y-axis is time [h]. Notice the quick reach of new particles to greater depth even at moderate events. Also notice the relatively high level of Péclet numbers in the young highly structured soil.

The situation here is very different. The flow is generally highly non-laminar. Even small events quickly reach to greater depth when the intensity is above $5\,\mathrm{mm\,h^{-1}}$. This results in a fast and even distribution of new particles over the soil profile. The development of a wetting front is less compared to the previous case. Occurrence of Péclet numbers above 0.5 is much more common and not related to a wetting front.

The apparent development of an unstable zone in the shallow subsurface could also be explained by a strong contrast of advective particles bypassing dry matrix with very low diffusivity. This also explains why the Péclet numbers remain very high for a long time: The model setup uses a strongly reduced macropore matrix interaction. Hence the contrast of dry and wet areas and hence fast and slow particles remains for a longer period. The model assumptions for this setup may deserve revision. Furthermore, also the lack of an included lateral structure at the superordinate hillslope-scale which would have drained much of the free water could be responsible for a probably underestimated system resilience.

4.8.2 Conclusions

In the test to use the echoRD model as virtual laboratory some of its potentials are shown. At the same time the previous success in modelling rapid subsurface flow in the Colpach test case needs to be

revised concerning the universality of the made scaling assumptions.

With regard to the longstanding debate about the role of preferential flow for more normal rain events, the results corroborate the importance of the process in soil water dynamics.

4.9 Intermediate conclusions of the echoRD model chapter

The first fundamental step was the presentation of an alternative representation of soil water diffusion based on a random walk of water particles (H1). I showed that this is a true alternative to solvers of the Richards equation performing even better compared to observations.

In the next step the model was extended to a lumped advection and diffusion representation in 1D (H2). Advective velocity of water in macroporous structures was estimated from observed tracer recovery of a sprinkler experiment (H3a) or defined by a constant initial value taken from literature (H3b). Although generally capable, the lumped model failed to self-limit advection without introducing any non-observable parameters.

Consequently I proposed a representative structured domain with a 2D matrix hosting topologically explicit 1D macropores (H4) as a physical and least adequate representation of the processes. Together with the concept of water as particles, thus was derived the echoRD model (eco-hydrological particle model based on representative structured domains).

After validating the model's capability to represent 2D diffusive flow and macropore-matrix exchange in general, I formulated hypotheses for the four main controls:

H4_I Infiltration and thus initialisation of the flow processes is simulated based on the concept of macropore drainage area (a) or based on maximising the power and thus flow against the driving potential (b).

H4_X Macropore-matrix exchange as crucial control of self-limiting advective water flow and redistribution is formulated as random walk exfiltration (a) or alternatively as friction controlled energy dissipation at the macropore-matrix interface (b).

H4_F Macropore flow is represented as dynamic film flow, with given initial velocity values and exchange taking place at the interface (a) or can be estimated by mean exchange acting on stream tubes (b).

For the model I could clearly ascertain that the proposed elements H4_Ia, H3b, H4_Xb, H4_Fa are performing well. The model is ca-

pable of dynamically simulating the variance of the diffusive and advective velocity field.

Concerning process understanding, the results corroborate the findings of Roth and Hammel [1996] that local hydrodynamic and molecular diffusion are sub-ordinate to the overall transport process – especially once the advective flow field has developed. Regarding the question of process exploration the findings propose a careful revision of the use of tracer profiles: While they are reasonable for flow path identification, inference of velocities based on unknown fixation times and spatially mixed samplings may be ambiguous. This calls for a revision of H3 and the experimental references.

The respective discussion is given in the following chapter 5.

5
Discussion

The different aspects of perceptual model, measurement and observation strategies, targeted experiments, and the application of models to test hypotheses are different aspects of the same theme. Some things repeat from aspect to aspect, others depend on each other. The discussion first emphasises specific aspects of the measurements and experiments. This is followed by the newly developed echoRD model. I then revise the question of functional unit identification. Finally a more general perspective is taken and the general scientific strategy of hydrological analyses is discussed.

5.1 Discussion of measurements and experiments

Before discussing the individual measurements and experiments, it shall be crucially acknowledged that tremendous development has been achieved in the field of environmental observations. Many experimentalists state that we may virtually measure anything in arbitrary resolution. Despite technical justification, this statement may overlook many fundamental limitations in loosely defined, open systems. This section emphasises the conceptual constraints of the employed soil-hydrological measurements rather than technical specifications of one device against another.

5.1.1 Soil moisture monitoring in structured soils

Apart from gauges, soil moisture sensors are probably THE device related to soil water dynamics. Since the attribution of the strong correlation of the dielectric permittivity of the soil-water-air continuum to soil moisture, plenty of sensors have been developed to measure soil dielectric permittivity through capacitive, frequency domain or time domain approaches. While these methods and the specific sensors have different strengths and limitations (stability of the signal, effect of diluted salts, temperature, soil mineral and organic composi-

tion, etc.), the measurement itself has also conceptual constraints due to the assumptions about the porous medium. In conditions of structured soils any local measurement of soil moisture quickly looses grounds:

In structured soils as in the Holtz experiment (section 3.3, p.57) I showed, that a great share of the event water bypassed large proportions of the soil. Moreover, much of the registered soil moisture change remained highly mobile in specific structures. A blind measurement with very few sensors or even the proposed TDR tube logs is prone to become non-informative if the overall setting is not taken into account. Hence in addition to the sensors uncertainty (precision, installation, etc.) the representation appears to be limited.

If the structures and the associated processes are evenly distributed, this can be simply attributed to heterogeneity. However, in most cases such distribution is highly skewed, multi-modal or structured. This also opens a dilemma of such measurements: the smaller the footprint, the less representative but the larger the footprint, the less sensitive to advective processes. Moreover, as soil moisture can only address the position of water but not its momentum, inference from state to process requires special care in addressing advective and diffusive movement. A steady macroporous film-flow cannot be distinguished from changes in capillary bound water by means of integral soil moisture measurement alone.

Another issue of soil moisture monitoring arises from a bias towards the diffusive part. Good contact to the soil matrix is prerequisite for all current soil moisture probes (and even more for tensiometers). As such the proper application avoids positioning in and close to structures. From a process perspective this directly means that water ultimately can reach the sensor only through diffusive transport. Even when the lateral redistribution is governed by advection, the strong difference between the order of magnitude of diffusive and advective transport will always have the tendency to bias soil moisture observations towards diffusive water.

Furthermore, the soil moisture sensors integrate the soil-water-air continuum in the connected matrix regardless of the distribution of the filled pore spectrum. With this an even distribution of the registered water to all pores or the fine ones may be erroneously assumed. Consequently this is often addressed as hysteresis.

To conclude this aspect, the measurement of soil moisture over time as surrogate for soil water dynamics is found problematic in structured soils. Especially quantitative inference from single observations need to clarify the validity of the given assumptions about the matrix states, continuity and process representation.

Accompanying soil moisture measurements with tensiometers or

sensors for soil water potential can largely reduce the ambiguity of the former. Although such sensors come with other technical limitations such as internal calibration functions, limited measurement ranges and sometimes very large uncertainty bounds, addressing the system's state though the measurement of a potential has some advantages over the assessment of the location of water in a heterogeneous substrate. However, the conceptual restrictions remain as challenging.

5.1.2 GPR tomography

Electrical resistivity tomography (ERT) and GPR are the most common geophysical imaging techniques which have been used in hydrology [e.g. BINLEY et al., 2002]. Since then the applications have evolved towards much higher resolution, non-invasive process observation in more complex settings [Klenk et al., 2015, Wehrer and Slater, 2015], and real-world applications [Westhoff, 2011].

While ERT has many advantages in terms of relatively easy setup and scalability its main limitations lie in the temporal and spatial resolution: The higher the desired resolution the finer the layout of the electrodes, the more electrodes the longer the measurement, the deeper the structure the more assumptions for its identification. In addition ERT detects resistivity which is not very sensitive to abrupt structures and which is strongly dependent on the convolution algorithm.

GPR on the contrary is known as the geophysical technique with the highest resolution. Allroggen et al. [2015] show its potential to even recalculate soil moisture changes from time-lapse surveys. Klenk et al. [2015] have shown means to derive capillary fringe dynamics from GPR measurements and inverse modelling. However, in heterogeneously structured soils the techniques' foundation of identifiable and to some degree continuous reflectors is strongly limited. So far quantitative estimates about distributed soil moisture changes remain challenging.

Our experiments have shown, that there are plenty of possibilities to advance the application of GPR in hydrology. One possibility lies in the close similarity of TDR and radar measurements which offers chances for cross calibration and parameter inference. Another option could be long-term installations of time-lapse GPR profiles or even 3D spots towards a new kind of field lysimeters. Once the measurements have been calibrated against extreme states and given sufficient temporal and spatial resolution this could evolve to a quantifiable tomographic process exploration tool.

5.1.3 *Inferring advective velocity distribution from recovered tracer concentrations*

To drive and test the echoRD model with data from structured soils I introduced a number of experimental references. Although each experiment has ample room for specific discussion I will summarise them to focus on the implications for model development.

I founded the model parameterisation on data about flow structures and dynamics derived from plot scale sprinkler experiments. The 1D model was parameterised with observed tracer profiles and recovered them well – although it could not account for self-limitation of advection due to macropore-matrix interaction. The full echoRD model employs structural findings from experiments as pdfs of macropore depth and density. Recovered tracer profiles are primarily used as validation reference.

Here experimental and conceptual concerns coincide. Experimentally, the degrees of freedom are not fully closed, since neither instantaneous nor time-lapsed sampling is possible (temporal dimension). Moreover, each sample contains a certain fraction of rapid flow structure and matrix. It relies on sorption of loaded water which contradicts the assumption of negligible macropore-matrix interaction. Furthermore, samples are limited to a small share of the total soil volume. Reconciling far from well-mixed conditions and poorly observed boundaries this imposes some considerable uncertainty to the measurement (spatial dimension).

Temporal dimension

Generally, we are challenged by a process which stretches over several orders of magnitude. While the fastest fraction may travel at $10^{-2}\,\mathrm{m\,s^{-1}}$, the slowest fraction – even in the advective phase – may be much more retarded, at $10^{-6}\,\mathrm{m\,s^{-1}}$ or less. By inferring advective velocities from recovered tracer depth distributions, I assume a monotonous flow field and equally distributed retention of the tracers by the matrix. In addition, the fixation time is an assumption scaling the advective velocities easily by several orders of magnitude.

To excavate a profile down to 1 or 2 m takes several hours. The sampling thus is likely biased towards the mid and slow fraction of the water. I also experimented using a percussion drill auger with 80 mm diameter for less invasive and faster sampling. On the one hand this enables to capture one profile "instantaneously". On the other hand it disturbs the sampled core and structures much more, remobilises free pore water and does not allow for structural inspection of its representation based on dye patterns.

Trials with time-lapse 3D ground penetrating radar (GPR) have

been more promising [Allroggen et al., 2015]. They enabled the observation of spatial distribution of irrigated water at different instances in time and thus also provide a much better approach to identify the fixation timing.

Given the fact that one sprinkler experiment alone accounts for several thousand Euro analytical costs and numerous working hours, these limitations strike harshly. If one cannot properly account for the temporal scale through complementary observations with 3D time-lapse GPR or tracer breakthrough curves, the experiments only reveal one snapshot of flow paths and macropore-matrix infiltration patterns.

Spatial dimension

We are also challenged by the fact that macropores are relatively small and thus the flow takes place in a small fraction of the total volume or even predominantly at the interfaces. However, excavation sampling techniques are rarely structure specific. Hence the measured recovered concentration is a mixture of the loaded flow paths and probably less-loaded matrix or vice versa. Moreover, one can only sample a comparatively small fraction of the total affected volume. It remains hypothetical, that the tracer recovery is representative – especially owing to the fact of local disequilibrium and structured flow paths.

Even 200-300 samples per profile account to far less than 0.24% of the total volume below the sprinkled surface. The total affected volume might be even larger, given additional lateral diffusive flow which has been found profound in experiments by Allroggen et al. [2015] and in the simulations (section 4.7.1, p.88). Experience also shows that succeeding profile faces may present highly different dye patterns when rapid flow paths channel the water. As such, the overall scaled mass balance of recovered tracer remains ambiguous when we cannot judge whether or not the sampled spectrum is representative and complete.

On the one hand, rapid and highly resolved sampling improves the resolution of the data base. On the other hand we remain at least one order of magnitude above the extent of the spatial structures. During the sampling process it is also unclear how much of the mostly air-filled structures are destroyed and thus not accounted for. The percussion drilled core samples were compacted by about 10 to 20%. From the phase shifts between the recovered profiles and the core log it can be concluded that this compaction is not the same over depth. Finally, we face the issue of tracing the water movement by means of dye, salt, isotope or radioactive tracers. This requires a spatial extent of the experiment that is much larger than the char-

acteristic lengths scale of the macropore system. As, the latter is not known, we need spatial replicates to judge whether the observations are representative or not [Zehe and Bloschl, 2004, Zehe et al., 2014].

Revision of the experiments

From a more general point of view I conclude that observing instantaneous velocity requires a different experimental setup than for average velocity. Macro-scale laboratory experiments can reduce artefacts although conserving heterogeneity. Additionally, they can give control over the lower boundary. Specific real-world experiments with complementary observation methods including multiple tracers, GPR and breakthrough curves can address the given shortcomings. Repeatability of such experiments with different intensities, under different states and at different locations will be a substantial improvement.

5.1.4 Plot sprinkling with multi-tracer and 3D time-lapse GPR

To accompany the sprinkler experiments with additional observation methods enable to step further towards completing the picture and to address some of the aforementioned shortcomings. The logs of stable isotopes provide an independent third tracer. The 3D time-lapse GRP measurements at three time instances allow for a qualitative insight into the advective flow field below $-0.4\,\mathrm{m}$ depth.

Tracer signals

The signal of the stable isotope concentration of the sprinkling water and soil water has a relatively low difference. Moreover, the calculations are based on one reference log some meters off the actual sprinkling sites. Interpretations of the results need to consider these limitations.

Despite the high heterogeneity, the recovered Bromide profiles and the Bromide core logs have a high agreement. This is supporting the sampling layout that one profile is representative for the plot. Although the recovery profiles are very patchy, the relatively high recovery coefficients point out that a large share of the soil without interaction with the sprinkling water was not sampled. Moreover, I neglected lateral spread and further percolation in deeper structures by referencing RC to an estimated soil cube spanned by the deepest sampling and the irrigated surface.

Bromide and Deuterium logs do not agree that well. Although both measurements have been conducted with the identical sample, no clear pattern of phase shift or dampening is identified. For the low sprinkling rate there is almost no reaction in the stable isotopes,

while Bromide, Brilliant Blue and GPR identify similar patchy flow paths as in the two other profiles. At the latter the stable isotopes suggest a much stronger exchange of the sprinkling water with the pore water. Contrastingly, the other methods show that large proportions of the soil have not been affected by sprinkling. However, the signal patterns of Bromide and Deuterium with some spikes at $-0.2\,\mathrm{m}$ and $-0.4\,\mathrm{m}$ are somehow similar.

3D time-lapse GPR

From the three 3D radargrams so far only a difference attribute of the signal amplitudes is calculated. This gives a qualitative insight into the overall spread of the irrigation water impulse in the subsurface. The acquisition of one 3D scan of this size took roughly 40 min. It remains unclear to what degree the propagation of the moisture plume after the second measurement is sensitive to a few minutes timing. With observed advective velocities of about $10^{-3}\,\mathrm{m\,s^{-1}}$ and with regard to the hillslope-scale experiment this needs a close revision as I assume that most of the advection was only active during and shortly after sprinkling. Hence it is unclear how critically the result is influenced by the acquisition timing.

Process understanding and coherent method development

Regarding the process it is noteworthy, that the relatively moderate sprinkling rate of $30\,\mathrm{mm\,h^{-1}}$ results in the same pattern, spreading over almost the same space as the stronger ones with $50\,\mathrm{mm\,h^{-1}}$. Thus the initialisation of the preferential flow structures appears to be immediate. Macropore-matrix exchange may have only a minor relevance in these soils.

The three multi-method plot sprinkler experiments can be seen as successful feasibility study for coherent plot-scale exploration of advective flow. The acquisition timing and speed of 3D GPR survey leaves room for improvement. It is planned to utilise a more advanced data analysis after Allroggen et al. [2015] to derive much more detailed and partly quantifiable information. Additional measurements during the experiment and more snapshots in time are found favourable.

Once the method is developed further, the use of Brilliant Blue and excavation could become obsolete. Percussion drilled sample logs can be used for tracer recovery. With this, multiple experiments (with different sprinkling intensity and duration) at the same plot become possible. The experimental and analytical efforts could be strongly reduced while gaining more information.

5.1.5 Hillslope experiment with GPR inferred trenching

The hillslope experiment is one realisation of the proposed specific hypothesis-driven approach combining plot scale and hillslope scale observations. It is designed based on findings from the plot-scale experiments (section 3.1.3, p.43), exploration of many percussion drill cores, measurements of hydraulic conductivity (section 2.3, p.25), analysis of event runoff generation and further data within the CAOS research group. Methodologically, I seek to analyse how subsurface structures, their dynamic connectivity and advective velocities can be explored at the hillslope-scale without excavations or trenches. With regard to process understanding the focus lies on the identification of preferential flow paths (especially lateral ones) and their contribution to water redistribution and runoff generation.

Time-lapse as key for subsurface structure exploration

The interpretation of the 3D GPR exploration of the hillslope towards a map of possible structures for rapid subsurface flow proved extraordinarily challenging. Different approaches resulted in contrasting maps. Much of the methodology is not yet established. Hence the referenced structure map in figure 3.19 is rather a best guess. On the contrary, the identification of active structures through time-lapse analysis of the GPR profiles gave a very robust signal. Although not quantified, it allows an insight into the relative intensities of the respective reaction.

Many soil-hydrological measurements assume state-invariance of the system. Even a relatively large number of samples does not suffice to extract signals from heterogeneity (section 2.3, p.25). To use time-lapse information can also be one key to separate much of the heterogeneity into either noise or structure because it provides a means to identify the relevant sections. In this respect I propose more repetitive measurements and the development of methods which are appropriate for that.

Timing, resolution and estimated depth

As highlighted earlier, the GPR methodology scratches only the surface of the needed spatial and temporal resolution. The limits in spatial resolution are mainly attributed to physical properties of the radar wave propagation, reflection and detection. Higher frequencies would enable higher resolution. But they have also a higher attenuation which limits the measurable depth strongly. Thus advances may be easier to gain in the temporal domain.

Besides the general resolution also the local positioning of the observed structures deserves attention. To assign a certain depth to

a signal in the radargram requires an estimate about the effective velocity of the medium which is not constant over depth and time. GPR measures the time and phase shift of a reflector. The propagation velocity of the radar wave is strongly dependent on the soil moisture content and its distribution with approximate velocities of $0.3\,\mathrm{m\,ns^{-1}}$, $0.03\,\mathrm{m\,ns^{-1}}$ and $0.1\,\mathrm{m\,ns^{-1}}$ for air, water and mineral matrix respectively. It is linked to dielectric permittivity ε given the low-loss assumption as:

$$v_{radar} = \frac{c}{\sqrt{\varepsilon}} \tag{5.1}$$

with c as speed of light ($0.3\,\mathrm{m\,ns^{-1}}$) and $\varepsilon \approx 1, 81, 5$ for air, water and mineral matrix.

The TDR logs propose themselves to close this gap. These measurements have a defined depth reference. However, the integral measurement over a depth increment of 0.1 m to 0.2 m is insufficient to precisely identify structures at length scales of one order of magnitude below.

Close relation of TDR and GPR

TDR uses basically the same principal to calculate the dielectric permittivity in the surrounding soil as surrogate for soil water content. It measures the timing and amplitude of the reflection of an electromagnetic pulse with 1 GHz along some guides. Joint application of the two methods could thus also be used to reduce the need for assumptions in the inversion model for GPR data interpretation. Vice versa, means to quantify the difference attributes of the time lapse GPR radargrams could evolve the method to a distributed soil moisture measurement [e.g. Steelman et al., 2012, Klenk et al., 2015, Allroggen et al., 2015].

Process understanding

Sprinkling intensity and duration were chosen to activate most of the potential flow paths. In addition the preceding storm event has initiated the preferential flow network. Furthermore, the rain shield imposed a strong divide to separate the lateral fraction of rapid subsurface storm flow. Hence the experiment is not intended to mimimic a natural event.

Without surface runoff, with a quick and strong reaction in deep layers and distant observation logs, and with a reach of the reaction in subsurface structures over 6 m downhill it is apparent that a substantial proportion of the water is transported advectively. This is also supported by the core area water balance in figure 5.1. Mass recovery drops below 100 % approximately 2 h after sprinkling start, indicating loss towards downhill areas but also to greater depth. Few

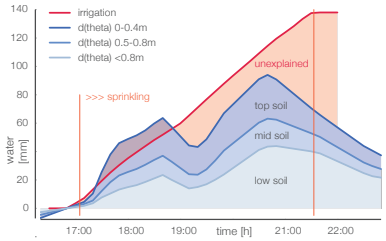

Figure 5.1: Water balance at core area. Explained water as soil moisture change in three soil layers as stapled curves (mean of 4 TDR logs).

minutes after sprinkling the mass recovery on the core area drops quickly below 50 %. Then 15% of the sprinkling water are recovered in the top $-0.4\,\mathrm{m}$.

2/3 of the water irrigated on the hillslope is advectively transported from the core area. This compares well to the estimates from the event water balance (section 2.2.2, p.22). The sub-basin consists of 30% slopes >9°. This results in a possible contribution to a quick runoff of about 20% of the precipitation. But only 5% of the event runoff reaction recovers in the first hump. This leads to the conclusion that a considerable proportion of the water is stored in the structures or percolates to greater depth.

5.1.6 *No advection in the "artificial macropore"*

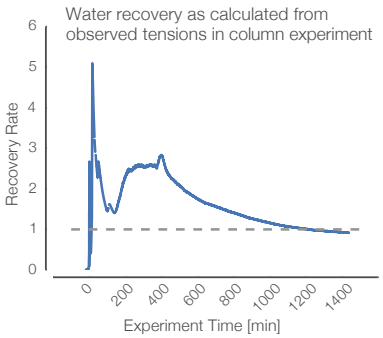

Figure 5.2: Observed moisture change (by means of tensiometers) in column experiment normalised by the applied irrigation water. One means full recovery.

In the first place I was very excited about the experimental data of Germer and Braun [2015] as a reference for macropore-matrix interaction, which is rarely observed – especially at this scale. However, it turned out that the representativeness is limited by the fact, that the "artificial macropore" has completely different properties to those of a natural air-filled one. In contrast with all reported flow velocities in macropores of around $0.075\,\mathrm{m\,s^{-1}}$ (table 4.3), the maximum apparent velocity is about $3.45 \times 10^{-5}\,\mathrm{m\,s^{-1}}$ as inferred from the first observed break-through. Moreover, the water balance could not be closed because of low precision of the conversion of observed matric head to soil moisture based on the step-like retention curve of the silica sand. Especially in the first hours of the experiment, the water content is considerably overestimated by a factor of 5.

A comparison of pure diffusive and advective-diffusive model runs discloses a very small difference between the two. A closer examination of the model behaviour revealed that the advective macropore (which is defined in the second hypothesis) rarely became active. There the matric head depleted the particle advection quickly and allowed for fast diffusion into the matrix in accordance with the experiment. This leads to the conclusion that diffusive transport dominated and corroborates the proposed macropore-matrix exchange formulation.

For process understanding, it can be highlighted that lateral diffusion is not always negligible and may become prevalent. For sprinkler experiments that means that under conditions of conductive and yet dry matrix special care should be given to account for this.

5.2 Discussion of the particle model

5.2.1 The 1D particle model for diffusive and lumped advective flow

In the first iteration we were able to prove that the our space domain random walk solves diffusive soil water dynamics equivalent to the Richards equation. Among others, a particular benefit is the possibility to treat and track each particle.

A less obvious benefit is the capability to combine stochastic and physical descriptions. As such, we are able to describe the advective flow field based on the depth distribution of recovered tracer concentrations. As shown in the second iteration the model is capable of reproducing the observed advection after 2 h but fails the self-limiting exchange process.

Although we aimed at a very parsimonious model, we did not see any other option to account for macropore-matrix interaction in a 1D representation without introducing non-observable parameters. As such, a lumped 1D representation of diffusion and advection failed.

5.2.2 Representative structured domain and particle concept

Building on the idea of self-similarity in flow networks going back to the works of Rodriguez-Iturbe and Rinaldo [1997], Rinaldo et al. [2014] we developed a topologically explicitly structured domain setup for the plot scale. The presence and importance of interfaces in soils [among others Hassanizadeh and Gray, 1990, Lehmann et al., 2012] led to the proposition for the combination of a 2D matrix, which accounts for non-equilibrium lateral and vertical diffusion, and multiple 1D vertically oriented advective structures, which account for fast vertical redistribution. The power of the particle approach can unfold within that domain. By modelling the interfacial processes and the behaviour within the respective domains with the same objects allows direct hypothesis testing.

The simulation results based on the Weiherbach dataset corroborate the feasibility of the approach. Both, domain and fluid, are described based on stochastic properties. However, the key problem of how to assess macropores and fluid processes remains.

From the beginning, we critically questioned, which parameters are reasonable with regard to their observation and representation. We also aimed at model-interfaces to other landscape models such as ecological species distribution or abundance simulations, or thermodynamic applications. Since macroporous systems especially underlie shrinking and swelling [Coppola et al., 2012] and taking up the ongoing debate about dynamic soil properties, all these data are considered as being dynamic and stochastic in nature.

5.2.3 *Diffusion and advection*

The Attert results point out that matrix diffusion is a strong control for the utilisation of the macropore capacity. It is not surprising that the structured, highly heterogeneous young soils do not develop full lateral diffusion. The matrix is characterised by voids, stones and discontinuities. As such, our hypothesis of a continuous layered 2D matrix may not be adequate for this setting. An alternative conclusion is that different macropore systems may also require more specific description. To some degree our hypothesis to reduce the multiple macropore settings in one abstraction may need revision with regard to both aspects: the macropore network and the soil matrix description.

Regarding process understanding, both test cases corroborate that local hydrodynamic and molecular diffusion are subordinate for the overall rapid transport process [Roth and Hammel, 1996]. This opens up the possibility to use the echoRD model to analyse the temporal autocorrelation of rapid flow under different conditions and forcing in order to formulate rapid flow as a Markov process of higher order in a 1D domain. There also a revision towards more efficient random walk solvers [e.g. Dentz et al., 2012] becomes possible.

General discussion of the particle approach and echoRD model The particle approach leaves the solid grounds of Eulerian hydrology, making it difficult to employ most of the accepted standard tools. We introduce new assumptions e.g. that particle interaction and fluid-fluid interfaces are negligible, which may ultimately be falsified.

Moreover, the particle approach is computationally very expensive. Because of the self-dependent state, we could not find any option to make use of the more efficient continuous time RW methodology [Metzler and Klafter, 2000, Delay and Bodin, 2001, Dentz et al., 2012]. Furthermore, I abandoned trials with grid-free methods to calculate the particle density e.g. by Voronoi polygon area calculation [Rycroft, 2009] as they required multiple calculation efforts. This will be left for future improvement (appendix 7.4.2).

Hence I advocate the echoRD model not as replacement for the established Richards solvers but as an extension for cases like rainfall driven conditions, where the diffusion assumption is not met. Since the particle domain can always be converted into a psi or theta field and vice versa, both approaches can work together.

Among others, a certain benefit is the possibility to treat and track each particle through different states and domains, where they state-dependently move diffusively and, if applicable, advectively. As demonstrated, the model became a powerful learning tool and virtual

laboratory due to the explicit topology of structures and hypothesis-driven process descriptions. As such it assists the exploration of model structural adequacy [Gupta et al., 2012].

Unravelling advective and diffusive fluxes implies an improved structural adequacy of the model and transferability of model structures to similar places. This is because matrix flow and preferential flow are dominated by different forces (either capillary forces or gravity) and deplete different gradients in free energy [Zehe et al., 2014]. Second, with soil matrix and preferential flow paths acting as independent factors that control subsurface flow resistances, they are independent sources of equifinality [e.g. Binley and Beven, 2003]. Preferential flow networks with different topological and hydraulic properties result in the same control volume resistance and thus match observed flow and transport equally well, even if all other model parameters are kept constant [Wienhöfer and Zehe, 2014]. Separate treatment of matrix flow as well as vertical and lateral preferential flow allows constraining the degrees of freedom in both flow domains independently.

By founding the model on physical and stochastic grounds without internal parameters, I also contribute to model falsifiability [e.g. Harte, 2002]. As it is making direct use of the laboriously gathered and valuable data from experiments, surveys and monitoring it also improves the matching of model concepts and hydrological observables Beven [1993, 2006a].

5.2.4 *Exploration of the impact of rainfall duration and intensity on soil water redistribution*

I used the validated echoRD model setups as virtual laboratory to test the impact of rainfall duration and intensity on soil water redistribution. It is also an evaluation of the model's capability as virtual lab.

Generally the model appears to capture the processes well and to deliver a basis for extrapolation from the validated case. It is also able to simulate the different flow regimes in the two examples. However, in the Colpach case the particles tend to remain advectively active for a long time. Although the experiments suggest strong activity during the event, they also have shown a relatively quick decline of advection afterwards. Thus the introduced scaling factors and the missing superordinate drainage need to be reconsidered. Unlike in the case of biopores here the interaction with the matrix was substantially scaled. This results in a general reduction of lateral diffusive transport. In combination with the coating factor the self-limitation of advection is counteracted and hence the universality of

the approach restricted.

From a model perspective also the necessity of the numerical stability criterions becomes apparent. All runs with a relaxed time step control exhibit a reduced advection in comparison to runs with similar or less forcing and restrained numerical stability.

From a process perspective, the results once more support the hypothesis that advection is a common dissipation path of mass-induced gradients in hydrological systems. Also low intensity and amount in rainfall can cause substantial vertical redistribution. The plots exhibit the advection as some kind of bulk movement which eventually is stopped and diffusively dispersed. With higher intensity and duration more of these bulks are triggered (grey stripes in Weiherbach case figure 4.14). This is less so in the Colpach case. Despite the extraordinarily spacious macropore network light rains do not cause much advection of new particles. On the other hand, the distribution of Péclet numbers resembles well the observed bypass of advective water in about $-0.3\,\mathrm{m}$ depth.

5.2.5 *Outlook on the echoRD model*

The echoRD model has hence also proven to be an adaptive learning tool. However, in its current state it requires considerable computational resources. This especially limits its application for long periods and larger areas.

Without a robust estimate of macropore distribution echoRD cannot be applied for structured soils. The next steps will consist of further development of the model parameterisation based on experiments accompanied by ground penetrating radar (GPR) campaigns [Allroggen et al., 2015]. On the other hand, the model will be linked to ecological models for abundances and activity of earth-dwelling species [van Schaik et al., 2013, Schröder, 2008].

We will further extend the scalable approach to the hillslope by means of definition of representative soil domains connected to an explicit lateral structure [Zehe et al., 2014]. Moreover, a full utilisation of the particles' advantages to carry heat and momentum will be explored.

Another future step is to work on a dynamic definition of temporal autocorrelation of advection using the echoRD model as a tool to establish definitions for a advection as a Markov process of higher order. This would open up ways to model simplification and connections to approaches at the hillslope scale such as Multiple Interacting Pathways (MIPs) model [Davies and Beven, 2012, Davies et al., 2013].

5.3 GIS and process analysis for functional unit identification

A functional unit (FU) is intended as concept which revises the static hydrological response units towards a process oriented description. The analysis for possible classification and FU identification based on remote sensing data and GIS derived indexes resulted in a strongly topography dominated picture. It somewhat contradicts the findings from the process analysis based on water balance calculations which is mostly driven by storage dynamics and the results from the functional soil examination.

5.3.1 Unravel storage and drainage

One major step in the identification of functional units is to acknowledge the relevant functions of the system. For soils I have shown, that despite fast advective flow of free water the retention curves describe silty characteristics with substantial storage also at higher tensions. The widely used models for water retention and hydraulic conductivity after Brooks and Corey [1964], Van Genuchten [1980] simplify the storage and drainage function into one. This is one fundament of most current hydrological process models.

Storage, as the capillary capacity to retain soil water against gravity and evaporative pressure, has been characterised by water balance calculations and soil sample analyses. Both present a distinct difference between the sandstone sub-basin against the marls and schists. The retention curves of the two latter sub-basins only deviate for the very low tensions. The larger pore space below field capacity corresponds to slightly more flashiness in the water balance dynamics in the Colpach basin.

Drainage and possible groundwater recharge is more related to the experimental findings and the existence of preferential flow paths. I have shown that such structures are governing the infiltration at large precipitation intensity. The resulting tracer depth distributions are not yet sufficient[1] to lead to a complementary standardisation to the retention curve or to extend the proposal of Vogel and Roth [1998]. Nevertheless, much points to a combination of network characteristics and lateral diffusive capacity of the soil matrix to control the processes.

[1] So far nine such plot-scale experiments are very few. In addition the sandstone examples happened to represent conditions in the marls since the locations have been in the lower part of the Huewelerbach sub-basin where the sands are covered by silts and clays.

5.3.2 Landscape delineation based on quasi-static data

On the one hand the ambiguous derivation of process-relevant units from static data is a theme which is recognised throughout the study. On the other hand the hypothesis of self-organisation would reversely mean that processes manifest themselves in structures and

site characteristics. From the perspective of the GIS analysis, it remains unclear if the data or the used indexes are causing this contradiction. Recently Ali et al. [2014] highlighted restrictions of wetness indexes, too. Oppositely, Gharari et al. [2011] successfully derived functional classes with the more conceptually driven HAND-approach in a nearby catchment.

The relatively good agreement of the mean local observations of soil characteristics with the hydrological processes also contradicts my findings from GIS analyses and remote sensing. With respect to soil water dynamics soil data appear to matter much more than topographic information.

Nonetheless, this apparent mismatch could also be a matter of different scales. Similar to the explorative means, a suitable time-lapse scheme could be key to reduce ambiguity. The satellite products used so far cannot provide the needed resolution - especially in time. This becomes particularly obvious when comparing the time scales of advective flow velocity ($10^{-3}\,\mathrm{m\,s^{-1}}$), event reaction[2] ($2 \times 10^{3}$ s to 2×10^{5} s) and remote sensing data[3] (1×10^{6} s to 2×10^{7} s). However, time-lapse remote sensing at the desired scale of events and hillslopes remains challenging.

[2] see section 2.2.2, p.22

[3] MODIS data is operational as 14-day integral. Landsat data reduce often to one or two scenes per year due to cloud cover.

Another option is a more hypothesis driven approach to FU delineation which is discussed in the following section.

5.4 *Pushing the basins and squeezing the models – a suggestion to step beyond rainfall-runoff analysis*

It has been shown in uncountable studies that given some information about a plot, hillslope or catchment, hydrological models are well capable to reproduce the observed behaviour to a satisfactory degree irrespective of all the uncertainty and equifinally coming with it. Alongside, substantial criticism on the common procedure of "blindly calibrating" model parameters and/or structures was formulated, too [e.g. Buytaert et al., 2008, Clark et al., 2011, Gupta et al., 2012, Gupta and Nearing, 2014].

This thesis presented a comprehensive argumentation for hydrological science relying on hydrological technologies. From this perspective, the thrill of rainfall-runoff modelling based on some standard soil parameters, topographic data and observed soil moisture and discharge dynamics is relatively low – although unarguably valuable for innumerable applications. The application of existing complex models with highly uncertain data and known restrictions and conflicts with the model concept and perception leaves us with a melange of unknowns hardly possible to unravel model artefacts from process insights. The multitude of processes and scales, limi-

tations of singular observations and the tools for their interpretation raise questions about getting trapped in circular reasoning, recovery of assumptions or ambiguity.

It has been suggested earlier, that hydrological sciences could benefit from more rigour in hypothesis testing based on the creation of controlled, repeatable and comparable settings. This has quite dramatic implications for hydrological process monitoring, experiments and modelling as it changes the order of how to adequately explore a system.

5.4.1 *Monitoring catchment dynamics*

Hydrological monitoring of catchment dynamics most often stands at the beginning of a study as we intend to analyse the processes in more detail. Based on the water mass balance $dS = P - Q - ET$ the standard setup will consist of monitoring stations for storage change (dS, through soil moisture sensors), precipitation input (P, as tipping bucket rain gauge) and stream discharge (Q, as gauge or water level sensor). Evapotranspiration (ET) is most often estimated based on the other terms. This is basically a manifestation of the perceptional model of a leaky bucket ignoring large parts of the literature of the past 35 years.

As I have discussed in section 5.1 (p.99), monitoring soil moisture state dynamics may not be as universal and informative as intended. Many studies have proven that an integral discharge volume signal can hardly be distinctly deconvoluted into the different contributing areas and flow paths. Other studies have proven that single tipping bucket rain gauges are barely sufficient to have a robust estimate of the incoming precipitation. Hence even within the leaky bucket concept there is lots of uncertainty, potential bias and equifinality.

Setting up a rain and stream gauge is still a good idea – as preliminray reference.

Referring to the debate of ungauged basins [Sivapalan et al., 2003, Blöschl et al., 2013] and because we cannot *a priori* know when to measure the most informative discharge data [Seibert and Beven, 2009] gauging a basin probably remains one of the best hydrological monitoring investments. Referring to the mismatch of the GIS analysis in section 2.4 (p.31) and the examination of the Attert flow regimes in section 2.2 (p.18) it is pointed out, that especially subsurface hydrological processes need ground truthing. However, this is just giving a foundation to formulate specific hypotheses about the basin.

Formulate hypotheses about dominating and specifically relevant processes, flow paths and controls

In the Attert basin a sequence of studies have sharpened the perceptional models of the hydrological processes [van den Bos et al., 2006, Fenicia et al., 2008, Wrede et al., 2014] based on due exploration of the water balance dynamics. The Delft-school models SUPERFLEX [Fenicia et al., 2011] and FLEX-topo [Savenije, 2010] have proven as impressively powerful tools to link mesoscale catchment organisation and rainfall-runoff modelling. Based on findings from such model applications one could not only explore multiple model hypotheses [Clark et al., 2011] but also formulate specific exploration hypotheses.

5.4.2 *The basins as laboratories – laboratories as basins*

Of course any simulation of natural systems needs data and computationally arranged process knowledge. As such some preliminary data about the mayor catchment properties is unarguably crucial as are reliable maps of soil-landscape elements.

Experimental proof and refinement of the perceptional models

Running specific hydrological process experiments as presented in chapter 3 (p.41) is fundamental to identify the scope of processes, appropriate means of observation and to test the formulated hypotheses. Multi-method approaches have been pointed out as highly beneficiary in this regard, although the major challenge is to coherently apply them.

Pushing the basins

To turn the basins into laboratories we need control over boundary conditions. On the one hand this is one crucial requirement for the observation setup. On the other hand we can and should create conditions which allow repeatable experiments. With the GPR inferred trenching in section 3.3 (p.57) I proposed one possible way to control conditions, separate processes (lateral subsurface storm flow in this example) and to non-invasively observe the response in the subsurface structures. Experiments like this should be repeatedly conducted to reduce uncertainty about controls of connectivity initiation and spatial persistence of active structures.

Such insights are hardly possible through less specific monitoring. As pointed out in the discussion of the hillslope-scale experiment, even the extremely dense network of 16 soil moisture sensor logs could not resolve the observed flow in very few distinct structures. This does not contradict the findings of Zehe et al. [2010a] that nested

soil moisture sensor clusters retain a high autocorrelation among the sensors. It is more an extension of the findings, that point observations remain a) uncertain about their spatial extrapolation and b) biased towards the diffusive phase as discussed in section 5.1 (p.99).

Coherent complementary observations

In section 3.2 (p.48) I presented findings from plot-scale sprinkler experiments using multiple tracers and observation techniques. It was especially insightful that the different methods did not agree *per se* and that only their complementary interpretation could reveal the full picture. Although successful, there is much room for improvement of methodological, spatial and temporal coherence of such methods.

Back to the lab

Another avenue to enable rigorous hypothesis testing is a revision of laboratory experiments. Much of hydrological experiments have to be conducted *in situ* to retain soil structures and local specifications. At the same time it is very challenging to control conditions and boundaries in the required precision in the field. Especially when it comes to processes at the macropore-scale and smaller, lab experiments offer a great opportunity to extend knowledge about processes such as macropore-matrix interaction. The latter was identified as crucial control for rapid subsurface storm flow. However, it is basically unknown (see section 4.5, p.77). Laboratory experiments can also strongly support the identification of adequate observation strategies for different settings.

5.4.3 *Squeezing the models to extend experiments in the real world*

With all enthusiasm to experimental hydrology it remains impossible to comprise the multitude of different states and forcing with real world experiments alone. Models have been employed to extend beyond single setups in virtual experiments [e.g. Graham and McDonnell, 2010, Klaus and Zehe, 2010, Smith et al., 2013].

Conceptual, physical and scientific rigour

Models are by definition limited in their representation of the natural complexity. Hence applying models to extend process understanding and experimental evidence needs to revise the capabilities of potential models. Since hydrological models evolved to complex and complicated code monsters it is not *a priori* given, that *physically-based* models are more physically sound than *conceptual* models. Gupta et al. [2012] highlight that any numerical model realisation is

founded on a perceptual model which formalises in a building process as conceptual model. Employing mathematical model schemes it is finally implemented as computational model.

It is thus a necessary step to revise the full chain for its applicability to the processes under study. It is no surprise when hydrological models which solve the Richards equation and are specifically developed for diffusive processes fail to perform well for advective flow in structured soils. Nevertheless, they are the most important tool in hydrological modelling – when the conceptual assumptions are met.

Diffusive and advective flow in structured soils

As one possible step further in this regard I presented the echoRD model (eco-hydrological particle model based on representative structured domains) in chapter 4 (p.67). Since structured soils prevail in nature and based on the physical meticulousness given to its development the model enables numerous hypothesis testings as the structured domain of diffusive soil matrix and advective macropores is unraveled and yet fully dynamically coupled. It relies on very few observable parameters and even manages to self-control macropore-matrix interaction.

6
Synopsis

Rapid subsurface flow in structured soils arises from imperfect lateral mixing of fast advective flow in structures and diffusive flow in the soil matrix. A physical process description and a unifying concept for structured soils is one of the long-standing challenges in hydrology. It is strongly linked to landscape organisation, heterogeneity and patterns, self-organisation of structures as dissipation paths, and a revision of exploratory strategies.

I presented examples from the Attert experimental basin in Luxembourg addressing landscape and process analysis (chapter 2), targeted experiments at the plot- and hillslope-scale (chapter 3) and the development of a novel model framework representing water as particles in a representative, structured domain (chapter 4).

Landscape analysis and functional unit identification

In section 2.2 and 2.4 I contrasted the analyses of the flow regimes against an investigation of GIS and remote sensing (RS) data. Both aspects contribute to the finding that the geological setting (although strongly impactive) is not the only descriptor in the basin. The study also suggests that functional unit (FU) identification and landscape delineation on GIS and RS alone can lead to classes which are inconsistent with observed processes in the subsurface such as runoff conversion. Although the study did not succeed in testing the FU hypothesis and developing a procedure to derive them, I extended the tools and theoretical concepts towards it.

Experiments to measure advective flow in structured soils

The experiments at the plot-scale show for all sites rapid subsurface flow in biogene, pedogene and geogene structures (section 3.1.3). While the binary Brilliant Blue stains allow the identification of preferential flow paths, recovered Bromide concentration profiles enabled a very detailed description of the advective flow field. The latter is

specific in the different settings. However, it also has a large uncertainty – especially about the representation based on high overall recovery rates and small sample volumes, and about transferring the results to different pre-event states and rainfall events.

Great progress was achieved through the coherent combination of different tracers (Brilliant Blue, Bromide, stable Isotopes) and methods (soil moisture monitoring, tracer recovery, 3D time-lapse GPR) (section 3.2). Primarily the discrepancies between the results sparked a revision of the perception of the processes and the exploratory methods.

In the hillslope-scale experiment (section 3.3) the findings from the plot-scale were extended. While vertically a fraction of the water largely bypassed the soil between $-0.4\,\mathrm{m}$ to $-1.1\,\mathrm{m}$ depth (v_{adv} $\approx 10^{-4}\,\mathrm{m\,s^{-1}}$) also lateral structures lead to fast transport ($v_{adv} \approx 10^{-3}\,\mathrm{m\,s^{-1}}$). Further it was found very challenging to identify hydrologically relevant structures from one exploration alone. However, the GPR inferred trenching based on repetitive measurements of the same profiles did clearly identify distinct flow paths. Hence exploration based on the differences during active and non-active states is proposed.

Nonetheless, the used methods are still far from being a standard in hydrology. Primarily the temporal and spatial resolution and secondly the coherence of different methods are found to deserve further enhancement. Still, a mere increase in resolution is not sufficient to overcome conceptual bounds of the methods.

The echoRD model

The presented new model framework of using water particles in a representative domain (chapter 4) is a fundamental innovation for hydrological process modelling. I have shown that a spatially explicit random walk performs very well for diffusive flow compared to Richards solvers and observations (section 4.3). Moreover I have presented that self-limitation of the advective flow in structures requires macropore-matrix interaction (section 4.4).

Consequently, the resulting echoRD model (section 4.5) is capable to simulate diffusive and advective flow in a structured domain. The particles' advection is represented as dynamic film flow with exchange to the matrix based on energy dissipation calculations. As such the model requires only soil physical parameters and a good estimate about the macropore depth and density distribution (derived from Brilliant Blue or GPR sprinkler experiments).

The greatest advance is the stochastic-physical foundation in which all parameters are determinable by measurement, process descriptions can be used as hypotheses and where parameters and

structures are allowed to change over time. It was further highlighted that a single estimate for maximal velocity in the macropore network is sufficient.

Process understanding of advective-diffusive water dynamics in structured soils

The experiments and the echoRD model addressed diffusive and advective soil water dynamics. The experiments underline that both paths are relevant and that the exploratory method may be biased to the one or the other domain.

In terms of process examination through the model, two results are highlighted: Friction control to advection appears realistic as self-limitation through additional drag at the macropore wall worked well. This corroborates the hypotheses of Roth [2008] for macropore flow and allows the utilisation of a relatively simple estimate of the maximum advection in the structures as reference. Moreover, infiltration based on macropore drainage areas after Weiler [2005] was successfully applied for biopores. With respect to not fully wetted topsoil surfaces the approach was extended by a scaling factor derived from horizontal Brilliant Blue dye stains.

Evolution of dissipative structures and thermodynamic limits of a landscape

The study did not succeed in an extension of the theoretical foundations of energy dissipation processes and heat engine limits of hydrological processes. Nonetheless the echoRD model is a tool which will help to explore these concepts further. Regarding processes understanding I showed that a thermodynamic control to friction in the macropores works well. In appendix 7.5 another model study corroborates that landscape setting impacts the hydrological system only when the dissipation limits (mass or energy) are reached.

The next steps will be to investigate the effect of decay and maintenance of such structures and possible optimality. This also enables one to approach the question of how the landscapes are impacted by the frequency of drying and wetting cycles.

Minimal adequacy of model complexity, geophysical exploration, functional unit identification and approximation of heterogeneity in hydrological systems

Aside from the specific findings, a major concern of this thesis is the joint consideration of theoretical concepts, experimental techniques and modelling approaches. I thus conclude this thesis by pointing

out that an answer to the initial question about minimal adequacy is less straightforward than initially anticipated. In many cases (as also in this study) a proposition of adequate tools can only be given *a posteriori* to extensive exploration. At this stage the many samples (section 2.3), landscape and process analyses (sections 2.2 & 2.4), and experiments (chapter 3) are still not sufficient to derive a functional, hydrological process specific soil map for the basin.

As I discussed (section 5.4) the mere application of some model to some data does not generate much insight. Similarly, a point measurement waiting for some event in a structured system has only a small chance of revealing new information about the system (section 3.3). At the same time it takes considerable effort to design coherent experiments with different complementary techniques (section 3.2), a strong control over all boundaries at appropriate spatial and temporal scales. Furthermore, there is much to learn from models when employed as conceptual hypotheses.

Hence I suggest revising the procedure to approach a catchment:

1. Preliminary exploration, data analysis and modelling of catchment dynamics and functional unit candidates to derive specific hypotheses about prevailing processes and perceptional models
2. Experimental testing of these hypotheses with coherent complementary observations of responses to controlled conditions and possibly repeated forcing
3. Extension of the experiments in models exhibiting conceptual adequacy, sufficient degrees of freedom and possibly self-controlled process interaction
4. Identification of adequate controls and observation techniques for the dominating processes and potential operational models for the respective sub-basins and monitoring applications

Likely, step 2 and 3 may need iterations to test the hypotheses throughout.

7
Appendix

7.1 GIT repository

As introduced and referred to earlier, most of this work is accessible through my GIT repository at `https://github.com/cojacoo`. Following this link will give you access to a readme-document describing the path and helping you navigate through the collection of analytical code, sample data and the echoRD model itself.

7.2 Maps

This section presents given and derived maps of the Attert experimental basin. Data basis have been the following sources:

- Topographical map of Luxembourg, Scale 1:20 000, 2008. Administration du Cadastre et de la Topographie. Grand-Duché de Luxembourg.
- Geological Map of Luxembourg, Scale 1:25 000, 1949. Service géologique du Luxembourg. Grand-Duché de Luxembourg.
- Land Cover, Occupation Biophysique du Sol, Scale 1:15 000, 1999. Based on color IR areal images. Grand-Duché de Luxembourg. And Carte d'Occupation du Sol de Wallonie, Scale 1:10 000, 2011, Service Public de Wallonie, Direction Générale opérationnelle Agriculture, Ressources Naturelles et Environnement
- Soils, Sols des plateaux et des pentes, Scale 1:100 000, 1969. Ministère de l'agriculture, de la viticulture et du Développement rural-Administration des services techniques de l'agriculture-Service de pédologie, Grand-Duché de Luxembourg. And Carte Numérique des Sols de Wallonie, 2007. Service Public de Wallonie, Direction Générale opérationnelle Agriculture, Ressources Naturelles et Environnement

- DEM, Modèle Numérique de Terrain de Luxembourg, 5m LIDAR. Relief de la Wallonie - Modèle Numérique de Surface, 10m LIDAR.
- MODIS near-IR reflection (2005-2011, 14 day timestep, 250 m resolution, MOD13Q1) (accessed through USGS Earth Explorer).
- Landsat 7 – 32 day composite of the Normalised Difference Vegetation Index (NDVI, using red (0.66 µm) and near-IR (0.83 µm) reflection bands, 30m resolution) (accessed through google earth engine).
- Landsat 7 – 8 day composite of the Normalised Difference Water Index (NDWI, using near-IR (0.83 µm) and mid-IR (1.65 µm) reflection bands, 30m resolution) (accessed through google earth engine).

The maps have been reprojected into EPSG:2169 Luxembourg 1930 / Gauss projection using GRASS GIS. The resolution of all maps has been harmonised to 10 m. The given map units are metre. While calculations have been performed in GRASS GIS, SAGA GIS and Whitebox GIS, the maps have been rendered using Quantum GIS.

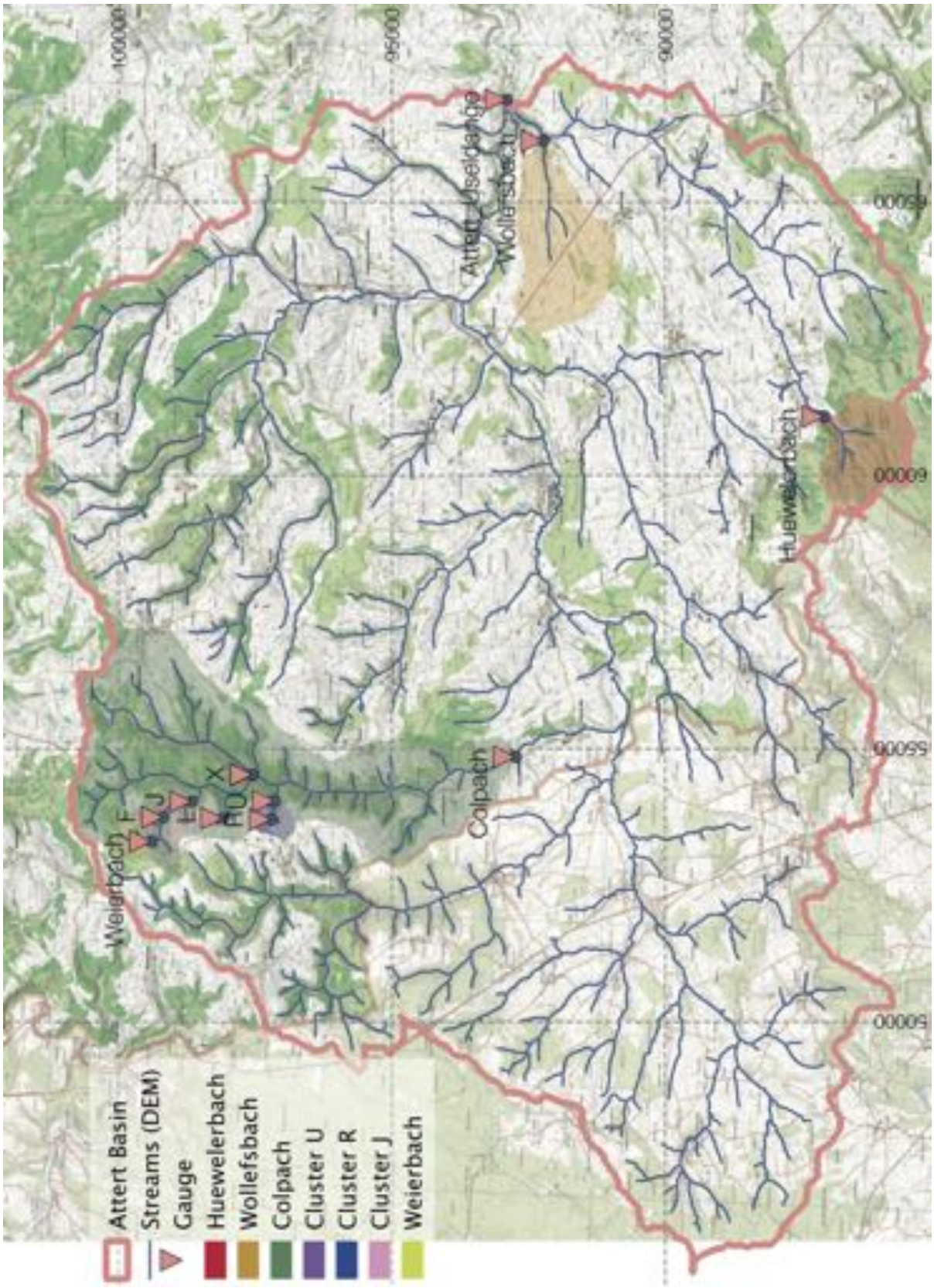

Figure 7.1: Attert experimental basin. Topographic map with marked gauges and subbasins. River network and watersheds derived from GIS analysis of the joint DEM.

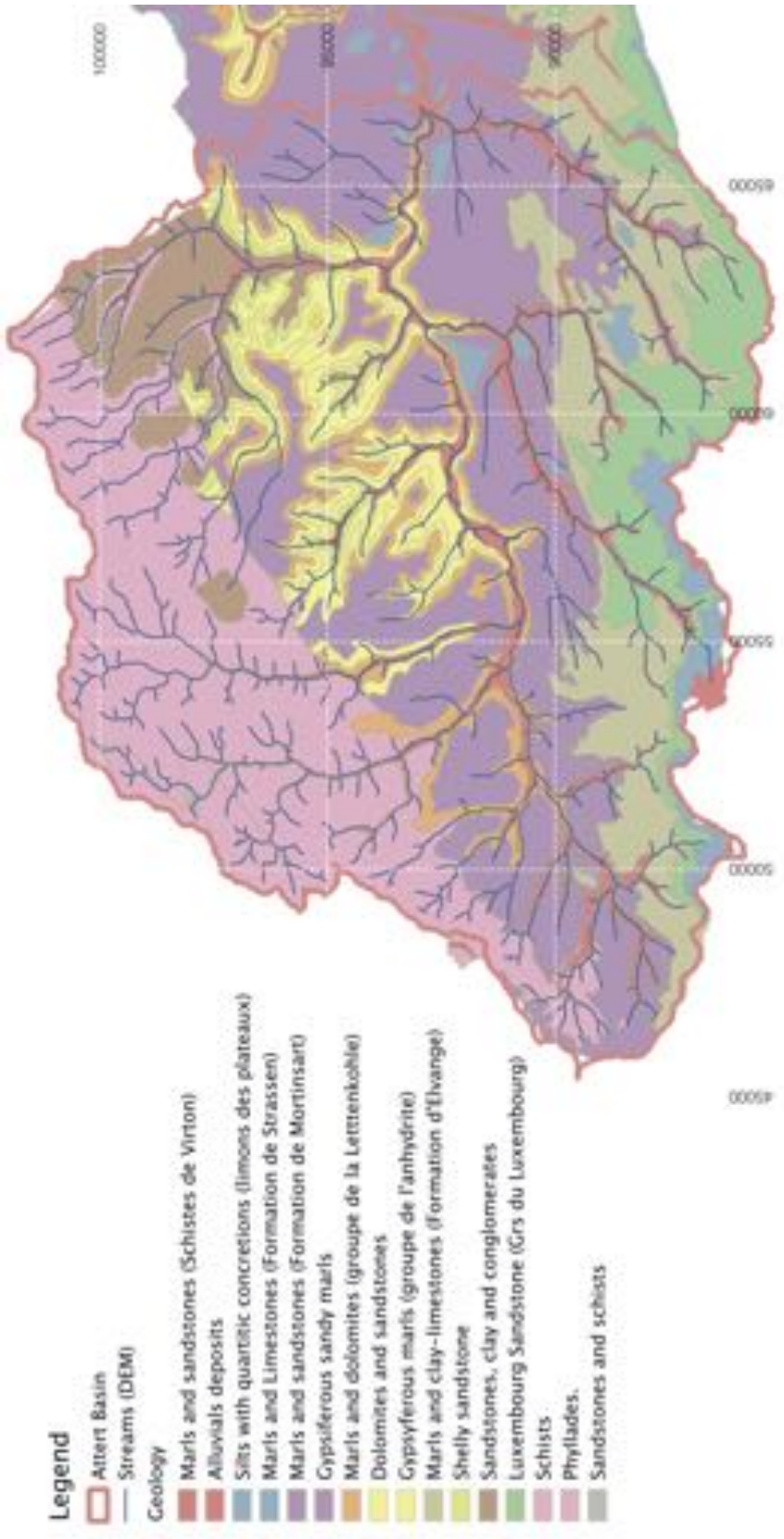

Figure 7.2: Attert experimental basin. Geology classes.

Figure 7.3: Attert experimental basin. Land cover classes based on land cover data.

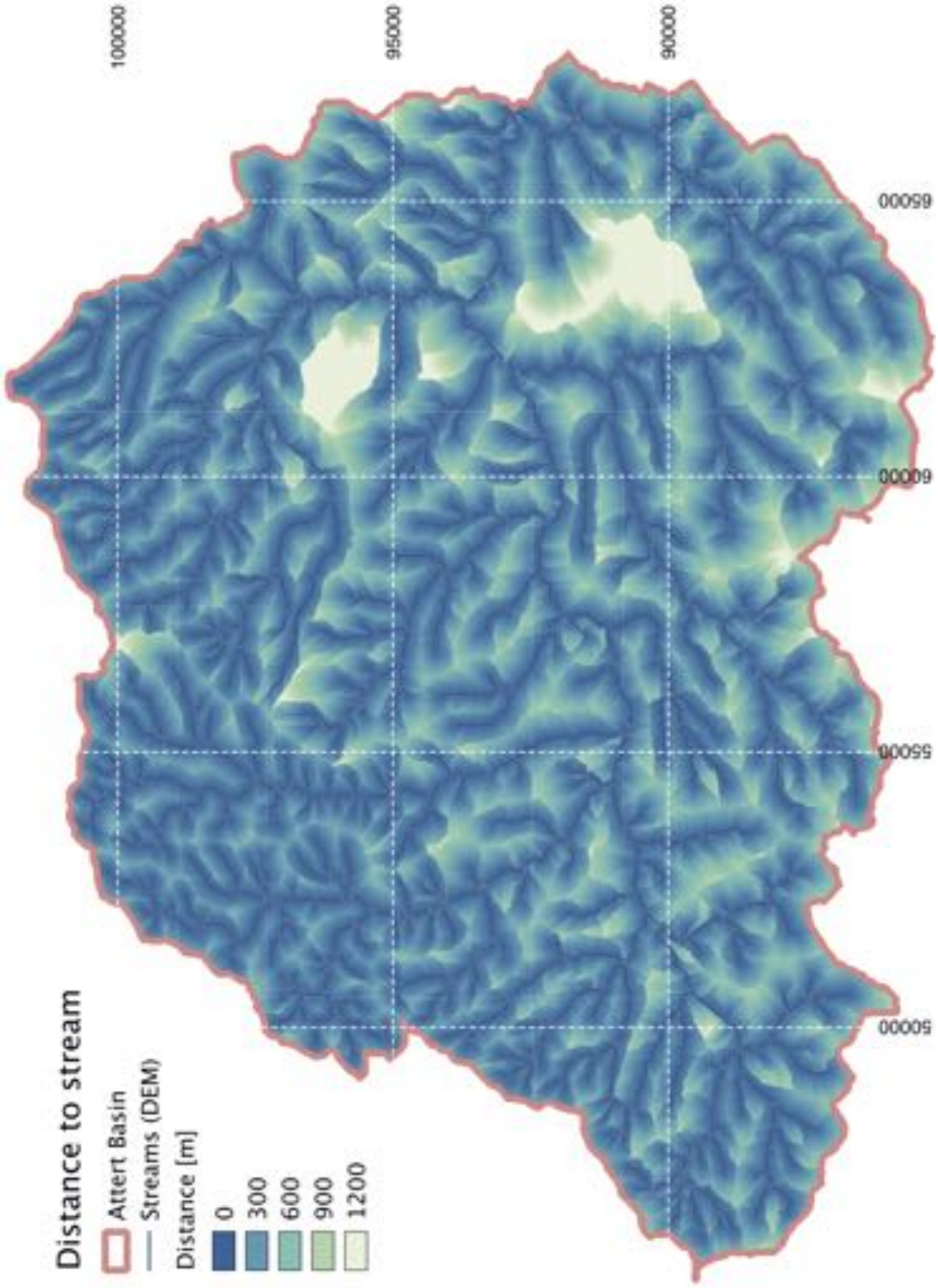

Figure 7.4: Attert experimental basin. Distance to stream calculated based on joint DEM in GRASS GIS using r.stream.distance [Jasiewicz and Metz, 2011] (downstream method).

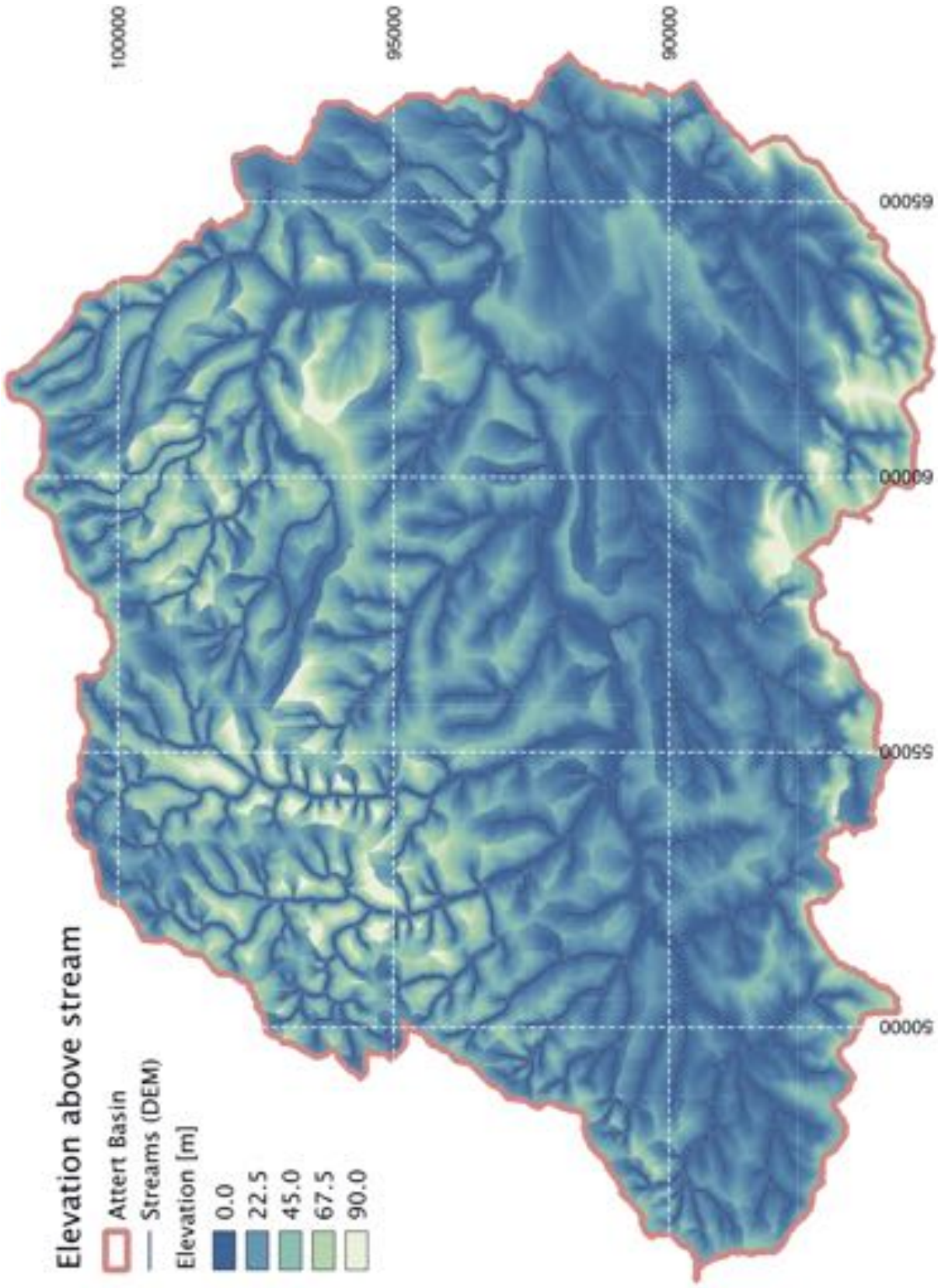

Figure 7.5: Attert experimental basin. Elevation above stream calculated based on joint DEM in GRASS GIS using r.stream.distance [Jasiewicz and Metz, 2011] (downstream method).

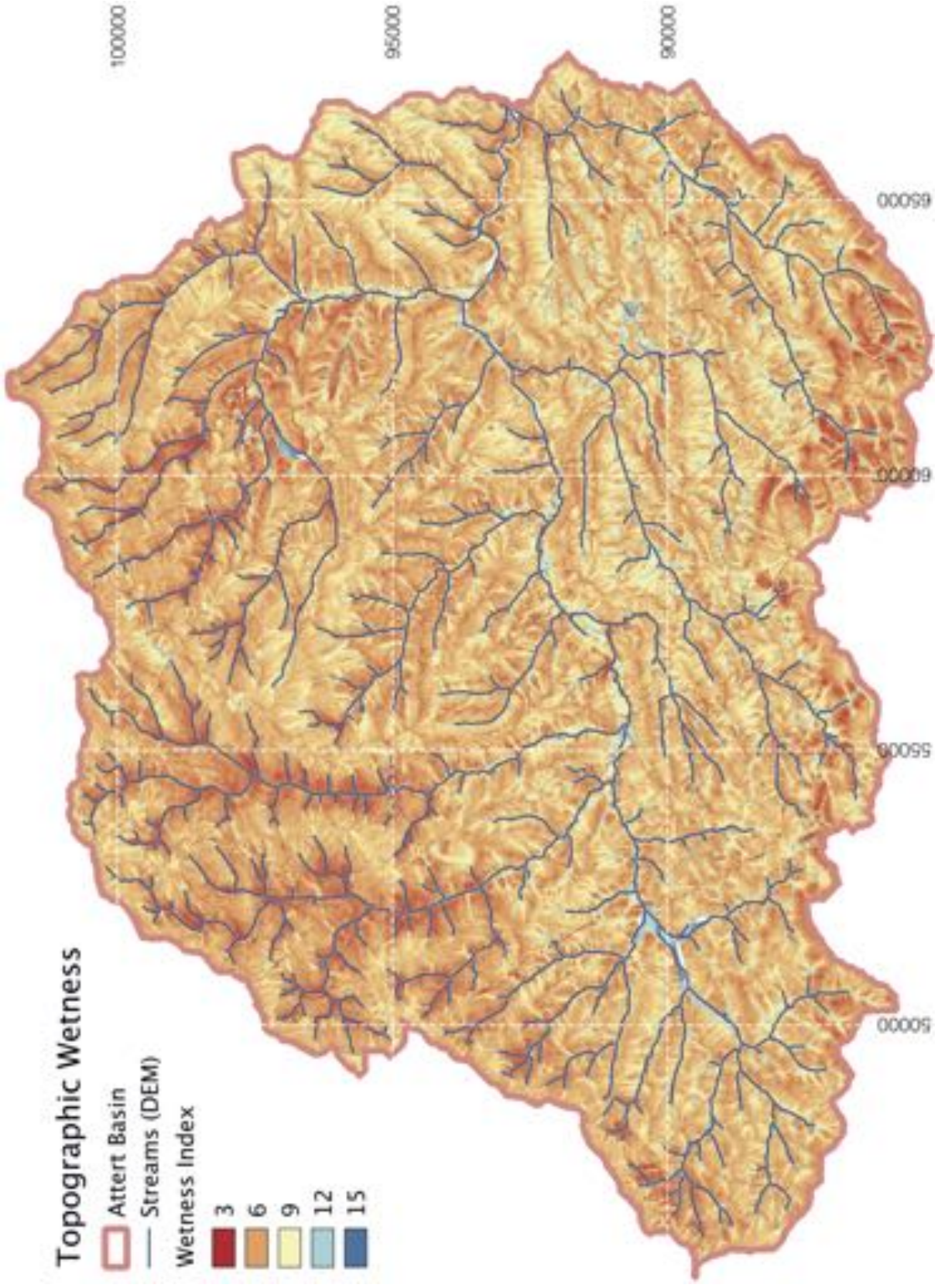

Figure 7.6: Attert experimental basin. Topographic wetness index [Beven and Kirkby, 1979] calculated based on joint DEM in SAGA GIS [Conrad, 2006].

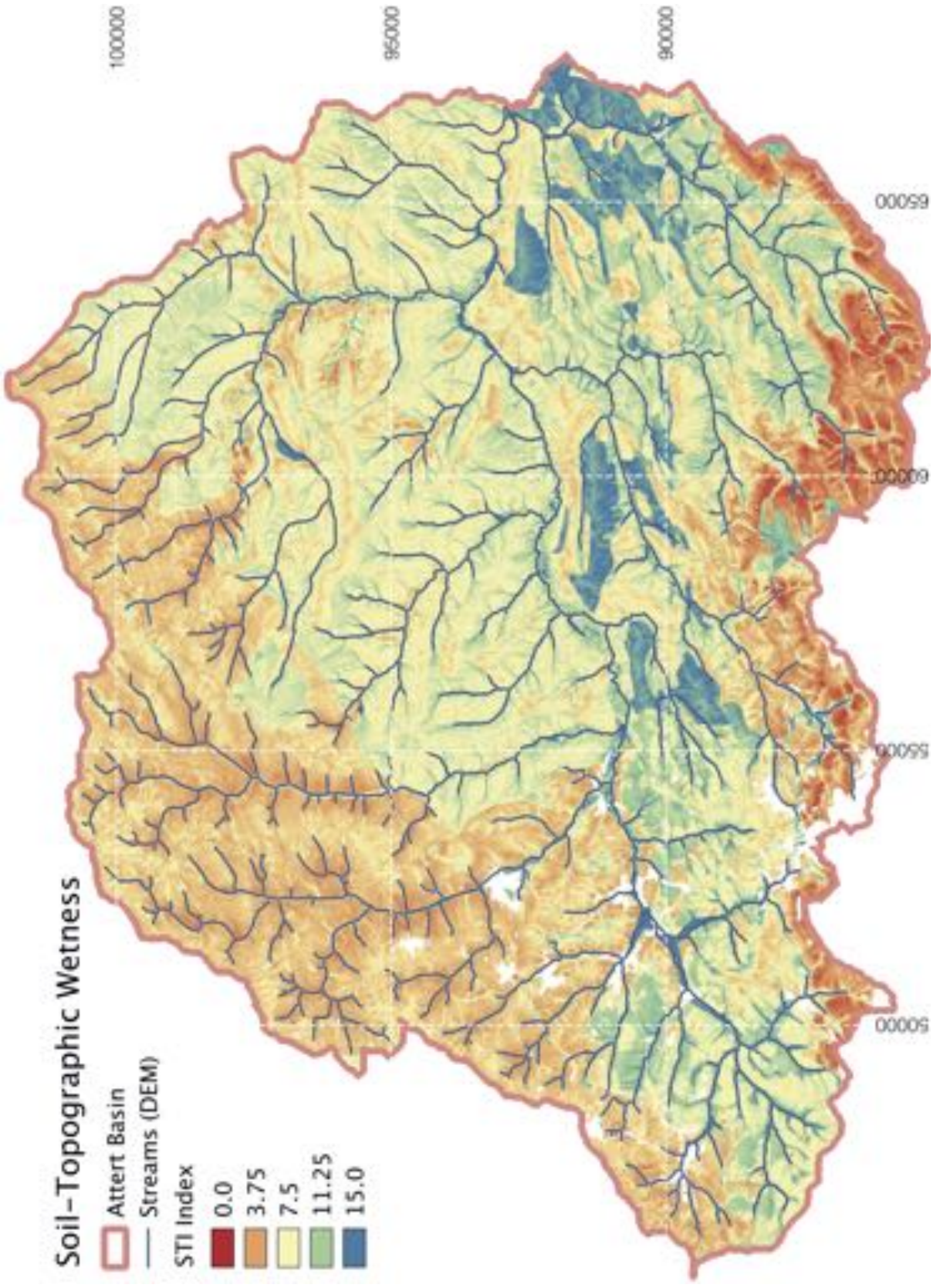

Figure 7.7: Attert experimental basin. Soil-topographic wetness index [Walter et al., 2002] calculated based on joint DEM, TWI (map 7.6) and soil parameter estimates as described in section in section 2.4.3 (p.33).

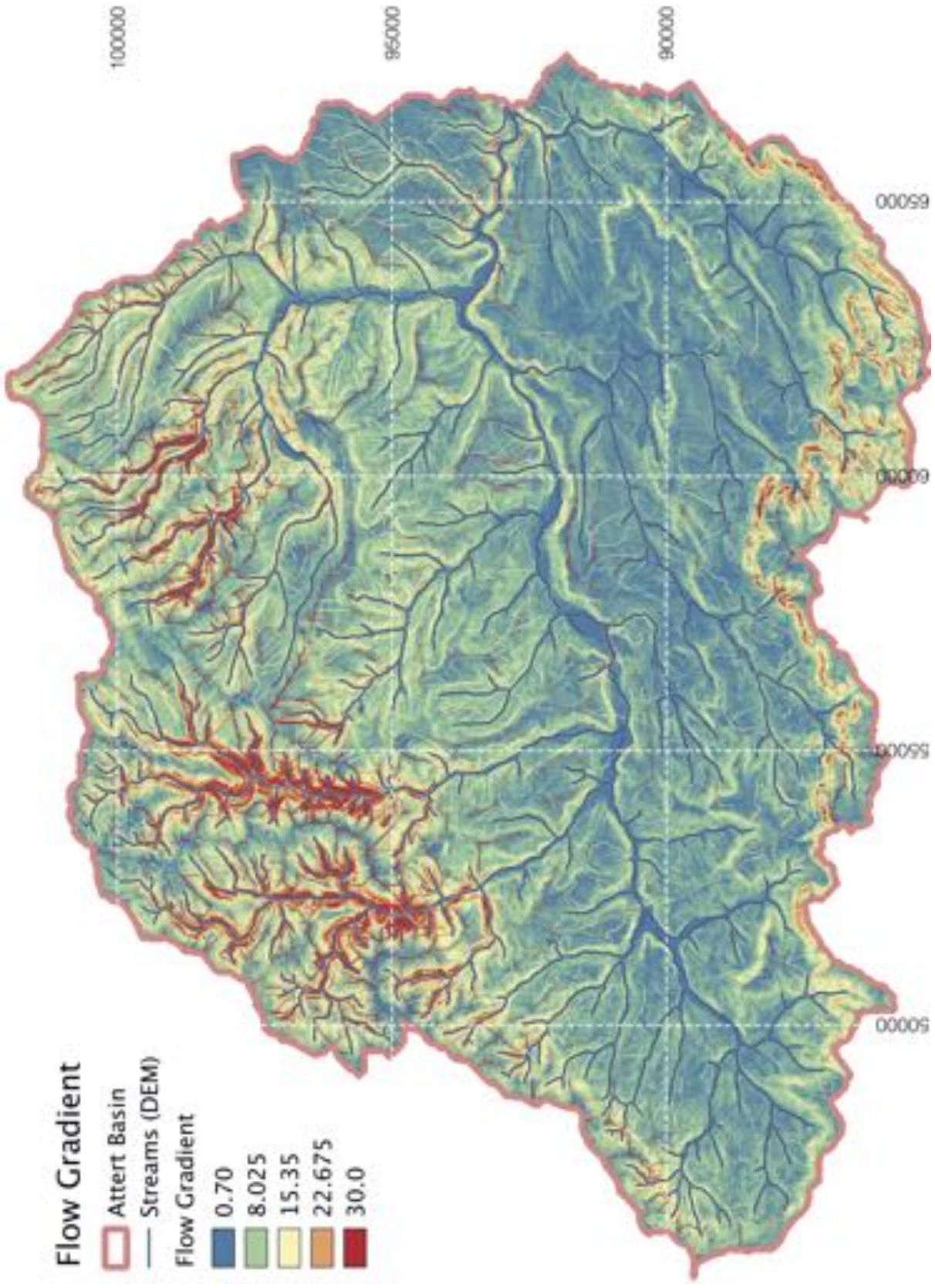

Figure 7.8: Attert experimental basin. Flow gradient calculated based on map 7.5 and 7.4 as described in section 2.4.3 (p.33).

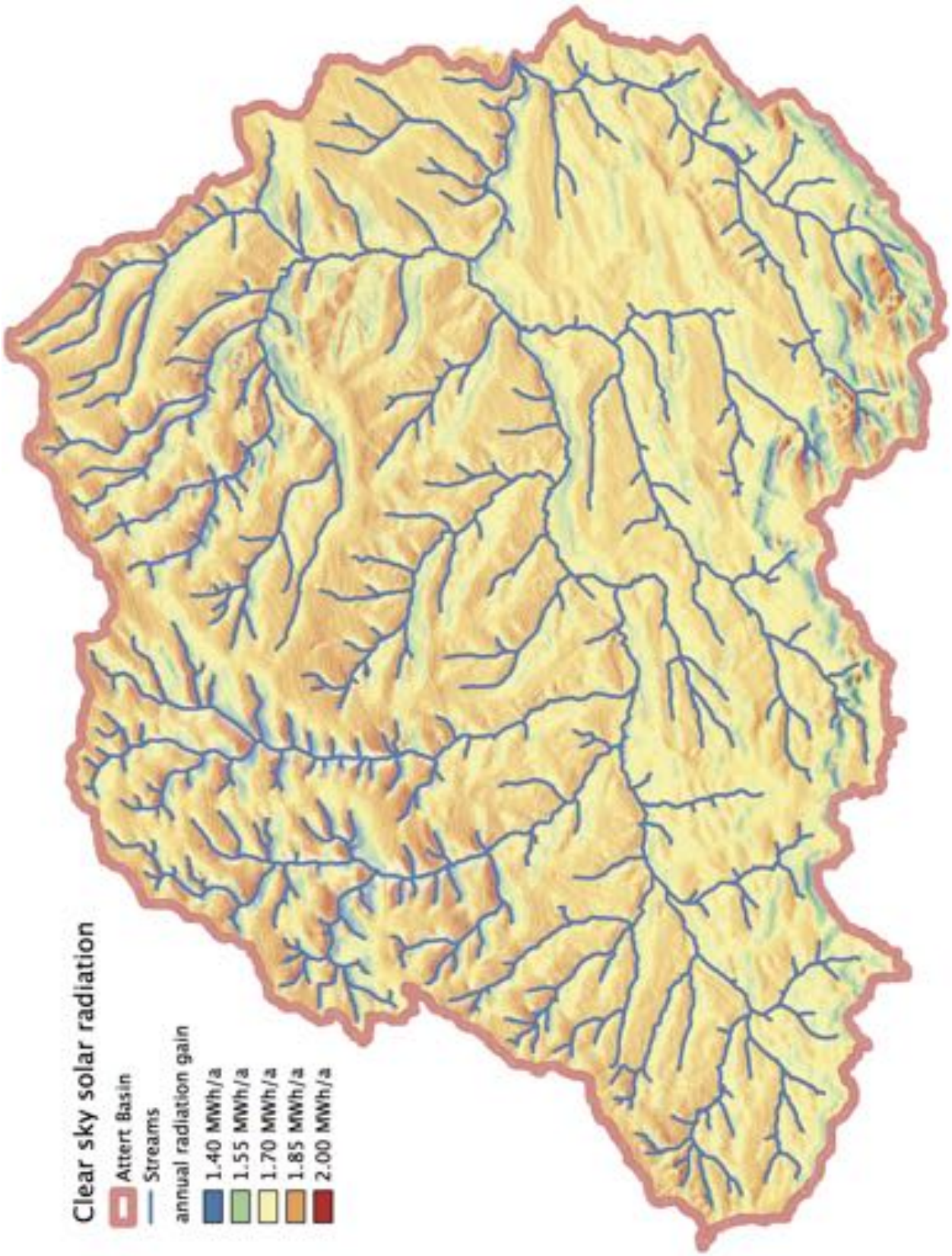

Figure 7.9: Attert experimental basin. Annual clear sky solar radiation gain calculated based on joint DEM in GRASS GIS using r.sun [Hofierka and Šúri, 2002].

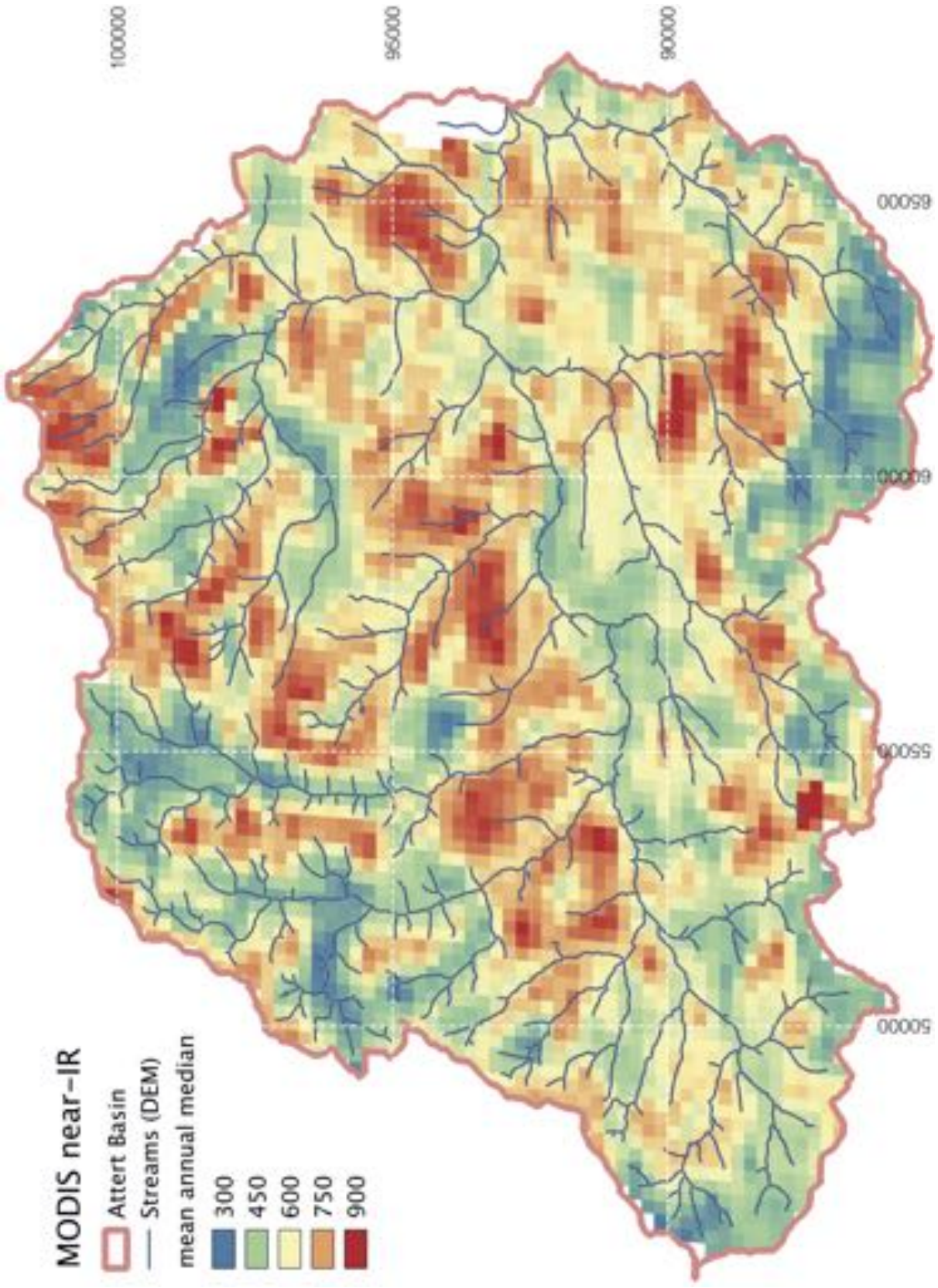

Figure 7.10: Attert experimental basin. MODIS near-IR reflection mean (over time) of 8-day data 2005-2011.

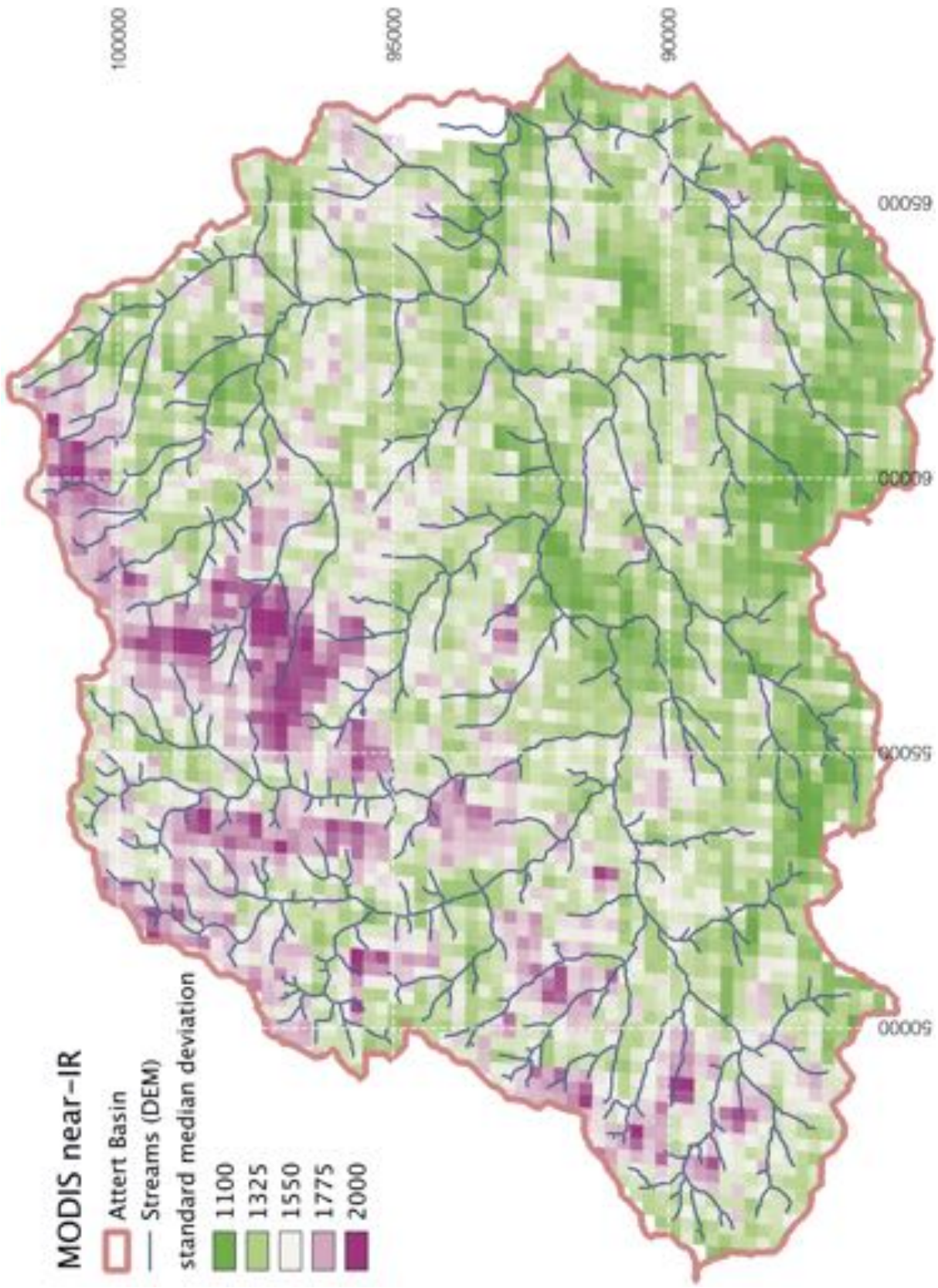

Figure 7.11: Attert experimental basin. MODIS near-IR reflection standard median deviation (over time) of 8-day data 2005-2011.

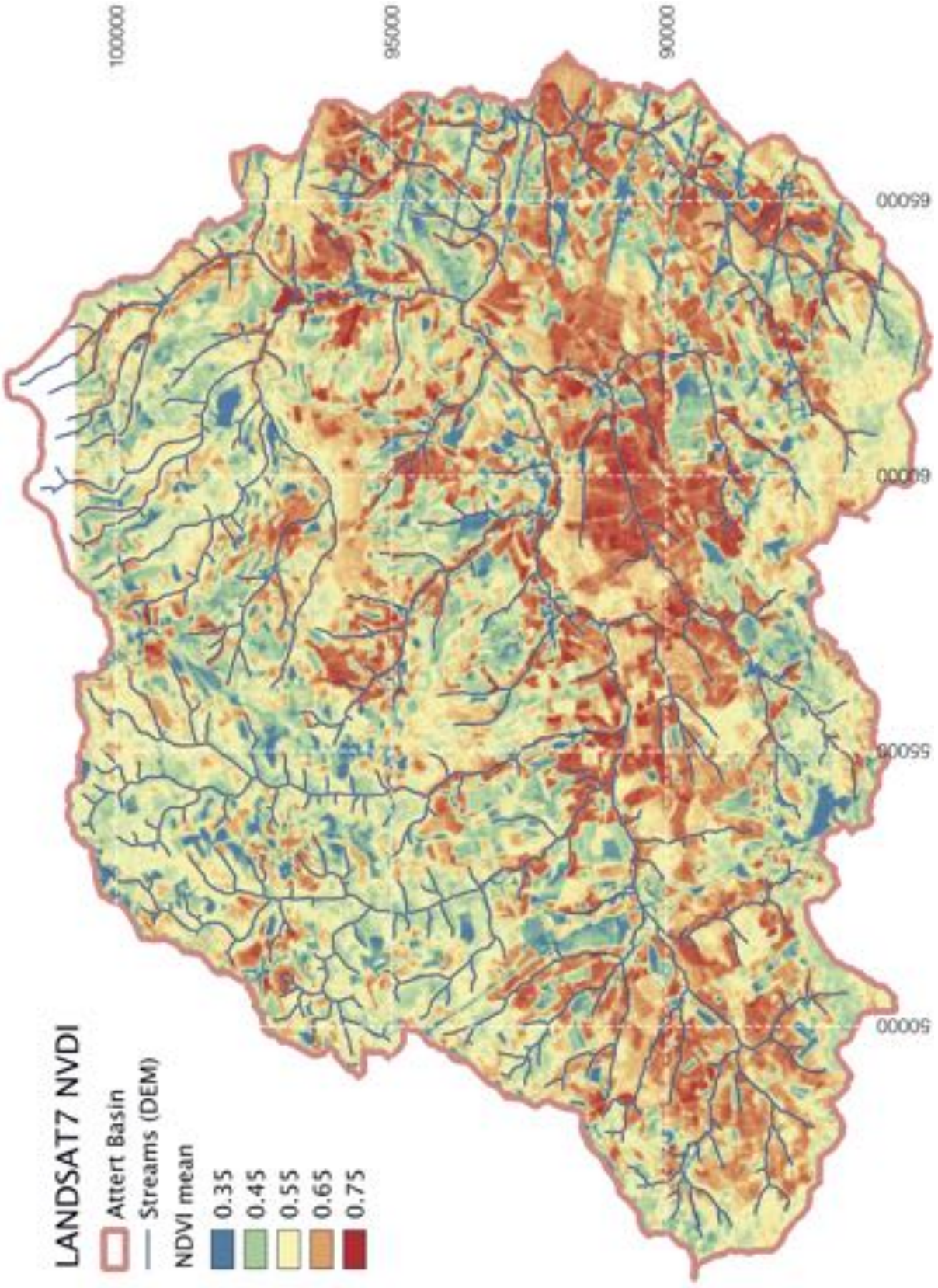

Figure 7.12: Attert experimental basin. Landsat 7 NDVI (spring and autumn 2011, 2013 and 2014) mean over time.

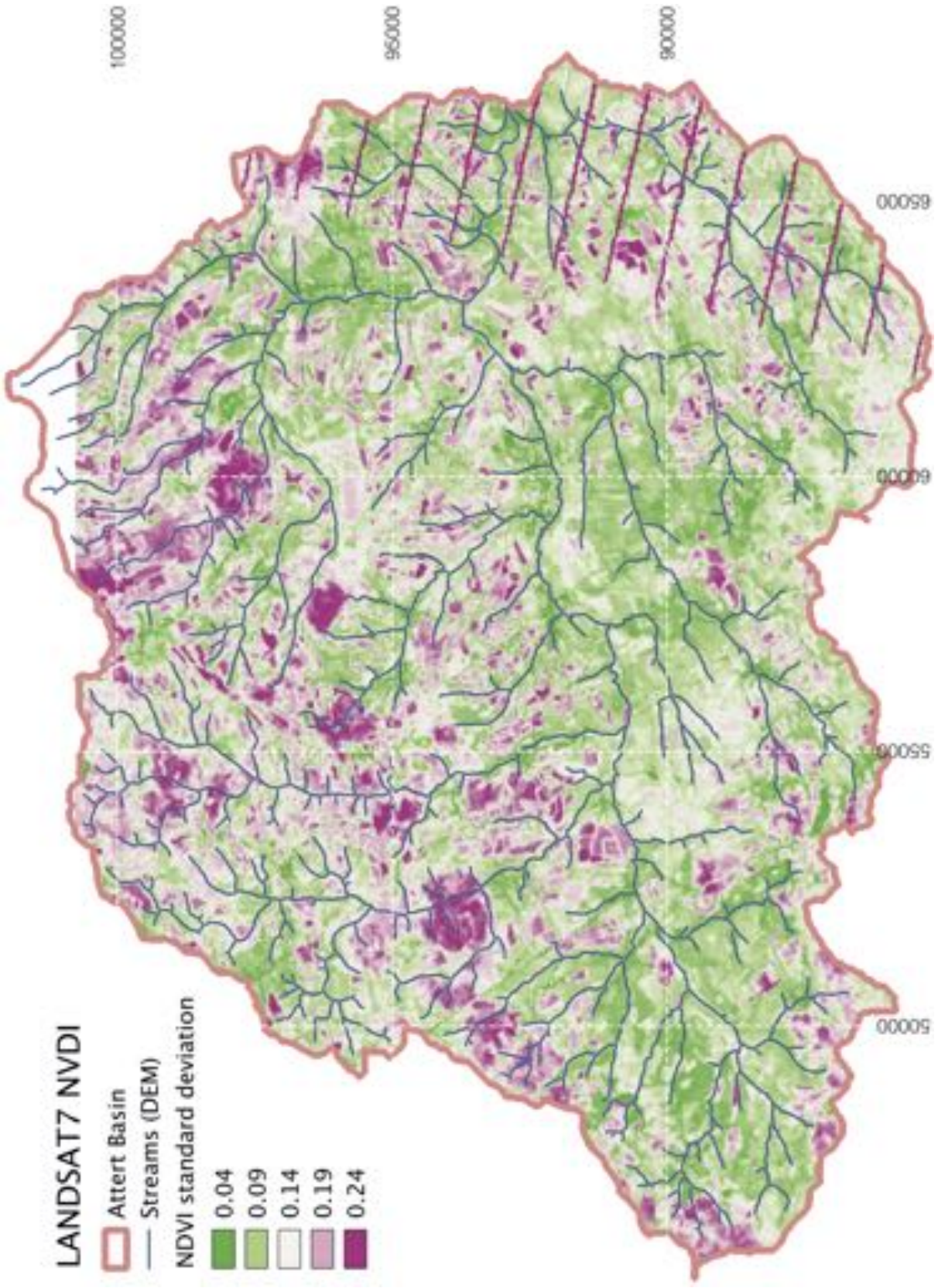

Figure 7.13: Attert experimental basin. Landsat 7 NDVI (spring and autumn 2011, 2013 and 2014) standard deviation over time.

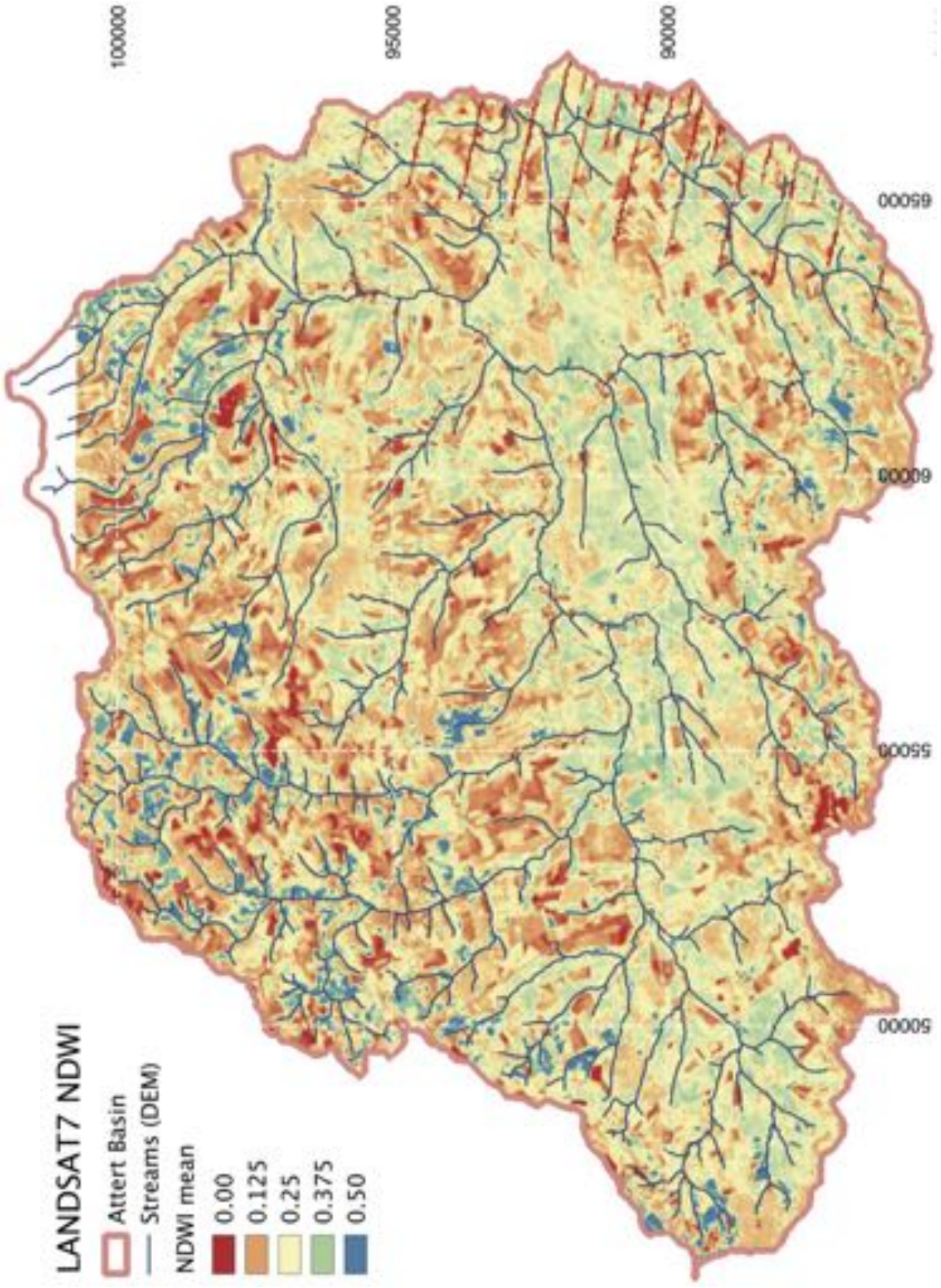

Figure 7.14: Attert experimental basin. Landsat 7 NDWI (spring and autumn 2011, 2013 and 2014) mean over time.

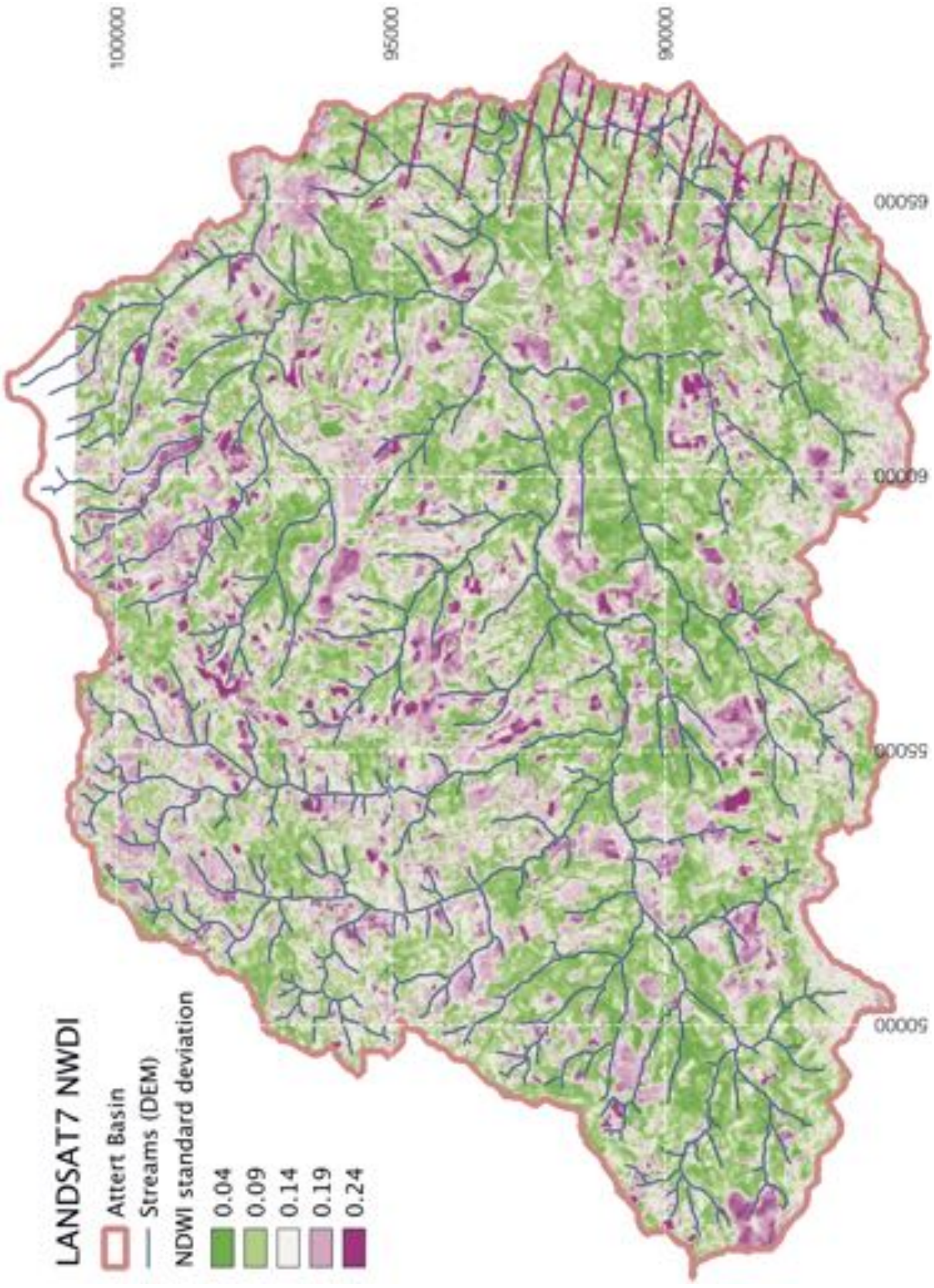

Figure 7.15: Attert experimental basin. Landsat 7 NDWI (spring and autumn 2011, 2013 and 2014) standard deviation over time.

7.3 Critical revisions of analytical tools and concepts

7.3.1 Texture analysis with different methods in different labs

Pedo-transfer-functions (PTFs) are a common tool in hydrological modelling. One of the most frequently used models is the vanGenuchten-Mualem approach referring hydrological properties to explorable parameters [Van Genuchten, 1980]. Since then it has been extended [e.g. Schaap and Leij, 2000] and explored [e.g. Ippisch et al., 2006]. Generally these parameters are again subject to PTFs on even more easily assessable properties such as bulk density and texture distributions [among others Scheinost et al., 1997, Mayr and Jarvis, 1999, Schaap et al., 2001, Wösten et al., 2001]. Because of this, the analysis of soil texture – especially clay content – can become crucial to the estimate of hydrological soil properties.

Currently, the standard is still the international pipette method after Köhn (DIN ISO 11277) relying on the sedimentation of suspended soil applying the stroke's law. Alternatively to successive pipette sampling one may use a hydrometre measuring the suspension density by means of buoyancy. New methods like laser diffraction and automated image analysis emerge and obtrude themselves as fast, automated alternatives. We tested all techniques on identical samples revealing a strong deficit in correct representation of the clay fraction, which was also highlighted by Konert and Vandenberghe [1997], Di Stefano et al. [2010]. This section presents the findings of the different techniques and an overall comparison of the analysis of 120 samples with laser diffraction (LD) and sieving and sedimentation (SS).

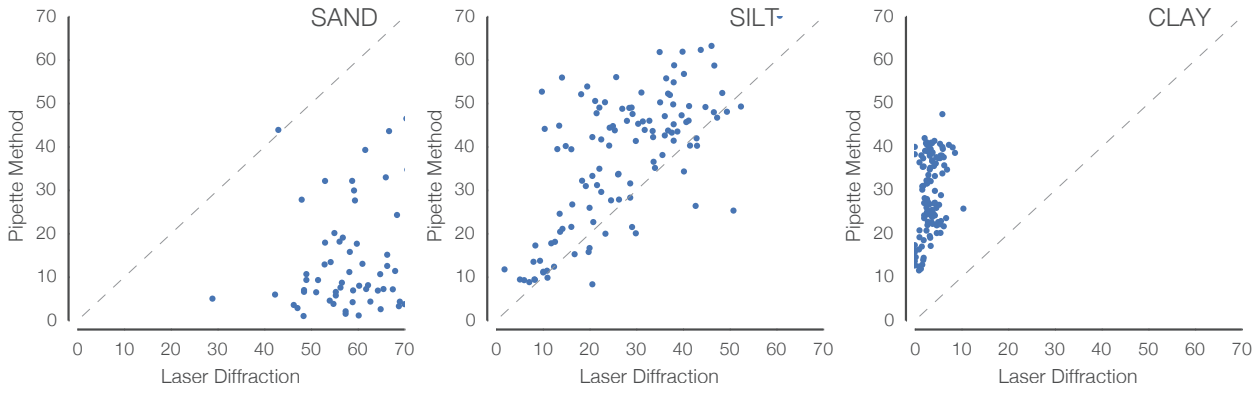

Figure 7.16: Soil texture analysis by different methods: Measured content of different fractions [%] by laser diffraction vs. pipette method in the same samples.

The results are presented in figure 7.16 which show dramatic de-

viance between the methods. The 120 samples cover a broad range of texture compositions and none is similarly measured by both methods. The deviations are also not simply caused by a bias. For sand LD identifies high values for all samples. It is noteworthy, that LD ranges from 40 % to 70 % while SS results from 0 % to 40 %. For silt both methods capture the full spectrum while SS mostly identifies higher values than LD. Clays cannot be measured with LD.

With this, it is strongly advised to rely on the standard of sieving and sedimentation analysis for the determination of texture composition. However, different sample preparation and workflows in the respective labs can also cause significant deviations within the same methodology. Figure 7.17 shows texture results of 8 samples which have been analysed based on the same method in different labs with slightly different preprocessing and handling standards.

It is noteworthy that the coarse fractions – hence those likely affected by the removal organic matter – are measured with higher proportion where organic matter has not been removed before analysis. There the clay fraction – hence the fraction most critical to proper suspension, salt removal and the dispersing agent Sodium hexametaphosphate – is measured with a negative bias.

Ad-hoc conclusion

Based on the presented findings it appears necessary to provide calibration standards to all methods and laboratories to avoid such strong deviation in texture analysis. It also poses questions about the universality of pedotransfer functions [e.g. Vereecken et al., 2010] when identical samples can deviate by 20%-points from lab to lab. As ad-hoc conclusion the processing of samples in one lab might result in the least errors. Consequently pedotransfer functions may need specific setup.

7.3.2 Saturation of core samples

During the processing of hundreds of soil core samples initial saturation already needs careful handling. Especially young soils appear to have the potential to change packing dramatically when fully saturated without any external influence. In one case we observed a reduction of the sample volume to <80% after having been left for full saturation for one week. This rendered the sample not representatively processable.

It also led to some questions about the standard procedure of laboratory analysis: Not all soils have been exposed to saturation in their genesis. Hence the main feature of loosely packed soils may exactly be the situation of being well-drained and not exhibiting a

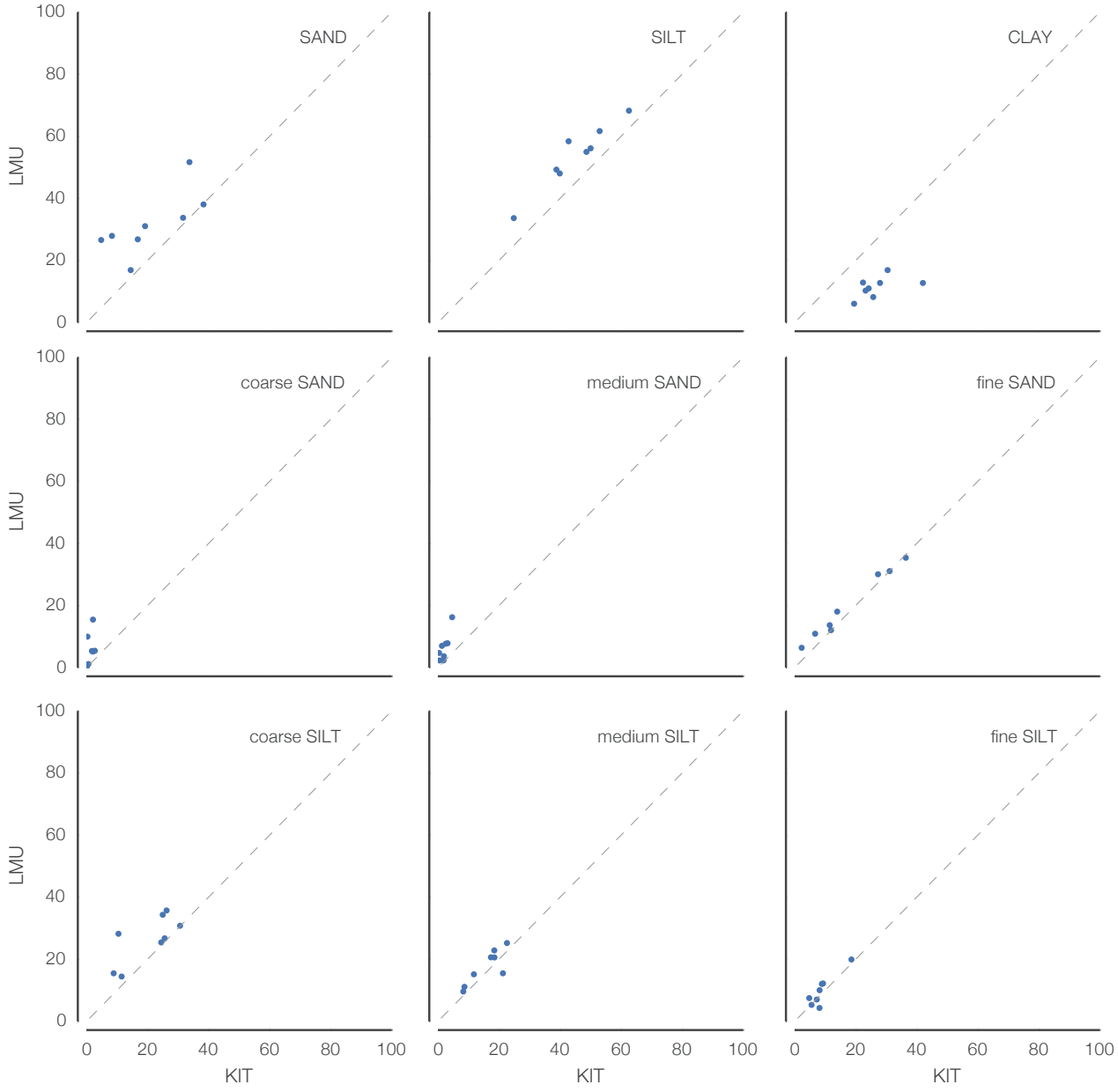

Figure 7.17: Soil texture analysis in different labs: Measured content of different texture fractions [%] by wet sieving and pipette method with identical samples.

pore system with continuous capillarity.

Under saturated conditions many soils lose their stability and thus may get (partly) suspended. Lessivation is a common pedogenic process altering pore spectrum and water retention properties. Hence the term saturated hydraulic conductivity may not be applicable to all soils. Because soil water dynamics are diffusive, advective and due to pressure wave conductance, also with respect to an adequate process representation the saturation concept may deserve revision. We should seek for methods with less bias towards the perception of diffusive flow and with particular attention to pedogenesis.

7.3.3 Discussion and conclusions

On the one hand retention properties are especially relevant for the storage behaviour of the soil. Hence a good estimate of the drying branch will deliver a solid foundation for respective estimates. On the other hand the water retention curve is only defined for pores which are small enough to develop capillary forces and which are sufficiently large to take part in the wetting and drying. Thus macropores and swelling clay minerals challenge the concept. Also field capacity as conceptual reference for free water is not as well defined [Assouline and Or, 2014].

In hydrology texture data is primarily used as proxy for the pore size distribution. Pedotransfer functions have been developed to derive soil hydraulic characteristics from available basic soil data [Wösten et al., 2001]. To account for the great differences in packing density they employ bulk density as descriptor. If the saturation reference as conceptual limits and if *basic soil data* as texture is neither reliable nor already *available* the general approach could be revised:

Joint measurement of matric potential and soil moisture is becoming more and more feasible thus allowing to observe soil water retention cycles in un- or less-disturbed conditions. Soil water retention models can be calibrated on this data directly. Moreover also these models could be replaced by a system describing diffusion, advection and active pore space.

7.4 Additional aspects and tools for the echoRD model

7.4.1 Projecting the half-cylindrical sandbox of the "artificial macropore" experiment

The results in figure 7.18 are based on the assumption of particles to diffusively travel in all three dimensions of the half-cylindrical sandbox. With this, the reference volume for moisture calculation

rises with distance to the central macropore.

If I neglect this geometry and calculate soil moisture only on the 2D pane, the results are astonishingly improved. Figure 7.18 presents runs with identical parametrisation but different geometry definitions.

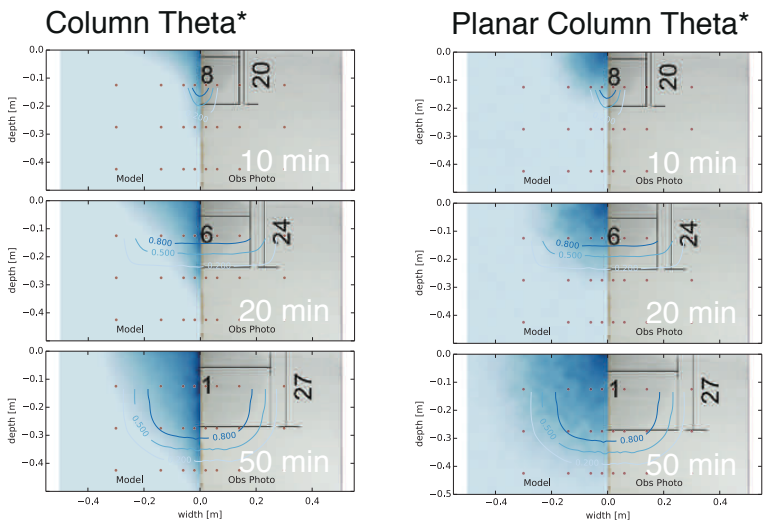

Figure 7.18: Simulation of sandbox experiment with an "artificial macropore" with different geometry deconvolution. Left: with half-cylindrical increase of the reference volume with distance to the central macropore. Right: planar 2D representation.

7.4.2 *Getting rid of the grid*

The particle approach requires the fundamental assumption of the size of such a particle. The first concepts have been framed around a more flexible formulation of such particles in terms of water bulks that exhibit some joint dynamics due to cohesive forces exceeding adhesive and interactive ones. A second fundament comes with the self-dependent property of especially diffusive flux (resulting from the fact that a water particle is still a great number of water molecules extending over several pores). The particle density needs to be frequently determined.

If we rely this determination on a grid, emerging properties below this scale cannot be resolved although the particles are selected much smaller than the grid cells. Thus I experimented with alternative means of particle density calculations such as tracking of neighbouring particles and network analytical methods. Especially the method based on Voronoi polygons was implemented using the package voro++ [Rycroft, 2009] and its Python wrapper Pyvoro (github.com/joe-jordan/pyvoro).

The result was a grid-free determination of the particle density based on the Voronoi tessellation of the particle field. The smaller the Voronoi polygon of a particle the higher the particle density. Hence

a direct relationship of polygon size to soil moisture, particle interaction or other properties can be established. However, the calculation of the Voronoi tessellation requires a multiple of the computational resources of grid-based derivation. Since this is already the premier numerical bottleneck and since appropriate assumptions of boundary effects and particle interaction were required I stalled further development in this regard. However, it is a very interesting field which may be taken up again at a later development stage with massively parallelised computation.

7.5 Energy perspective – virtual experiments with Catflow

In order to examine the physical foundations of the GIS analysis above this section presents virtual experiments using the physical hydrological process model *CATFLOW* [Zehe et al., 2001]. We analyse the dynamics of Helmholtz Free Energy (F) and partly the dynamics of entropy (H) in hydrological systems under different landscape arrangements by means of a scenario analysis to address the question of topology and optimality in hydrologic systems.

Three different real hillslopes were setup as virtual experiment environments in *CATFLOW* based on successfully applied parameters from the cited studies[1]. The vegetation of each hillslope was consecutively altered to the variations shown in figure 7.19. The resulting time series of soil moisture and matrix head were used to calculate F of the soil water. Additionally the energy flux of latent heat was calculated from simulated evapo-transpiration time series.

The three cases are:

1. Malalcahuello, Southern Chile, layered young volcanic ash soils, high precipitation [Blume et al., 2008]
2. Menzingen, Kraichtal, Western Germany, intensively managed loess soils, conditioned irrigation [Zehe et al., 2001]
3. Rehefeld, Ore Mountains, Eastern Germany, highly variable loamy soils formed by weathering in Weichsel cold age, cold humid [Graeff et al., 2012]

Helmholz Free Energy F, as measure of dissipative energy in a system is defined as:

$$dF = \underbrace{-SdT}_{\approx E_{rad}-\lambda_{ET}} \underbrace{-pdV}_{\equiv 0} + \underbrace{\mu dM}_{=E_{grav}+E_{bind}} \tag{7.1}$$

The respective energy terms are:

$$E_{grav} = M = p\theta V \tag{7.2}$$

$$E_{bind} = \mu(\theta) = g(z + \psi(\theta(x,y,z))) \tag{7.3}$$

$$E_{rad} = A(dRAD) \tag{7.4}$$

$$\lambda_{ET} = m_{ET} q_{vap} \tag{7.5}$$

Based on these equations the *CATFLOW* outputs are processed for the resulting time series of free energy given.

[1] I especially thank Theresa Blume, Thomas Gräff and Erwin Zehe for sharing their established model setups with me.

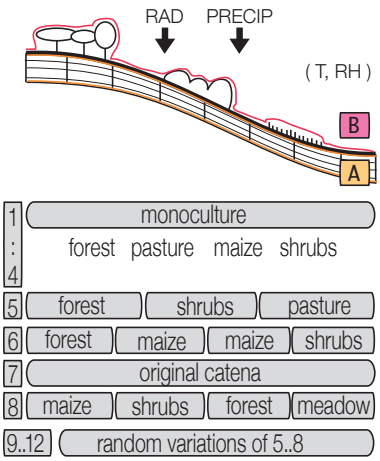

Figure 7.19: Virtual experiments analysing the effect of vegetation organisation along a hillslope using *CATFLOW*. A&B describe the soil water domain and entropy and heat exchange respectively. The different catena scenarios are outlined as 1..12.

Results

The resulting simulated time series of the respective free energy are given in figure 7.20. At Malalcahuello we initially used the observed, very large precipitation which resulted in no deviation between the different land use scenarios. After scaling precipitation to 10% slight deviation occurs during dry spells. Note that precipitation here is one order of magnitude higher than in the two other test cases. Malalcahuello and Menzingen have well drained soils. In both cases cumulated $-SdT$ is maximised with maize monoculture. It is very low under forest. However the ranks of the scenarios differ.

In Rehefeld with loamy soils this picture is almost reversed where maize ranks very low. It is also noteworthy that the random variations dramatically differ. This underlines the impact of catena topology as was also found by Zehe et al. [2013].

Another important point is, that E_{grav}, E_{bind} and SdT range several orders of magnitude apart. E_{grav} ranges near $1\,\mathrm{J\,m^{-2}}$ to $10\,\mathrm{J\,m^{-2}}$. E_{bind} can rise to $10^3\,\mathrm{J\,m^{-2}}$ during dry spells. SdT ranges easily at $10^8\,\mathrm{J\,m^{-2}}$ to $10^{10}\,\mathrm{J\,m^{-2}}$.

Conclusions from this small experiment are that:

Dissipation paths matter with regard to the maximisation of free energy dissipation. During *mass-driven* conditions the gradient of E_{grav} has to be depleted by mass export with high mass but low energy turnover. A share of the input mass will also deplete the gradient of E_{bind}. During *energy-driven* conditions ET will deplete the strong gradient at the atmospheric boundary with low mass but high energy turnover. Both cases are mediated through specific structures such as macropores and vegetation respectively.

The **MEP principle** cannot be applied directly to single hillslopes since a mere balance over all kinds of energy will always neglect the *mass-driven* case.

The **systems behaviour** will only deviate under stress. Only if there is a limitation by precipitation or radiation different land use settings led to different dissipation of free energy.

$$\frac{dE_{cap}}{V} = \rho g \frac{\partial \Psi}{\partial \theta} d\theta \tag{7.6}$$

$$\frac{dE_{pot}}{V} = \rho g z d\theta \tag{7.7}$$

$$\Psi_H = \Psi + z \tag{7.8}$$

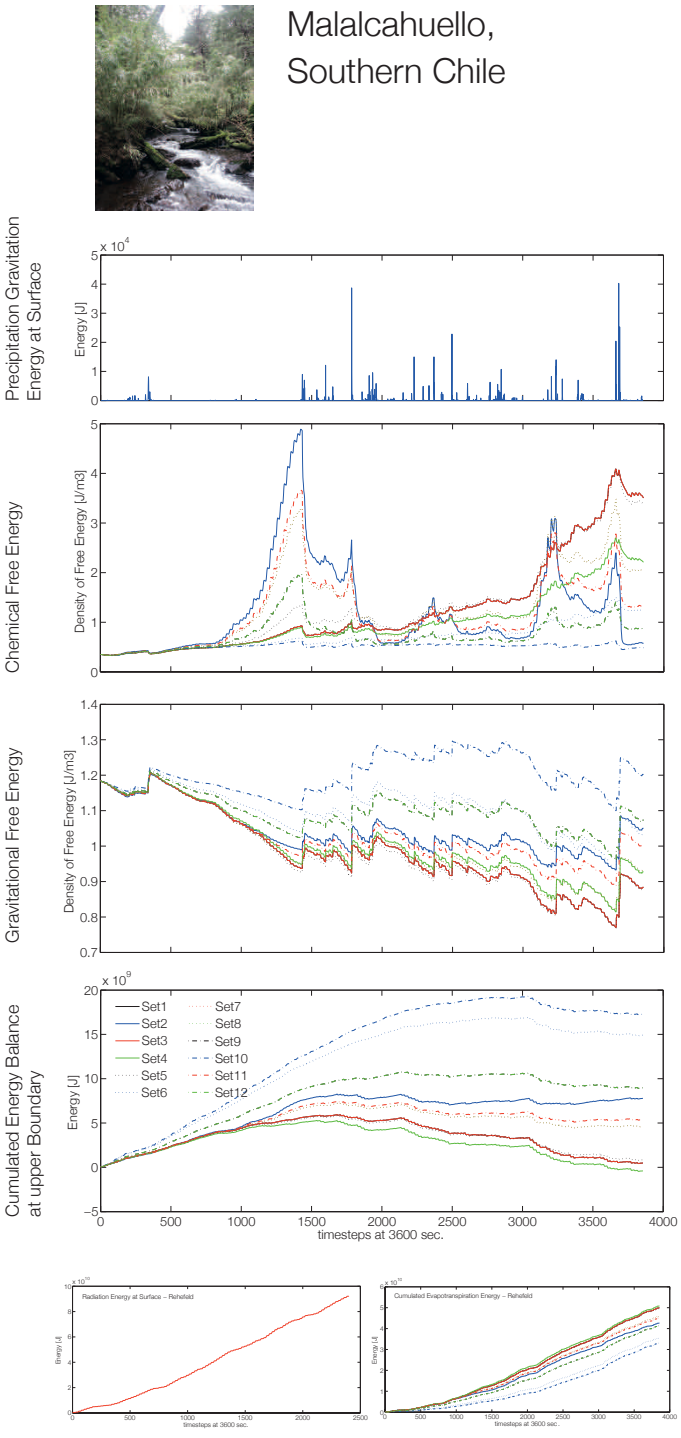

Figure 7.20: Modelled free energy dynamics under different land cover settings at three different hillslopes.

Menzingen, Kraichtal,
Western Germany

Rehefeld, Ore Mts.,
Eastern Germany

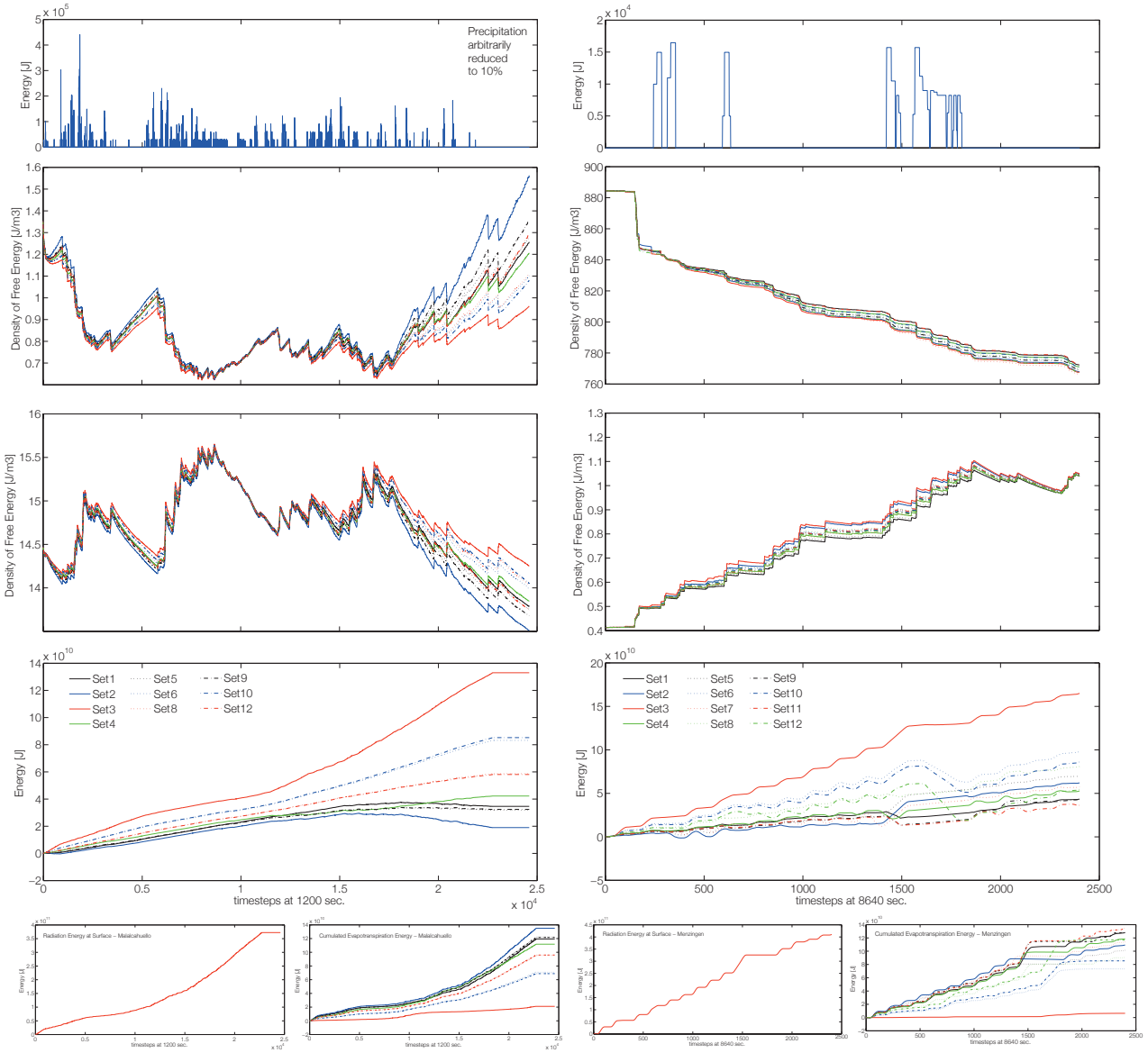

Bibliography

Geneviève Ali, Doerthe Tetzlaff, Chris Soulsby, Jeffrey J McDonnell, and René Capell. A comparison of similarity indices for catchment classification using a cross-regional dataset. *ADVANCES IN WATER RESOURCES*, 40(1):11–22, 2012. DOI: doi: 10.1016/j.advwatres.2012.01.008.

Geneviève Ali, Christian Birkel, Doerthe Tetzlaff, Chris Soulsby, Jeffrey J McDonnell, and Paolo Tarolli. A comparison of wetness indices for the prediction of observed connected saturated areas under contrasting conditions. *Earth Surface Processes and Landforms*, 39(3):399–413, March 2014. DOI: 10.1002/esp.3506.

RG Allen, LS Pereira, D Raes, and M Smith. Crop evapotranspiration - Guidelines for computing crop water requirements, 1998.

Niklas Allroggen, N Loes M B van Schaik, and Jens Tronicke. 4D ground-penetrating radar during a plot scale dye tracer experiment. *Journal of Applied Geophysics*, 118(0):139–144, 2015. DOI: 10.1016/j.jappgeo.2015.04.016.

Shmuel Assouline and Dani Or. The concept of field capacity revisited: Defining intrinsic static and dynamic criteria for soil internal drainage dynamics. *WATER RESOURCES RESEARCH*, 50(6):4787–4802, June 2014. DOI: 10.1002/2014WR015475.

Sophie Bachmair and Markus Weiler. Interactions and connectivity between runoff generation processes of different spatial scales. *HYDROLOGICAL PROCESSES*, pages n/a–n/a, March 2013.

L E Band, J J McDonnell, J M Duncan, A Barros, A Bejan, T Burt, W E Dietrich, R E Emanuel, T Hwang, G Katul, Y Kim, B McGlynn, B Miles, A Porporato, C Scaife, and P A Troch. Ecohydrological flow networks in the subsurface. *Ecohydrology*, 7(4):1073–1078, August 2014. DOI: 10.1002/eco.1525.

Philippe C Baveye and Magdeline Laba. Moving away from the geostatistical lamppost: Why, where, and how does the spatial

heterogeneity of soils matter? *ECOLOGICAL MODELLING*, 298(0): 24–38, February 2015.

Adrian Bejan and Sylvie Lorente. The constructal law and the evolution of design in nature. *Physics of Life Reviews*, 8(3):209–240, 2011. DOI: doi: 10.1016/j.plrev.2011.05.010.

S Bergström. Development and application of a conceptual runoff model for Scandinavian catchments. Technical report, Norrköping, Sweden, 1976.

Brian Berkowitz, Andrea Cortis, Marco Dentz, and Harvey Scher. Modeling non-Fickian transport in geological formations as a continuous time random walk. *Reviews of Geophysics*, 44(2):RG2003, June 2006. DOI: 10.1029/2005RG000178.

K Beven. Searching for the Holy Grail of scientific hydrology: $Q_t = H(S, R, \Delta t)A$ as closure. *HYDROLOGY AND EARTH SYSTEM SCIENCES*, 10(5):609–618, 2006a.

K Beven. A manifesto for the equifinality thesis. *JOURNAL OF HYDROLOGY*, 320(1-2):18–36, 2006b.

Keith Beven. Prophecy, reality and uncertainty in distributed hydrological modelling. *ADVANCES IN WATER RESOURCES*, 16(1): 41–51, 1993. DOI: 10.1016/0309-1708(93)90028-E.

Keith Beven. What we see now: Event-persistence and the predictability of hydro-eco-geomorphological systems. *ECOLOGICAL MODELLING*, 298(0):4–15, February 2015.

Keith Beven and Peter Germann. WATER FLOW IN SOIL MACROPORES II. A COMBINED FLOW MODEL. *Journal of Soil Science*, 32 (1):15–29, 1981. DOI: 10.1111/j.1365-2389.1981.tb01682.x.

Keith Beven and Peter Germann. Macropores and water flow in soils. *WATER RESOURCES RESEARCH*, 18(5):1311–1325, October 1982. DOI: 10.1029/WR018i005p01311.

Keith Beven and Peter Germann. Macropores and water flow in soils revisited. *WATER RESOURCES RESEARCH*, pages n/a–n/a, February 2013. DOI: 10.1002/wrcr.20156.

KJ Beven and MJ Kirkby. A physically-based variable contributing area model of basin hydrology. *Hydrol. Sci. Bull.*, 24(1):43–69, 1979.

Branko Bijeljic, Ali Raeini, Peyman Mostaghimi, and Martin J Blunt. Predictions of non-Fickian solute transport in different classes of porous media using direct simulation on pore-scale images.

Physical Review E, 87(1):013011, January 2013. DOI: 10.1103/PhysRevE.87.013011.

A BINLEY, G Cassiani, R Middleton, and P Winship. Vadose zone flow model parameterisation using cross-borehole radar and resistivity imaging. *JOURNAL OF HYDROLOGY*, 267(3-4):147–159, October 2002.

Andrew Binley and Keith Beven. Vadose Zone Flow Model Uncertainty as Conditioned on Geophysical Data. *GROUND WATER*, 41 (2):119–127, March 2003. DOI: 10.1111/j.1745-6584.2003.tb02576.x.

G Bloschl and M Sivapalan. Scale issues in hydrological modelling: A review. *HYDROLOGICAL PROCESSES*, 9(3-4):251–290, April 1995. DOI: 10.1002/hyp.3360090305.

G Blöschl and E Zehe. On hydrological predictability. *HYDROLOGICAL PROCESSES*, 19(19):3923–3929, 2005.

Günter Blöschl, Murugesu Sivapalan, Thorsten Wagener, Alberto Viglione, and Hubert Savenije. *Runoff Prediction in Ungauged Basins*. Synthesis Across Processes, Places and Scales. Cambridge University Press, April 2013. ISBN 9781107028180.

M Blouin, M E Hodson, E A Delgado, G Baker, L Brussaard, K R Butt, J Dai, L Dendooven, G Peres, J E Tondoh, D Cluzeau, and J J Brun. A review of earthworm impact on soil function and ecosystem services. *European Journal of Soil Science*, 64(2):161–182, January 2013. DOI: 10.1111/ejss.12025.

T Blume, E Zehe, D E Reusser, A Iroume, and A Bronstert. Investigation of runoff generation in a pristine, poorly gauged catchment in the Chilean Andes I: A multi-method experimental study. *HYDROLOGICAL PROCESSES*, 22(18):3661–3675, August 2008.

Theresa Blume and H J Ilja van Meerveld. From hillslope to stream: methods to investigate subsurface connectivity. *Wiley Interdisciplinary Reviews: Water*, pages n/a–n/a, February 2015. DOI: 10.1002/wat2.1071.

Johannes Botschek, Simone Krause, Thekla Abel, and Armin Skowronek. Hydrological parameterization of piping in loess-rich soils in the Bergisches Land, Nordrhein-Westfalen, Germany. *Journal of Plant Nutrition and Soil Science*, 165(4):506–510, August 2002. DOI: 10.1002/1522-2624(200208)165:4<506::AID-JPLN506>3.0.CO;2-7.

J Bouma, C F M Belmans, and L W DEKKER. Water Infiltration and Redistribution in a Silt Loam Subsoil with Vertical Worm Channels1. *Soil Science Society of America Journal*, 46(5):917, 1982. DOI: 10.2136/sssaj1982.03615995004600050006x.

George E P Box. Science and Statistics. *Journal of the American Statistical Association*, 71(356):791–799, December 1976. DOI: 10.1080/01621459.1976.10480949.

R H Brooks and A T Corey. Hydraulic Properties of Porous Media. Hydrology Papers, Colorado State University, Fort Collins, Colorado, 1964.

Wilfried Brutsaert and Han Stricker. An advection-aridity approach to estimate actual regional evapotranspiration. *WATER RESOURCES RESEARCH*, 15(2):443–450, April 1979. DOI: 10.1029/WR015i002p00443.

B P Buchanan, M Fleming, R L Schneider, B K Richards, J Archibald, Z Qiu, and M T Walter. Evaluating topographic wetness indices across central New York agricultural landscapes. *Hydrol. Earth Syst. Sci.*, 18(8):3279–3299, August 2014. DOI: 10.5194/hess-18-3279-2014.

Wouter Buytaert, Dominik Reusser, Stefan Krause, and J-P Renaud. Why can't we do better than Topmodel? *HYDROLOGICAL PROCESSES*, 22(20):4175–4179, September 2008. DOI: 10.1002/hyp.v22:20.

Robert F. Carsel and Rudolph S. Parrish. Developing joint probability distributions of soil water retention characteristics. *WATER RESOURCES RESEARCH*, 24(5):755–769, 1988. DOI: 10.1029/WR024i005p00755.

KK Caylor, S Manfreda, and et al. On the coupled geomorphological and ecohydrological organization of river basins. *ADVANCES IN WATER RESOURCES*, 2005.

M Celia, E Bouloutas, and R Zarba. A General Mass-Conservative Numerical-Solution for the Unsaturated Flow Equation. *WATER RESOURCES RESEARCH*, 26(7):1483–1496, July 1990.

Martyn Clark, Dmitri Kavetski, and Fabrizio Fenicia. Pursuing the method of multiple working hypotheses for hydrological modeling. *WATER RESOURCES RESEARCH*, 47(9):W09301, September 2011.

R Cockett, S Kang, L G Heagy, A Pidlisecky, and W D Oldenburg. SimPEG: An open-source framework for simulation and parameter estimation in geophysical applications. *Computers & Geosciences*, 2015.

Olaf Conrad. *SAGA Entwurf, Funktionsumfang und Anwendung eines Systems für Automatisierte Geowissenschaftliche Analysen*. PhD thesis, Georg-August-Universität zu Göttingen, Göttingen, November 2006.

Antonio Coppola, Horst H Gerke, Alessandro Comegna, Angelo Basile, and Vincenzo Comegna. Dual-permeability model for flow in shrinking soil with dominant horizontal deformation. *WATER RESOURCES RESEARCH*, 48(8):W08527 1–21, August 2012. DOI: 10.1029/2011WR011376.

J. Davies and K Beven. Comparison of a Multiple Interacting Pathways model with a classical kinematic wave subsurface flow solution. *Hydrological Sciences Journal*, 57(2):203–216, January 2012. DOI: doi: 10.1080/02626667.2011.645476.

J. Davies, K Beven, A Rodhe, L Nyberg, and K Bishop. Integrated modeling of flow and residence times at the catchment scale with multiple interacting pathways. *WATER RESOURCES RESEARCH*, 49(8):4738–4750, August 2013. DOI: 10.1002/wrcr.20377.

Jessica Davies, Keith Beven, Lars Nyberg, and Allan Rodhe. A discrete particle representation of hillslope hydrology: hypothesis testing in reproducing a tracer experiment at Gårdsjön, Sweden. *HYDROLOGICAL PROCESSES*, pages n/a–n/a, 2011. DOI: 10.1002/hyp.8085.

Frédérick Delay and Jacques Bodin. Time domain random walk method to simulate transport by advection-dispersion and matrix diffusion in fracture networks. *Geophysical Research Letters*, 28(21): 4051–4054, January 2001. DOI: 10.1029/2001GL013698.

Frédérick Delay, Anne Kaczmaryk, and Philippe Ackerer. Inversion of a Lagrangian time domain random walk (TDRW) approach to one-dimensional transport by derivation of the analytical sensitivities to parameters. *ADVANCES IN WATER RESOURCES*, 31(3): 484–502, 2008.

Marco Dentz. Concentration statistics for transport in heterogeneous media due to stochastic fluctuations of the center of mass velocity. *ADVANCES IN WATER RESOURCES*, 36(0):11–22, February 2012. DOI: 10.1016/j.advwatres.2011.04.005.

Marco Dentz, Philippe Gouze, Anna Russian, Jalal Dweik, and Frédérick Delay. Diffusion and trapping in heterogeneous media: An inhomogeneous continuous time random walk approach. *ADVANCES IN WATER RESOURCES*, 49(0):13–22, 2012.

RC Dewar. Maximum entropy production and the fluctuation theorem. *Journal of Physics A: Mathematical and General*, 38(21), 2005.

C Di Stefano, V Ferro, and S Mirabile. Comparison between grain-size analyses using laser diffraction and sedimentation

methods. *Biosystems Engineering*, 106(2):205–215, June 2010. DOI: 10.1016/j.biosystemseng.2010.03.013.

James Dooge. Looking for hydrologic laws. *WATER RESOURCES RESEARCH*, 22(9S):46S–58S, 1986.

Peter Droogers and Richard G Allen. Estimating reference evapotranspiration under inaccurate data conditions. *Irrigation and Drainage Systems*, (16):33–45, 2002.

U Ehret, H V Gupta, M Sivapalan, S V Weijs, S J Schymanski, G Bloschl, A N Gelfan, C Harman, A Kleidon, T. A. Bogaard, D Wang, T Wagener, U Scherer, E Zehe, M F P Bierkens, G Di Baldassarre, J Parajka, L P H van Beek, A van Griensven, M C Westhoff, and H C Winsemius. Advancing catchment hydrology to deal with predictions under change. *Hydrol. Earth Syst. Sci.*, 18(2): 649–671, 2014. DOI: 10.5194/hess-18-649-2014.

John Ewen. 'SAMP' model for water and solute movement in unsaturated porous media involving thermodynamic subsystems and moving packets: l. Theory. *JOURNAL OF HYDROLOGY*, 182(1–4): 175–194, July 1996. DOI: 10.1016/0022-1694(95)02925-7.

F Fenicia, H H G Savenije, P Matgen, and L Pfister. A comparison of alternative multiobjective calibration strategies for hydrological modeling. *WATER RESOURCES RESEARCH*, 43(3), 2007.

Fabrizio Fenicia, Hubert H G Savenije, Patrick Matgen, and Laurent Pfister. Understanding catchment behavior through stepwise model concept improvement. *WATER RESOURCES RESEARCH*, 44(1): 1–13, 2008. DOI: 10.1029/2006WR005563.

Fabrizio Fenicia, Dmitri Kavetski, and Hubert H G Savenije. Elements of a flexible approach for conceptual hydrological modeling: 1. Motivation and theoretical development. *WATER RESOURCES RESEARCH*, 47(11):W11510, January 2011. DOI: 10.1029/2010WR010174.

Fabrizio Fenicia, Dmitri Kavetski, Hubert H G Savenije, Martyn P. Clark, Gerrit Schoups, Laurent Pfister, and Jim Freer. Catchment properties, function, and conceptual model representation: is there a correspondence? *HYDROLOGICAL PROCESSES*, 28(4):2451–2467, February 2014. DOI: 10.1002/hyp.9726.

Igor V Florinsky. *Digital Terrain Analysis in Soil Science and Geology*. Academic Press, 2012. ISBN 0123850363.

Markus Flury, Hannes Flühler, William A Jury, and Jörg Leuenberger. Susceptibility of soils to preferential flow of water: A field

study. *WATER RESOURCES RESEARCH*, 30(7):1945–1954, July 1994. DOI: 10.1029/94WR00871.

Horst H Gerke. Preferential flow descriptions for structured soils. *Journal of Plant Nutrition and Soil Science*, 169(3):382–400, June 2006. DOI: 10.1002/jpln.200521955.

Horst H Gerke. Macroscopic Representation of the Interface between Flow Domains in Structured Soil. *VADOSE ZONE JOURNAL*, 11(3):0, 2012. DOI: 10.2136/vzj2011.0125.

Peter F Germann. Preferential Flow. Geographica Bernensia, Institute of Geography, University of Bern, Bern, 2014. ISBN 9783905835342.

K Germer and J Braun. Macropore-matrix water flow interaction around a vertical macropore embedded in fine sand – laboratory investigations. *VADOSE ZONE JOURNAL*, n/a(n/a), 2015. DOI: 10.2136/vzj2014.03.0030.

S Gharari, M Hrachowitz, F Fenicia, and H H G Savenije. Hydrological landscape classification: investigating the performance of HAND based landscape classifications in a central European mesoscale catchment. *Hydrol. Earth Syst. Sci.*, 15(11):3275–3291, November 2011. DOI: 10.5194/hess-15-3275-2011.

S Gillies. The Shapely User Manual. Technical report, December 2013.

T. Graeff, E Zehe, T Blume, T Francke, and B Schroder. Predicting event response in a nested catchment with generalized linear models and a distributed watershed model. *HYDROLOGICAL PROCESSES*, 26(24):3749–3769, November 2012. DOI: 10.1002/hyp.8463.

Chris B Graham and Jeffrey J McDonnell. Hillslope threshold response to rainfall: (2) Development and use of a macroscale model. *JOURNAL OF HYDROLOGY*, 393(1–2):77–93, October 2010.

RB Grayson, G Bl oschl, AW Western, and TA McMahon. Advances in the use of observed spatial patterns of catchment hydrological response. *ADVANCES IN WATER RESOURCES*, 25(8-12):1313–1334, 2002.

Rodger Grayson and Günter Blöschl, editors. *Spatial Patterns in Catchment Hydrology: Observations and Modelling*. Cambridge University Press, August 2001. ISBN 0521633168.

Rodger B Grayson, Andrew W Western, Francis H S Chiew, and Günter Blöschl. Preferred states in spatial soil moisture patterns:

Local and nonlocal controls. *WATER RESOURCES RESEARCH*, 33 (12):2897–2908, December 1997. DOI: 10.1029/97WR02174.

A Güntner, MS Krol, JC De Araujo, and A Bronstert. Simple water balance modelling of surface reservoir systems in a large data-scarce semiarid region. *HYDROLOGICAL SCIENCES JOURNAL-JOURNAL DES SCIENCES HYDROLOGIQUES*, 49(5):901–918, 2004. DOI: 10.1623/hysj.49.5.901.55139.

Hoshin Gupta, Martyn P. Clark, Jasper A. Vrugt, Gab Abramowitz, and Ming Ye. Towards a Comprehensive Assessment of Model Structural Adequacy. *WATER RESOURCES RESEARCH*, 48(8):1–40, August 2012. DOI: 10.1029/2011WR011044.

Hoshin V. Gupta and Grey S Nearing. Debates—the future of hydrological sciences: A (common) path forward? Using models and data to learn: A systems theoretic perspective on the future of hydrological science. *WATER RESOURCES RESEARCH*, 50(6):5351–5359, June 2014. DOI: 10.1002/2013WR015096.

C Harman, P Rao, N Basu, G McGrath, P Kumar, and M Sivapalan. Climate, soil, and vegetation controls on the temporal variability of vadose zone transport. *WATER RESOURCES RESEARCH*, 47(1): WooJ13, September 2011.

Ciaran J Harman. Time-variable transit time distributions and transport: Theory and application to storage-dependent transport of chloride in a watershed. *WATER RESOURCES RESEARCH*, pages n/a–n/a, January 2015. DOI: 10.1002/2014WR015707.

John Harte. Toward a synthesis of the Newtonian and Darwinian worldviews. *Physics Today*, 55(10):29–34, October 2002. DOI: 10.1063/1.1522164.

S M Hassanizadeh and W Gray. Mechanics and thermodynamics of multiphase flow in porous media including interphase boundaries. *ADVANCES IN WATER RESOURCES*, 13(4):169–186, 1990.

Hugo Hellebrand, Christoph Müller, Patrick Matgen, Fabrizio Fenicia, and Huub Savenije. A process proof test for model concepts: Modelling the meso-scale. *Physics and Chemistry of the Earth, Parts A/B/C*, 36(1-4):42–53, 2011. DOI: doi: 10.1016/j.pce.2010.07.019.

Katja Heller. *Einfluss periglazialer Deckschichten auf die oberflächennahen Fließwege am Hang - eine Prozessstudie im Osterzgebirge, Sachsen*. PhD thesis, Technical University Dresden, July 2012.

S Hergarten, G Winkler, and S Birk. Transferring the concept of minimum energy dissipation from river networks to subsurface flow

patterns. *Hydrol. Earth Syst. Sci.*, 18(10):4277–4288, October 2014. DOI: 10.5194/hess-18-4277-2014.

Ingrid Hincapié and Peter Germann. Water Content Wave Approach Applied to Neutron Radiographs of Finger Flow. *VADOSE ZONE JOURNAL*, 9(2):278, 2010. DOI: 10.2136/vzj2009.0102.

Jaroslav Hofierka and Marcel Šúri. The solar radiation model for Open source GIS: implementation and applications. *Proceedings of the Open source GIS - GRASS users conference 2002*, 2002.

B K P Horn. Hill shading and the reflectance map. *Proceedings of the IEEE*, 69(1):14–47, January 1981. DOI: 10.1109/PROC.1981.11918.

Marijke Huysmans and Alain Dassargues. Review of the use of Péclet numbers to determine the relative importance of advection and diffusion in low permeability environments. *Hydrogeology Journal*, 13(5-6):895–904–904, 2005. DOI: 10.1007/s10040-004-0387-4.

O Ippisch, H-J Vogel, and P Bastian. Validity limits for the van Genuchten-Mualem model and implications for parameter estimation and numerical simulation. *ADVANCES IN WATER RESOURCES*, 29(12):1780–1789, 2006.

T Iserloh, J B Ries, A Cerdà, M T Echeverría, W Fister, C Geißler, N J Kuhn, F J León, P Peters, M Schindewolf, J Schmidt, T Scholten, and M Seeger. Comparative measurements with seven rainfall simulators on uniform bare fallow land. *Zeitschrift für Geomorphologie Supplement*, 57(1):11–26, March 2013. DOI: 10.1127/0372-8854/2012/S-00085.

Conrad Jackisch, Erwin Zehe, Luis Samaniego, and Anupam K Singh. An experiment to gauge an ungauged catchment: rapid data assessment and eco-hydrological modelling in a data-scarce rural catchment. *Hydrological Sciences Journal*, 59(12):2103–2125, November 2014. DOI: 10.1080/02626667.2013.870662.

N. J. Jarvis. A review of non-equilibrium water flow and solute transport in soil macropores: principles, controlling factors and consequences for water quality. *European Journal of Soil Science*, 58 (3):523–546, 2007. DOI: 10.1111/j.1365-2389.2007.00915.x.

JarosŁaw Jasiewicz and Markus Metz. A new GRASS GIS toolkit for Hortonian analysis of drainage networks. *Computers & Geosciences*, 37(8):1162–1173, August 2011. DOI: 10.1016/j.cageo.2011.03.003.

Kelsey G Jencso and Brian L. McGlynn. Hierarchical controls on runoff generation: Topographically driven hydrologic connectivity,

geology, and vegetation. *WATER RESOURCES RESEARCH*, 47(11): W11527, January 2011. DOI: 10.1029/2011WR010666.

Jérôme Juilleret, Jean François Iffly, Laurent Pfister, and Christophe Hissler. Remarkable Pleistocene periglacial slope deposits in Luxem-bourg (Oesling): pedological implication and geosite potential. *Bulletin de Société des Naturalistes Luxembourgeois*, 2011.

W. A. Jury, D Or, Y. Pachepsky, H Vereecken, J. W. Hopmans, L. R. Ahuja, B. E. Clothier, K L Bristow, G. J. Kluitenberg, P. Moldrup, J Simunek, M. Th van Genuchten, and R. Horton. Kirkham's Legacy and Contemporary Challenges in Soil Physics Research. *Soil Science Society of America Journal*, 75(5):1589–1601, August 2011.

William A Jury and Kurt Roth. *Transfer functions and solute movement through soil*. theory and applications. Birkhauser, Basel, 1990.

William A Jury, Zhi Wang, and Atac Tuli. A Conceptual Model of Unstable Flow in Unsaturated Soil during Redistribution. *VADOSE ZONE JOURNAL*, (2):61–67, February 2003. DOI: 10.2136/vzj2003.6100.

MJ Kirkby and R J Chorley. Throughflow, overland flow and erosion. *International Association of Scientific Hydrology. Bulletin*, 12(3): 5–21, September 1967. DOI: 10.1080/02626667709493533.

Peter Kitanidis. Particle-tracking equations for the solution of the advection-dispersion equation with variable coefficients. *WATER RESOURCES RESEARCH*, 30(11):3225–3227, November 1994.

J Klaus and E Zehe. A novel explicit approach to model bromide and pesticide transport in connected soil structures. *Hydrol. Earth Syst. Sci.*, 15(7):2127–2144, July 2011. DOI: 10.5194/hess-15-2127-2011.

J Klaus, E Zehe, M Elsner, C Külls, and J J McDonnell. Macropore flow of old water revisited: experimental insights from a tile-drained hillslope. *Hydrol. Earth Syst. Sci.*, 17(1):103–118, January 2013. DOI: 10.5194/hess-17-103-2013.

Julian Klaus and Erwin Zehe. Modelling rapid flow response of a tile-drained field site using a 2D physically based model: assessment of 'equifinal' model setups. *HYDROLOGICAL PROCESSES*, 24 (12):1595–1609, 2010. DOI: 10.1002/hyp.7687.

A Kleidon. Beyond Gaia: Thermodynamics of life and earth system functioning. *CLIMATIC CHANGE*, 66(3):271–319, 2004.

A Kleidon and M. Renner. Thermodynamic limits of hydrologic cycling within the Earth system: concepts, estimates and implications. *Hydrol. Earth Syst. Sci.*, 17(7):2873–2892, July 2013. DOI: 10.5194/hess-17-2873-2013.

A Kleidon and S Schymanski. Thermodynamics and optimality of the water budget on land: A review. *Geophysical Research Letters*, 35 (20):6, October 2008. DOI: 10.1029/2008GL035393.

A Kleidon, M. Renner, and P Porada. Estimates of the climatological land surface energy and water balance derived from maximum convective power. *Hydrol. Earth Syst. Sci.*, 18(6):2201–2218, June 2014. DOI: 10.5194/hess-18-2201-2014.

Axel Kleidon. Nonequilibrium thermodynamics and maximum entropy production in the Earth system. *Naturwissenschaften*, 96(6): 653–677, June 2009. DOI: 10.1007/s00114-009-0509-x.

Axel Kleidon. How does the Earth system generate and maintain thermodynamic disequilibrium and what does it imply for the future of the planet? *Philosophical Transactions of the Royal Society of London A: Mathematical, Physical and Engineering Sciences*, 370(1962): 1012–1040, March 2012. DOI: 10.1098/rsta.2011.0316.

P Klenk, S Jaumann, and K Roth. Quantitative high-resolution observations of soil water dynamics in a complicated architecture using time-lapse ground-penetrating radar. *Hydrol. Earth Syst. Sci.*, 19(3):1125–1139, 2015. DOI: 10.5194/hess-19-1125-2015-supplement.

John Koestel and Mats Larsbo. Imaging and quantification of preferential solute transport in soil macropores. *WATER RESOURCES RESEARCH*, 50(5):4357–4378, May 2014. DOI: 10.1002/2014WR015351.

John Köhne, Sigrid Köhne, and Jirka Šimůnek. A review of model applications for structured soils: b) Pesticide transport. *JOURNAL OF CONTAMINANT HYDROLOGY*, 104(1-4):36–60, February 2009a. DOI: doi: 10.1016/j.jconhyd.2008.10.003.

John Köhne, Sigrid Köhne, and Jirka Šimůnek. A review of model applications for structured soils: a) Water flow and tracer transport. *JOURNAL OF CONTAMINANT HYDROLOGY*, 104(1-4):4–35, February 2009b. DOI: doi: 10.1016/j.jconhyd.2008.10.002.

Martin Konert and Jef Vandenberghe. Comparison of laser grain size analysis with pipette and sieve analysis: a solution for the underestimation of the clay fraction. *Sedimentology*, 44(3):523–535, June 1997. DOI: 10.1046/j.1365-3091.1997.d01-38.x.

D Koutsoyiannis. HESS Opinions "A random walk on water". *HYDROLOGY AND EARTH SYSTEM SCIENCES*, 14(3):585–601, 2010. DOI: 10.5194/hess-14-585-2010.

M Kutilek and PF Germann. Converging hydrostatic and hydromechanic concepts of preferential flow definitions. *JOURNAL OF CONTAMINANT HYDROLOGY*, 104(1-4):61–66, February 2009. DOI: doi: DOI: 10.1016/j.jconhyd.2008.06.004.

M Kutìlek and DR Nielsen. *Soil Hydrology*. 1995.

Hanne Laine Kaulio, Soile Backnäs, Tuomo Karvonen, Harri Koivusalo, and Jeffrey J McDonnell. Lateral subsurface stormflow and solute transport in a forested hillslope: A combined measurement and modeling approach. *WATER RESOURCES RESEARCH*, 50 (10):8159–8178, October 2014. DOI: 10.1002/2014WR015381.

Michele Di Lazzaro. Correlation between channel and hillslope lengths and its effects on the hydrologic response. *JOURNAL OF HYDROLOGY*, 362(3-4):260–273, 2008. DOI: DOI: 10.1016/j.jhydrol.2008.08.022.

P Lehmann, I Neuweiler, J Vanderborght, and H-J Vogel. Dynamics of Fluid Interfaces and Flow and Transport across Material Interfaces in Porous Media—Modeling and Observations. *VADOSE ZONE JOURNAL*, 11(3):0, 2012. DOI: 10.2136/vzj2012.0105.

HuiMin Lei, DaWen Yang, Stanislaus J Schymanski, and Murugesu Sivapalan. Modeling the crop transpiration using an optimality-based approach. *Science in China, Technological Science*, 51(2):60–75, 2008. DOI: doi: 10.1007/s11431-008-6008-z.

Christian Leibundgut, Piotr Maloszewski, and Christoph Külls. *Tracers in Hydrology*. Wiley, August 2011. ISBN 9781119965015.

Brian Lepore, Cristine Morgan, John Norman, and Christine Molling. A Mesopore and Matrix infiltration model based on soil structure. *GEODERMA*, 152(3-4):301–313, September 2009. DOI: doi: 10.1016/j.geoderma.2009.06.016.

M Leue, H H Gerke, and R H Ellerbrock. Millimetre-scale distribution of organic matter composition at intact biopore and crack surfaces. *European Journal of Soil Science*, 64(6):757–769, December 2013. DOI: 10.1111/ejss.12098.

H Lin. Earth's Critical Zone and hydropedology: concepts, characteristics, and advances. *Hydrol. Earth Syst. Sci.*, 14(1):25–45, January 2010. DOI: 10.5194/hess-14-25-2010.

T Mayr and N. J. Jarvis. Pedotransfer functions to estimate soil water retention parameters for a modified Brooks–Corey type model. *GEODERMA*, 91(1–2):1–9, 1999.

J McDonnell, M Sivapalan, K Vaché, S Dunn, G Grant, R Haggerty, C Hinz, R Hooper, J Kirchner, M Roderick, J Selker, and M Weiler. Moving beyond heterogeneity and process complexity: A new vision for watershed hydrology. *WATER RESOURCES RESEARCH*, 43, July 2007.

Jeffrey J McDonnell. Are all runoff processes the same? *HYDROLOGICAL PROCESSES*, 27(26):4103–4111, December 2013. DOI: 10.1002/hyp.10076.

Jeffrey J McDonnell and Keith Beven. Debates—The future of hydrological sciences: A (common) path forward? A call to action aimed at understanding velocities, celerities and residence time distributions of the headwater hydrograph. *WATER RESOURCES RESEARCH*, 50(6):5342–5350, June 2014. DOI: 10.1002/2013WR015141.

Kevin J McGuire and Jeffrey J McDonnell. Hydrological connectivity of hillslopes and streams: Characteristic time scales and nonlinearities. *WATER RESOURCES RESEARCH*, 46(10):W10543–n/a, October 2010. DOI: 10.1029/2010WR009341.

Wes McKinney. *Python for Data Analysis*. O'Reilly Media, Inc., October 2012. ISBN 9781449323615.

T A McMahon, M C Peel, L Lowe, R Srikanthan, and T R McVicar. Estimating actual, potential, reference crop and pan evaporation using standard meteorological data: a pragmatic synthesis. *Hydrol. Earth Syst. Sci.*, 17(4):1331–1363, April 2013. DOI: 10.5194/hess-17-1331-2013-supplement.

M Metz, H Mitasova, and R S Harmon. Efficient extraction of drainage networks from massive, radar-based elevation models with least cost path search. *Hydrol. Earth Syst. Sci.*, 15(2):667–678, February 2011. DOI: 10.5194/hess-15-667-2011.

Ralf Metzler and Joseph Klafter. The random walk's guide to anomalous diffusion: a fractional dynamics approach. *Physics Reports*, 339(1):1–77, 2000.

Ralf Metzler and Joseph Klafter. The restaurant at the end of the random walk: recent developments in the description of anomalous transport by fractional dynamics. *Journal of Physics A: Mathematical and General*, 37(31):R161, 2004.

Franziska Moebius and Dani Or. Interfacial jumps and pressure bursts during fluid displacement in interacting irregular capillaries. *Journal of Colloid and Interface Science*, 377(1):406–415, July 2012. DOI: 10.1016/j.jcis.2012.03.070.

F I Morton. Operational estimates of areal evapotranspiration and their significance to the science and practice of hydrology. *JOURNAL OF HYDROLOGY*, 66(1–4):1–76, 1983.

Nadezhda Nadezhdina, Teresa S David, Jorge S David, Maria Isabel Ferreira, Michal Dohnal, Miroslav Tesar, Karl Gartner, Ernst Leitgeb, Valeriy Nadezhdin, Jan Cermak, Maria Soledad Jimenez, and Domingo Morales. Trees never rest: the multiple facets of hydraulic redistribution. *Ecohydrology*, 3(4):431–444, December 2010. DOI: 10.1002/eco.148.

Insa Neuweiler and Hans-Jörg Vogel. Upscaling for unsaturated flow for non-Gaussian heterogeneous porous media. *WATER RESOURCES RESEARCH*, 43(3):W03443, March 2007. DOI: 10.1029/2005WR004771.

Insa Neuweiler, Daniel Erdal, and Marco Dentz. A Non-Local Richards Equation to Model Unsaturated Flow in Highly Heterogeneous Media under Nonequilibrium Pressure Conditions. *VADOSE ZONE JOURNAL*, 11(3):0, 2012. DOI: 10.2136/vzj2011.0132.

John R Nimmo. Preferential flow occurs in unsaturated conditions. *HYDROLOGICAL PROCESSES*, 26(5):786–789, December 2011. DOI: 10.1002/hyp.8380.

Guo-Yue Niu, Claudio Paniconi, Peter A. Troch, Russell L Scott, Matej Durcik, Xubin Zeng, Travis Huxman, and David C Goodrich. An integrated modelling framework of catchment-scale ecohydrological processes: 1. Model description and tests over an energy-limited watershed. *Ecohydrology*, 7(2):427–439, April 2014. DOI: 10.1002/eco.1362.

John F O'Callaghan and David M Mark. The extraction of drainage networks from digital elevation data. *Computer Vision, Graphics, and Image Processing*, 28(3):323–344, December 1984. DOI: 10.1016/S0734-189X(84)80011-0.

Travis E Oliphant. Python for Scientific Computing. *Computing in Science & Engineering*, 9(3):10–20, 2007. DOI: 10.1109/MCSE.2007.58.

D Or. Scaling of capillary, gravity and viscous forces affecting flow morphology in unsaturated porous media. *ADVANCES IN WATER RESOURCES*, 31(9):1129–1136, September 2008. DOI: 10.1016/j.advwatres.2007.10.004.

Dani Or and Shmuel Assouline. The foam drainage equation for unsaturated flow in porous media. *WATER RESOURCES RESEARCH*, 49(10):6258–6265, October 2013.

Juliane Palm, N Loes M B van Schaik, and Boris Schröder. Modelling distribution patterns of anecic, epigeic and endogeic earthworms at catchment-scale in agro-ecosystems. *Pedobiologia*, 56(1): 23–31, 2012. DOI: 10.1016/j.pedobi.2012.08.007.

L Pfister and L Hoffmann. Experimental hydro-climatological atlas of the Alzette river basin. *Centre de Recherche Public – Gabriel Lippmann*, 2002.

Hrsg Erich J Plate and Erwin Zehe, editors. *Hydrologie und Stoffdynamik kleiner Einzugsgebiete*. Schweizerbart Science Publishers, Stuttgart, Germany, March 2008. ISBN 9783510652389.

P Reggiani, M Sivapalan, and S M Hassanizadeh. A unifying framework for watershed thermodynamics: balance equations for mass, momentum, energy and entropy, and the second law of thermodynamics. *ADVANCES IN WATER RESOURCES*, 22(4):367–398, 1998.

Andrea Rinaldo, Riccardo Rigon, Jayanth R Banavar, Amos Maritan, and Ignacio Rodriguez-Iturbe. Evolution and selection of river networks: Statics, dynamics, and complexity. *Proceedings of the National Academy of Sciences*, 111(7):2417–2424, February 2014.

I Rodriguez-Iturbe. Ecohydrology: A hydrologic perspective of climate-soil-vegetation dynamics. *WATER RESOURCES RESEARCH*, 36(1):3–9, 2000. DOI: 10.1029/1999WR900210.

Ignacio Rodriguez-Iturbe and Andrea Rinaldo. *Fractal River Basins Chance and Self-Organization*. Cambridge University Press, Cambridge UK, 1 edition, 1997. ISBN 0-521-47398-5.

Helmut Rogasik, Stefan Schrader, Ingrid Onasch, Joachim Kiesel, and Horst H Gerke. Micro-scale dry bulk density variation around earthworm (Lumbricus terrestris L.) burrows based on X-ray computed tomography. *GEODERMA*, 213:471–477, January 2014. DOI: 10.1016/j.geoderma.2013.08.034.

K Roth. Scaling of water flow through porous media and soils. *European Journal of Soil Science*, 59(1):125–130, February 2008. DOI: 10.1111/j.1365-2389.2007.00986.x.

K Roth, W. A. Jury, H Flühler, and W Attinger. Transport of Chloride Through an Unsaturated Field Soil. *WATER RESOURCES RESEARCH*, 27(10):2533–2541, October 1991. DOI: 10.1029/91WR01771.

Kurt Roth and Klaus Hammel. Transport of conservative chemical through an unsaturated two-dimensional Miller-similar medium with steady state flow. *WATER RESOURCES RESEARCH*, 32(6): 1653–1663, June 1996. DOI: 10.1029/96WR00756.

Franziska Anna Rühle, Christine Klier, and Christine Stumpp. Changes in Water Flow and Solute Transport Pathways During Long-Term Column Experiments. *VADOSE ZONE JOURNAL*, 12(3): 0, 2013. DOI: 10.2136/vzj2013.01.0032.

Franziska Anna Rühle, Nadine Zentner, and Christine Stumpp. Changes in water table level influence solute transport in uniform porous media. *HYDROLOGICAL PROCESSES*, 29(6):875–888, March 2015. DOI: 10.1002/hyp.10200.

Chris H Rycroft. VORO++: A three-dimensional Voronoi cell library in C++. *Chaos: An Interdisciplinary Journal of Nonlinear Science*, 19(4): –, 2009. DOI: 10.1063/1.3215722.

Luis Samaniego, András Bárdossy, and Rohini Kumar. Streamflow prediction in ungauged catchments using copula-based dissimilarity measures. *WATER RESOURCES RESEARCH*, 46(2):W02506, February 2010.

Till Sander and Horst H Gerke. Modelling field-data of preferential flow in paddy soil induced by earthworm burrows. *JOURNAL OF CONTAMINANT HYDROLOGY*, 104(1–4):126–136, February 2009. DOI: 10.1016/j.jconhyd.2008.11.003.

Emily C Sanders, Majdi R Abou Najm, Rabi H Mohtar, Eileen Kladivko, and Darrell Schulze. Field method for separating the contribution of surface-connected preferential flow pathways from flow through the soil matrix. *WATER RESOURCES RESEARCH*, 48(4): n/a–n/a, April 2012. DOI: 10.1029/2011WR011103.

H H G Savenije. HESS Opinions "Topography driven conceptual modelling (FLEX-Topo)". *Hydrol. Earth Syst. Sci.*, 14(12):2681–2692, December 2010. DOI: 10.5194/hess-14-2681-2010-supplement.

M G Schaap, F J Leij, and M Th Van Genuchten. Rosetta: A computer program for estimating soil hydraulic parameters with hierarchical pedotransfer functions. *JOURNAL OF HYDROLOGY*, 251 (3-4):163–176, 2001.

Marcel G Schaap and Feike J Leij. Improved Prediction of Unsaturated Hydraulic Conductivity with the Mualem-van Genuchten Model. *Soil Science Society of America Journal*, 64(3):843–851, 2000.

K Scharmer and J Greif. The European solar radiation atlas. Les Presses de l'École des Mines, Paris, March 2000. ISBN 2-911762-21-5.

A C Scheinost, W Sinowski, and K Auerswald. Regionalization of soil water retention curves in a highly variable soilscape, I. Developing a new pedotransfer function. *GEODERMA*, 78(3–4):129–143, 1997.

B Schröder. Pattern, process, and function in landscape ecology and catchment hydrology - How can quantitative landscape ecology support predictions in ungauged basins? *HYDROLOGY AND EARTH SYSTEM SCIENCES*, 10(6):967–979, 2006.

B Schröder. Challenges of species distribution modeling belowground. *J. Plant Nutr. Soil Sci*, 2008.

K Schulz, R Seppelt, E Zehe, H Vogel, and S Attinger. Importance of spatial structures in advancing hydrological sciences. *WATER RESOURCES RESEARCH*, 42, February 2006.

S Schymanski, M Sivapalan, M Roderick, L Hutley, and J Beringer. An optimality-based model of the dynamic feedbacks between natural vegetation and the water balance. *WATER RESOURCES RESEARCH*, 45, January 2009.

S J Schymanski, M Sivapalan, M L Roderick, J Beringer, and L B Hutley. An optimality-based model of the coupled soil moisture and root dynamics. *HYDROLOGY AND EARTH SYSTEM SCIENCES*, 12 (3):913–932, 2008. DOI: 10.5194/hess-12-913-2008.

Stanislaus Josef Schymanski. Transpiration as the Leak in the Carbon Factory: A Model of Self-Optimising Vegetation. *Thesis, University of Western Australia, School of Environmental Systems Engineering*, page 236, November 2006.

J Seibert and K Beven. Gauging the ungauged basin: how many discharge measurements are needed? *HYDROLOGY AND EARTH SYSTEM SCIENCES*, 13(6):883–892, June 2009.

Jan Seibert and Brian L. McGlynn. A new triangular multiple flow direction algorithm for computing upslope areas from gridded digital elevation models. *WATER RESOURCES RESEARCH*, 43(4): W04501, April 2007. DOI: 10.1029/2006WR005128.

M J Shipitalo and K R Butt. Occupancy and geometrical properties of Lumbricus terrestris L. burrows affecting infiltration. *Pedobiologia*, 43(6):782–794, 1999.

W Shuttleworth and J Wallace. Evaporation from sparse crops-an energy combination theory. *Quarterly Journal of the Royal Meteorological Society*, 111(469):839–855, 1985. DOI: 10.1002/qj.49711146910.

Jirka Šimůnek, Nick J Jarvis, M Th Van Genuchten, and Annemieke Gärdenäs. Review and comparison of models for describing non-equilibrium and preferential flow and transport in the vadose zone. *JOURNAL OF HYDROLOGY*, 272(1-4):14–35, March 2003. DOI: 10.1016/S0022-1694(02)00252-4.

M Sivapalan. Pattern, Process and Function: Elements of a Unified Theory of Hydrology at the Catchment Scale. *Encyclopedia of Hydrological Sciences*, 2005.

M Sivapalan, K Takeuchi, S W Franks, V K Gupta, H Karambiri, V Lakshmi, X Liang, J J McDonnell, E M Mendiondo, P E O'Connell, T Oki, J W Pomeroy, D Schertzer, S Uhlenbrook, and E Zehe. IAHS Decade on Predictions in Ungauged Basins (PUB), 2003-2012: Shaping an exciting future for the hydrological sciences. *Hydrological Sciences Journal*, 48(6):857–880, 2003.

Tyler Smith, Lucy Marshall, Brian McGlynn, and Kelsey Jencso. Using field data to inform and evaluate a new model of catchment hydrologic connectivity. *WATER RESOURCES RESEARCH*, 49(10): 6834–6846, 2013. DOI: 10.1002/wrcr.20546.

Michal Snehota, Vladimira Jelinkova, Martina Sobotkova, Jan Sacha, Peter Vontobel, and Jan Hovind. Water and entrapped air redistribution in heterogeneous sand sample: Quantitative neutron imaging of the process. *WATER RESOURCES RESEARCH*, pages n/a–n/a, January 2015. DOI: 10.1002/2014WR015432.

C Soulsby, D Tetzlaff, and M Hrachowitz. Are transit times useful process-based tools for flow prediction and classification in ungauged basins in montane regions? *HYDROLOGICAL PROCESSES*, 24(12):1685–1696, January 2010. DOI: 10.1002/hyp.7578.

L Stadler, I Martinez-Noguez, R Hinkelmann, and K Germer. Simulating Water Flow into a Soil Matrix with a Cylindrical Macropore. In Lehfeldt and Kopmann, editors, *ICHE Conference 2014, Bundesanstalt für Wasserbau*, pages 287–293, Hamburg, 2014.

I Stavi, R Shem-Tov, M Chocron, and H Yizhaq. Geodiversity, self-organization, and health of three-phase semi-arid rangeland ecosystems, in the Israeli Negev. *Geomorphology*, 234:11–18, 2015. DOI: 10.1016/j.geomorph.2015.01.004.

Colby M Steelman, Anthony L Endres, and Jon P Jones. High-resolution ground-penetrating radar monitoring of soil moisture dynamics: Field results, interpretation, and comparison with unsaturated flow model. *WATER RESOURCES RESEARCH*, 48(9): W09538, September 2012. DOI: 10.1029/2011WR011414.

Jozsef Szilagyi and Janos Jozsa. New findings about the complementary relationship-based evaporation estimation methods. *JOURNAL OF HYDROLOGY*, 354(1–4):171–186, June 2008. DOI: 10.1016/j.jhydrol.2008.03.008.

F. Terribile, A. Coppola, G. Langella, M. Martina, and A. Basile. Potential and limitations of using soil mapping information to understand landscape hydrology. *HYDROLOGY AND EARTH SYSTEM SCIENCES*, 15(12):3895–3933, January 2011.

D Tetzlaff, S Carey, H Laudon, and K McGuire. Catchment processes and heterogeneity at multiple scales—benchmarking observations, conceptualization and prediction. *HYDROLOGICAL PROCESSES*, 24(16):2203–2208, 2010. DOI: 10.1002/hyp.7784.

F Tian, H Hu, Z Lei, and M Sivapalan. Extension of the Representative Elementary Watershed approach for cold regions via explicit treatment of energy related processes. *HYDROLOGY AND EARTH SYSTEM SCIENCES*, 10(5):619–644, 2006.

Gerard Uffink. *Analysis of Dispersion by the Random Walk Method*. PhD thesis, Proefschrift, Technische Universiteit Delft, February 1990.

Gerard Uffink, Amro Elfeki, Michel Dekking, Johannes Bruining, and Cor Kraaikamp. Understanding the Non-Gaussian Nature of Linear Reactive Solute Transport in 1D and 2D. *Transport in Porous Media*, 91(2):547–571, 2012. DOI: 10.1007/s11242-011-9859-x.

Stefan Uhlenbrook. Catchment hydrology - a science in which all processes are preferential. *HYDROLOGICAL PROCESSES*, 20(16): 3581–3585, 2006.

N Ursino and S Contarini. Stability of banded vegetation patterns under seasonal rainfall and limited soil moisture storage capacity. *ADVANCES IN WATER RESOURCES*, 29(10):1556–1564, 2006.

Jos C van Dam, Piet Groenendijk, Rob FA Hendriks, and Joop G Kroes. Advances of Modeling Water Flow in Variably Saturated Soils with SWAP. *VADOSE ZONE JOURNAL*, 7(2):640–653, 2008. DOI: 10.2136/vzj2007.0060.

Rudi van den Bos, Lucien Hoffmann, Jérôme Juilleret, Patrick Matgen, and Laurent Pfister. Conceptual modelling of individual HRU's as a trade-off between bottom-up and top-down modelling, a case study. *iemss.org*, (12), 2006.

Stéfan van der Walt, Johannes L Schönberger, Juan Nunez-Iglesias, François Boulogne, Joshua D Warner, Neil Yager, Emmanuelle Gouillart, and Tony Yu. scikit-image: image processing in Python. *PeerJ*, 2:e453, June 2014. DOI: 10.7717/peerj.453.

M Th Van Genuchten. CLOSED-FORM EQUATION FOR PREDICTING THE HYDRAULIC CONDUCTIVITY OF UNSATURATED SOILS. *Soil Science Society of America Journal*, 44(5):892–898, 1980.

H J van Meerveld, J Seibert, and N E Peters. Hillslope-riparian-stream connectivity and flow directions at the Panola Mountain Research Watershed. *HYDROLOGICAL PROCESSES*, pages n/a–n/a, April 2015. DOI: 10.1002/hyp.10508.

Loes van Schaik, Juliane Palm, Julian Klaus, Erwin Zehe, and Boris Schröder. Linking spatial earthworm distribution to macropore numbers and hydrological effectiveness. *Ecohydrology*, pages n/a–n/a, January 2013. DOI: 10.1002/eco.1358.

H Vereecken, M Weynants, M Javaux, Y. Pachepsky, M G Schaap, and M Th van Genuchten. Using Pedotransfer Functions to Estimate the van Genuchten–Mualem Soil Hydraulic Properties: A Review. *VADOSE ZONE JOURNAL*, 9(4):795, 2010. DOI: 10.2136/vzj2010.0045.

H J Vogel and K Roth. A new approach for determining effective soil hydraulic functions. *European Journal of Soil Science*, 49(4):547–556, 1998. DOI: 10.1046/j.1365-2389.1998.4940547.x.

H-J Vogel and K Roth. Moving through scales of flow and transport in soil. *JOURNAL OF HYDROLOGY*, 272(1-4):95–106, March 2003. DOI: 10.1016/S0022-1694(02)00257-3.

H-J Vogel, I Cousin, O Ippisch, and P Bastian. The dominant role of structure for solute transport in soil: experimental evidence and modelling of structure and transport in a field experiment. *HYDROLOGY AND EARTH SYSTEM SCIENCES*, 10(4):495–506, January 2006.

T Wagener, M Sivapalan, P Troch, and R Woods. Catchment Classification and Hydrologic Similarity. *Geography Compass*, 1(4):901–931, 2007.

John Wainwright, Laura Turnbull, Tristan Ibrahim, Irantzu Lexartza-Artza, Steven Thornton, and Richard Brazier. Linking environmental régimes, space and time: Interpretations of structural and functional connectivity. *Geomorphology*, 126(3-4):387–404, March 2011. DOI: doi: 10.1016/j.geomorph.2010.07.027.

M Todd Walter, Tammo S Steenhuis, Vishal K Mehta, Dominique Thongs, Mark Zion, and Elliot Schneiderman. Refined conceptualization of TOPMODEL for shallow subsurface flows. *HYDROLOGICAL PROCESSES*, 16(10):2041–2046, July 2002. DOI: 10.1002/hyp.5030.

D Wang, J M Norman, B Lowery, and K McSweeney. Nondestructive Determination of Hydrogeometrical Characteristics of Soil Macropores. *Soil Science Society of America Journal*, 58(2):294, 1994. DOI: 10.2136/sssaj1994.03615995005800020005x.

Markus Wehrer and Lee D Slater. Characterization of water content dynamics and tracer breakthrough by 3-D electrical resistivity tomography (ERT) under transient unsaturated conditions. *WATER RESOURCES RESEARCH*, pages n/a–n/a, January 2015. DOI: 10.1002/2014WR016131.

Steven V Weijs and Nick van de Giesen. Accounting for Observational Uncertainty in Forecast Verification: An Information-Theoretical View on Forecasts, Observations, and Truth. *Mon. Wea. Rev.*, 139(7):2156–2162, March 2011. DOI: 10.1175/2011MWR3573.1.

Markus Weiler. An infiltration model based on flow variability in macropores: development, sensitivity analysis and applications. *JOURNAL OF HYDROLOGY*, 310(1-4):294–315, August 2005. DOI: doi: DOI: 10.1016/j.jhydrol.2005.01.010.

Markus Weiler and Hannes Flühler. Inferring flow types from dye patterns in macroporous soils. *GEODERMA*, 120(1–2):137–153, May 2004. DOI: 10.1016/j.geoderma.2003.08.014.

Markus Weiler and J McDonnell. Conceptualizing lateral preferential flow and flow networks and simulating the effects on gauged and ungauged hillslopes. *WATER RESOURCES RESEARCH*, 43, March 2007.

Markus Weiler and Felix Naef. Simulating surface and subsurface initiation of macropore flow. *JOURNAL OF HYDROLOGY*, 273(1-4): 139–154, March 2003. DOI: doi: DOI: 10.1016/S0022-1694(02)00361-X.

Markus Helmut Weiler. *Mechanisms controlling macropore flow during infiltration. Dye tracer experiments and simulations.* PhD thesis, ETH Zürich, 2001.

M C Westhoff. *High resolution temperature observations to identify different runoff processes*. PhD thesis, PhD Thesis, TU Delft, October 2011.

J Wienhöfer and E Zehe. Predicting subsurface stormflow response of a forested hillslope – the role of connected flow paths. *Hydrol. Earth Syst. Sci.*, 18(1):121–138, 2014. DOI: 10.5194/hess-18-121-2014.

J H M Wösten, Ya A Pachepsky, and W.J. Rawls. Pedotransfer functions: bridging the gap between available basic soil data and missing soil hydraulic characteristics. *JOURNAL OF HYDROLOGY*, 251(3–4):123–150, 2001.

Sebastian Wrede, Fabrizio Fenicia, Núria Martínez-Carreras, Jérôme Juilleret, Christophe Hissler, Andreas Krein, Hubert H G Savenije, Stefan Uhlenbrook, Dmitri Kavetski, and Laurent Pfister. Towards more systematic perceptual model development: a case study using 3 Luxembourgish catchments. *HYDROLOGICAL PROCESSES*, pages n/a–n/a, December 2014. DOI: 10.1002/hyp.10393.

E Zehe and G Bloschl. Predictability of hydrologic response at the plot and catchment scales: Role of initial conditions. *WATER RESOURCES RESEARCH*, 40(10), October 2004. DOI: 10.1029/2003WR002869.

E Zehe and H Flühler. Preferential transport of isoproturon at a plot scale and a field scale tile-drained site. *JOURNAL OF HYDROLOGY*, 247(1-2):100–115, June 2001. DOI: 10.1016/S0022-1694(01)00370-5.

E Zehe, T Maurer, J Ihringer, and E Plate. Modeling water flow and mass transport in a loess catchment. *PHYSICS AND CHEMISTRY OF THE EARTH PART B-HYDROLOGY OCEANS AND ATMOSPHERE*, 26(7–8):487–507, January 2001. DOI: 10.1016/S1464-1909(01)00041-7.

E Zehe, R Becker, A Bardossy, and E Plate. Uncertainty of simulated catchment runoff response in the presence of threshold processes: Role of initial soil moisture and precipitation. *JOURNAL OF HYDROLOGY*, 315(1-4):183–202, 2005.

E Zehe, T. Graeff, M. Morgner, A Bauer, and A Bronstert. Plot and field scale soil moisture dynamics and subsurface wetness control on runoff generation in a headwater in the Ore Mountains.

HYDROLOGY AND EARTH SYSTEM SCIENCES, 14(6):873–889, January 2010a.

E Zehe, U Ehret, T Blume, A Kleidon, U Scherer, and M Westhoff. A thermodynamic approach to link self-organization, preferential flow and rainfall-runoff behaviour. *Hydrol. Earth Syst. Sci.*, 17(11): 4297–4322, 2013. DOI: 10.5194/hess-17-4297-2013.

E Zehe, U Ehret, L Pfister, T Blume, B Schroder, M Westhoff, C Jackisch, S J Schymanski, M Weiler, K Schulz, N Allroggen, J Tronicke, L van Schaik, P Dietrich, U Scherer, J Eccard, V Wulfmeyer, and A Kleidon. HESS Opinions: From response units to functional units: a thermodynamic reinterpretation of the HRU concept to link spatial organization and functioning of intermediate scale catchments. *Hydrol. Earth Syst. Sci.*, 18(11):4635–4655, November 2014. DOI: 10.5194/hess-18-4635-2014.

Erwin Zehe. *Stofftransport in der ungesättigten Bodenzone auf verschiedenen Skalen*. PhD thesis, Mitteilungen des Instituts für Wasserwirtschaft und Kulturtechnik der Universität Karlsruhe (TH), December 1999.

Erwin Zehe, Theresa Blume, and Günter Blöschl. The principle of 'maximum energy dissipation': a novel thermodynamic perspective on rapid water flow in connected soil structures. *Philosophical Transactions of the Royal Society B: Biological Sciences*, 365(1545):1377–1386, 2010b. DOI: 10.1098/rstb.2009.0308.